TESIS DE LA UNIVERSIDAD DE ZARAGOZA
2021
182

Lucía Rivero Cuesta

Paleoenvironmental assessment across key Eocene climatic events based on benthic foraminifera.

Director/es
Alegret Badiola, María Laia

ISSN 2254-7606

Prensas de la Universidad
Universidad Zaragoza

ISSN 2254-7606

Universidad Zaragoza
1542

Tesis Doctoral

PALEOENVIRONMENTAL ASSESSMENT ACROSS KEY EOCENE CLIMATIC EVENTS BASED ON BENTHIC FORAMINIFERA.

Autor

Lucía Rivero Cuesta

Director/es

Alegret Badiola, María Laia

UNIVERSIDAD DE ZARAGOZA
Escuela de Doctorado

2021

Paleoenvironmental assessment across key Eocene climatic events based on benthic foraminifera

Lucía Rivero Cuesta

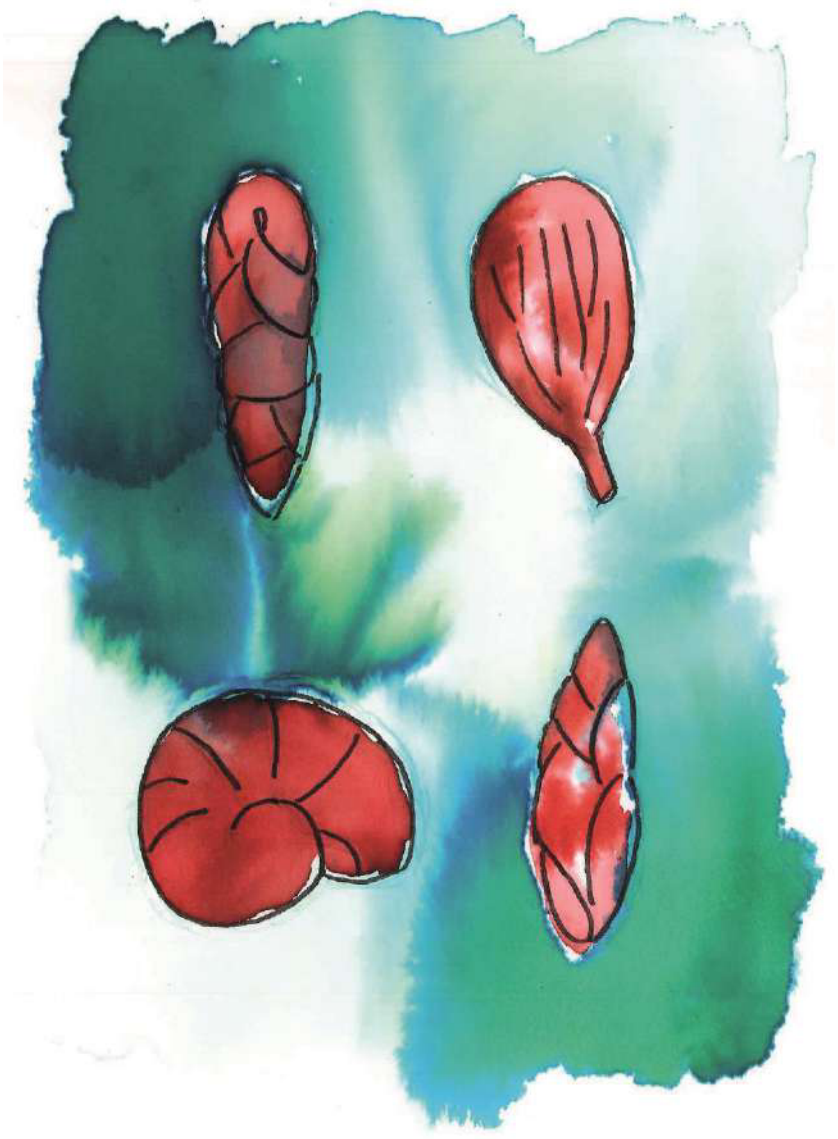

Cover artwork/ilustración de portada: Llanos Sanz

Departamento de Ciencias de la Tierra
Universidad Zaragoza

Instituto Universitario de Investigación en Ciencias Ambientales de Aragón
Universidad Zaragoza

PhD THESIS / TESIS DOCTORAL

Paleoenvironmental assessment across key Eocene climatic events based on benthic foraminifera

Lucía Rivero Cuesta

Supervisor/Directora:

Laia Alegret Badiola

Departamento de Ciencias de la Tierra

Facultad de Ciencias

Universidad de Zaragoza

2020

This document presents a PhD Thesis consisting of a collection of five scientific papers, which are listed below chronologically. All of the publications have been published in journals included in the Journal Citation Reports (JCR).

§

Esta tesis se presenta en formato de compendio de publicaciones. Para cumplir con la normativa vigente de la Universidad de Zaragoza, la tesis contiene cinco artículos científicos publicados en revistas incluidas en el Journal Citation Reports (JCR):

Grira, C., Karoui-Yaakoub, N., Hédi Negra, M., **Rivero-Cuesta**, L., and Molina, E., 2018. Paleoenvironmental and ecological changes during the Eocene-Oligocene transition based on foraminifera from the Cap Bon Peninsula in North East Tunisia. *Journal of African Earth Sciences*, 143, 145-161.

Rivero-Cuesta, L., Molina, E., and Alegret, L., 2018. Eocene (Bartonian) benthic foraminifera and paleoenvironmental changes in the Western Tethys. *Palaeogeography, Palaeoclimatology, Palaeoecology*, 503, 102-111.

Rivero-Cuesta, L., Westerhold, T., Agnini, C., Dallanave, E., Wilkens, R., and Alegret, L., 2019. Paleoenvironmental changes at ODP Site 702 (South Atlantic): anatomy of the Middle Eocene Climatic Optimum. *Paleoceanography and Paleoclimatology*, 34, PA003806.

Rivero-Cuesta, T. Westerhold, L., and Alegret, L., 2020. The Late Lutetian Thermal Maximum (middle Eocene): first record of deep-sea benthic foraminifera response. *Palaeogeography, Palaeoclimatology, Palaeoecology,* 545, 109637.

Cotton, L., **Rivero-Cuesta**, L., Franceschetti, G., Iakovleva, A., Alegret, L., Dinarès-Turell, J., Hooker, L., King, C., Fluegeman, R., Yager, S., and Monechi, S., 2020. Reassessing the Bartonian unit stratotype at Alum Bay (Isle of Wight, UK): an integrated approach. *Newsletters on Stratigraphy*, 54(1), 17-42.

This PhD Thesis aims for the doctoral degree with international mention. In order to reach this goal, two foreign specialists have reviewed this document and evaluated its quality: Carolina Náñez (Servicio Geológico Minero Argentino and CONICET, Argentina) and Carlos Alberto Sánchez Quiñonez (Universidad Nacional de Colombia).

During the course of the PhD, two research stays with a total duration of four months were done at MARUM (Bremen) under the supervision of Thomas Westerhold. High-resolution isotopic analysis, data integration, data analysis and discussion were the main tasks performed by the doctoral student during these research stays, which have contributed to the development of this Thesis.

The publications that integrate this PhD Thesis are included in their original version and in the language in which they were published (English). The main body of this document is presented in English, whereas the abstract and conclusions are shown both in English and in Spanish.

§

La presente tesis doctoral se postula para mención internacional. Para ello, dos especialistas extranjeros han evaluado la calidad de este documento: Carolina Náñez (Servicio Geológico Minero Argentino y CONICET, Argentina) y Carlos Alberto Sánchez Quiñonez (Universidad Nacional de Colombia).

Durante el doctorado se han realizado dos estancias de investigación con una duración total de cuatro meses en el centro de investigación MARUM (Bremen, Alemania) bajo la supervisión de Thomas Westerhold. Durante las estancias, la doctoranda realizó análisis isotópicos de alta resolución, integración de datos y discusión de resultados entre otras tareas, que han repercutido positivamente en el resultado final de la tesis.

Las publicaciones que integran esta tesis doctoral están incluidas en su versión original y en el idioma en el que han sido publicadas (inglés). El cuerpo principal de este documento es en inglés, mientras que el resumen y las conclusiones se presentan tanto en inglés como en castellano.

A mis padres

"*Gentlemen, here is this chit of a girl, right out of college, telling us that we can use Foraminifera to determine the age of a formation.*

Gentlemen, you know that it can't be done!"

Professor J. J. Galloway in response to Esther Richards Applin's presentation at the Paleontological Society meeting, 1921

Agradecimientos/ Acknowledgements

Esta tesis doctoral ha sido financiada por el Ministerio de Economía y Competitividad de España a través del contrato predoctoral BES-2015-075140. Las actividades realizadas durante la tesis doctoral han contado con el apoyo económico de los proyectos de investigación CGL 2014-58794-P y CGL 2017-84693-R (Ministerio de Economía y Competitividad y fondos FEDER), el grupo de investigación E33_17R "Extinción y reconstrucción paleoambiental desde el Cretácico al Cuaternario" (Gobierno de Aragón y Fondo Social Europeo) y el Instituto Universitario de Investigación en Ciencias Ambientales de Aragón (IUCA).

Me gustaría agradecer en primer lugar a mis supervisores de tesis, Laia Alegret y Eustoquio Molina†, por seleccionarme para realizar este trabajo. Han sido años de intenso aprendizaje tanto profesional como personal. Aunque por desgracia Eustoquio no ha podido llegar a ver el final de esta tesis, estoy segura de que estaría satisfecho con ella. Extender mis agradecimientos a Ignacio Arenillas (Univ. Zaragoza), Francisco Sierro (Univ. Salamanca), Gabriela de Jesús Arreguín Rodríguez (Univ. Baja California Sur), Carolina Náñez (Servicio Geológico Minero Argentino) y José Antonio Arz (Univ. Zaragoza) por acceder a formar parte del tribunal de esta tesis. De la misma manera agradezco al revisor externo que ha evaluado esta tesis, Carlos Sánchez (Univ. Nacional de Colombia); así como a los coautores de los artículos que componen esta tesis y los editores y revisores de las revistas donde se han publicado. Gracias por vuestro tiempo.

My "internationalization" would not have been possible without the collaboration of Thomas Westerhold, who kindly had me visiting not once but twice at MARUM. Thank you for your interest in my research (and the bike!); it has been a pleasure working alongside you. I felt very welcome by the team: Edo, Roy, Anna, Ulla, Alex, Holger, Henning; as well as by many other people from MARUM/AWI/Bremen Uni (Gema, Diederik, Dharma, Heather, Diana, Amanda, Jeroen,…). Those months in Bremen were memorable, not just because of the science but also the climbing sessions, the (maybe too many) visits to Muchos Más with my twin Lucía and the GoT nights at Mariem and Will's. Big thank you to all!

Durante estos años he podido contar con compañeros de faenas bastante majicos: Raquel, Vicente, Ester, Jara, Manu, Edu, Julia, Carmen, Álvaro, Fernando, Christian, Toni, Elisa; además de compañeros de departamento (Nacho, Jose Antonio, Gloria, Iñaki, Enrique, Isa) y veteranos de las trincheras de la ciencia (Esteve, Miguel, Gaska, Diego, Víctor, Luismi, Pere, Roi) que han hecho que este tiempo haya sido considerablemente mejor, muchas gracias a todos. Queda pendiente un piscolabis. Merece una línea a parte mi "partner in crime" Alba, el primer hilo de unión con Zaragoza y la chispa que inició todo esto en los pasillos del Geocentrum (y alguna katuskha): eskerrik asko!

Another part of this journey has been the courses, congresses and meetings. They have allowed me to meet amazing people: Ángela, Marina, Rowan, Vivor, Catarinas, Iván, Marisa… thanks for being amazing scientists and wonderful people too.

Y esta aventura ha sido aún más redonda gracias a personicas que, sin darme cuenta, han acabado siendo mis pilares zaragozanos. Llanos, Alain y Montse consiguieron ser los primeros en colarse en mi círculo entre swings in y swings out, mientras que con pies de gato, cuerdas y alguna(s) cerveza(s) conocí a mis compañeros de montaña: Andrea, Ana, Enrique, Julia y demás familia del CAU, en especial a la otra mitad de mi cordada, Icíar. Si juntas algo que disfrutas con gente estupenda, el resultado no puede ser mejor. Más tarde pero con fuerza entró el equipo Bulderland, las sesiones de yoga con Ana y las peripecias artísticas con Sofi. Muchas gracias a todos por haberme hecho sentir como en casa.

A los que, aún en la distancia, habéis sido un gran apoyo. Empezando por las más guapitas (MariLai, MariIne y MariCar), min favorit svenska Linnea, "los de siempre" (Vir, Jose y Manu), los futuros funcionarios (Carlos, Nuria y Rafa) y la resistencia salmantina (Marina, Marta, Dani, Raksha): gracias por estar siempre ahí. No m'oblido del que ha hagut de donar-me extra ànims: moltes gràcies Albert, per creure en mi quan jo no ho vaig fer.

Pero no estaría escribiendo esto si no fuese por mis padres, que siempre tienen una palabra de aliento cuando más lo necesito. Va por vosotros.

Table of contents

Abstract **1**
Resumen 3

Chapter 1: Introduction **6**
1.1 Benthic foraminifera 7
1.1.1 Ecology of benthic foraminifera 8
1.1.2 Applications of benthic foraminifera 10
1.1.3 Fossil benthic foraminifera assemblages 12
1.2 Eocene climate 15
1.2.1 The Late Lutetian Thermal Maximum 19
1.2.2 The Middle Eocene Climatic Optimum 20
1.2.3 The Eocene/Oligocene transition 21
1.3 Missing formal boundary stratotypes of the Paleogene: the base of the Bartonian, a GSSP in progress 23

Chapter 2: Objectives **26**

Chapter 3: Material and methods **28**
3.1 Initial deskwork 29
3.2 Study site and sections 29
3.3 Sample collection and processing 32
3.4 Taxonomic classification 33
3.5 Quantitative analyses and diversity 34
3.6 Multivariate statistical analyses 34
3.7 Assessment of benthic foraminiferal assemblages
3.7.1 Paleoenvironment and paleoecology 35
3.7.2 Paleobathymetry 37
3.8 Paleoceanographic proxies
3.8.1 Stable carbon and oxygen isotopes 38
3.8.2 Calcium carbonate content 39
3.8.3 Accumulation rates 39
3.9 Contribution to biostratigraphy and sedimentation rates 40

Chapter 4: Results **41**

4.1 Benthic foraminiferal turnover across Eocene climatic events

4.1.1 Late Lutetian Thermal Maximum (middle Eocene): first record of deep-sea benthic foraminiferal response 42

4.1.2 Paleoenvironmental changes at ODP Site 702 (South Atlantic): anatomy of the Middle Eocene Climatic Optimum 54

4.1.3 Eocene (Bartonian) benthic foraminifera and paleoenvironmental changes in the Western Tethys 75

4.1.4 Paleoenvironmental and ecological changes during the Eocene-Oligocene transition based on foraminifera from the Cap Bon Peninsula in North East Tunisia 86

4.2 Contribution to the definition of the Bartonian GSSP

4.2.1 Reassessing the Bartonian unit stratotype at Alum Bay (Isle of Wight, UK): an integrated approach 104

Chapter 5: Discussion **131**

5.1. Benthic foraminifera response to Eocene climatic events

5.1.1 The Late Lutetian Thermal Maximum 132

5.1.2 The MECO 135

5.1.3 Comparison of climatic events 142

5.2. Stratigraphic boundaries

5.2.1 Benthic turnover across the Eocene Oligocene transition 148

5.2.2 The Bartonian GSSP 150

Conclusions **154**

Conclusiones 157

References **160**

Appendices **183**

Appendix I: information about the published articles 184

Appendix II: Supplementary material (Rivero-Cuesta et al., 2020) 186

Appendix III: Supplementary material (Rivero-Cuesta et al., 2019) 188

Appendix IV: Supplementary material (Rivero-Cuesta et al., 2018) 202

ABSTRACT

The Eocene was a period of intense climatic variability in Earth's history. It comprised a long-term climatic transition from the early Eocene greenhouse to the Oligocene icehouse state, and this general trend was punctuated by short warming events coeval with temporary perturbations of the global carbon cycle, called hyperthermal events. Early Eocene hyperthermals have received much attention, but the middle to late Eocene events such as the Late Lutetian Thermal Maximum (LLTM) are largely underrepresented in the current literature. Additionally, one of the most intriguing events of this epoch, the Middle Eocene Climatic Optimum, shows an unusual long duration and its trigger mechanisms are still enigmatic. This thesis aims to analyse the faunal response of benthic foraminifera and interpret the paleoecological and paleoenvironmental changes across the MECO and LLTM climatic events, as well as across the Lutetian/Bartonian and Eocene/Oligocene stratigraphic boundaries in order to contribute to the broad picture of the middle to late Eocene climate. Taxonomic, quantitative and statistical studies of benthic foraminiferal assemblages were combined with geochemical analyses and integrated in five multidisciplinary publications.

Benthic foraminiferal assemblages from three land sections (Torre Cardela in Spain, Alum Bay in England and Menzel Bou Zelfa in Tunisia) and an ocean drilling site (ODP Site 702, South Atlantic Ocean) were studied across several key, middle to late Eocene climatic (LLTM, MECO) and stratigraphic events (Lutetian/Bartonian and Eocene/Oligocene boundaries). Overall, the warming events studied did not have a large impact on the benthic fauna, but temporary shifts in their assemblages related to changes in the food supply to the seafloor. The environmental instability recorded by these transient changes on the benthic fauna lasted longer than the isotopic excursion that defines the LLTM and MECO events. This stresses the importance of paleoenvironmental assessment and multidisciplinary studies across enigmatic events such as the MECO.

Correlation between the carbon isotope values and changes in abundance of certain benthic taxa across the warming intervals suggests that the main ecological driver of the faunal turnover was related to changes in the organic matter flux to

the seafloor rather than to temperature. Warming across the LLTM and MECO seems to have affected the accumulation rates of benthic (rather than their diversity) and planktic foraminifera, pointing to a temperature threshold possibly related to increased metabolic rates of these organisms.

RESUMEN

El Eoceno fue un periodo de intensa variabilidad climática en la historia de la Tierra. Esta época abarca una transición climática a largo plazo, desde el estado "invernadero" del Eoceno inferior hasta un planeta con hielo permanente en el Oligoceno. Esta transición climática estuvo salpicada de breves eventos de calentamiento global relacionados con perturbaciones temporales en el ciclo del carbono, llamados eventos hipertermales. Los hipertermales del Eoceno inicial han recibido mucha atención, pero los del Eoceno medio y terminal, como el Máximo Térmico del Luteciense superior (LLTM por sus siglas en inglés), están ampliamente infrarrepresentados en la literatura. Además, uno de los eventos más insólitos de esta época, el Óptimo Climático del Eoceno medio (MECO por sus siglas en inglés), muestra una duración excepcionalmente larga y los mecanismos que lo generaron aún son un enigma. Esta tesis tiene como objetivo analizar la respuesta de los foraminíferos bentónicos e interpretar su paleoecología y los cambios paleoambientales a través de los eventos climáticos del LLTM y al MECO, así como a través de los límites estratigráficos Luteciense/Bartoniense y Eoceno/Oligoceno, y así obtener nuevos datos para contribuir a la visión global del Eoceno medio y superior. Los estudios taxonómicos, cuantitativos y estadísticos de las asociaciones de foraminíferos bentónicos se combinaron con análisis geoquímicos en cinco publicaciones multidisciplinares.

Se han estudiado las asociaciones de foraminíferos de tres afloramientos (Torre Cardela en España, Alum Bay en Inglaterra y Menzel Bou Zelfa en Túnez) y un sondeo oceánico (ODP Site 702, Atlántico Sur) a través de varios eventos climáticos (LLTM, MECO) y límites estratigráficos (Luteciense/Bartoniense y Eoceno/Oligoceno) claves del Eoceno medio y superior. En general, los eventos de calentamiento analizados no muestran un gran impacto sobre la fauna bentónica, pero sí modificaciones temporales en sus asociaciones, relacionadas con cambios en el aporte alimenticio al fondo oceánico. La inestabilidad ambiental revelada por estos cambios temporales de la fauna bentónica persistió más que la excusión isotópica que define el LLTM y el MECO. Este descubrimiento acentúa la

importancia de la evaluación paleoambiental y los estudios multidisciplinares en eventos complejos como el MECO.

La correlación entre los valores isotópicos del carbono y la abundancia de ciertos taxones observados en los eventos de calentamiento estudiados sugiere que el mayor factor ecológico que controló estos cambios de abundancia estuvo relacionado con modificaciones del flujo de la materia orgánica hacia los fondos oceánicos en vez de con el aumento de la temperatura. El calentamiento asociado a los eventos LLTM y MECO afectó a las tasas de acumulación de los foraminíferos bentónicos (en lugar de a su diversidad) y planctónicos, sugiriendo un límite de temperatura posiblemente relacionado con las tasas metabólicas de estos organismos.

Acronyms

AR(s)	Accumulation rate(s)
BCR	Bremen core repository
BFAR(s)	Benthic foraminifera accumulation rate(s)
CCD	Calcium compensation depth
CFAR(s)	Coarse fraction accumulation rate(s)
CIE	Carbon isotopic excursion
DIC	Dissolved inorganic carbon
DIS	Drilling information system
ECORD	European Consortium for Ocean Research Drilling
EECO	Early Eocene Climatic Optimum
EOB	Eocene Oligocene Boundary
GSSP	Global Boundary Stratotype Section and Point
ICS	International Commission on Stratigraphy
IODP	Integrated Ocean Discovery Program
LLTM	Late Lutetian Thermal Maximum
MBSF	Meters below sea floor
MBZ	Menzel Bou Zelfa section
MECO	Middle Eocene Climatic Optimum
ODP	Ocean Drilling Program
OIE	Oxygen isotopic excursion
PET	Phytodetritus exploiting taxa
PETM	Paleocene-Eocene Thermal Maximum
TROX	Trophic Oxygen model

Chapter 1: Introduction

1.1 Benthic foraminifera

Benthic foraminifera are eukaryotic unicellular microorganisms (protists) that inhabit the seafloor, from shallow settings to abyssal depths (Phleger, 1960). They are the most abundant organisms in the benthic realm (Snider et al., 1984; Gooday et al., 1992), occurring at all latitudes and in a wide range of marine environments, from warm, brackish lagoons (e.g. Reizopoulou and Nicolaidou, 2004) to cold Antarctic deep waters (e.g. Mikhalevich, 2004). Ecological studies have documented more than 2100 living species of benthic foraminifera, although their actual diversity could be even two times higher (Murray, 2007). Molecular techniques have improved the understanding of actual foraminifera diversity (Pawlowski, 2000), revealing a larger number of biological species than previous estimates by morphological classifications (Pawlowski and Holzmann, 2008). Genetically, foraminifera (order Foraminiferida) belong to the Rhizaria supergroup (Adl et al., 2005), which is characterised by the presence of thread-like pseudopods (rhizopodia) for feeding or/and locomotion.

Benthic foraminifera cover their cytoplasmic body with a test, which is either made of calcium carbonate ($CaCO_3$) or by agglomeration of mineral grains embedded in organic cement. Foraminifera with no test, called "naked" foraminifera, have also been reported (Gooday, 1986; Pawlowski et al., 1998). Tests range from a simple single chamber with an aperture to more complex, multi-chambered morphologies (Boersma, 1998). Possible functions of the test include protection against adverse environmental condition, and to aid reproduction and cell growth, among others (Murray, 2006).

Test composition and morphology (chamber arrangement and shape) have been historically used to classify benthic foraminifera into families, genera and species (therefore, they are morphospecies, not biological species). Alfred R. Loeblich and Helen Tappan compiled a comprehensive classification (Loeblich and Tappan, 1987) that is currently the most widely used one at the supra-specific level, although it has undergone revisions and updates (e.g. uniserial morphologies by Hayward et al., 2012). Molecular studies suggest that chamber shape, mode of coiling and distance between apertures correspond better to the main

evolutionary trends in foraminifera than test composition and structure (Pawlowski et al., 2013). Matching the molecular and morphological approaches in benthic foraminifera classification is one of the current challenges for taxonomists to tackle (e.g. Tsuchiya et al., 2000).

Because of their abundance and ubiquity, benthic foraminifera have been increasingly studied since the XIX century despite their small size, which can range from a few microns to several centimetres. Large benthic foraminifera are usually found in shallow-water settings, where they are able to grow large due to the presence of sunlight and symbionts hosted within their tests (Hallock, 1985; Lee and Anderson, 1991). Small benthic foraminifera are found at all depths and they become dominant in deep-water settings. There are records of benthic foraminifera since the Late Proterozoic (Gaucher and Sprechmann, 1999) and their long, continuous and abundant fossil record makes them one of the most useful fossil groups in paleoenvironmental reconstructions and paleoclimate research (Holbourn et al., 2013).

1.1.1 Ecology of benthic foraminifera

Ecology explores patterns of distribution and abundance of organisms and the causes behind them, considering interactions between individuals and their physical and chemical environment. Despite the widespread presence of benthic foraminifera, ecology studies have commonly reported the occurrence of specific benthic taxa in particular ocean environments and habitats (see Murray, 2007 for particular cases). It is now widely accepted that benthic foraminifera distribution is strongly controlled by their environment (Murray, 2006) and that most species are adapted to inhabit specific marine settings. Broad distribution patterns can be defined in relation to major environmental controls (Cushman, 1948; Boltovskoy and Wright, 1976; Culver and Buzas, 2000). At local scales, however, there are too many factors involved, preventing identification of narrower distribution patterns (Gooday, 1999).

Temperature, salinity, oxygen concentration, food supply, sediment characteristics and hydrodynamics are believed to be the main environmental parameters controlling benthic foraminiferal distribution and abundance (Murray,

2007). However, the importance of each factor varies within marine settings. Salinity and temperature, for example, play an important role controlling shallow-water benthic foraminifera distribution, while they become less relevant in deeper environments where these parameters are steadier. Experimental studies have been able to artificially isolate individual factors in order to determine critical thresholds of a particular species (i.e. the lower and upper limits for survival). These studies usually show more extreme critical limits than those observed in field studies (Murray, 2001 and references therein). "*No one factor controls the benthic community. Nearly all factors are coupled and their relative importance at different sites determines benthic community structure*" (Flach, 2003; pp. 351-352). In nature, factors operate and co-vary together, which may produce different thresholds, explaining why in one particular environment there is a strong correlation between certain species and one particular factor, while this correlation is not observed in another setting (Murray, 1991).

The deep-sea is the largest and most stable ecosystem on Earth (Verity et al., 2002), and one of the least explored areas on Earth. The most important parameters controlling deep-sea benthic foraminifera distribution and abundance are thought to be the amount organic matter (Corliss and Emerson, 1990; Jorissen et al., 1992, 1995; Hohenegger et al., 1993; Linke and Lutze, 1993; Wollenburg and Meckensen, 1998) and oxygen availability at the seafloor (Sen Gupta, 1999; van der Zwaan et al., 1999; Gooday, 2003; Jorissen et al., 2007 and references therein). This hypothesis was first proposed by Corliss and Emerson (1990), then Jorissen et al. (1995) formalised it into a conceptual model named TROX (TRophic OXygen model), which explains benthic foraminiferal distribution and abundance based on these two parameters. The type, quality and seasonality of food supply also play an important role (Lee et al., 1977; Altenbach, 1992; Smart et al., 1994; Loubere, 1998; Gooday, and Rathburn 1999; Den Dulk et al., 2000; Fontainer et al., 2005), suggesting that the abundance and distribution of deep-sea benthic foraminifera is more complex than a two-axis model.

Opportunistic species, for instance, do not follow the TROX model. These species increase quickly in abundance when conditions change in their favour, and decrease again once conditions are reverted, with individuals still existing in small

numbers for long periods of time (e.g. Finger and Lipps, 1981; Alve and Murray, 1997; Scott et al., 2003). For example, species with preference for refractory organic matter (i.e., low quality organic matter, of terrestrial origin) rather than labile (fresh) organic matter have been reported to have this opportunistic behaviour (Jorissen et al., 1998; Loubère and Fariduddin, 1999; Gooday, 2003; Fenero et al., 2012; Arreguín-Rodríguez et al., 2014; Giusberti et al., 2016). Another good example is the seasonal input of phytodetritus that provides a temporary source of food to phytodetritus-eating species, which rapidly increase in abundance (Gooday, 2002). Species showing this opportunistic behaviour have been defined as phytodetritus species (Gooday, 1988; 1993) or phytodetritus exploiting taxa (PET, Jorissen et al., 2007; Smart et al., 2007), and have been reported in numerous deep-sea benthic foraminifera studies (e.g. Thiel et al., 1988; Gooday and Turley, 1990; Lambshead and Gooday, 1990; Gooday and Hughes, 2002; Boscolo-Galazzo et al., 2015). Species that thrive during seasonal phytodetritus blooms such as *Alabamina weddellensis* and *Epistominella exigua* have the ability to cope with a rapid change, rather than having tolerance to a specific environmental parameter (Alve, 2003).

The diversity of deep-sea benthic foraminifera is also restricted by $CaCO_3$-corrosivity of bottom waters: $CaCO_3$ saturation decreases with depth, starting to decrease at the lysocline and being completely depleted below the carbonate compensation depth (CCD). Consequently, there is an increase in agglutinated tests with increasing water depth as the amount of calcareous tests decreases. Below the CCD, only agglutinated and organic-walled foraminifera exist, hence $CaCO_3$ saturation is a strong limiting factor for calcareous taxa besides oxygen and food availability.

1.1.2 Applications of benthic foraminifera

The widespread distribution of benthic foraminifera across geographic space and geological time, and their rapid response to ecological changes makes them a powerful tool for analysing benthic oceanic processes (Gooday et al., 1992; Murray, 2000; Gooday, 2003). All their applications must involve an understanding of their ecology, as their distribution and abundance are strongly controlled by environmental parameters (see section 1.1.1). In this thesis, benthic foraminifera

and their paleoecology have been used to obtain paleoenvironmental inferences. The comparison of fossil and modern assemblages has been traditionally used in paleoenvironmental inferences, although the interpretation of past environments based on modern taxa becomes less accurate with age. The niche of a given fossil species may or may not be the same as its extant representatives; in fact it is known that organisms adapt to the dynamics of their environment through time. Furthermore, the habitats of modern species are calibrated to the ranges of modern environments. If a past environmental factor exceeded the limits of modern analogues (e.g. higher atmospheric CO_2 concentration), there are no real modern analogues and interpretations are therefore partially speculative. Nevertheless, general features of the assemblages such as wall composition (relative abundance of calcareous and agglutinated tests) or diversity (e.g. Fisher-alpha index) are more conservative features in deep time (Murray, 2006). Short-term (e.g. diurnal) natural variability is time-averaged in the sedimentary record while longer-term climatic changes are preserved, usually shown by changes in the fossil assemblages or even by extinction events.

Paleoenvironmental studies do not allow direct measures of environmental variables, but the use of proxies, based on strong statistical correlation between the value of a single environmental factor and the abundance of a benthic foraminiferal species (Murray, 2006), helps reconstructing past conditions such as bottom-water temperature, salinity, oxygen concentration, organic matter flux to the seafloor, etc. (e.g. Herguera and Berger, 1991; Schmield et al., 1997; Schönfeld, 2002; Alegret and Thomas, 2009; Friedrich, 2010). Common proxies are based on assumptions, hence they present numerous challenges such as interpretation, errors and other uncertainties. The most robust paleoceanographic interpretations are based on interdisciplinary studies that analyse an array of techniques, such as the geochemistry of the foraminiferal tests (e.g., stable isotopes, Ca/Mg ratio; see Katz et al., 2010) together with the abundance of taxa and their paleoecological interpretation.

Benthic foraminifera are also widely applied to estimate water paleodepth. Benthic species show distinct bathymetric boundaries between environments such as marsh, lagoon, continental shelf, bathyal and abyssal depths (Van Morkhoven et

al., 1986). They are commonly used to determine relative changes (e.g. oceanic transgression from inner shelf to outer shelf) rather than providing absolute water depths (e.g. Li et al., 2003). In more recent timescales, benthic foraminifera have been used to monitor contemporary environmental change and disturbance caused by anthropogenic activities. Marginal marine and inner shelf environments are particularly affected as they are closest to pollutant sources, both chemical (e.g. organic sewage, nitrite, hydrocarbons and heavy metals) and physical (e.g. thermal pollution, Titelboim et al., 2016). Historical studies of benthic foraminifera assemblages have been able to differentiate pre-pollution from pollution periods although there are difficulties separating natural climatic variability from changes induced by pollution (Alve, 1995; Sen Gupta, 1999; Lee and Hallock, 2000; Martin, 2000; Scott et al., 2001; Haslett, 2002). Despite certain benthic foraminifera species being adapted to extreme changes (e.g. Weinmann and Langer, 2017), current climate change is threatening even these resilient organisms (Uthicke et al., 2013). While "*the present is the key to the past*" (Charles Lyell) applies for paleoceanographic reconstructions, this can be turned around as the analysis of benthic foraminifera fossil assemblages can help predicting future environmental and climatic changes.

1.1.3 Fossil benthic foraminifera assemblages

Benthic foraminifera are useful for reconstructing conditions of the past. When performing paleoecological and paleoenvironmental analysis, it is necessary to assess to what extent the fossil assemblage is representative of the original living assemblage. This section discusses the taphonomic processes that influence post-mortem assemblage composition, abundance and preservation.

Empty tests are sedimentary grains that are hence subject to transport, either as bed load or suspended load depending on their size, mass and shape. These mechanisms are common in marginal marine and inner-shelf environments, caused by tidal currents and waves; however contour currents can transport sedimentary material in continental margins and bathyal depths (Schönfeld, 1997). This transport produces loss of tests in source areas and gain of tests in depositional areas (Alve and Murray, 1994). Turbidity currents, submarine canyons and sediment mass flows also transport foraminiferal tests from shallow

to deeper environments (e.g. Vénec-Peyré and Le Calvez, 1986, Wynn et al., 2002). Plants can be an active transport mechanism for certain species such as epiphytic taxa, which live attached to seaweed and seagrasses that can be carried away by storms and currents to a different setting (e.g. Bock and Moore, 1968; Boltovskoy and Lena, 1969; Spindler, 1980). Their natural habitat is not the associated sandy sediment where their dead tests accumulate, hence their distribution and abundance in dead and fossil assemblages should be carefully interpreted (e.g. García-Gallardo et al., 2017).

As opposed to transport, which occurs laterally, bioturbation disturbs benthic faunas vertically into the sediment, up to a maximum depth of 1 m, and infaunal organisms move through the sediment, which causes mixing and homogenization.

The diversity of the original assemblage can decrease due to the loss of agglutinated tests, which have been recorded to decrease downcore due to bacterial or chemical decay of the cement (e.g. Douglas et al., 1980; Denne and Sen Gupta, 1989; Edelman-Furstenberg et al., 2001; Murray and Pudsey, 2004). This is thought to affect assemblage diversity more than the loss of calcareous tests by dissolution (Murray, 2006), although understanding carbonate dissolution is still a challenge (Morse and Arvidson, 2002). Corrosive pore water due to organic matter decay can lead to different intensities of $CaCO_3$ dissolution, from etched surfaces to chamber breakage or even the total destruction of calcareous tests. Dissolution largely depends on wall thickness, structure and composition (Peebles and Lewis, 1991; Boltovskoy, 1991), with thinner, smaller and hyaline tests being more prone to dissolution. There is an inverse correlation between the amount of broken tests and $CaCO_3$ levels (Corliss and Honjo, 1981), except for high-energy environments. An agglutinated-dominated assemblage can evidence total dissolution, and occasionally glauconite infillings (preserved as moulds) can be found after the dissolution of the calcareous tests (George and Murray, 1977).

Loss of benthic foraminifera tests can also be related to sample processing, however this is more difficult to assess and the extraction of foraminifera from the sediment should be done carefully, avoiding the use of strong acids and mechanical methods. In cases when micropaleontological criteria are unclear, the geological

context can be helpful. Diagenesis and weathering should also be assessed, especially if foraminiferal tests are used for geochemical analyses (e.g. stable isotopes) because their primary signal could have been altered. Post-mortem and depositional processes must be taken into account to ensure accurate paleoecological interpretations of fossil assemblages.

1.2 Eocene climate

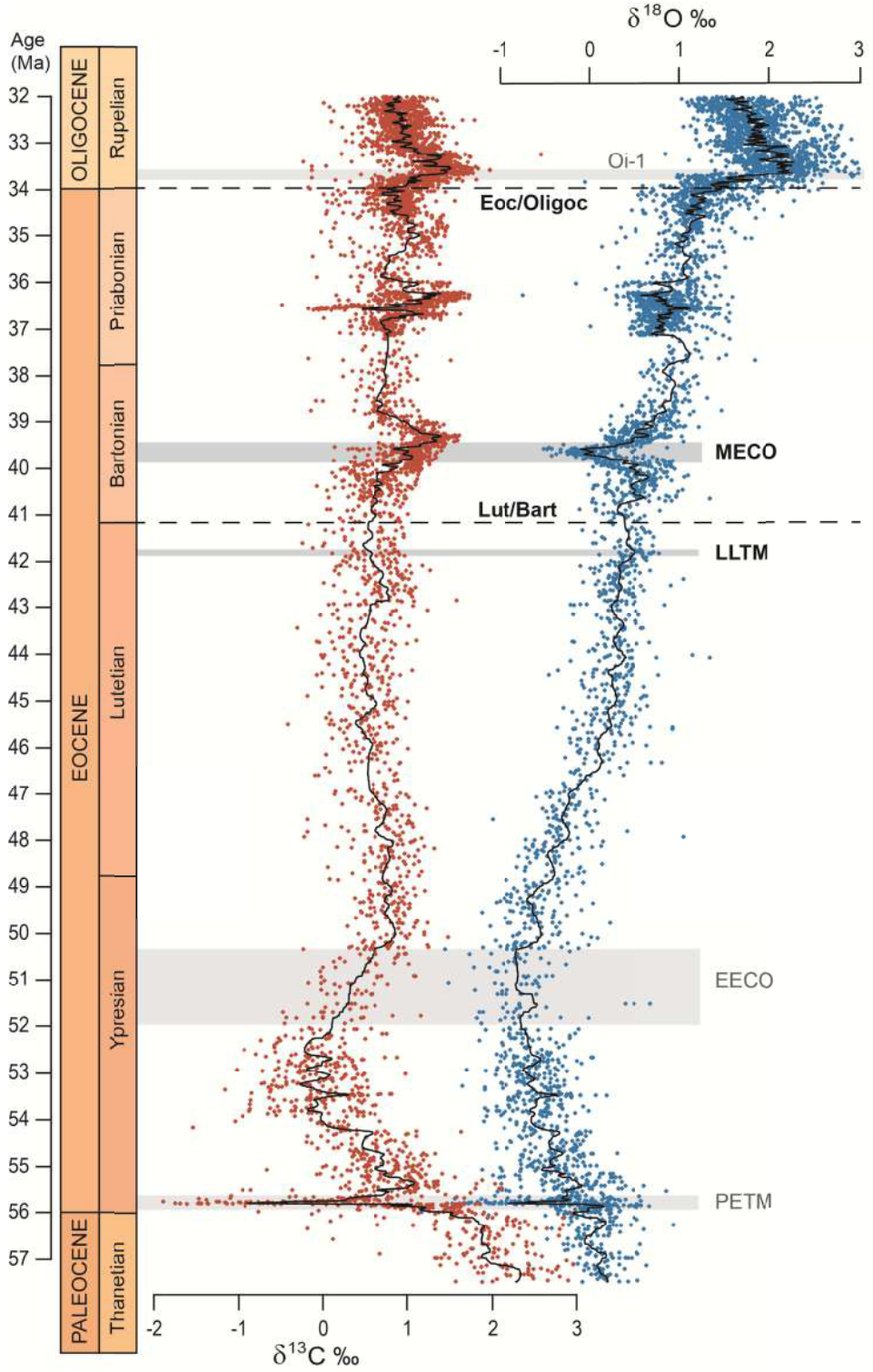

Figure 1. Foraminifera Carbon and Oxygen stable isotopes across the **E**ocene (Cramer et al., 2009). Bold letters indicate the events studied in this thesis. The events are positioned according to the age model from Cramer et al. (2009), however some ages do not coincide with those mentioned in the chapters of the thesis, which are related to the age model used in each case study.

The Eocene epoch (33.9 – 56.0 Ma, Gradstein et al., 2012) was a period of intense climate variability in Earth's history. The Eocene has increasingly received attention in paleoclimate research due to its high potential to reconstruct Earth's carbon cycle dynamics and climate evolution (Zachos et al., 2008). Analyses of oxygen and carbon isotopes in deep-sea sediments reflect climatic changes, with the warmest period of the Paleogene represented by the early Eocene, followed by global cooling in the middle and late Eocene, especially at high latitudes (Miller et al., 1987; Zachos et al., 1993, 2001, 2008; Lear et al., 2000; Cramer et al., 2009; Littler et al. 2014; Barnet et al., 2019; Westerhold et al., 2020). The Early Eocene Climatic Optimum (EECO, 50 - 52 Ma) represents the tipping point towards heavier oxygen isotopic values and a cooler climate during the Eocene (Fig. 1).

The gradual cooling trend from a greenhouse to an icehouse state concluded at the Eocene-Oligocene transition (Coxall et al., 2005), which culminated in a major cooling event during the early Oligocene (Oi-1 glaciation, 33.5 Ma; Wade and Pälike, 2004) that settled the climatic conditions for modern life (Zachos et al., 1996; Zachos, 2001). Earth's long term trends are commonly related to important tectonic phenomena. Rifting and associated volcanism in the North Atlantic during the early Eocene may have contributed to the EECO, whilst the reduction of seafloor spreading rates is connected to the Eocene/Oligocene transition (Vandenberghe et al., 2012).

Superimposed on this general warming-cooling trend, several transient global warming events have been described. These events, known as hyperthermals, have a short duration (from tens to a few hundred thousand years) and are characterised by global warming and perturbations of the carbon cycle (Lyle et al., 2005; McInerney and Wing, 2011; Tipple et al., 2011; Luciani et al., 2016; Zeebe et al., 2017; Giorgioni et al., 2019), showing paired negative oxygen and carbon isotope excursions (e.g., Thomas et al., 2000; Cramer et al., 2003; Lourens et al., 2005; Bowen et al., 2006; Zachos et al., 2010; Sluijs et al., 2012; Kirtland Turner and Ridgwell, 2013; Littler et al., 2014; Lauretano et al., 2015). They are usually associated with ocean acidification, deep-sea carbonate dissolution, perturbations of the hydrological cycle and increased continental erosion (e.g. Thomas et al., 2000; Cramer et al., 2003; Lourens et al., 2005; Zachos,

2005; Nicolo et al., 2007; Sluijs et al., 2009; Leon-Rodriguez and Dickens, 2010; Stap et al., 2010a, b; Sexton et al., 2011; Payros et al., 2012; Littler et al., 2014; Lauretano et al., 2015). These features make them very interesting events as analogues of current global warming because of their relation to increasing CO_2 atmospheric levels (e.g. Bijl et al., 2010; Pearson, 2010). Hyperthermal events provide a perfect testing ground to investigate the feedbacks and mechanisms of the climate system during periods of transient global warming, especially regarding the carbon cycle under greenhouse conditions in timescales of 10s to 100s kyr.

The most extreme and widely recognized of these events was the Paleocene-Eocene Thermal Maximum (PETM; Miller et al., 1987b; Kennett and Stott, 1991; Thomas and Shackleton, 1996; Wing et al., 2005; Zachos et al., 2006; Thomas, 2007; Alegret et al., 2020) at the base of the Eocene (Fig. 1). A massive input of isotopically light carbon into the ocean-atmosphere system, reflected by a 2 – 3‰ negative carbon isotopic excursion, is commonly accepted as the cause (e.g., McInerney and Wing, 2001; Sluijs et al., 2007; Littler et al., 2014 and references therein). However the sources, rate and triggering mechanisms of ^{12}C release are still under debate. Due to the similarities among the PETM and the smaller hyperthermal events, it has been suggested that they should have had a common cause, ruling out the possibility of singular causes such as asteroid impacts. Hyperthermal events are thought to have been paced or triggered by Earth's orbital eccentricity (Cramer et al., 2003; Zachos et al., 2010; Sexton et al., 2011; Lauretano et al., 2015, 2016), although the PETM has been argued to be out of phase (Cramer et al., 2003; Lourens et al., 2005; Westerhold et al., 2007; Zachos et al., 2010; Littler et al., 2014).

The biotic consequences of the PETM have been documented in detail, including a major extinction (35-55%) of deep-sea benthic foraminifera species (Tjalsma and Lohman, 1983; Thomas, 1989, 1990, 2007; Katz and Miller, 1991; Alegret et al., 2009a, b, 2018; Giusberti et al., 2009, 2016; Arreguín-Rodríguez et al., 2016; Giraldo-Gómez et al., 2018). It is the largest extinction of the Cenozoic (Thomas, 1998, 2007; Alegret et al., 2009a, b, 2020), which makes the PETM a key biotic event considering that deep-sea benthic foraminifera survived other global

extinction events such as the Cretaceous/Paleogene boundary (e.g. Alegret and Thomas, 2005). Numerous studies have documented perturbation (but no extinction) of benthic foraminifera across late Paleocene and early Eocene smaller hyperthermal events, including decreased diversity and absolute abundance of benthic foraminifera (e.g. Bernaola et al., 2007; Agnini et al., 2009; Coccioni et al., 2010; Stap et al., 2010a; D'haenens et al., 2012, 2014; Payros et al., 2012; Sprong et al., 2012, 2013; Foster et al., 2013; Jennions et al., 2015; Frontalini et al., 2016; Arreguín-Rodriguez and Alegret, 2016; Arreguín-Rodríguez et al., 2016; Thomas et al., 2018). Middle and late Eocene hyperthermal events (Wade and Kroon, 2002; Bohaty and Zachos, 2003; Tripati et al., 2005; Sexton et al., 2006; Edgar et al., 2007; Ivany et al., 2008; Bohaty et al., 2009), however, have not received the same attention.

The middle to late Eocene covers a critical period during which benthic foraminifera shifted from warm to cold-type assemblages across the Eocene at lower and abyssal depths (e.g. Thomas, 1992; Ortiz and Thomas, 2015). This middle late Eocene turnover has also been recorded in the fossil record of nannoplankton (Aubry, 1992; Newsam et al., 2017) and radiolaria (Kamikuri and Wade, 2012), indicating significant ecological changes at both surface and deep waters during this interval. A recent compilation on Paleogene deep-sea benthic foraminifera showed that the middle Eocene was a critical period of several millions of years of faunal turnover (possibly linked to long-term changes in functional types of dominant phytoplankton) and establishment of latitudinal diversity gradients (Alegret et al., 2020). The late Lutetian to early Bartonian interval (44-38 Ma) is of particular interest due to the uncertainties about the presence and volume of polar ice sheets across this period (Prentice and Matthews, 1988; Zachos et al., 1994; 2001; Tripati et al., 2005; Edgar et al., 2007; Burgess et al., 2008; Koeberl and Montanari, 2009). This interval encompasses the Middle Eocene Climatic Optimum (MECO, Bohaty and Zachos, 2003) and the Late Lutetian Thermal Maximum (LLTM), also known as the C19r event (Edgar et al., 2007).

1.2.1 The Late Lutetian Thermal Maximum

The oldest hyperthermal event analysed in this thesis is the C19r event (Edgar et al., 2007) or Late Lutetian Thermal Maximum (LLTM), a short-lived warming event recorded at 41.52 Ma (Westerhold et al., 2018) in the upper part of magnetochron C19r. This event has been identified by short and sharp negative excursions in the oxygen and carbon isotopic records coupled with dissolution in the deep-sea, similar to most Eocene hyperthermals. The LLTM has been documented in the Atlantic Ocean, ODP Sites 1260, 1263 and 702 (Edgar et al., 2007; Westerhold and Röhl, 2013; Westerhold et al., 2018) and in a land section in Cape Oyambre, Spain (Intxauspe-Zubiaurre et al., 2018).

The total duration of the LLTM carbon isotopic excursion (CIE) is estimated to be ca. 30 kyr calculated by orbital tuning, a duration similar to that of other early Eocene hyperthermals. The magnitude of the carbon and oxygen isotope excursions across the LLTM is comparable to the H2 event in the early Eocene (53.6 Ma), suggesting a similar behaviour of the climate system during carbon cycle perturbations (Kirtland Turner et al., 2014; Westerhold et al., 2018). The LLTM occurred at the highest insolation value of the last 45 Ma (Westerhold and Röhl, 2003 using La 2004 solution) and this exceptional strong insolation could have crossed a threshold leading to the rapid release of carbon into the ocean-atmosphere system; a very similar mechanism as proposed for early Eocene hyperthermals H1, H2, I1, I2, J and K (Lourens et al. 2005; Galeotti et al., 2010; Stap et al., 2010a; Zachos et al., 2010; Lunt et al., 2011; Lauretano et al., 2015).

The duration and magnitude of the isotopic excursion and a potential orbital trigger of the LLTM are characteristics similar to those observed across other early Eocene hyperthermals (e.g. Lourens et al, 2005; Edgar et al., 2007; Stap et al., 2010b) that have been linked to release of dissolved organic carbon due to orbital driven changes in ocean ventilation (Sexton et al., 2011). Nevertheless, the LLTM occurred in slightly cooler climate several million years after the EECO. Paleoecological data could shed some light on the similarities and differences among events, however the ecological response to this event is underrepresented in the current scientific literature, with only one paleoecological study (Intxauspe-Zubiaurre et al. 2018) published since the discovery of the LLTM. Chapter 4.1.1

(Rivero-Cuesta et al., 2020) of this thesis shows the first benthic foraminifera record across this event and discusses its paleoecological significance.

1.2.2 The Middle Eocene Climatic Optimum

The Middle Eocene Climatic Optimum (MECO, Bohaty and Zachos, 2003) is one of the most puzzling warming events of the Eocene. It was documented for the first time at several Southern Ocean deep-sea sites (Bohaty and Zachos, 2003) that showed a conspicuous negative oxygen isotopic excursion (OIE, ca. – 1 ‰ in bulk sediment and benthic foraminiferal records). The MECO is considered a global event as it has been recognized at globally distributed ocean drilling sites and on-land sections (Jovane et al., 2007; Bohaty et al., 2009; Spofforth et al., 2010; Boscolo Galazzo et al., 2014). The associated OIE has been interpreted as a temperature signal since ice sheets were small or absent during the Eocene (Bohaty and Zachos, 2003; Edgar et al., 2007), suggesting a transient global warming of 4-6ºC in both surface and deep waters (Bohaty and Zachos, 2003; Bohaty et al., 2009; Bijl et al., 2010; Edgar et al., 2010).

Like most Eocene hyperthermals, the MECO is associated with an increase in atmospheric pCO_2 concentrations (Bijl et al., 2010), shoaling of the carbonate compensation depth (Bohaty et al., 2009; Pälike et al., 2012) and related decline in carbonate accumulation at abyssal sites (Lyle et al., 2005). However, it usually lacks a clear CIE accompanying the OIE, with carbon isotopic values even rising rather than declining during MECO warming (Bohaty and Zachos, 2003). Some study sites show records of a brief CIE (-0.5 ‰ in bulk sediment) coinciding with OIE peak conditions, but this is not consistent across sites (Boscolo Galazzo et al., 2014).

The MECO OIE peak coincides with the base of Chron C18n.2n (40.14 Ma, Gradstein et al., 2012), which provides a reliable age constraint (Bohaty et al., 2009). In addition to the identification of the base of Chron C18n.2n, high-resolution carbon and oxygen isotope records are arguably the best tool available to compare and correlate the MECO among different sites due to their distinctive patterns (Bohaty et al., 2009). Estimations of MECO duration based on isotopic records vary from ~500 kyr (Bohaty et al., 2009), ~600 kyr (Bohaty and Zachos,

2003) to ~750 kyr (Edgar et al., 2010). An accurate estimation of the duration of this event is essential to discuss its mechanisms, and robust age models are needed to assess its relation with orbital cycles as it is thought to coincide with a very long eccentricity minimum (Lunt et al., 2011; Westerhold et al., 2014, 2015; Giorgioni et al., 2019).

The duration of the MECO, its gradual warming/rapid cooling pattern and its unusual CIE trend have raised questions about how well we understand carbon cycle mechanisms across warming periods, with models struggling to recreate the trends displayed by MECO records (Sluijs et al., 2013). The characteristics of this event provide a unique opportunity to analyse the complex relationship between climate and the carbon cycle during past periods of increased atmospheric pCO_2 and global warming on timescales of 100s kyr. Analysis of benthic foraminiferal fauna across the MECO (Boscolo-Galazzo et al., 2013, 2015; Moebius et al., 2014, 2015) show that its impact on deep-sea environments seems to vary bathymetrically, in latitude and within oceans. This thesis explores in detail the response of benthic foraminifera to the MECO at South Atlantic ODP site 702 (Chapter 4.1.2; Rivero-Cuesta et al., 2019) and in the Torre Cardela section (Spain), western Tethys (Chapter 4.1.3; Rivero-Cuesta et al., 2018).

1.2.3 The Eocene/Oligocene transition

The Eocene-Oligocene transition (EOT; 34 Ma) was a period of global cooling (Zachos et al., 2001; DeConto and Pollard, 2003; Coxall and Pearson, 2007; Lear et al., 2008; Liu et al., 2009; Miller et al., 2009) associated with sea level fall (e.g. Miller et al., 1991, 2009; Pekar et al., 2002), deepening of the calcite compensation depth (Van Andel, 1975; Coxall et al., 2005; Rea and Lyle, 2005) and reorganization of the carbon cycle (Shackleton and Kennet, 1975; Diester-Haass and Zahn, 1996; Zachos et al., 2001; Coxal et al., 2005; Merico et al., 2008). This transition includes the Oi-1 glaciation event (Miller et al., 1991; Zachos et al., 2001), which is associated with the establishment of a permanent ice-sheet in Antarctica (Kennett et al., 1975; Liu et al., 2004; Miller et al., 2009). The EOT global cooling is coupled with atmospheric CO_2 decrease (Pearson and Palmer, 2000; Pagani et al., 2005) and tectonic and paleoceanographic changes, especially in Antarctica and nearby continents (e.g. Lawver and Gahgan, 2003). The onset of a

permanent ice-sheet in Antarctica in the late Eocene-early Oligocene and a bipolar glaciated world had a major role in oceanographic reorganization, heat distribution and global climate (Zachos et al., 2001).

The EOT has been identified on deep-sea benthic foraminiferal oxygen and carbon isotopes (Coxall et al., 2005) reflecting the cooling of the oceans and the development of large ice sheets in Antarctica (Shackleton and Kennett, 1975; Zachos et al., 1996; DeConto and Pollard, 2003; Coxall et al., 2005; Lear et al., 2008). This period of global climatic reorganization is coeval with marine biotic turnovers (Aubry, 1992; Dunkley Jones et al., 2008; Funakawa and Nishi, 2008; Pearson et al., 2008; Suto, 2006; Villa et al., 2008; Wade and Pearson, 2008), terrestrial faunal and floral changes (e.g. Francis, 1999; Hooker et al., 2004; Jaramillo et al., 2006), increased marine productivity (Diester-Haass and Zahn, 1996; Salamy and Zachos, 1999; Diester-Haass and Zachos, 2003; Anderson and Delaney, 2005) and the extinction of several species of phytoplankton and zooplankton (Funakawa et al., 2006; Pearson et al., 2008). Planktic foraminifera suffered a rapid but gradual extinction event across the E/O boundary (Molina, 2015 and references therein), characterized by the extinction of hantkeninids and turborotalids. The E/O boundary is also reported to coincide with the extinction of the hantkeninids at the Italian Massignano section (Premoli Silva and Jenkins, 1993).

Larger foraminifera living in shallow platforms show faunal turnover but no extinction across the E/O boundary (Molina et al., 2016), although the magnitude of the turnover is not well known. Studies on small benthic foraminifera living in bathyal and abyssal environments are scarce and their extinction pattern across the E/O boundary is not yet known, although published works suggest they were little affected (Bolli et al., 1994; Molina et al., 2006; Hayward et al., 2010; among others). Chapter 4.1.4 (Grira et al., 2018) of this thesis explores the response of benthic foraminifera in detail across the EOT at the Bou Zelfa and Jhaff composite section (Tunisia) and discusses its paleoecological significance.

1.3 Missing formal boundary stratotypes of the Paleogene: the base of the Bartonian, a GSSP in progress

A high-resolution timescale of the Earth's geological history requires the definition of unit stratotypes for global correlation. The International Commission on Stratigraphy (ICS) developed the concept of Global Boundary Stratotype Section and Point (GSSP) to define boundary stratotypes in well-documented, well-preserved and accessible outcrops. Within the Eocene epoch, three stages (Ypresian, Lutetian, Priabonian) have formally ratified GSSPs (Dupuis et al., 2003; Aubry et al., 2007; Molina et al., 2011; Agnini et al., formally ratified by ICS in January 2020 and publication in prep.), with only one GSSP pending formal definition by the International Subcommission on Paleogene Stratigraphy (ISPS): the base of the Bartonian stage (Vandenberghe et al., 2012). This is also the last GSSP that remains to the defined within the whole Paleogene (ISPS website, www.paleogene.org). The locality (stratotype) where this boundary was originally described (before the creation of the GSSP concept) was defined by local or regional features that hinder correlation at a global level. Consequently, there is a need for finding a viable GSSP and to define characteristic geological markers that allow long distance correlation of the base of the Bartonian.

The Bartonian unit stratotype (Mayer-Eymar, 1858) was originally defined in marine clays and sands (Barton Beds) of a coastal outcrop in the Hampshire Basin (Barton-on-sea, central southern England), which contains well-preserved Paleocene sedimentary sequences (Curry, 1981). The base of the Bartonian was initially defined by a horizon rich in large benthic foraminifera *Nummulites prestwichianus* (Curry, 1981). Larger benthic foraminifera (LBF) are restricted to shallow platform environments and are facies dependent, therefore they are a limited marker. Accordingly, the characteristic *Nummulites prestwichianus* bed is a local feature that cannot be correlated outside the Hampshire and Paris basins (Murray and Wright, 1974). Hooker (1986) shifted the base of the Bartonian downwards to a thin glauconitic and pebbly omission surface, so that it would coincide with a major lithological boundary rather than with a local biostratigraphic level. More recently Ogg et al. (2008) suggested that the base of the Bartonian occurs close to the C19n/C18r magnetochron boundary. In the last

version of the geological timescale (Gradstein et al., 2012), the C19n/C18r magnetochron boundary was proposed as a marker for the base of the Bartonian (Vandenberghe et al., 2012) because magnetostratigraphic events are global, geologically instantaneous and identifiable in both land and marine sections.

To test the validity of this magnetostratigraphic boundary and aiming to find further stratigraphic markers, Bartonian outcrops outside the Hampshire Basin have been explored. The Basque-Cantabrian basin (Spain) hosts three Paleogene GSSPs: the Selandian, Thanetian and Lutetian (Schmitz et al., 2008, 2011; Molina et al., 2011) and auxiliary stratotypes for the Danian and Ypresian Stages (Molina et al., 2009), therefore being a favourable area. After the analysis of several outcrops, Cape Oyambre yielded valuable information (Payros et al., 2015) but discrepancy on planktic foraminifera bioevents hindered the definition of the GSSP at this locality.

A well-documented section near the classical Contessa Highway section (Italy) suggests the top of Chron C19r has potential to mark the base of the Bartonian (Jovane et al., 2007; 2010). This section also contains planktic foraminifera biostratigraphic markers below the base of the Bartonian, and a noticeable oxygen and carbon isotope excursion that starts about 6 m above the C19n/C18r magnetochron boundary, which is accompanied by significant planktic foraminifera turnover. This is comparable to the MECO as observed in several deep-sea cores (Bohaty and Zachos, 2003; Bohaty et al. 2007) and it has also been identified in the Barton Clay Formation of the Hampshire Basin (Dawber et al., 2011). The Contessa section seems to be the most promising option to place the Bartonian GSSP, however the presence of faults and accessibility issues hinder its ratification as GSSP. To endorse the proposed events around the base of the Bartonian and to aim for further biological markers for correlation, fossiliferous-rich Bartonian outcrops with good preservation and adequate thickness are being studied, as the Torre Cardela section presented in this thesis (section 4.1.3; Rivero-Cuesta et al., 2018).

Regional and global correlation at the Bartonian stratotype locality remains problematic due to the lack of comprehensive studies combining multidisciplinary records. The parastratotype section, located 7 km from the Barton stratotype, is

found in a coastal outcrop on the Isle of Wight (Curry, 1981) and it has been reported to have potential for correlation (Hooker and King, 2019). This parastratotype section of Alum Bay has been reassessed in detail by members of the ISPS in order to assess, confirm and extend potential correlations and placements for this boundary. This thesis has contributed to this multidisciplinary approach, which integrates nannofossil, smaller and large benthic foraminifera, dinoflagellates and paleomagnetic studies (section 4.2.1, Cotton et al., 2020).

Chapter 2: Objectives

The main aim of this PhD thesis is to analyse deep-sea benthic foraminiferal assemblages across key Eocene climatic events of different nature, magnitude and duration in order to identify the most relevant environmental factors that controlled the structure and changes of the assemblages. In order to achieve this goal, the following specific objectives have been addressed:

- To produce the first quantitative dataset of benthic foraminiferal assemblages across the Late Lutetian Thermal Maximum (LLTM) and to analyse its paleoecological and paleoenvironmental implications.
- To evaluate the impact of the Middle Eocene Climatic Optimum (MECO) on the benthic fauna at a low latitude setting and its differences with records from other latitudes and settings.
- To compare the response of benthic foraminifera to two different middle and late Eocene climatic events, the LLTM and the MECO, at the same site.
- To identify any critical thresholds controlling the impact of environmental changes on benthic foraminifera across the studied climatic events.
- To analyse the paleoenvironmental changes recorded on the benthic fauna associated with the climatic changes across the Eocene/Oligocene transition.
- To contribute to the definition of the GSSP of the Bartonian with new paleoenvironmental data at the parastratotype section.
- To better understand the response of benthic foraminifera to the Eocene climate variability and its paleoenvironmental consequences.

Chapter 3: Materials and methods

This chapter includes the studied material and the methodology followed in this thesis related to benthic foraminifera and paleoceanographic proxies. Methodologies followed by co-authors of the publications and specific details of each study section can be found in each publication.

3.1 Initial deskwork

The author of this thesis performed a thorough literature review on the response of benthic foraminifera to Eocene hyperthermal events in order to gain understanding of the topic, previous results and main hypotheses, as well as the scientific problems that were still unresolved. Events which were understudied, such as the LLTM, or which are not fully understood, such as the MECO, were preferentially chosen in order to obtain new, novel data. Background on the taxonomy of Eocene benthic foraminifera as well as on their paleoecological, paleoenvironmental and paleoceanographic applications was acquired.

Sites and sections suitable for benthic foraminifera analysis were selected based on an extensive literature review and discussions with co-authors and other colleagues who kindly shared information (e.g., Kirsty Edgar, Univ. Birmingham). Spain belongs to the European Consortium for Ocean Research Drilling (ECORD), therefore scientists working in Spanish institutions are granted access to International Ocean Discovery Program (IODP) drilling cores material and facilities. A formal sampling request was submitted to and approved by the IODP Bremen Core Repository (BCR) in Germany, where the sampling took place.

3.2 Study site and sections

The samples studied in this thesis were collected from a deep-sea drilling ocean site located in the South Atlantic (Ocean Drilling Program –ODP- Site 702) and three land sections located in the Betic Cordillera in Southern Spain (Torre Cardela section), the Cap Bon peninsula in Northeast Tunisia (Menzel Bou Zelfa or MBZ section) and the Isle of White in Southern England (Alum Bay section) (Fig. 2 and Table 1).

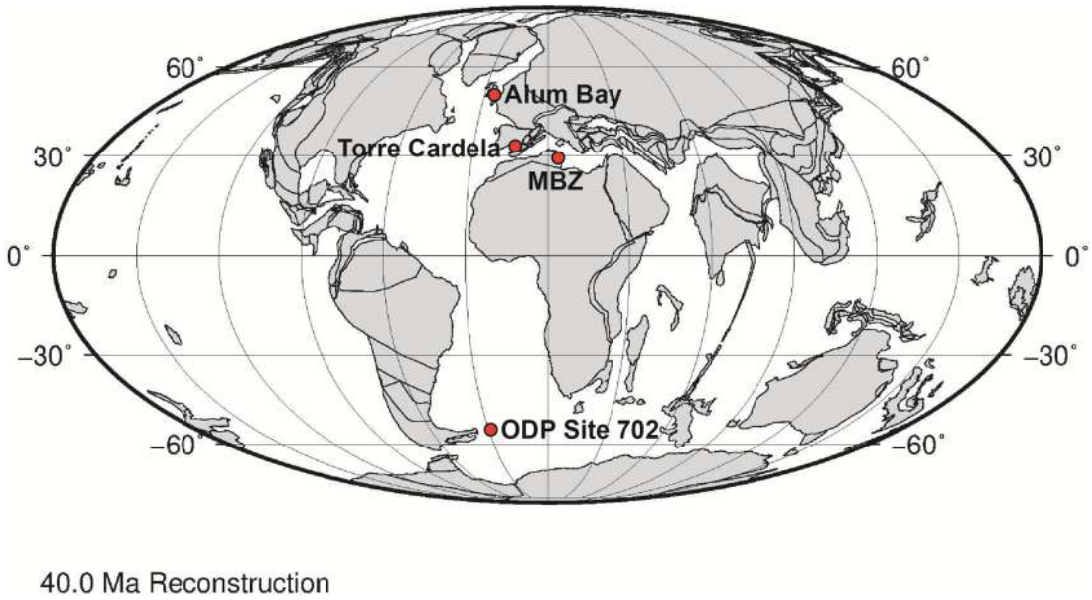

Figure 2. Location of the site and sections studied in this thesis. Paleogeographic reconstruction of 40 Ma from Ocean Drilling Stratigraphic Network (ODSN).

	ODP Site 702 (Rivero-Cuesta et al., 2019, 2020)	**Alum Bay** (Cotton et al., 2020)	**Torre Cardela** (Rivero-Cuesta et al., 2018)	**Menzel Bou Zelfa -MBZ** (Grira et al., 2018)
Location	Islas Orcadas Rise South Atlantic Ocean	Hampshire Basin North Atlantic Ocean	Western Tethys Ocean	Southern Tethys Ocean
Paleodepth	Lower bathyal 1000-2000 m	Photic zone > 100 m	Middle to lower bathyal	Upper to middle bathyal
Event studied	LLTM and MECO	Bartonian base	Bartonian base and MECO	Eocene-Oligocene transition

Table 1. Summary of the ODP site and land-based sections studied in this thesis.

ODP Site 702 was drilled in the South Atlantic Ocean (Fig. 2), in the central area of the Islas Orcadas Rise (50° 56.760′ S, 26° 22.122′ W, 3083.4 m water depth) where extensive deposition of homogeneous nannofossil ooze and chalk took place in a lower bathyal setting (1000–2000 m paleodepth) during the Paleogene (Ciesielski and Kristoffersen, 1991; Katz and Miller, 1991). A total of 60 sediment samples from Hole B (Site 702) were extracted between 90.25 and 89.9 meters below sea floor (mbsf) coinciding with the LLTM (41.52 Ma) and between

83.29 and 63.75 mbsf comprising the MECO event (ca. 40 Ma). Samples were collected during two sampling visits at the IODP Bremen Core Repository (Germany) by the author of this thesis, who processed them at the micropaleontology laboratory of the University of Zaragoza.

The Torre Cardela section is located in the southern part of the Iberian Peninsula, within the External Zones of the Betic Cordillera (37° 29′ 02.4″ N, 3° 20′ 43.8″ W, Fig. 2). The studied sedimentary succession is a 145 m-thick sequence composed of a rhythmic series of 25 to 35 cm-thick sandy carbonate (calcarenite) layers interbedded with 1 to 20 m-thick grey silty-marly intervals, deposited during the Eocene in the Western part of the Tethys Ocean. These levels contain abundant calcareous microfossils that reveal a middle to late Eocene age (Gonzalvo and Molina, 1996). A set of 25 samples collected and processed by E. Molina and C. Gonzalvo (Univ. Zaragoza) for planktonic foraminifera biozonation have been used in the study presented in this thesis.

The Menzel Bou Zelfa (MBZ) section is located in the Cap Bon peninsula, North-Eastern Tunisia (Fig. 2). The stratigraphic series is composed of marls, limestones and sands ranging from the middle Eocene to the Quaternary. Since the E/O boundary interval is covered with Quaternary deposits, it was necessary to carry out an auxiliary sampling across the E/O boundary in a better exposed section (Jhaff section) 1 km south of the MBZ section which has been integrated in a composite section. A set of 27 samples was collected in MBZ and Jhaff sections by C. Grira (Univ. Carthage) for the study presented in this thesis.

The Alum Bay section is a coastal outcrop with near vertical bedding situated in the Isle of White (South England) (Fig. 2). These sediments were deposited in a series of transgressive and regressive cycles during the Paleogene, and consist of near-shore shelf sediments. At Alum Bay the Barton Clay succession comprises a series of glauconitic and non-glauconitic clays and sands spanning the upper Lutetian to upper Bartonian. A total of 32 samples were collected across an almost 100 m transect section by L. Alegret and other components of the Bartonian Working Group of the ISPS in 2015. A set of 25 samples were selected and processed by the author of this thesis at the micropaleontology laboratory of the University of Zaragoza for the study presented in this thesis.

3.3 Sample collection and processing

Samples from ODP Site 702 were collected from the working half of drilling cores. Each sample (10 cc of sediment) was individually labelled and introduced into a database (Bremen Core Repository Drilling Information System i.e. BCR DIS) that can be consulted freely. Standard procedures for sampling drilling cores were followed and sediment from the centre of the core was preferentially sampled, avoiding the edges of the core in contact with the liner, which can be contaminated during drilling.

Sediment samples from ODP Site 702 and Alum Bay section were processed by standard procedures in order to obtain loose benthic foraminifera. About two thirds of the sample was processed, and one third was reserved for isotopic analysis on bulk sediment, or in case the sample had to be processed again. The part of the sample to be processed was individually labelled and dried in the oven at <50°C for 24 h, then weighed to obtain the bulk dry weight. Samples were then soaked in water or a weak acid such as $(NaPO_3)_6$ or H_2O_2 to disaggregate the sediment. After complete disaggregation of the samples (timing depending on its compaction), they were washed under running water through a 63 µm sieve. For the study presented in Grira et al. (2018), a column of three interlocking sieves (meshes size 250 µm, 150 µm and 63 µm) was used.

Sieves were washed and dyed with a methylene blue solution after processing each sample to avoid contamination. Sieve size influences species abundance and assemblage composition (Gooday, 2003), and the use of a 63 µm sieve is recommended for quantitative ecological studies because some dominant species are small and concentrated in the finer fraction (e.g., Thomas, 1985; Rathburn and Corliss, 1994; Kurbjeweit et al., 2000), especially small key species such as *Epistominella exigua* are severely underrepresented in larger size fractions (e.g. 125, 150, 250 or 300 µm; Murray, 2006). The sediment fraction collected in the mesh (>63 µm) was oven-dried at <50°C and weighed. It is important not exceed this temperature to avoid possible alteration of the geochemical signal (stable isotopes) of the foraminiferal tests.

The analysis of fossil assemblages usually requires counting more than 250 specimens per sample to be representative (Murray, 2006). Around 300 specimens of benthic foraminifera were picked from a representative split of each sample, and all the specimens were mounted with water-based glue on microslides for identification and storage. In Grira et al. (2018), the 63 and 150 μm fractions were combined before doing representative splits and picking the 300 specimens.

3.4. Taxonomic classification

Classification to the generic level was performed following the classification by Loeblich and Tappan (1988), and determinations at the species level largely followed the taxonomic concepts of Tjalsma and Lohmann (1983), Van Morkhoven et al. (1986), Bolli et al. (1994), Alegret and Thomas (2001), Holbourn et al. (2013) and Arreguín-Rodríguez et al. (2018). In addition, the exhaustive revision of uniserial taxa with complex apertures by Hayward et al. (2012), including modifications of some genera and/or species, was adopted in all the publications included in this thesis.

Careful taxonomic revision of benthic foraminiferal species is required because different authors may use distinct taxonomical concepts. This is partly related to the fact that description of most extinct species is based on their test morphology, but they may show intraspecific variability, including the occurrence of different micro- and megalospheric forms. In order to clearly identify the various taxonomic concepts used in the literature, a bibliographic revision was carried out and benthic foraminiferal species were compared between several publications that included images and/or descriptions of Eocene benthic foraminifera species (e.g. Grünig, 1985; Katz and Miller, 1991; Müller-Merz and Oberhänsli, 1991; Katz et al., 2003; Ortiz and Thomas, 2006; Alegret et al., 2008; Fenero et al., 2012; Boscolo-Galazzo et al., 2015). Descriptions of several type species were consulted in the Ellis and Messina online catalogue of Foraminifera (www.micropress.org), and holotypes images were obtained from the Smithsonian Paleobiology Collections (https://collections.nmnh.si.edu) when available.

The most representative species considering their abundance, evolution across particular intervals or paleoecological significance were illustrated to better

document the species identified. Scanning electron micrographs (SEM) were performed at the facilities of the University of Zaragoza (Servicio de Apoyo a la Investigación, SAI) except for those shown in Grira et al. (2018), which were obtained at the ETAP (Tunisian National Oil Company).

3.5 Quantitative analyses and diversity

The publications that form the main body of this thesis rely on quantitative studies based on representative splits of ~300 specimens per sample. The resulting data sets are the basis for the paleoecological and paleoenvironmental interpretation of the benthic foraminifera assemblages. The relative abundance (percentage) was calculated for each taxon or species in every sample, and absolute abundance (number of specimens of each taxon or species per gram of bulk sediment) was calculated for the most representative species in Rivero-Cuesta et al. (2019, 2020). The relative abundances of all taxa within the assemblages at Torre Cardela (Rivero-Cuesta et al., 2018) were recalculated excluding allochthonous taxa in order to obtain an accurate paleoenvironmental interpretation.

As diversity indices, the Fisher-α diversity index (Fisher et al., 1943) and the heterogeneity index H(S) (Shannon, 1948; Hayek and Buzas, 1997) were calculated. All the publications presented include the Fisher-α diversity index, which correlates the number of specimens (or individuals, N) and the number of species (S, i.e. species richness) in a sample. The heterogeneity index H(S) (in Rivero-Cuesta et al., 2018, 2019, 2020) considers the number of species and their relative abundances within a sample. The H(S) index shows less variability than the number of species (N), as it reduces de influence of the presence or absence of rare species. For the Atlantic Ocean, there is a linear relationship between Fisher-α and H(S) and the correlation is high (r = 0.87) (Murray, 2006).

3.6 Multivariate statistical analyses

Multivariate analyses were performed using the PAST free software (Hammer et al., 2001) on datasets including species with relative abundance > 1% (Rivero-Cuesta et al., 2020), > 1.5% (Rivero-Cuesta et al., 2019) and > 2% (Rivero-

Cuesta et al., 2018) in at least one sample and excluding informal taxonomic groups. They are a useful tool to evaluate the response of benthic foraminiferal assemblages to environmental changes.

Hierarchical cluster analyses were performed in R-mode (Rivero-Cuesta et al., 2018, 2019, 2020) and Q-mode (Rivero-Cuesta et al., 2018) using the Pearson similarity index and the unweighted pair-group average algorithm (UPGMA). These analyses group together species (R-mode) or samples (Q-mode) with a similar distribution pattern across the studied interval. Additionally, as an attempt to identify the environmental variables that may have controlled the distribution pattern of benthic foraminifera (Hammer and Harper, 2005) and the results derived from clustering, detrended correspondence analysis (DCA) in both R-mode (species, Rivero-Cuesta et al., 2019, 2020) and Q-mode (samples, Rivero-Cuesta et al., 2018) were also performed on the same datasets.

The visualization (graphs and plots) of quantitative and multivariate analyses have been performed with Grapher, Adobe Illustrator and IGOR Pro software.

3.7 Assessment of benthic foraminiferal assemblages

3.7.1 Paleoenvironment and paleoecology

The ratio between calcareous and agglutinated taxa was calculated in all samples as a qualitative measure of the carbonate saturation of bottom waters. An increase in agglutinated taxa may indicate a decrease in carbonate availability, although other factors such as trophic levels can also play a role (e.g. Gooday et al., 2008), hence the interpretation of the calcareous-agglutinated ratio must be made in combination with other proxies.

Morphogroups analysis allowed us to calculate the infaunal-epifaunal ratio. According to the TROX model (e.g., Jorissen et al., 1995, 2007) (Fig. 3), their relative abundance can be used as a proxy for oxygen levels and trophic conditions in deep sea settings. A high relative abundance of infaunal taxa is thought to be indicative of a high food supply and/or low oxygen availability, and a low

percentage of infaunal taxa indicative of oligotrophic and/or well-oxygenated conditions at the seafloor.

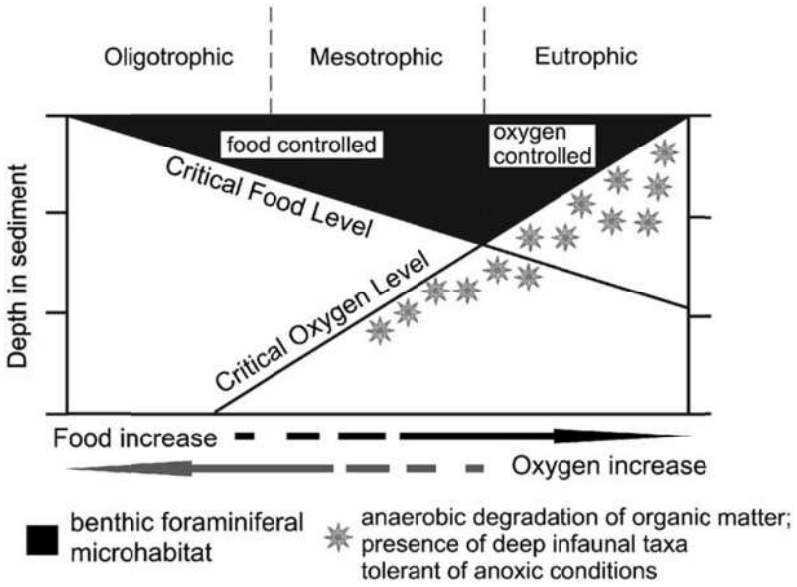

Figure 3. TROX model from Jorissen et al. (2007).

In oxic environments (e.g. most abyssal plains and lower bathyal zones), oxygen is not a limiting factor. These types of environments fall in the oligotrophic side of the TROX model, being food availability the main ecological parameter controlling benthic foraminifera abundance. Food availability is a primary limiting factor for benthic biomass in the deep sea (Gage and Tyler, 1991), and there is a positive correlation between food availability (measured as organic carbon flux) and benthic species abundance, at least at water depths greater than 1000 m (Altenbach and Struck, 2001). In these deep-sea settings, the main food supply derives from phytoplankton primary productivity in surface waters. The amount of food that reaches the deep sea is controlled by the productivity (nutrients availability) of surface waters, the aggregation of organic matter into marine snow and the remineralisation of organic matter through the water column. As a result, only 1-3% of this surface primary productivity reaches the seafloor in open ocean settings, and the major part of this organic matter is consumed by benthic fauna, largely benthic foraminifera (Meyer-Reil and Köster, 1991).

The assignment to infaunal or epifaunal microhabitats is based on test morphotypes: epifaunal species are thought to have milioline coiling, planoconvex

and biconvex trochospiral tests, biconvex planispiral, rounded and flat tests, tubular, and leaf-like forms. Species with cylindrical, spherical, ovoid, unilocular globose, rounded planispiral and streptospiral shapes, and those with a neck are thought to be mostly infaunal (e.g., Corliss, 1985, 1991; Jones and Charnock, 1985; Corliss and Chen, 1988; Rathburn and Corliss, 1994; Jorissen, 1999; Murray, 2006). Nevertheless, this division between infaunal and epifaunal is not straightforward. Observations have shown that species can be epifaunal or infaunal according to different environmental conditions (Gross, 2002) and some authors consider taxa living in the top first cm of sediment as epifaunal (Corliss, 1991); hence this classification is not restrictive and applies loosely in some cases (Jorissen, 1999; van der Zwaan et al., 1999). Even for many living taxa, the relation between morphology and microhabitat is not well established (e.g., Jorissen, 1999), and assignments seem to be accurate only about 75% of the times (Buzas et al., 1993). Despite these, the infaunal/epifaunal ratio provides a basic evaluation of the relationship between benthic foraminifera and the main environmental conditions controlling their assemblages (Gooday, 2003).

The relative and absolute abundances of ecologically key species, i.e., species with a well-known affinity to some environmental parameters, can be crucial in paleoenvironmental interpretations. Species associated to inputs of phytodetritus, called phytodetritus exploiting taxa (PET), have been of particular interest in this thesis (Rivero-Cuesta et al., 2019, 2020). These species (e.g., *Epistominella exigua*, *Alamabina weddellensis* and *Caucasina* spp.) are related to seasonality or pulsed deposition of labile organic matter to the seafloor (Gooday, 1993, 2003; Smart et al., 1994; Thomas et al., 1995; Thomas and Gooday, 1996; Ohkushi et al., 2000; Boscolo-Galazzo et al., 2015). They show an opportunistic life strategy, and are likely to have fast reproduction rates due to their small size.

3.7.2 Paleobathymetry

Paleobathymetric reconstructions are based on the occurrence and abundance of depth-related species and their upper depth limits (e.g. Van Morkhoven et al., 1986; Alegret and Thomas, 2001; Ortiz and Thomas, 2006; Fenero et al., 2012), and on comparison between fossil and recent assemblages. Paleobathymetry is also inferred from comparison with assemblages from ocean

drilling sites where paleodepths have been established by independent methods such as backtracking (Grünig and Herb, 1980; Ingle, 1980; Tjalsma and Lohmann, 1983; Thomas, 1990; Speijer, 1994; Bignot, 1998; Alegret and Thomas, 2001; Katz et al., 2003; Ortiz and Thomas, 2006). The publications in this thesis follow the bathymetric divisions defined by Van Morkhoven et al. (1986): neritic (0-200 m), upper bathyal (200-600 m), middle bathyal (600-1000 m), lower bathyal (1000-2000 m) and abyssal (>2000 m).

This thesis has contributed to the estimation of the paleobathymetry at Torre Cardela (Rivero-Cuesta et al., 2008) and MBZ section (Grira et al., 2018) and has corroborated the paleodepth estimations at Alum Bay (Cotton et al., 2020). Paleodepth estimates were already available for ODP Site 702.

3.8 Paleoceanographic proxies

3.8.1 Stable carbon and oxygen isotopes

The isotopic composition of benthic foraminiferal calcareous tests is an extremely useful tool in paleoceanographic reconstructions (Rohling and Cooke, 1999). In deep-sea settings, epifaunal taxa are closer to isotopic equilibrium with ambient seawater (Bemis et al., 1998), as infaunal taxa are exposed to pore water which may have different isotopic values than the overlying bottom water (Rathburn et al., 2003; Mackensen and Licari, 2004). Tests can show $\delta^{13}C$ disequilibrium due to various causes, including uptake of metabolic CO_2 during shell secretion, growth rate or variation on carbonate-ion concentration in ambient water (Murray, 2006). Disequilibrium in $\delta^{18}O$ values of calcite secreted under stable low temperature suggests that microhabitats play a role.

Species-specific carbon and oxygen stable isotopes analyses were performed in Rivero-Cuesta et al. (2018) and Rivero-Cuesta et al. (2019) at the Leibniz Laboratory for Radiometric Dating and Stable Isotope Research (Kiel University, Germany) and at MARUM Isotope Laboratory (Bremen University) respectively. Full details on procedures and mass spectrometers are explained in each publication.

Species-specific analyses were mainly made on *Nuttallides truempyi* (Rivero-Cuesta et al., 2019, 2020), in the size range between 100 and 500 μm. Larger individuals were preferentially chosen to avoid intraspecific variability between juveniles and adult specimens. *N. truempyi* is typically used in paleoceanographic records due to its abundance, size, thick carbonate wall and epifaunal mode of life. In Rivero-Cuesta et al. (2018), the infaunal species *Bolivinoides crenulata* was extracted from five samples that did not yield enough specimens of *N. truempyi* for the analyses. Additionally, two control samples were selected to perform analyses in both benthic species (*N. truempyi* and *B. crenulata*) and two planktic species (*Acarinina bullbrooki* and *Catapsydrax unicavus*) for paleoenvironmental assessment across the water column. The selection was preferential for well-preserved specimens in order to avoid diagenetic distortion of the isotopic signal of the tests.

3.8.2 Calcium carbonate content

Bulk wt % CaCO3 was analysed in Rivero-Cuesta et al. (2019) with a manocalcimeter at the University of Zaragoza, which yielded the total % $CaCO_3$ of the sediment. This proxy complements the benthic calcareous/agglutinated ratio in order to identify intervals of dissolution or corrosive waters.

3.8.3 Accumulation rates

Benthic foraminifera accumulation rates (BFAR, Herguera and Berger, 1991) and coarse fraction accumulation rates (CFAR, Diester-Haass, 1995) were calculated in Rivero-Cuesta et al. (2019, 2020). Both have been calculated with linear sedimentation rate (LSR) and dry bulk sediment (DBS) values.

The BFAR is the number of benthic foraminifera per gram of bulk sediment, and it is considered as a proxy for total organic matter flux reaching the seafloor, i.e. export productivity (Herguera, 2000; Gooday, 2003; Jorissen et al., 2007). In sediments deposited above the lysocline, the number of benthic foraminifera per unit of space and time depends on the water depth and on the supply of organic matter (Herguera and Berger, 1991), hence the BFAR primarily depends on the organic material that makes it to the seafloor in above-lysocline and open ocean conditions. It has been observed that variations in oceanic organic carbon fluxes

derived from geochemical proxies in Paleogene sediments of the Southern Ocean show a similar signal as faunal proxies such as BFAR (Diester-Haass and Faul, 2019)

CFAR calculates the amount (gr) of coarse material (> 63 μm) per gram of sediment and it is an approximation of planktic foraminiferal accumulation rates, hence heterotrophs´ productivity (e.g. Diester-Haass, 1995; Boscolo-Galazzo et al., 2014). Additionally, the carbonate mass accumulation rate (CMAR) determines the amount (gr) of $CaCO_3$ per gram of sediment, which is also an additional proxy for carbonate dissolution and deposition.

3.9 Contribution to biostratigraphy and sedimentation rates

Planktic foraminifera biozones were revised and updated at the Torre Cardela section. These were originally defined by Gonzalvo and Molina (1996), who documented zones P12, P13 and P14 across the section, comprising most of the Bartonian. Since the late 90´s, the Eocene planktic foraminifera biozonation has been revised and updated, and zones P12, P13 and P14 have been redefined to E11, E12, E13, E14 (Berggren and Pearson, 2005). Sedimentation rates were then calculated based on the duration of the revised planktic biozones, calibrated to astronomical ages (Pälike et al., 2006; Wade et al., 2011).

Linear sedimentation rates from the shipboard report of ODP Site 702 (Ciesielski and Kristoffersen, 1988) were extrapolated and compared with the sedimentation rates derived from the age model generated in Rivero-Cuesta et al. (2019), yielding similar results.

Chapter 4:

Results

4.1 Benthic foraminiferal turnover across Eocene climatic events

4.1.1. Late Lutetian Thermal Maximum (middle Eocene): first record of deep-sea benthic foraminiferal response

Lucía Rivero-Cuesta, Thomas Westerhold & Laia Alegret, 2020

Palaeogeography, Palaeoclimatology, Palaeoecology 545, 109637

Supplementary material of this article can be found in Appendix II

Palaeogeography, Palaeoclimatology, Palaeoecology 545 (2020) 109637

Contents lists available at ScienceDirect

Palaeogeography, Palaeoclimatology, Palaeoecology

journal homepage: www.elsevier.com/locate/palaeo

The Late Lutetian Thermal Maximum (middle Eocene): first record of deep-sea benthic foraminiferal response

Lucía Rivero-Cuesta[a,*], Thomas Westerhold[b], Laia Alegret[a]

[a] Departamento de Ciencias de la Tierra & Instituto Universitario de Ciencias Ambientales (IUCA), Universidad de Zaragoza, Spain
[b] MARUM – Center for Marine and Environmental Sciences, University of Bremen, Germany

ARTICLE INFO

Keywords:
Hyperthermal
C19r event
Site 702
Paleoecology
Paleoenvironment
Metabolic rates

ABSTRACT

Understanding the role of deep-sea biota across global warming events in the past is key to unravel climate system dynamics during periods of increased pCO_2 levels. Here we present the first record of the benthic foraminiferal response to a middle Eocene transient warming event named the Late Lutetian Thermal Maximum (LLTM; 41.52 Ma) at ODP Site 702 in the South Atlantic Ocean. Changes in benthic foraminiferal assemblages such as a decrease in absolute abundance of certain taxa (e.g. *Bulimina elongata*) are correlated with the negative carbon isotope excursion corresponding to the LLTM event. Paleoecological interpretations of the assemblage turnover suggest changes in the type of organic matter arriving to the seafloor during the LLTM. Benthic foraminifera and coarse fraction accumulation rates (BFARs and CFARs) decreased across the warming period of the LLTM, coeval with the negative $\delta^{18}O$ excursion associated with ~2 °C deep-sea warming. We suggest that increased temperatures led to enhanced metabolic rates in heterotroph organisms such as foraminifera, triggering a population decline in food-limiting environments such as the meso-oligotrophic setting of Site 702. A similar ecological response and a decrease in export productivity, as inferred from decreased CFARs and BFARs, have also been reported across the Middle Eocene Climatic Optimum at this site, and support the hypothesis that metabolic rates accelerated during warming events, in spite of their different magnitude and duration.

1. Introduction

The climatic transition from the early Eocene greenhouse to the Oligocene icehouse state (Miller et al., 1987; Lear, 2000; Zachos, 2001; Cramer et al., 2009) was not steady: several transient, global warming events spiced up the middle to late Eocene cooling, as shown by short but sharp negative excursions in the oxygen and carbon isotopic records (Wade and Kroon, 2002; Bohaty and Zachos, 2003; Sexton et al., 2006; Ivany et al., 2008; Bohaty et al., 2009). These events, some of which are categorised as "hyperthermals" (Thomas et al., 2000; Cramer et al., 2003; Lourens et al., 2005; Bowen et al., 2006; Zachos et al., 2010; Sluijs et al., 2012; Kirtland Turner and Ridgwell, 2013; Littler et al., 2014; Lauretano et al., 2015), are usually associated with carbonate dissolution (e.g. Leon-Rodriguez and Dickens, 2010; Sexton et al., 2011) and increased levels of atmospheric CO_2 (e.g. Bijl et al., 2010; Pearson, 2010), evidencing changes in the global carbon cycle (Lyle et al., 2005; McInerney and Wing, 2011; Tipple et al., 2011; Luciani et al., 2016; Zeebe et al., 2017; Giorgioni et al., 2019). They provide a perfect testing ground to investigate the feedbacks and mechanisms of the climate system during periods of transient global warming, especially regarding the carbon cycle in timescales of 10s to 100 s kyr.

One of those short-lived warming events was the C19r event (Edgar et al., 2007) or Late Lutetian Thermal Maximum (LLTM), a hyperthermal event that is recorded 41.52 Ma ago (Westerhold et al., 2018) in the upper part of magnetochron C19r. Similar to most Eocene hyperthermals, this event has been defined by a short and sharp negative excursion in the oxygen and carbon isotopic records in the Atlantic Ocean, including ODP Sites 1260, 1263 and 702 (Edgar et al., 2007; Westerhold and Röhl, 2013; Westerhold et al., 2018) and a land section in Cape Oyambre, Spain (Intxauspe-Zubiaurre et al., 2018). It has also been associated with dissolution in the deep-sea, documented by decreased $CaCO_3$ values and a dark clay layer in deep-sea sediments (Westerhold et al., 2018). A detailed and complete record of the LLTM at Site 702 (South Atlantic Ocean) confirms the extent of this event at high latitudes (Westerhold et al., 2018). At this site, deep-sea temperatures increased by 2 °C in 7 kyr (Westerhold et al., 2018). So far, no studies on the response of the deep-sea biota to this warming event have been carried out. The ecological response to this event is underrepresented in the current scientific literature, with only one paleoecological study (Intxauspe-Zubiaurre et al., 2018) published since the

* Corresponding author at: Pedro Cerbuna 12, Departamento de Ciencias de la Tierra, Universidad de Zaragoza, 50009, Spain.
E-mail address: Lrivero@unizar.es (L. Rivero-Cuesta).

https://doi.org/10.1016/j.palaeo.2020.109637
Received 3 October 2019; Received in revised form 27 January 2020; Accepted 27 January 2020
Available online 08 February 2020
0031-0182/

discovery of the LLTM, hence records from deep-sea fauna are missing.

Benthic foraminifera are excellent paleoenvironmental proxies, and they show a shift from warm to cold-type assemblages across the Eocene at lower bathyal and abyssal depths (e.g. Thomas, 1992; Ortiz and Thomas, 2015). Over the last decade, multiple studies on benthic foraminifera have contributed to reconstruct key Eocene climatic events and their paleoenvironmental consequences. Some of these events include the Paleocene-Eocene Thermal Maximum (PETM; e.g., Thomas, 2007; Alegret et al., 2009a, 2009b; Giusberti et al., 2009, 2016; Nagy et al., 2013; Arreguín-Rodríguez et al., 2016; Alegret et al., 2018; Giraldo-Gómez et al., 2018), several early Eocene hyperthermals (e.g., Foster et al., 2013; D'haenens et al., 2014; Thomas et al., 2018) and the Middle Eocene Climatic Optimum (MECO; Boscolo-Galazzo et al., 2013, 2015; Moebius et al., 2014, 2015; Rivero-Cuesta et al., 2018, 2019). High-resolution paleoecological analyses are needed to understand and interpret the causes and consequences of significant climatic events in the past.

The role that benthic fauna played within the biological pump across these events is largely unknown. Oceanic organic matter through the biological pump was an important regulator of atmospheric CO_2 during the Eocene (Hilting et al., 2008), as it is today (Passow and Carlson, 2012), and paleoecological studies across middle to late Eocene hyperthermals have reported shifts in both surface and deep-sea fauna, suggesting fluctuations in the biological pump (Spofforth et al., 2010; Toffanin et al., 2011; Boscolo-Galazzo et al., 2014; Rivero-Cuesta et al., 2019). Organic carbon burial in marine sediments is an important carbon sink, facilitated by the biological carbon pump. Benthic fauna, especially benthic foraminifera as a main component of this fauna, have a significant role within the biological pump by regulating the rate of organic carbon burial at the seafloor. The analysis of these organisms will contribute to understand paleoecological and paleoenvironmental changes and their role within the ocean organic carbon budget, shedding light into the mechanisms behind the LLTM.

The main goals of this study are: 1) to record for the first time the response of the benthic fauna to the LLTM event at Site 702, where high-resolution carbon and oxygen isotopic analyses and a reliable age model are available; 2) to analyze, quantitatively and statistically, benthic foraminiferal changes in assemblage composition and paleoecology as a result of the fast 2 °C warming reported in the deep-sea; and 3) to reconstruct the paleoceanographic conditions across the LLTM in the deep-sea at a high latitude site, contributing to disentangle the biotic role of benthic foraminifera across this event.

2. Location and setting

Ocean Drilling Program (ODP) Site 702 was drilled in the South Atlantic Ocean (Fig. 1), in the central area of the Islas Orcadas Rise (50° 56.760′ S, 26° 22.122′ W, 3083.4 m water depth). Islas Orcadas is a N-NW trending aseismic ridge over 1000 m above the adjacent seafloor (Ciesielski and Kristoffersen, 1988).

The Islas Orcadas Rise was likely formed during the early Paleogene (Ciesielski and Kristoffersen, 1988) and subsided to its present water depth after the late Eocene, suggesting that late Paleocene to Eocene subsidence of Site 702 was only minor (Ciesielski and Kristoffersen, 1991). Extensive deposition of homogeneous nannofossil ooze and chalk took place at lower bathyal (1000–2000 m) paleodepths during the Paleogene (Ciesielski and Kristoffersen, 1991; Katz and Miller, 1991). Eocene sediments are characterized by high carbonate content (85% to 95%; Ciesielski and Kristoffersen, 1991) with a relatively minor contribution of foraminifera (< 10%). The occurrence of diverse and well-preserved benthic foraminifera across middle-upper Eocene sediments, together with its relatively expanded and continuous record, makes Site 702 a suitable location to perform high-resolution micropaleontological analyses.

3. Methods

In order to perform a detailed sampling across the short-lived LLTM event at Site 702, we used as a guideline the high-resolution isotopic record available from Westerhold et al. (2018). According to this study, the event had a total duration of 30 kyr between 89.9 and 90.25 meters below sea floor (mbsf) in Hole 702B. Sampling was performed at the Bremen Core Repository (BCR) facilities of the International Ocean Discovery Program (IODP), where 24 samples of 10 cc were extracted between core 10×, section 5, interval 3–5 cm (88.34 mbsf) and core 10×, section 7, interval 22–24 cm (91.53 mbsf) of Hole 702B. Sampling comprises 3.19 m of core, more than twice the duration of the LLTM, in order to include the pre- and post-stages of the event. Sampling resolution ranges between 20 and 6 cm (highest across the event), which equals to a 16 to 5 kyr resolution.

A total of 24 sediment samples were oven-dried at 50 °C for 24 h and weighted before being washed. Benthic foraminifera were extracted by disaggregation of sediment samples in H_2O over 12–24 h. Soaked samples were individually sieved under running water and the ≥63 μm size fraction was collected, oven-dried (50 °C for 24 h) and weighted again. Assemblage work of benthic foraminifera was performed on representative splits of ca. 300 individuals per sample. A total of 62 taxa (58 calcareous and 4 agglutinated) were recognized at species or higher taxonomic level (Supplementary Table 1). Classification at the generic level mainly follows Loeblich and Tappan (1987), except for uniserial taxa (Hayward et al., 2012). Species identification follows Tjalsma and Lohmann (1983), Van Morkhoven et al. (1986), Katz and Miller (1991); Müller-Merz and Oberhänsli (1991), Ortiz and Thomas (2006), Holbourn et al. (2013), Boscolo-Galazzo et al. (2015) and Arreguín-Rodríguez et al. (2018). Preservation of foraminiferal tests is commonly good, and allows observation of diagnostic morphological features. The most representative specimens were photographed using the Scanning Electron Micrograph imaging facilities at the University of Zaragoza (Spain) (Plate I).

The relative abundance of each species was calculated from the raw data matrix that contains the original assemblage counts. Diversity (Fisher-α and Shannon-Weaver H (S) indices; Murray, 1991) and the percentage of calcareous and agglutinated tests were calculated for paleoecological assessment. Taxa were assigned to infaunal or epifaunal morphogroups according to their morphology, following Jones and Charnock (1985), Corliss and Chen (1988) and Corliss (1991). The TROX model (Jorissen et al., 1995) was followed to infer food supply and oxygenation at the seafloor according to the microhabitat distribution of benthic foraminifera, which is extrapolated by comparing with modern, morphologically similar taxa (e.g. Jorissen, 1999). Note that foraminifera are not static but actively move through the sediment (Bornmalm, 1997; Gooday and Rathburn, 1999; Gross, 2000; Fontanier et al., 2002), and this may lead to inaccuracies when assigning microhabitats.

Hierarchical cluster analysis was performed using the PAST software (Hammer et al., 2001) on a data matrix containing all common taxa (species > 1% in at least one sample) using the Pearson similarity index and the unweighted pair-group (UPGMA) algorithm. Detrended Correspondence Analysis (DCA) was carried out with the same software and on the same dataset to further analyze the results derived from clustering, and to investigate the relationship between foraminifera and environmental variables (Hammer and Harper, 2005).

The number of benthic foraminifera per gram of bulk sediment was calculated and multiplied by the linear sedimentation rate (LSR) and the dry bulk sediment (DBS) (data from Ciesielski and Kristoffersen, 1988) to determine benthic foraminiferal accumulation rates (BFAR, Herguera and Berger, 1991). The coarse fraction accumulation rate (CFAR) was determined by calculating the amount (g) of coarse material (> 63 μm) per gram of sediment and multiplying it by the LSR and the DBS (Diester-Haass, 1995). Individual accumulation rates of the most common (> 10%) species were calculated following the same method, obtaining the number of specimens of the selected species per

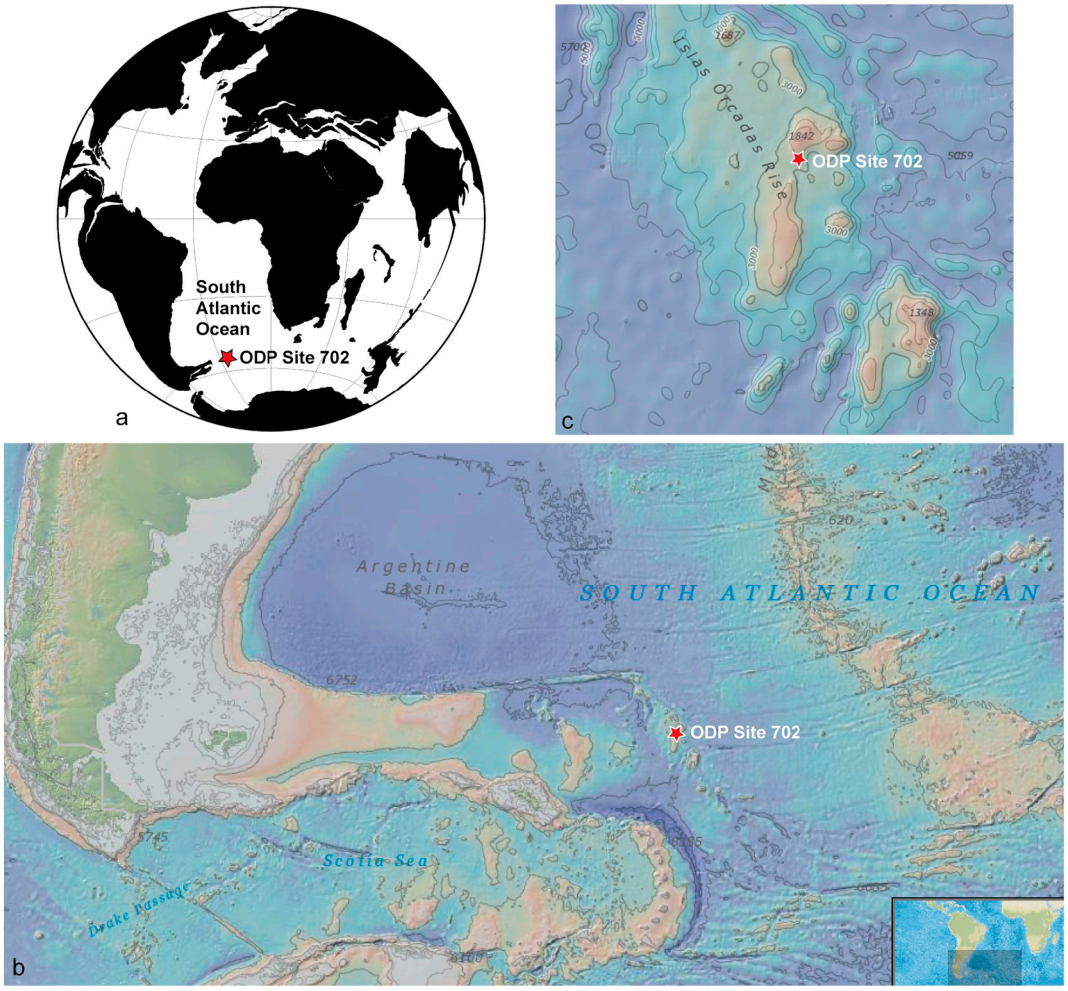

Fig. 1. Position of ODP Site 702 (red star) a) at 41 Ma, plotted on a paleogeographic reconstruction from the Ocean Drilling Stratigraphic Network (GEOMAR, Kiel, Germany); b) and c) at present, plotted on a bathymetry map form NOAA Bathymetric Data viewer. (For interpretation of the references to colour in this figure legend, the reader is referred to the web version of this article.)

g of bulk sediment and multiplying by the LSR and the DBS.

The CFAR is an approximation of planktic foraminiferal accumulation rates, hence heterotrophs productivity (e.g. Diester-Haass, 1995; Boscolo-Galazzo et al., 2014). The BFAR is considered as a proxy for total organic matter flux reaching the seafloor, i.e. export productivity (Herguera, 2000; Gooday, 2003; Jorissen et al., 2007), as the organic matter produced in the photic zone and exported to the deep-sea provides food for benthic foraminifera at the seafloor. In sediments deposited above the lysocline, the number of benthic foraminifera per unit of space and time depends on the water depth and on the supply of organic matter (Herguera and Berger, 1991), hence BFAR primarily depends on the organic material that makes it to the seafloor in below-lysocline and open ocean conditions. It has been observed that variations in oceanic organic carbon fluxes derived from geochemical proxies in Paleogene sediments of the Southern Ocean show a similar signal as faunal proxies such as BFAR (Diester-Haass and Faul, 2019). Additionally, and as an independent proxy to check the validity of our results, we used the wt%$CaCO_3$ data from Westerhold et al. (2018) to calculate carbonate mass accumulation rates (CMAR) by multiplying the amount of carbonate per gram of sediment by the LSR and the DBS.

4. Results

4.1. Benthic foraminifera assemblages and cluster analysis

No extinctions of benthic foraminifera have been recorded across the study interval at Site 702, but there are noticeable changes in the relative abundance of certain species (Figs. 2 and 3) and overall diversity of the assemblages (Fig. 4). The Fisher-α diversity index ranges between 9.95 and 18.09, with higher values (> 14.5) in the lowermost part of the studied interval and between 90.9 and 90.1 mbsf (Fig. 4). Benthic foraminifera assemblages are strongly dominated by calcareous taxa, and agglutinated species only make up to 3.6% of the assemblages (Fig. 4). Relative abundance of infaunal and epifaunal morphogroups is steady across the study interval, with infaunal taxa slightly dominating the assemblages (Fig. 4).

All the taxa that make up > 1% of the assemblages in at least one sample are represented in Figs. 2 and 3. Among epifaunal taxa (Fig. 2), *Alabamina weddelensis*, *Nuttallides truempyi*, *Cibicidoides micrus*, *Epistominella exigua* and *Anomalinoides* spp. dominate. Among infaunal taxa (Fig. 3), *Bulimina elongata*, *Oridorsalis umbonatus*, *Globocassidulina subglobosa*, *Nonion havanense* and Stilostomellids are most abundant. In order to better assess the benthic foraminiferal assemblages, a classical hierarchical cluster analysis with 30 benthic species (n = 30) was performed, and three main clusters (1, 2 and 3) with similarity < 0 were identified (Fig. 4, Supplementary Fig. 1).

Cluster 1 includes *Bulimina elongata* as the most abundant species, which is also one of the main components of the benthic assemblages at Site 702. It also contains *Cibicidoides micrus*, and three other species with minor representation (< 2% in relative abundance, Supplementary Fig. 1). The relative abundance of this cluster ranges from 12.46 to 32.88% across the study interval, recording lower values

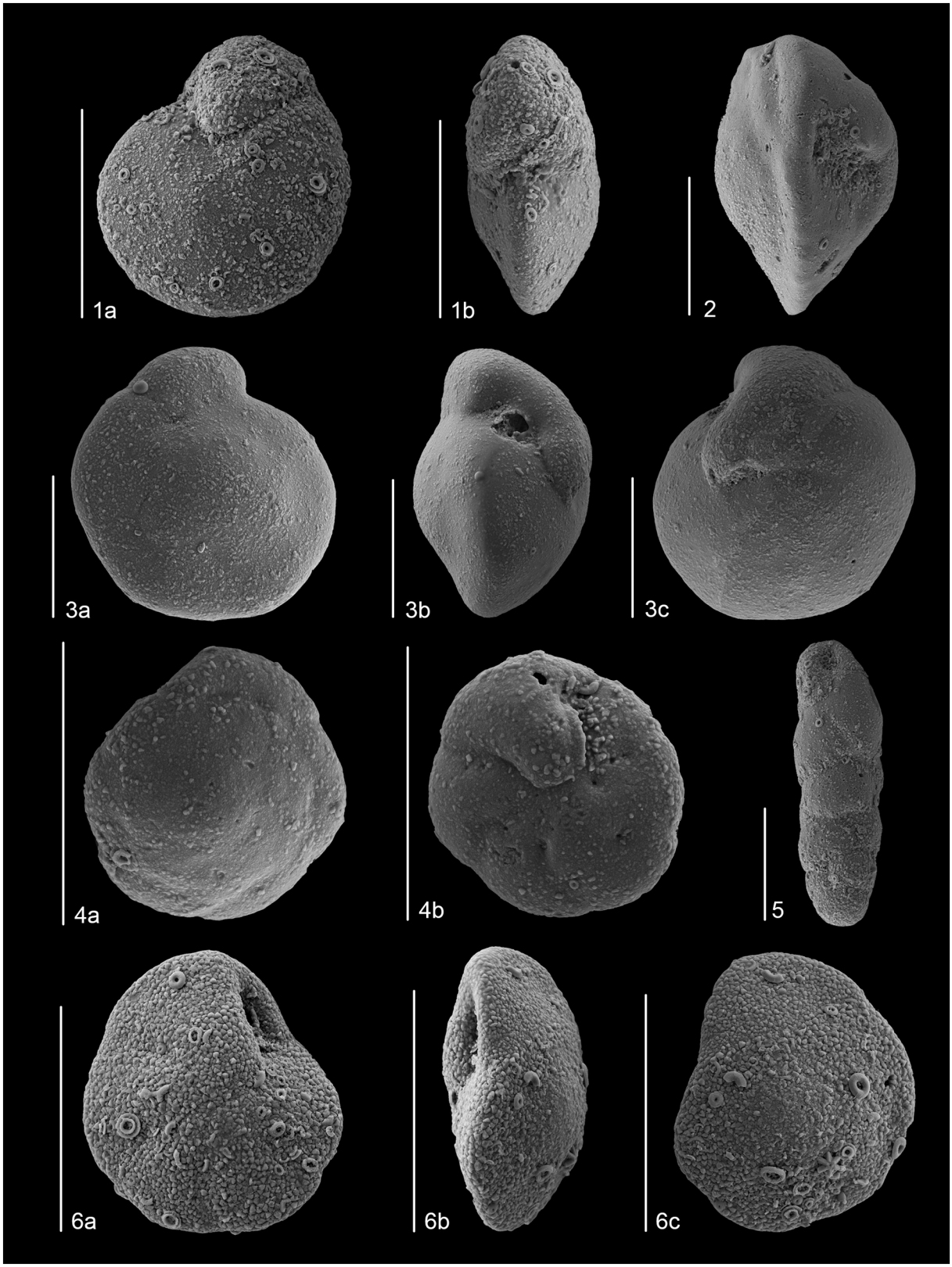

Plate I. SEM images of the most common benthic foraminiferal species at Site 702 across the LLTM. 1, *Cibicidoides micrus* (sample 10 × 5, 3–5 cm): a) ventral side, b) apertural view; 2, *Nuttallides truempyi* (sample 10 × 5, 3–5 cm), apertural view; 3, *Oridorsalis umbonatus* (sample 10 × 5, 13–15 cm): a) dorsal side, b) apertural view, c) ventral side; 4, *Alabamina weddellensis* (sample 10 × 5, 13–15 cm): a) dorsal side, b) ventral side; 5, *Bulimina elongata* (sample 10 × 5, 3–5 cm); 6, *Epistominella exigua* (sample 10 × 5, 33–35 cm): a) ventral side, b) apertural view, c) dorsal side. All scale bars = 100 μm.

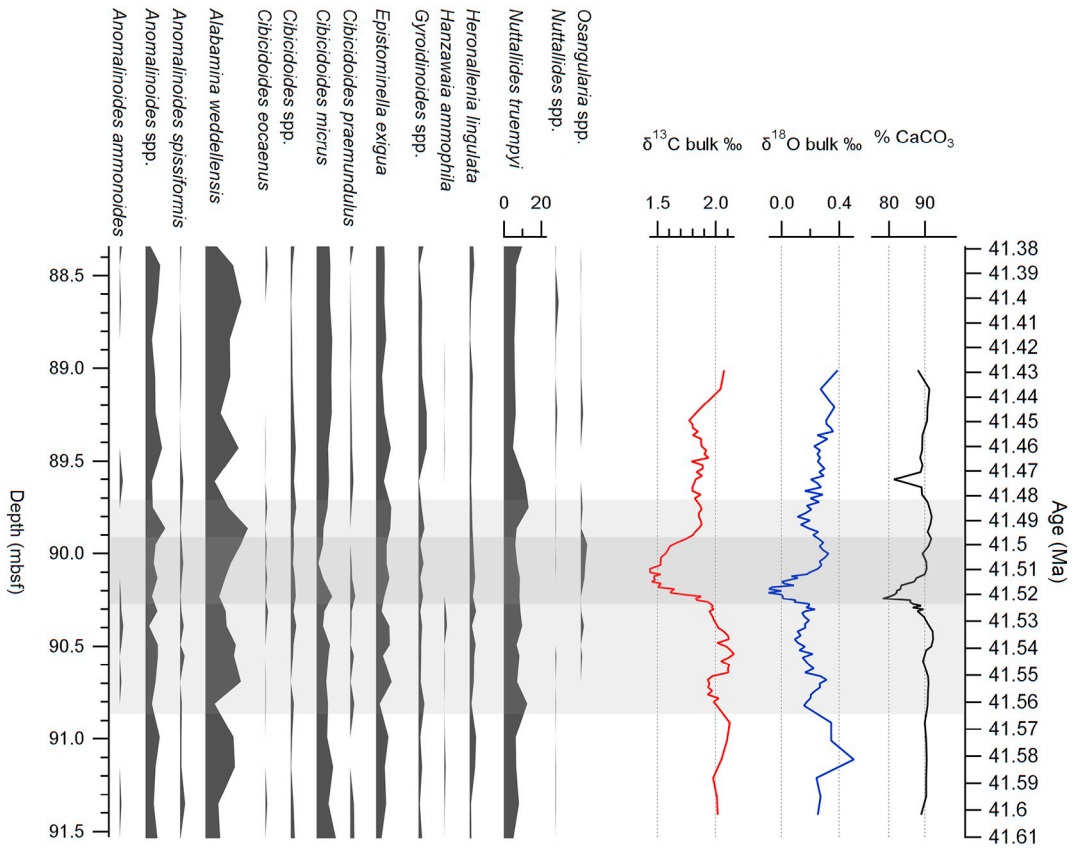

Fig. 2. Relative abundance of benthic epifaunal taxa at Site 702 against depth (mbsf). Geochemical data from Westerhold et al. (2018). Dark grey box indicates the position of the LLTM, light grey box indicates the duration of the paleoecological changes recorded.

(< 21%) in the interval between 90.9 and 89.7 mbsf (Fig. 4).

Cluster 2 is the most diverse one (n = 14), and it is dominated by *Oridorsalis umbonatus* and *Nuttallides truempyi*. Other common species (> 2% in relative abundance) include *Nonion havanense*, *Gyroidinoides beisselli*, *Anomalinoides spissiformis* and *Cibicidoides praemundulus*, sorted from more to less frequent (Supplementary Fig. 1). This cluster presents

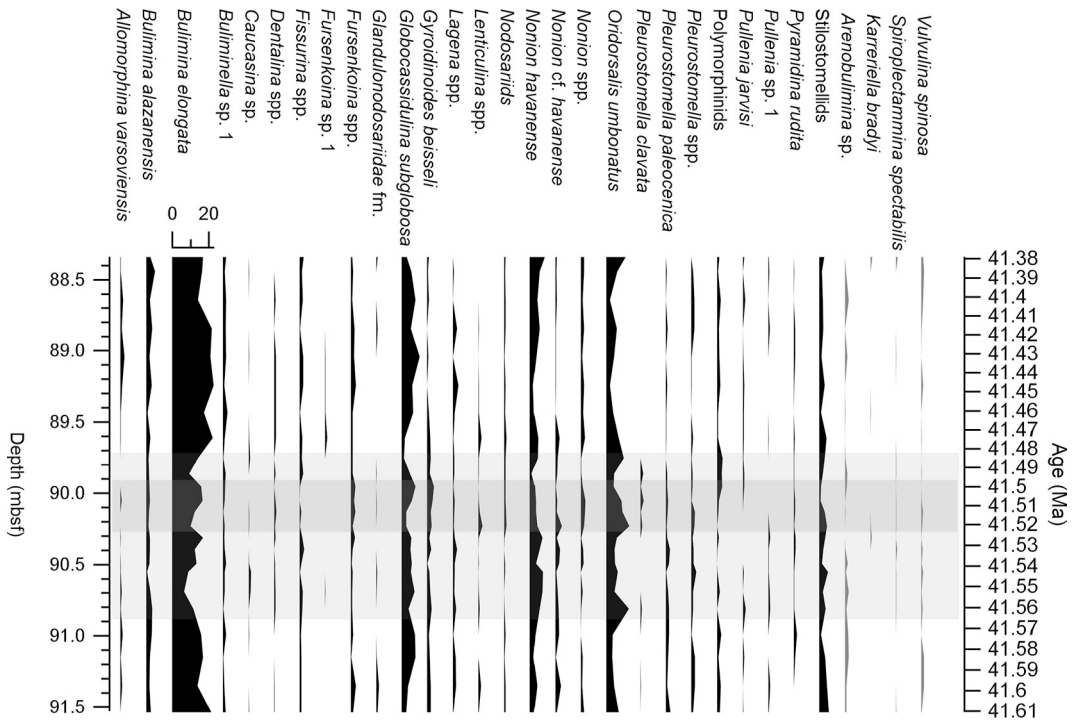

Fig. 3. Relative abundance of benthic infaunal taxa at Site 702 against depth (mbsf). Dark grey box indicates the position of the LLTM, light grey box indicates the duration of the paleoecological changes recorded.

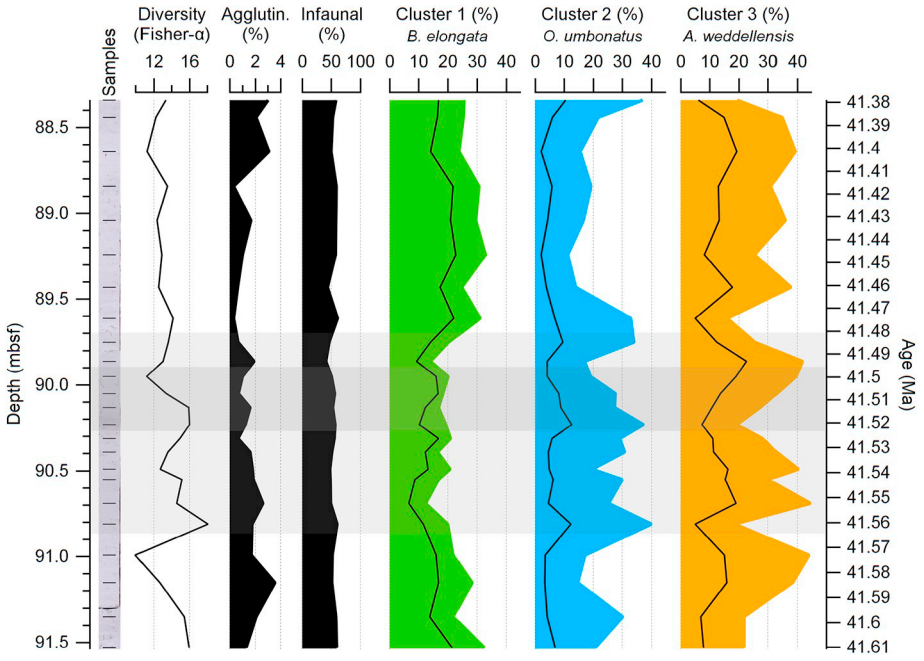

Fig. 4. Benthic foraminiferal diversity (Fisher-α) and relative abundance of agglutinated taxa, infaunal morphogroups and clusters, including the most representative species of each cluster (black solid lines within each colour plot, species names on top of each plot). All data plotted against depth (mbsf) at Site 702. Dark grey box indicates the position of the LLTM, light grey box indicates the duration of the paleoecological changes recorded. (For interpretation of the references to colour in this figure legend, the reader is referred to the web version of this article.)

the largest changes in relative abundance, ranging from 11.2% to 40%. The highest values (> 25%) are mainly recorded within the interval between 90.9 and 89.5 mbsf, coinciding with the lowest abundance of cluster 1 (Fig. 4), and in the uppermost sample.

Overall, cluster 3 (n = 11) is the most common one but its relative abundance strongly fluctuates across the studied interval, ranging from 16% to 44.59% of the assemblages (Fig. 4). *Alabamina weddellensis* is the most common species, and it is a main component of the whole assemblage together with *B. elongata* (cluster 1). Other common species in cluster 3 include *Globocassidulina subglobosa* and *Epistominella exigua* (< 5% in relative abundance).

4.2. Accumulation rates and DCA analysis

Accumulation rates (AR) have been calculated for the two most abundant species of each cluster (Fig. 5). The ARs of *B. elongata* and *C. micrus* (cluster 1) are low (below average values) in the lower part of the study interval, particularly between 90.8 and 89.6 mbsf, and they increase in the upper part, between 89.5 and 88.8 mbsf. *O. umbonatus* and *N. truempyi* ARs (cluster 2) remain fairly steady across the study interval. The ARs of the most abundant species of cluster 3, *A. weddellensis* and *E. exigua*, strongly fluctuate and show a general trend somehow similar to *B. elongata* ARs, with low values in the lower part and high values in the upper part of the study interval. Note that the ARs of the most common species (*B. elongata* and *A. weddellensis*, Fig. 5) have the largest range of AR values (up to 80 N/cm^2*kyr) as compared to the ARs of other taxa, which do not exceed 30 N/cm^2*kyr.

Benthic foraminiferal accumulation rates (BFARs) of the full assemblage show a general trend similar to *A. weddellensis* ARs (Fig. 5), with overall low values in the lower to middle part of the study interval (in the lowermost 30 cm, and between 90.8 and 89.6 mbsf), and positive peaks especially in the middle-upper part, with maximum values at 89.45 mbsf. The coarse fraction (> 63 μm) accumulation rates (CFARs) show continuous low values between 90.6 and 90.1 mbsf and a low peak at 89.75 mbsf (Fig. 5). The carbonate mass accumulation rates (CMARs), calculated from weight % $CaCO_3$ data (Westerhold et al., 2018), show uniform values except for two low peaks at 90.23 and 89.61 mbsf (Fig. 5).

To further interpret the paleoecology of benthic foraminiferal assemblages across the LLTM event, a DCA analysis was performed on the same dataset as the cluster analysis (species > 1% in relative abundance, Fig. 6). As a general trend, species are more spread along axis 1, with members of cluster 2 to the right half of this axis, and species from cluster 3 towards the left. Species from cluster 1 show intermediate values along axis 1, and positive values along axis 2. Species from cluster 2 record mostly negative values along axis 2, and cluster 3 shows intermediate values (Fig. 6).

5. Interpretation

5.1. Paleoenvironmental interpretation based on benthic foraminifera

The lack of last occurrences of benthic species across the studied interval suggests that the fast (7 kyr), 2 °C deep-sea warming recorded at Site 702 during the LLTM (Westerhold et al., 2018) did not cause any extinctions among benthic foraminifera. The $CaCO_3$% decrease from ~90% to 80% across the LLTM (Fig. 2, data from Westerhold et al., 2018) coincide with a slightly increase in corrosion-resistant species (*Oridorsalis umbonatus*, *Lenticulina* spp.) and in some infaunal taxa (*Nonion* spp.). These results might indicate a subtle increase in $CaCO_3$ corrosivity of bottom waters, but assemblages do not support $CaCO_3$ dissolution at the seafloor, as they were strongly dominated by calcareous taxa (Fig. 4) and the preservation of the tests do not show any signs of carbonate dissolution.

Benthic foraminifera do show, however, changes in their assemblages across the studied interval, and provide information about their ecological response across the LLTM for the first time. The most relevant changes are recorded between 90.8 and 89.7 mbsf (Fig. 7), where the relative abundance of cluster 2 increases and that of cluster 1 decreases. Both the relative abundance of cluster 1 (Fig. 4) and the ARs of the most abundant species of cluster 1 (*B. elongata* and *C. micrus*, Fig. 5) decrease across this interval, suggesting an actual decrease in absolute abundance of these species. In contrast, cluster 2 records its highest relative abundance across the same interval (Fig. 4). The ARs of *O. umbonatus* and *N. truempyi* (main components of cluster 2) do not show notable changes (Fig. 5) and indicate that their increase in abundance is only relative and not absolute. *O. umbonatus* is an extant cosmopolitan species with a broad environmental tolerance (Thomas and Shackleton, 1996; Katz, 1999; Foster et al., 2013) and *N. truempyi* is considered as an indicator of oligotrophic conditions, resistant to

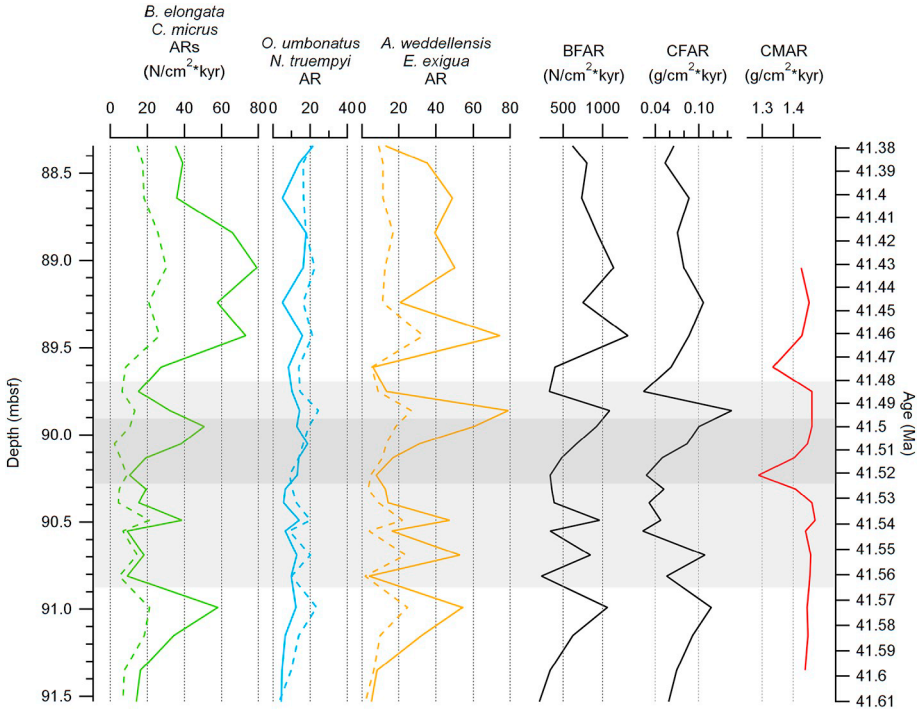

Fig. 5. Accumulation rates of the most abundant species (coloured solid lines) and the second most abundant species (dashed lines) of each cluster (same colour-code as Fig. 4). Benthic foraminifera, coarse fraction and carbonate mass accumulation rates. All data plotted against depth (mbsf) at Site 702. Dark grey box indicates the position of the LLTM, light grey box indicates the duration of the paleoecological changes recorded. (For interpretation of the references to colour in this figure legend, the reader is referred to the web version of this article.)

$CaCO_3$-corrosive waters (e.g. Tjalsma and Lohmann, 1983; Thomas, 1998; Alegret et al., 2018). Their abundance in cluster 2 points to a high resilience of the species included in this cluster (incl. *N. havanense*, *G. beisseli*, *A. spissiformis* and *C. praemundulus*).

The constant infaunal/epifaunal ratio (between 40.6% and 60.9%, Fig. 4) rules out large changes in bottom water oxygenation or organic matter flux, suggesting that the oligo-mesotrophic conditions at the seafloor did not vary noticeably across the studied interval. In addition, no evidence for low oxygenation at the seafloor has been found across the LLTM (e.g., species tolerant to low-oxygen conditions, dark organic-rich sediments) at Site 702. Species from cluster 1 (particularly *B. elongata*) decrease in abundance across the 90.8–89.7 mbsf interval (Fig. 4), possibly due to changes in the type of organic matter rather than to decreased food supply to the seafloor. We speculate that species from cluster 2 (mainly *O. umbonatus* and *N. truempyi*), which are interpreted as more resilient and are able to cope with oligotrophic conditions, were less affected by changes in the type of organic matter reaching the seafloor. This is further supported by the lack of changes in their absolute abundance (Fig. 5).

The relative abundance of cluster 3 does not show any clear trends related to the LLTM, but it strongly fluctuates across the entire study interval. Two of its most common species, *A. weddellensis* and *E. exigua*, are considered to be phytodetritus exploiting taxa (PET taxa), associated with enhanced seasonality in food delivery to the seafloor (e.g. Gooday, 2003; Boscolo-Galazzo et al., 2015; Ortiz and Thomas, 2015). The relative and absolute abundance of these PET species shows noticeable changes but no distinct patterns, suggesting non-steady conditions across the entire study interval, possibly related to periods of

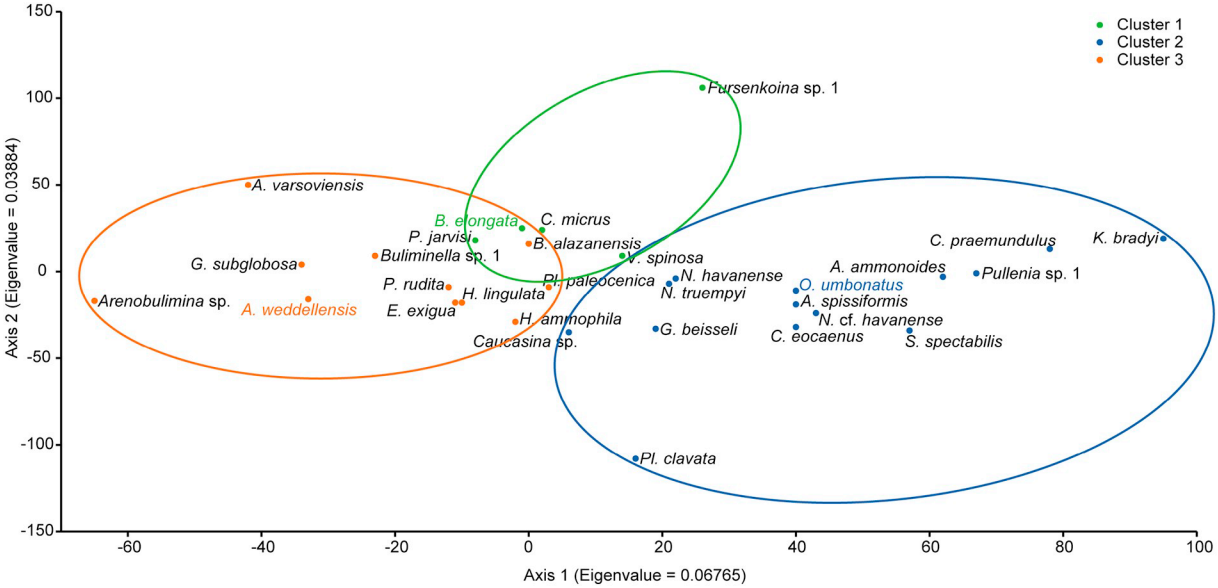

Fig. 6. R-mode (species) Detrended correspondence analysis (DCA) results from Site 702 across the LLTM event. The most common species of each cluster are colour-coded (see legend). (For interpretation of the references to colour in this figure legend, the reader is referred to the web version of this article.)

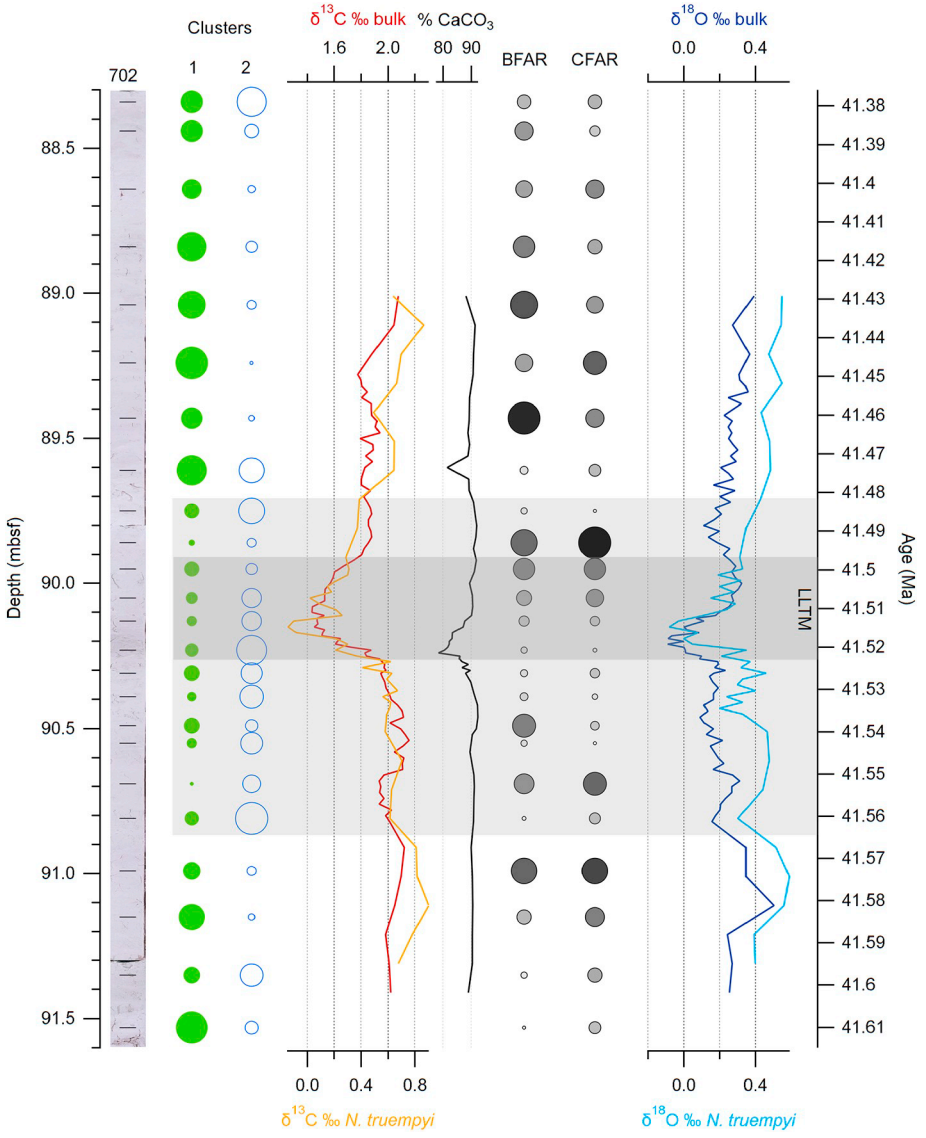

Fig. 7. Compilation of the most relevant data from this study, and C and O isotope records at Site 702 from Westerhold et al. (2018). The light grey box highlights the interval where most relevant faunal changes are recorded and the dark grey box highlights the LLTM event defined by the $\delta^{13}C$ bulk excursion. The size and/or colours of circles correspond to absolute values of the proxy represented, with smaller/lighter circles corresponding to lower values. Absolute ages are derived from Westerhold et al. (2018). All data plotted against depth (mbsf). (For interpretation of the references to colour in this figure legend, the reader is referred to the web version of this article.)

increased seasonality of the food flux.

The R-mode DCA analysis (Fig. 6) groups species from cluster 2 to the right (positive values) of axis 1, including cosmopolitan species such *N. truempyi* and *O. umbonatus* which show stable ARs across the studied interval. We argue that these species were little affected by changes in food supply to the seafloor. Negative values along this axis include species with an opportunistic behavior that show highly variable ARs across the studied interval, such as the PET species from cluster 3 (e.g. *A. weddellensis* and *E. exigua*) which likely responded to seasonality of food supply. Species from cluster 1 show mid-range values along axis 1. These species may have reacted to changes in the type (rather than seasonality) of food supply to the seafloor. DCA axis 1 thus may be indicative of ecological stability, showing resilient cosmopolitan species to the right and opportunistic, seasonally-related species to the left of axis 1.

5.2. Paleoecological changes across the LLTM and MECO events

The negative $\delta^{13}C_{bulk}$ excursion that defines the LLTM has a duration of 30 kyr at Site 702, from onset to recovery to background levels (Westerhold et al., 2018). The interval of benthic faunal change recorded by our data at this site comprises ca. 80 kyr, which includes the duration of the LLTM plus the pre- and post-event phases (Fig. 7). The assemblage turnover points to environmental instability across an interval (90.8 and 89.7 mbsf) that coincides with decreased $\delta^{13}C_{benthic}$ and $\delta^{18}O_{benthic}$ values, and suggests changes in the type of food supply to the seafloor. A similar ecological response has been documented across the longer (300 kyrs), Middle Eocene Climatic Optimum (MECO) at this site (Rivero-Cuesta et al., 2019).

Low CFARs values correlate with low $\delta^{18}O$ bulk values (Fig. 7), and the linear regression in the CFAR vs. $\delta^{18}O_{bulk}$ cross-plot supports the hypothesis that the production of organic matter at the surface decreased during the warming interval (Supplementary Fig. 2). Low $\delta^{18}O$ values in bulk sediment and benthic foraminifera across the LLTM have been attributed to a 2 °C increase in surface and bottom waters lasting 10 kyr (Westerhold et al., 2018). Warmer temperatures could lead to a decrease in heterotroph biomass according to the metabolic hypothesis (Olivarez Lyle and Lyle, 2006; O'Connor et al., 2009; Boscolo-Galazzo et al., 2014; Arreguín-Rodríguez et al., 2016). Increased temperature accelerates metabolic rates because of metabolism temperature dependency, especially of heterotroph organisms (Boscolo-Galazzo et al., 2018), which then require a higher food consumption to maintain the same population. In oligo-mesotrophic settings such as Site 702, food availability is a limiting factor, and an increase in food demand would increase competition, eventually leading to a decrease in the heterotroph population. This mechanism could account for the low CFAR and

BFAR values recorded between 90.5 and 90.1 mbsf (Fig. 7). A decrease in CFARs and BFARs coinciding with a negative $\delta^{18}O$ bulk isotopic excursion has also been recorded across the MECO interval at Site 702 (Rivero-Cuesta et al., 2019). The magnitude of the $\delta^{18}O$ excursions is different in each event (~1‰ during the MECO and ~0.5‰ across the LLTM), suggesting that metabolic rates accelerate during warm events in spite of their different magnitude and duration.

6. Conclusions

- The benthic foraminiferal turnover across the Late Lutetian Thermal Maximum (41.52 Ma, late middle Eocene) at South Atlantic Ocean Site 702 is here documented for the first time. It records assemblage changes lasting longer than the carbon isotopic excursion that defines the LLTM.
- Benthic foraminifera did not suffer extinction of species across the LLTM, but moderate assemblage changes point to environmental perturbations, likely related to changes in the type of organic matter delivered to the seafloor.
- The relative and absolute abundance of the benthic species *Bulimina elongata* (and other species of cluster 1) decreased across the paleoecological instability interval including the LLTM, suggesting a higher sensitivity than other species to changes in the type of organic matter delivered to the seafloor. A similar ecological response has been also documented across the MECO at the same site.
- BFAR and CFAR values show a positive correlation with the $\delta^{18}O$ record, suggesting a link between accumulation rates and temperature. Increased metabolic rates of heterotroph organisms under warmer temperatures may account for the decreased CFAR and BFAR values across the LLTM, as across the MECO. This might have led to a decrease in the rate of carbon burial at the seafloor, but the role of this possible positive feedback mechanism needs to be further explored.

Supplementary data to this article can be found online at https://doi.org/10.1016/j.palaeo.2020.109637.

Declaration of competing interest

The authors declare that they have no known competing financial interests or personal relationships that could have appeared to influence the work reported in this paper.

Acknowledgments

We thank Roy H. Wilkens for software support, Holger Huhlmann and Alex Wülbers for sampling assistance at BCR. Authors would like to acknowledge the use of Servicio General de Apoyo a la Investigación-SAI, Universidad de Zaragoza and Cristina Gallego for SEM imaging. Samples and data used in this research were provided by the International Ocean Discovery Program (IODP), which is sponsored by the U.S. National Science Foundation (NSF) and participating countries. Financial support was provided by the Spanish Ministry of Economy and Competitiveness and FEDER funds (Project CGL 2017-84693-R and predoctoral grant BES-2015-075140), and by the Aragon government (Reference Group E33_17R), co-financed with the European Regional Development Fund (ERDF 2014-2020) "Building Europe from Aragon". TW was funded by the Deutsche Forschungsgemeinschaft (DFG, German Research Foundation) project number 320221997. Data reported are tabulated in the supporting information. This research is part of the PhD thesis of the first author.

References

Alegret, L., Ortiz, S., Molina, E., 2009a. Extinction and recovery of benthic foraminifera across the Paleocene–Eocene Thermal Maximum at the Alamedilla section (Southern Spain). Palaeogeogr. Palaeoclimatol. Palaeoecol. 279, 186–200.
Alegret, L., Ortiz, S., Orue-Etxebarria, X., Bernaola, G., Baceta, J.I., Monechi, S., Apellaniz, E., Pujalte, V., 2009b. The Paleocene-Eocene Thermal Maximum: new data on microfossil turnover at the Zumaia Section, Spain. PALAIOS 24, 318–328.
Alegret, L., Reolid, M., Vega Pérez, M., 2018. Environmental instability during the latest Paleocene at Zumaia (Basque-Cantabric Basin): the bellwether of the Paleocene-Eocene Thermal Maximum. Palaeogeogr. Palaeoclimatol. Palaeoecol. 497, 186–200.
Arreguín-Rodríguez, G.J., Alegret, L., Thomas, E., 2016. Late Paleocene-middle Eocene benthic foraminifera on a Pacific seamount (Allison Guyot, ODP Site 865): greenhouse climate and superimposed hyperthermal events: Benthic Foraminifera on Pacific Seamount. Paleoceanography 31, 346–364.
Arreguín-Rodríguez, G.J., Thomas, E., D'haenens, S., Speijer, R.P., Alegret, L., 2018. Early Eocene deep-sea benthic foraminiferal faunas: recovery from the Paleocene Eocene Thermal Maximum extinction in a greenhouse world. PLoS One 13, e0193167.
Bijl, P.K., Houben, A.J.P., Schouten, S., Bohaty, S.M., Sluijs, A., Reichart, G.-J., Damsté, J.S.S., Brinkhuis, H., 2010. Transient Middle Eocene atmospheric CO_2 and temperature variations. Science 330, 819–821.
Bohaty, S.M., Zachos, J.C., 2003. Significant Southern Ocean warming event in the late middle Eocene. Geology 31, 1017–1020.
Bohaty, S.M., Zachos, J.C., Florindo, F., Delaney, M.L., 2009. Coupled greenhouse warming and deep-sea acidification in the middle Eocene. Paleoceanography 24 (PA2207).
Bornmalm, L., 1997. Taxonomy and paleoecology of Late Neogene Benthic Foraminifera from the Caribbean Sea and eastern equatorial Pacific Ocean. In: Fossils and Strata. Scandinavian Univ. Press, Oslo.
Boscolo-Galazzo, F., Giusberti, L., Luciani, V., Thomas, E., 2013. Paleoenvironmental changes during the Middle Eocene Climatic Optimum (MECO) and its aftermath: the benthic foraminiferal record from the Alano section (NE Italy). Palaeogeogr. Palaeoclimatol. Palaeoecol. 378, 22–35.
Boscolo-Galazzo, F., Thomas, E., Pagani, M., Warren, C., Luciani, V., Giusberti, L., 2014. The middle Eocene climatic optimum (MECO): a multiproxy record of paleoceanographic changes in the southeast Atlantic (ODP Site 1263, Walvis Ridge): MECO repercussions in the SE Atlantic. Paleoceanography 29, 1143–1161.
Boscolo-Galazzo, F., Thomas, E., Giusberti, L., 2015. Benthic foraminiferal response to the Middle Eocene Climatic Optimum (MECO) in the South-Eastern Atlantic (ODP Site 1263). Palaeogeogr. Palaeoclimatol. Palaeoecol. 417, 432–444.
Boscolo-Galazzo, F., Crichton, K.A., Barker, S., Pearson, P.N., 2018. Temperature dependency of metabolic rates in the upper ocean: a positive feedback to global climate change? Glob. Planet. Chang. 170, 201–212.
Bowen, G.J., Bralower, T.J., Delaney, M.L., Dickens, G.R., Kelly, D.C., Koch, P.L., Kump, L.R., Meng, J., Sloan, L.C., Thomas, E., Wing, S.L., Zachos, J.C., 2006. Eocene hyperthermal event offers insight into greenhouse warming. Eos, Transactions American Geophysical Union 87, 165.
Ciesielski, P.F., Kristoffersen, Y., 1988. Proceedings of the Ocean Drilling Program, Initial Reports. vol. 114 Ocean Drilling Program, College Station, Texas.
Ciesielski, P.F., Kristoffersen, Y., 1991. Proceedings of the Ocean Drilling Program, Scientific Results. vol. 114 Ocean Drilling Program, College Station, Texas.
Corliss, B.H., 1991. Morphology and microhabitat preferences of benthic foraminifera from the northwest Atlantic Ocean. Mar. Micropaleontol. 17, 195–236.
Corliss, B.H., Chen, C., 1988. Morphotype patterns of Norwegian Sea deep-sea benthic foraminifera and ecological implications. Geology 16, 716–719.
Cramer, B.S., Wright, J.D., Kent, D.V., Aubry, M.-P., 2003. Orbital climate forcing of $\delta^{13}C$ excursions in the late Paleocene-early Eocene (chrons C24n-C25n). Paleoceanography 18 (4), 1097.
Cramer, B.S., Toggweiler, J.R., Wright, J.D., Katz, M.E., Miller, K.G., 2009. Ocean overturning since the Late Cretaceous: inferences from a new benthic foraminiferal isotope compilation. Paleoceanography 24 (PA4216).
D'haenens, S., Bornemann, A., Claeys, P., Röhl, U., Steurbaut, E., Speijer, R.P., 2014. A transient deep-sea circulation switch during Eocene Thermal Maximum 2. Paleoceanography 29, 370–388.
Diester-Haass, L., 1995. Middle Eocene to early Oligocene paleoceanography of the Antarctic Ocean (Maud rise, ODP Leg 113, Site 689): change from a low to a high productivity ocean. Palaeogeogr. Palaeoclimatol. Palaeoecol. 113, 311–334.
Diester-Haass, L., Faul, K., 2019. Paleoproductivity reconstructions for the Paleogene Southern Ocean: a direct comparison of geochemical and micropaleontological proxies. Paleoceanogr. Paleocl. 34, 79–97.
Edgar, K.M., Wilson, P.A., Sexton, P.F., Suganuma, Y., 2007. No extreme bipolar glaciation during the main Eocene calcite compensation shift. Nature 448, 908–911.
Fontanier, C., Jorissen, F.J., Licari, L., Alexandre, A., Anschutz, P., Carbonel, P., 2002. Live benthic foraminiferal faunas from the Bay of Biscay: faunal density, composition, and microhabitats. Deep-Sea Res. I Oceanogr. Res. Pap. 49, 751–785.
Foster, L.C., Schmidt, D.N., Thomas, E., Arndt, S., Ridgwell, A., 2013. Surviving rapid climate change in the deep sea during the Paleogene hyperthermals. Proc. Natl. Acad. Sci. 110, 9273–9276.
Giorgioni, M., Jovane, L., Rego, E.S., Rodelli, D., Frontalini, F., Coccioni, R., Catanzariti, R., Özcan, E., 2019. Carbon cycle instability and orbital forcing during the Middle Eocene Climatic Optimum. Sci. Rep. 9, 9357.
Giraldo-Gómez, V.M., Mutterlose, J., Podlaha, O.G., Speijer, R.P., Stassen, P., 2018. Benthic foraminifera and geochemistry across the Paleocene–Eocene thermal maximum interval in Jordan. J. Foraminifer. Res. 48, 100–120.
Giusberti, L., Coccioni, R., Sprovieri, M., Tateo, F., 2009. Perturbation at the sea floor during the Paleocene–Eocene Thermal Maximum: evidence from benthic foraminifera at Contessa Road, Italy. Mar. Micropaleontol. 70, 102–119.
Giusberti, L., Boscolo-Galazzo, F., Thomas, E., 2016. Variability in climate and productivity during the Paleocene–Eocene Thermal Maximum in the western Tethys (Forada section). Clim. Past 12, 213–240.

Gooday, A.J., 2003. Benthic foraminifera (protista) as tools in deep-water Palaeoceanography: environmental influences on faunal characteristics. Adv. Mar. Biol. 46, 1–90.
Gooday, A.J., Rathburn, A.E., 1999. Temporal variability in living deep-sea benthic foraminifera: a review. Earth Sci. Rev. 46, 187–212.
Gross, O., 2000. Influence of temperature, oxygen and food availability on the migrational activity of bathyal benthic foraminifera: evidence by microcosm experiments. In: Liebezeit, G., Dittmann, S., Kröncke, I. (Eds.), Life at Interfaces and Under Extreme Conditions. Springer Netherlands, Dordrecht, pp. 123–137.
Hammer, Ø., Harper, D., 2005. Paleontological Data Analysis. Blackwell Publishing, Oxford.
Hammer, Ø., Harper, D.A.T., Ryan, P.D., 2001. PAST: Paleontological statistics software package for education and data analysis. Paleontol. Electron. 4 (1), 9.
Hayward, B.W., Kawagata, S., Sabaa, A., Grenfell, H., Van Kerckhoven, L., Johnson, K., Thomas, E., 2012. The Last Global Extinction (Mid-Pleistocene) of Deep-sea Benthic Foraminifera (Chrysalogoniidae, Ellipsoidinidae, Glandulonodosariidae, Plectofrondiculariidae, Pleurostomellidae, Stilostomellidae), Their Late Cretaceous-Cenozoic History and Taxonomy. Cushman Foundation for Foraminiferal Research Special Publication. Cushman Foundation for Foraminiferal Research Special Publication.
Herguera, J.C., 2000. Last glacial paleoproductivity patterns in the eastern equatorial Pacific: benthic foraminifera records. Mar. Micropaleontol. 40, 259–274.
Herguera, J.C., Berger, W.H., 1991. Paleoproductivity from benthic foraminifera abundance: glacial to postglacial change in the west-equatorial Pacific. Geology 19, 1173–1176.
Hilting, A.K., Kump, L.R., Bralower, T.J., 2008. Variations in the oceanic vertical carbon isotope gradient and their implications for the Paleocene-Eocene biological pump. Paleoceanography 23.
Holbourn, A., Henderson, A.S., MacLeod, N., 2013. Atlas of Benthic Foraminifera, Natural History Museum. Wiley-Blackwell.
Intxauspe-Zubiaurre, B., Martínez-Braceras, N., Payros, A., Ortiz, S., Dinarès-Turell, J., Flores, J.-A., 2018. The last Eocene hyperthermal (Chron C19r event, ~41.5 Ma): chronological and paleoenvironmental insights from a continental margin (Cape Oyambre, N Spain). Palaeogeogr. Palaeoclimatol. Palaeoecol. 505, 198–216. https://doi.org/10.1016/j.palaeo.2018.05.044.
Ivany, L.C., Lohmann, K.C., Hasiuk, F., Blake, D.B., Glass, A., Aronson, R.B., Moody, R.M., 2008. Eocene climate record of a high southern latitude continental shelf: Seymour Island, Antarctica. Geol. Soc. Am. Bull. 120, 659–678.
Jones, R.W., Charnock, M.A., 1985. "Morphogroups" of agglutinated foraminifera. Their life positions and feeding habits and potential applicability in (paleo)ecological studies. Rev. Palèobiol. 4 (2), 311–320.
Jorissen, F.J., 1999. Benthic foraminiferal microhabitats below the sediment-water interface. In: Modern Foraminifera. Springer Netherlands, Dordrecht, pp. 161–179.
Jorissen, F.J., de Stigter, H.C., Widmark, J.G., 1995. A conceptual model explaining benthic foraminiferal microhabitats. Mar. Micropaleontol. 26, 3–15.
Jorissen, F.J., Fontanier, C., Thomas, E., 2007. Chapter seven: paleoceanographical proxies based on deep-sea benthic foraminiferal assemblage characteristics. In: Developments in Marine Geology. Elsevier, pp. 263–325.
Katz, M.E., 1999. The source and fate of massive carbon input during the latest Paleocene thermal maximum. Science 286, 1531–1533.
Katz, M.E., Miller, K.G., 1991. Early Paleogene benthic foraminiferal assemblages and stable isotopes in the Southern Ocean. In: Ciesielski, P.F., Kristoffersen, Y. (Eds.), Proc. ODP. Sci. Results, pp. 481–512.
Kirtland Turner, S., Ridgwell, A., 2013. Recovering the true size of an Eocene hyperthermal from the marine sedimentary record. Paleoceanography 28, 700–712.
Lauretano, V., Littler, K., Polling, M., Zachos, J.C., Lourens, L.J., 2015. Frequency, magnitude and character of hyperthermal events at the onset of the Early Eocene Climatic Optimum. Clim. Past 11, 1313–1324.
Lear, C.H., 2000. Cenozoic deep-sea temperatures and global ice volumes from Mg/Ca in benthic foraminiferal calcite. Science 287, 269–272.
Leon-Rodriguez, L., Dickens, G.R., 2010. Constraints on ocean acidification associated with rapid and massive carbon injections: the early Paleogene record at ocean drilling program site 1215, equatorial Pacific Ocean. Palaeogeogr. Palaeoclimatol. Palaeoecol. 298, 409–420.
Littler, K., Röhl, U., Westerhold, T., Zachos, J.C., 2014. A high-resolution benthic stable-isotope record for the South Atlantic: implications for orbital-scale changes in Late Paleocene–Early Eocene climate and carbon cycling. Earth Planet. Sci. Lett. 401, 18–30.
Loeblich Jr., A.R., Tappan, H., 1987. Foraminiferal Genera and Their Classification. Van Nostrand Reinhold Company.
Lourens, L.J., Sluijs, A., Kroon, D., Zachos, J.C., Thomas, E., Röhl, U., Bowles, J., Raffi, I., 2005. Astronomical pacing of late Palaeocene to early Eocene global warming events. Nature 435, 1083–1087.
Luciani, V., Dickens, G.R., Backman, J., Fornaciari, E., Giusberti, L., Agnini, C., D'Onofrio, R., 2016. Major perturbations in the global carbon cycle and photosymbiont-bearing planktic foraminifera during the early Eocene. Clim. Past 12, 981–1007.
Lyle, M., Lyle, A.O., Backman, J., Tripati, A.K., 2005. Biogenic sedimentation in the Eocene equatorial pacific - the stuttering greenhouse and Eocene carbonate compensation depth. Proc. ODP Sci. Results 199, 1–35.
McInerney, F.A., Wing, S.L., 2011. The Paleocene-Eocene thermal maximum: a perturbation of carbon cycle, climate, and biosphere with implications for the future. Annu. Rev. Earth Planet. Sci. 39, 489–516.
Miller, K.G., Fairbanks, R.G., Mountain, G.S., 1987. Tertiary oxygen isotope synthesis, sea level history, and continental margin erosion. Paleoceanography 2, 1–19.
Moebius, I., Friedrich, O., Scher, H.D., 2014. Changes in Southern Ocean bottom water environments associated with the Middle Eocene Climatic Optimum (MECO). Palaeogeogr. Palaeoclimatol. Palaeoecol. 405, 16–27.
Moebius, I., Friedrich, O., Edgar, K.M., Sexton, P.F., 2015. Episodes of intensified biological productivity in the subtropical Atlantic Ocean during the termination of the Middle Eocene Climatic Optimum (MECO): intensified productivity during the MECO. Paleoceanography 30, 1041–1058.
Müller-Merz, E., Oberhänsli, H., 1991. Eocene bathyal and abyssal benthic foraminifera from a South Atlantic transect at 20–30 S. Palaeogeogr. Palaeoclimatol. Palaeoecol. 83, 117–171.
Murray, J.W., 1991. Ecology and paleoecology of benthic foraminifera. Longman, Harlow 1–397.
Nagy, J., Jargvoll, D., Dypvik, H., Jochmann, M., Riber, L., 2013. Environmental changes during the Paleocene–Eocene Thermal Maximum in Spitsbergen as reflected by benthic foraminifera. Polar Res. 32, 19737.
O'Connor, M.I., Piehler, M.F., Leech, D.M., Anton, A., Bruno, J.F., 2009. Warming and resource availability shift food web structure and metabolism. PLoS Biol. 7, e1000178.
Olivarez Lyle, A., Lyle, M.W., 2006. Missing organic carbon in Eocene marine sediments: is metabolism the biological feedback that maintains end-member climates? Paleoceanography 21 (PA2007).
Ortiz, S., Thomas, E., 2006. Lower-middle Eocene benthic foraminifera from the Fortuna section (Betic Cordillera, southeastern Spain). Micropaleontology 52, 97–150.
Ortiz, S., Thomas, E., 2015. Deep-sea benthic foraminiferal turnover during the early–middle Eocene transition at Walvis Ridge (SE Atlantic). Palaeogeogr. Palaeoclimatol. Palaeoecol. 417, 126–136.
Passow, U., Carlson, C., 2012. The biological pump in a high CO_2 world. Mar. Ecol. Prog. Ser. 470, 249–271.
Pearson, P.N., 2010. Increased atmospheric CO_2 during the Middle Eocene. Science 330, 763–764.
Rivero-Cuesta, L., Molina, E., Alegret, L., 2018. Eocene (Bartonian) benthic foraminifera and paleoenvironmental changes in the Western Tethys. Palaeogeogr. Palaeoclimatol. Palaeoecol. 503, 102–111.
Rivero-Cuesta, L., Westerhold, T., Agnini, C., Dallanave, E., Wilkens, R.H., Alegret, L., 2019. Paleoenvironmental changes at ODP Site 702 (South Atlantic): anatomy of the Middle Eocene Climatic Optimum. Paleoceanogr. Paleocl. 34. https://doi.org/10.1029/2019PA003806.
Sexton, P.F., Wilson, P.A., Norris, R.D., 2006. Testing the Cenozoic multisite composite $\delta^{18}O$ and $\delta^{13}C$ curves: new monospecific Eocene records from a single locality, Demerara Rise (Ocean Drilling Program Leg 207). Paleoceanography 21 (PA2019).
Sexton, P.F., Norris, R.D., Wilson, P.A., Pälike, H., Westerhold, T., Röhl, U., Bolton, C.T., Gibbs, S., 2011. Eocene global warming events driven by ventilation of oceanic dissolved organic carbon. Nature 471, 349–352.
Sluijs, A., Zachos, J.C., Zeebe, R.E., 2012. Constraints on hyperthermals. Nat. Geosci. 5, 231.
Spofforth, D.J.A., Agnini, C., Pälike, H., Rio, D., Fornaciari, E., Giusberti, L., Luciani, V., Lanci, L., Muttoni, G., 2010. Organic carbon burial following the middle Eocene climatic optimum in the central western Tethys. Paleoceanography 25 (PA3210).
Thomas, E., 1992. Middle Eocene-Late Oligocene bathyal benthic foraminifera (Weddell Sea): faunal changes and implications for ocean circulation. In: Prothero, D.R., Berggren, W.A. (Eds.), Eocene-Oligocene Climatic and Biotic Evolution. Princeton University Press, Princeton.
Thomas, E., 1998. The biogeography of the Late Paleocene benthic foraminiferal extinction. In: Aubry, M.P., Lucas, S., Berggren, W.A. (Eds.), Late Paleocene-Early Eocene Biotic and Climatic Events in the Marine and Terrestial Records. Columbia University Press, New York, pp. 214–243.
Thomas, E., 2007. Cenozoic mass extinctions in the deep sea: What perturbs the largest habitat on Earth? In: Special Paper 424: Large Ecosystem Perturbations: Causes and Consequences. Geological Society of America, pp. 1–23.
Thomas, E., Shackleton, N.J., 1996. The Paleocene-Eocene benthic foraminiferal extinction and stable isotope anomalies. Geol. Soc. Lond., Spec. Publ. 101, 401–441.
Thomas, E., Zachos, J.C., Bralower, T.J., 2000. Deep-sea environments on a warm earth: latest Paleocene-early Eocene. In: Huber, B.T., Macleod, K.G., Wing, S.L. (Eds.), Warm Climates in Earth History. Division III Faculty Publications. Cambridge University Press, Cambridge, pp. 132–160.
Thomas, E., Boscolo-Galazzo, F., Balestra, B., Monechi, S., Donner, B., Röhl, U., 2018. Early Eocene Thermal Maximum 3: biotic response at Walvis Ridge (SE Atlantic Ocean). Paleoceanogr. Paleocl. 33, 862–883.
Tipple, B.J., Pagani, M., Krishnan, S., Dirghangi, S.S., Galeotti, S., Agnini, C., Giusberti, L., Rio, D., 2011. Coupled high-resolution marine and terrestrial records of carbon and hydrologic cycles variations during the Paleocene–Eocene Thermal Maximum (PETM). Earth Planet. Sci. Lett. 311, 82–92.
Tjalsma, R.C., Lohmann, G.P., 1983. Paleocene - Eocene bathyal and abyssal benthic foraminifera from the Atlantic Ocean. In: Micropaleontology Special Edition, pp. 89.
Toffanin, F., Agnini, C., Fornaciari, E., Rio, D., Giusberti, L., Luciani, V., Spofforth, D.J.A., Pälike, H., 2011. Changes in calcareous nannofossil assemblages during the Middle Eocene Climatic Optimum: clues from the central-western Tethys (Alano section, NE Italy). Mar. Micropaleontol. 81, 22–31.
Van Morkhoven, F.P.C.M., Berggren, W.A., Edwards, A.S., 1986. Cenozoic Cosmopolitan Deep-Water Benthic Foraminifera, Bull. Centres Rech. Explor.-Prod. Elf-Aquitaine.
Wade, B.S., Kroon, D., 2002. Middle Eocene regional climate instability: evidence from the western North Atlantic. Geology 30, 1011–1014.
Westerhold, T., Röhl, U., 2013. Orbital pacing of Eocene climate during the Middle Eocene climate optimum and the chron C19r event: missing link found in the tropical western Atlantic: orbital pacing of Eocene climate. Geochem. Geophys. Geosyst. 14, 4811–4825.
Westerhold, T., Röhl, U., Donner, B., Frederichs, T., Kordesch, W.E.C., Bohaty, S.M., Hodell, D.A., Laskar, J., Zeebe, R.E., 2018. Late Lutetian Thermal Maximum-crossing

a thermal threshold in Earth's climate system? Geochemistry, Geophysics, Geosystems 19, 73–82.
Zachos, J.C., 2001. Trends, rhythms, and aberrations in global climate 65 Ma to present. Science 292, 686–693.
Zachos, J.C., McCarren, H., Murphy, B., Röhl, U., Westerhold, T., 2010. Tempo and scale of late Paleocene and early Eocene carbon isotope cycles: implications for the origin of hyperthermals. Earth Planet. Sci. Lett. 299, 242–249.
Zeebe, R.E., Westerhold, T., Littler, K., Zachos, J.C., 2017. Orbital forcing of the Paleocene and Eocene carbon cycle. Paleoceanography 32, 440–465.

4.1 Benthic foraminiferal turnover across Eocene climatic events

4.1.2. Paleoenvironmental changes at ODP Site 702 (South Atlantic): anatomy of the Middle Eocene Climatic Optimum

Lucía Rivero-Cuesta, Thomas Westerhold, Claudia Agnini, Edoardo Dallanave, Roy Wilkens & Laia Alegret, 2019

Paleoceanography and Paleoclimatology 34, PA003806

Supplementary material of this article can be found in Appendix III

Paleoceanography and Paleoclimatology

RESEARCH ARTICLE
10.1029/2019PA003806

Key Points:
- High-resolution C and O isotope and XRF data allowed detailed identification of the MECO at Site 702, and suggest a duration of ~300 kyr
- Benthic phytodetritus taxa proliferation and a positive C isotopic excursion predate the start of MECO, suggesting changes in food supply
- Increasing warm-water calcareous nannoplankton taxa during the MECO indicates migration toward higher latitudes due to rising temperature

Supporting Information:
- Supporting Information S1
- Table S1
- Table S2
- Table S3

Correspondence to:
L. Rivero-Cuesta,
lrivero@unizar.es

Citation:
Rivero-Cuesta, L., Westerhold, T., Agnini, C., Dallanave, E., Wilkens, R. H., & Alegret, L. (2019). Paleoenvironmental changes at ODP Site 702 (South Atlantic): Anatomy of the Middle Eocene Climatic Optimum. *Paleoceanography and Paleoclimatology*, *34*. https://doi.org/10.1029/2019PA003806

Received 12 NOV 2019
Accepted 14 NOV 2019
Accepted article online 27 NOV 2019

Paleoenvironmental Changes at ODP Site 702 (South Atlantic): Anatomy of the Middle Eocene Climatic Optimum

L. Rivero-Cuesta[1], T. Westerhold[2], C. Agnini[3], E. Dallanave[4], R. H. Wilkens[5], and L. Alegret[1]

[1]Departamento de Ciencias de la Tierra & Instituto Universitario de Ciencias Ambientales, Universidad de Zaragoza, Zaragoza, Spain, [2]MARUM-Center for Marine Environmental Sciences, University of Bremen, Bremen, Germany, [3]Dipartamento di Geoscienze, Università di Padova, Padua, Italy, [4]Faculty of Geosciences, University of Bremen, Bremen, Germany, [5]Hawaii Institute of Geophysics & Planetology, University of Hawai'i at Mānoa, Honolulu, HI, USA

Abstract The Middle Eocene Climatic Optimum (MECO) was an unusual global warming event that interrupted the long-term Eocene cooling trend ca. 40 Ma. Here we present new high-resolution bulk and benthic isotope records from South Atlantic ODP Site 702 to characterize the MECO at a high latitude setting. The MECO event, including early and peak warming as well as recovery to background levels, had an estimated ~300 Kyr duration (~40.51 to ~40.21 Ma). Cross-plots ($\delta^{18}O$ vs. $\delta^{13}C$) suggest that the mechanisms driving coupled changes in O and C isotope values across the MECO were weaker or absent before the event. The paleoecological response has been evaluated by quantitative analysis of calcareous nannofossils and benthic foraminifera assemblages. We document a shift in the biogeographical distribution of warm and temperate calcareous nannoplankton taxa, which migrated toward higher latitudes due to increased temperatures during the MECO. Conversely, changes in the organic matter flux to the seafloor appear to have controlled benthic foraminifera dynamics at Site 702. Benthic phytodetritus exploiting taxa increased in abundance coinciding with a positive $\delta^{13}C$ excursion, ~150 Kyr before the start of the $\delta^{18}O$ negative excursion that marks the start of MECO warming. Our data suggest that paleoecological disturbance in the deep sea predates MECO $\delta^{18}O$ excursion and that it was driven by changes in the type and/or amount of organic matter reaching the seafloor rather than by increased temperature.

1. Introduction

The Eocene was a period of significant change in Earth's climate. It comprises a long-term transition from the greenhouse state of the early Eocene to the icehouse state at the Eocene-Oligocene transition (Miller et al., 1987; Zachos, 2001). The middle to late Eocene cooling was punctuated by short-lived, transient warming events (Edgar et al., 2007; Ivany et al., 2008; Sexton et al., 2006; Tripati, 2005; Wade & Kroon, 2002), with the Middle Eocene Climatic Optimum (MECO; Bohaty & Zachos, 2003) being one of the most puzzling events described. The MECO was first recognized by a negative oxygen isotopic excursion (OIE; approximately –1‰ in $\delta^{18}O_{bulk}$ and $\delta^{18}O_{benthic}$ records) at different Southern Ocean sites (Bohaty & Zachos, 2003). It was further documented at globally distributed ocean drilling sites and on-land sections (Bohaty et al., 2009; Boscolo Galazzo et al., 2014; Jovane et al., 2007; Spofforth et al., 2010), hence considered a global event. The OIE recorded across the MECO has been interpreted mainly as a temperature signal as ice sheets were likely small or absent during the Eocene (Bohaty & Zachos, 2003; Edgar et al., 2007), suggesting a transient global warming of 4–6 °C in both surface and deep waters (Bohaty & Zachos, 2003; Bohaty et al., 2009; Bijl et al., 2010).

The MECO OIE peak appears to be synchronous with the base of Chron C18n.2n (40.14 Ma, Gradstein et al., 2012), providing a reliable age constraint (Bohaty et al., 2009). Another useful dating event is the short planktonic foraminifera biozone E12 (Berggren & Pearson, 2005), defined by the total range of *Orbulinoides beckmanni*, that was believed to coincide with the MECO event (e.g., Bohaty et al., 2009) However, this species is diachronous, as it appeared earlier at low latitudes and successively spread toward higher latitudes (Edgar et al., 2010). Nannofossil biozones provide further tie points across the MECO (Agnini et al., 2014) even at high latitudes (Villa et al., 2008; Wei & Thierstein, 1991), although there is also slight diachroneity of certain biostratigraphic events between high and low latitudes

(Bohaty et al., 2009). In order to compare and correlate the MECO among different sites and in addition to the identification of the base of Chron C18n.2n, high-resolution carbon and oxygen isotope records are arguably the best tool available due to their distinctive patterns (Bohaty et al., 2009). Estimations of MECO duration based on isotopic records vary from ~500 Kyr (Bohaty et al., 2009), ~600 Kyr (Bohaty & Zachos, 2003) to ~750 Kyr (Edgar et al., 2010). Robust age models are needed to better constrain the duration of this event, to discuss its mechanisms, and to assess its relation with orbital cycles (Giorgioni et al., 2019; Westerhold et al., 2014, 2015).

Like other Eocene warming events, the MECO is associated with a decline in carbonate accumulation at abyssal sites (Lyle et al., 2005) and related increase in atmospheric pCO_2 concentrations (Bijl et al., 2010). However, it usually lacks a clear carbon isotope excursion (CIE) accompanying the OIE, with carbon isotopic values even rising rather than declining during MECO warming (Bohaty & Zachos, 2003). Some study sites show records of a brief CIE (−0.5‰ $\delta^{13}C_{bulk}$) coinciding with OIE peak conditions, but this is not consistent across sites (Boscolo Galazzo et al., 2014). The duration of the MECO, its gradual warming/rapid cooling pattern, and its unusual CIE trend have raised questions about how well we understand carbon cycle mechanisms across warm periods, with models struggling to recreate the trends displayed by MECO records (Sluijs et al., 2013). The characteristics of this event provide a unique opportunity to analyze the complex relationship between climate and the carbon cycle during past periods of increased atmospheric pCO_2 and global warming on a hundreds of Kyr timescale.

Carbon-containing organic matter is an important component of the carbon cycle, and its cycling is driven by both abiotic and biotic processes. Oceanic organic matter through the biological pump was the main regulator of atmospheric CO_2 during the Eocene (Hilting et al., 2008). However, only a small part of the organic matter produced in the surface reaches the deep sea, especially at high latitudes (Diester-Haass & Faul, 2019) where recycling across the water column is particularly high. The remaining organic carbon is consumed by deep-sea heterotrophs (e.g., benthic foraminifera) and ultimately removed from the ocean-atmosphere system by burial (Arndt et al., 2013). Paleoecological studies across the MECO have reported shifts in both surface and deep-sea faunas (e.g., Toffanin et al., 2011; Boscolo Galazzo et al., 2014; 2015), suggesting changes in the biological pump. Surface primary productivity has been reported to increase or decrease depending on the study site (e.g., Luciani et al., 2010; Takata et al., 2013; Toffanin et al., 2011, 2013). Similarly, reported changes in benthic foraminifera assemblages across the MECO range from significant and transient restructuring of the fauna (Ocean Drilling Program [ODP] Site 738, Moebius et al., 2014) to unchanged benthic assemblages (ODP Site 1263, Boscolo Galazzo et al., 2015). In order to characterize this perturbation of the global carbon cycle and to improve our understanding of its paleoenvironmental consequences, we generated geochemical and paleontological proxies across the MECO interval at ODP Site 702 (Leg 114, South Atlantic Ocean). New, high-resolution bulk and benthic $\delta^{18}O$ and $\delta^{13}C$ isotope records as well as XRF, magnetostratigraphy, and calcium carbonate content (%$CaCO_3$) are presented to assess paleoceanographic changes. Paleoecological inferences are based on calcareous nannofossil and benthic foraminifera assemblages.

A comprehensive reconstruction of the paleoceanographic conditions of surface and deep-sea realms at this high latitude site is here presented, addressing the changes in organic carbon flux across the MECO and its consequences on deep-sea biota. Additionally, we provide constrains on the timing of the $\delta^{18}O$ and $\delta^{13}C$ isotopic excursions in the bulk and benthic records identifying their similarities and differences, which may contribute to improve our understanding of the mechanisms triggering and controlling the MECO.

2. Location and Setting

ODP Site 702 was drilled during Leg 114 (March–May 1987) in the central area of the Islas Orcadas Rise (50° 56.760′S, 26°22.122′W, 3,083.4 m water depth) in the South Atlantic Ocean (Figure 1). Islas Orcadas is a north-northwest-trending aseismic ridge more than 500 km long, 90 to 180 km wide, and over 1,000 m above the adjacent seafloor (Ciesielski & Kristoffersen, 1988). Circumpolar Deep Water bathes the central region of the Islas Orcadas Rise, and surface waters have a strong easterly flow created by the Antarctic Circumpolar Current (Reid et al., 1977). The Antarctic Convergence Zone, or polar front, today lies 60 km north of Site 702 (Gordon et al., 1977).

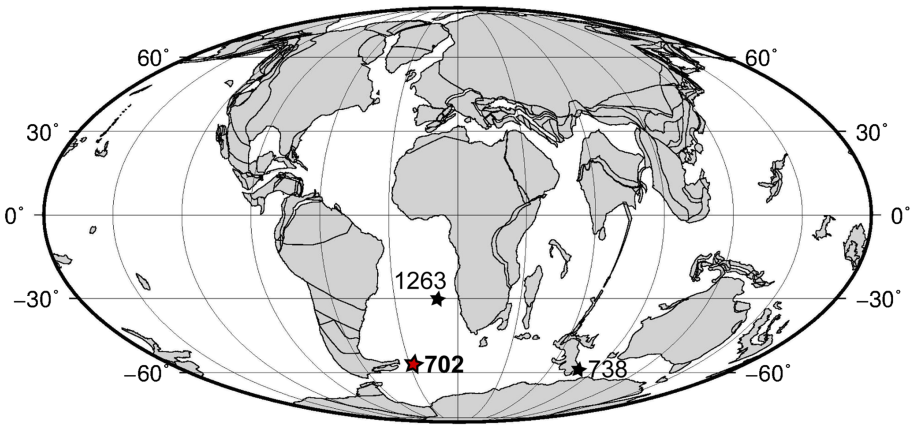

Figure 1. Map of ODP sites where benthic foraminifera assemblages have been studied across the MECO: Site 702 (this study), Site 738 (Moebius et al., 2014), and Site 1263 (Boscolo Galazzo et al., 2015). High-resolution isotope and XRF data from these sites have been used to generate the age model used in this study. Approximate positions at 40 Ma are plotted on a paleogeographic reconstruction from the Ocean Drilling Stratigraphic Network (GEOMAR, Kiel, Germany).

The Islas Orcadas Rise was likely formed during the early Paleogene, at a propagating rift that also produced the Meteor Rise (Ciesielski & Kristoffersen, 1988). Rifting and seafloor spreading separated the Islas Orcadas and Meteor rises in the Eocene, forming a deep passageway that allowed less-restricted communication of deep water from the South Atlantic to the north (Ciesielski & Kristoffersen, 1988). Site 702 subsided to near its present water depth after the late Eocene, suggesting that late Paleocene to Eocene subsidence of Site 702 was only minor; by middle to late Eocene, the polar front was located south of the Islas Orcadas Rise (Ciesielski & Kristoffersen, 1991). Extensive deposition of homogeneous nannofossil ooze and chalk, with relatively minor contribution of foraminifera (<10%) and a high carbonate content (85% to 95%; Ciesielski & Kristoffersen, 1991), took place at lower bathyal (1,000–2,000 m) paleodepths at that time (Ciesielski & Kristoffersen, 1991).

The occurrence of abundant, diverse, and well-preserved benthic foraminifera and calcareous nannofossils across middle-late Eocene sediments, together with its relatively expanded and continuous record, make Site 702 a suitable location to perform paleontological and geochemical analyses at high resolution.

3. Materials and Methods

ODP Site 702 Hole B was sampled at the International Ocean Discovery Program Bremen Core Repository. Sediment samples between Core 8X, Section 1, interval 44–46 cm (63.74 m below sea floor [mbsf]) and Core 10X, Section 1, interval 98–100 cm (83.28 mbsf) were taken at high resolution (see details below). The MECO was first identified at Hole 702B by a sharp OIE between 75 and 70.5 mbsf (Bohaty et al., 2009), which served as a baseline for our study.

3.1. Inorganic Geochemistry and XRF Measurements

Bulk stable C and O isotope analyses were performed on 238 sediment samples between 81.00 and 64.90 mbsf (5 to 10 cm resolution, ~4–8 Kyr; supporting information Table S1). Analyses were performed at the MARUM Isotope Laboratory (Bremen University) using a Finnigan MAT 252 gas isotope ratio mass spectrometer with Kiel III/Kiel IV automated carbonate preparation device. Data are reported relative to the Vienna Pee Dee Belemnite international standard, determined via adjustment to calibrated in-house standard (Solnhofen limestone) and NBS-19. The standard deviation of house standard over the measurement period was 0.04‰ for $\delta^{13}C$ and 0.07‰ for $\delta^{18}O$. Species-specific C and O isotope analyses were carried out on benthic foraminiferal tests, using a set of 72 samples between 80.85 and 64.90 mbsf, with a sample resolution between 50 and 8 cm (higher around the OIE). Between 8 and 15 specimens of well-preserved *Nuttallides truempyi* were analyzed per sample. Large specimens from the ≥100 μm fraction were used to avoid intraspecific variation of juvenile and adult specimens. Bulk wt%$CaCO_3$ was analyzed on 41 samples between 80.85 and 64.90 mbsf (sampling resolution from 1.5 m to 25 cm, with higher resolution across the OIE).

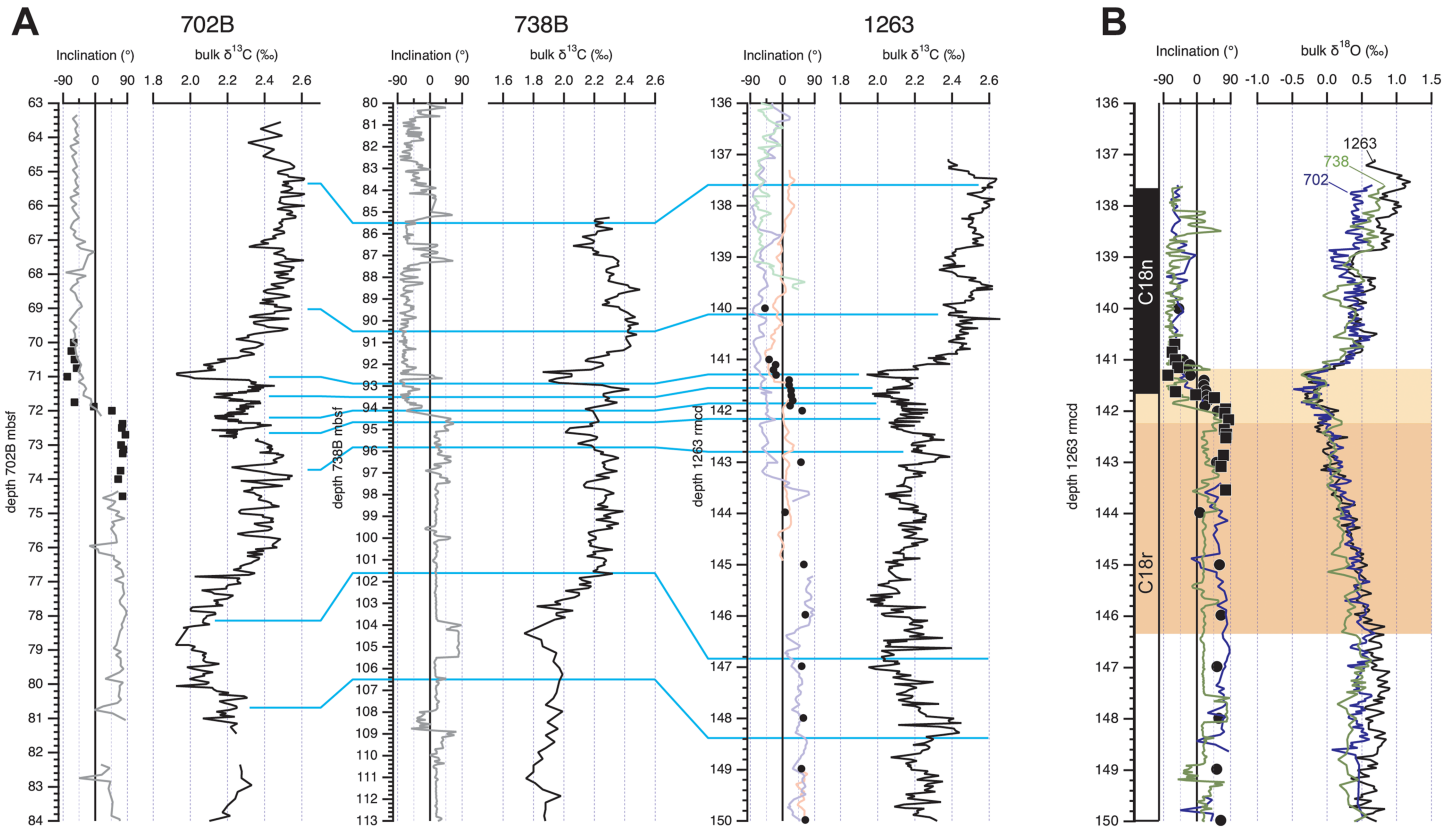

Figure 2. (a) Correlation of Hole 702B with Hole 738B and Site 1263 by high-resolution carbon isotope records (bulk sediment) and (b) magnetostratigraphic data. Data in Table S5.

The analyses were performed with a manocalcimeter (Geoservices) by addition of 5 ml of HCl (50 %) to 1 g of pulverized sediment. The pCO_2 produced during this reaction was measured in vacuum, and the result is given in % $CaCO_3$ of the total sediment analyzed.

Sediment Cores 702B7X to 702B10X from Hole 702B (archive half) were analyzed with an XRF Core Scanner III at MARUM-University of Bremen. Data were obtained every 2 cm down core over a 1 cm^2 area using a generator setting of 10 kV, 0.150 mA, and a sampling time of 15 s. XRF Scanner III was operated with a Canberra X-PIPS Silicon Drift Detector (Model SXD 15C-150-500) with 150 eV X-ray resolution, the Canberra Digital Spectrum Analyzer DAS 1000 and an Oxford Instruments 100W Neptune X-ray tube with rhodium (Rh) target material. Data are complementary to the set published in Westerhold et al. (2018).

3.2. Magnetostratigraphy

Shipboard paleomagnetic measurements of the natural remanent magnetization (NRM) were performed on the archive halves after maximum alternating field (AF) cleaning of 5 or 9 mT (Clement & Hailwood, 1991). Despite the low level of demagnetization, this analysis resulted in a shift from negative (up-pointing) to positive (down-pointing) paleomagnetic inclination interpreted as the C18n.2n-C19r Chron boundary. However, the shipboard data do not provide a continuous and fully reliable magnetic polarity record through the interval of interest at Hole 702B, and the archive halves measurements are not supported by discrete sample analysis because the intensity of the NRM signal is too low for the equipment available at the time. The CIE related to the MECO has been found near the C18n.2n-C18r Chron boundary (Bohaty et al., 2009). In order to improve the shipboard-based magnetostratigraphy, we collected a total of 23 oriented discrete samples between 70.14 and 74.43 mbsf (Figure 2), where this Chron boundary was originally placed (Clement & Hailwood, 1991). After selecting sedimentary layers not affected by coring deformation, samples were collected by pushing standard 8 cm^3 plastic cubes into the core.

To determine the paleomagnetic component of the NRM, all samples were demagnetized using three-axes AF technique, adopting 5 mT steps from 5 to 50 mT and 10 mT steps from 50 up to 100 mT, measuring the NRM after each demagnetization step. After AF demagnetization, we investigated the magnetic mineralogy of the samples by means of isothermal remanent magnetization (IRM) acquisition on a representative set of eight samples. Samples were magnetized using 22 steps with field ranging from 10 to 700 mT, and the IRM was measured after each step. All magnetic remanence measurements were performed with a 2G-Enterprises cryogenic magnetometer placed in line with an ASC AF demagnetizer and a pulse magnetizer (Mullender et al., 2016) at the University of Bremen.

The characteristic remanent magnetization (ChRM) of the sediment has been isolated by means of visual inspection of vector end points demagnetization diagrams (Zijderveld, 1967). We isolated the vector components linearly decaying to the origin of the demagnetization axes using the principal component analysis of Kirschvink (1980). ChRM components failing to trend linearly to the origin of the axes are estimated applying the spherical statistic of Fisher (1953) to the vector end points. Since the cores are azimuthally not oriented, the magnetic polarity stratigraphy has been interpreted using only the inclination of the ChRM, whereby directions with negative inclination were acquired during a normal geomagnetic field, while positive inclination represents reversed field. Analyses were performed using the PuffinPlot freeware (Lurcock & Wilson, 2012).

3.3. Correlation and Age Model

Records of carbon and oxygen stable isotopes on bulk carbonate and benthic foraminifera are key to identifying and correlating the MECO between different ocean regions (Bohaty & Zachos, 2003; Bohaty et al., 2009). Our new, high-resolution bulk carbon isotope records were used to correlate ODP Sites 702B, 738B, and 1263 based on the identification of characteristic and unique features across magnetic polarity Chrons C18r and C18n2n (Figure 2). Bulk oxygen isotope and magnetostratigraphic data (inclination) reinforce the correlation confirming that the reversal from C18r to C18n2n is located in the second of three prominent carbon isotope swings in the peak-MECO. After depth correlation, the age model for ODP Site 1263 has been adopted providing a consistent stratigraphic framework for the sites across the MECO interval. The age model for Site 1263 is based on astronomical tuning of high-resolution bulk carbonate stable carbon isotope data to the La2010b (Laskar et al., 2011) solution for orbital eccentricity. Variations in Site 1263 bulk carbon isotope data show clear imprint of short (100 Kyr) and long (405 Kyr) eccentricity, as already documented and applied for orbital tuning for the early and middle Eocene records from Site 1263 (Westerhold et al., 2015, 2017, 2018). Tuning was done by correlating the long eccentricity cycle related lighter carbon isotope data to the maxima in the La2010b eccentricity solution (Figure S1). Bulk carbon isotope data from Hole 702B reinforce the tuning of Site 1263 carbon isotope data, particularly in 405 Kyr eccentricity cycle 102 where Hole 702B data show a clearer expression of the cycle compared to Site 1263 as already presented in Westerhold et al., 2018 (see Figure S6 and S7 therein). This procedure results in a new astronomically tuned age model fully encompassing the MECO event. A previous tuned age model combining International Ocean Discovery Program Expedition 320 records from the equatorial Pacific with records from ODP 1051, 1172A, and 1260 (Westerhold et al., 2014) is lacking of high-quality, high-resolution stable isotope data due to dissolution of carbonate during the MECO and rely on low quality magnetostratigraphic data from 1172A.

3.4. Benthic Foraminifera

Quantitative analyses on benthic foraminifera were carried out on 36 samples between 83.29 and 63.75 mbsf; sampling resolution varied from 1.5 m to 25 cm, ~120 to 20 Kyr (higher resolution across the OIE). Samples were oven-dried (<50 °C for 24 hr), weighed, and disaggregated in $(NaPO_3)_6$ for 3 hr. Each sample was sieved under running water, and the ≥63 μm size fraction was collected, oven-dried (<50 °C for 24 hr), and weighed again.

Assemblage work was performed on representative splits of around 300 specimens per sample. A total of 73 taxa (70 calcitic and 3 agglutinated) was recognized at species or higher taxonomic level (Table S2). Classification at the generic level mainly follows Loeblich and Tappan (1987), except for uniserial taxa (Hayward et al., 2012). Species identification follows Tjalsma and Lohmann (1983), Van Morkhoven et al. (1986), Müller-Merz and Oberhänsli (1991), Ortiz and Thomas (2006), Holbourn et al. (2013), Boscolo

Galazzo et al. (2015), and Arreguín-Rodríguez et al. (2018). Preservation of foraminiferal tests is commonly good, suitable to detect diagnostic morphological features. The most representative specimens were photographed using the SEM imaging facilities at the University of Zaragoza (Spain) (Figure S2).

The relative abundance of each species was calculated from the raw data matrix. Diversity (Fisher-α) and dominance indices (Murray, 1991) and the percentage of calcareous and agglutinated tests were calculated. Taxa were assigned to infaunal or epifaunal morphogroups according to their morphology, following Jones and Charnock (1985), Corliss and Chen (1988), and Corliss (1991). The TROX model (Jorissen et al., 1995) was followed to infer food supply and oxygenation at the seafloor according to the microhabitat distribution of benthic foraminifera, which is extrapolated by comparing with modern, morphologically similar taxa (e.g., Jorissen, 1999). Note that foraminifera are not static but actively move through the sediment (e.g., Bornmalm, 1997; Fontanier et al., 2002; Gooday & Rathburn, 1999; Gross, 2000; Jorissen, 1999), and this may lead to inaccuracies when assigning microhabitats.

Hierarchical cluster analysis was performed (PAST package, Hammer et al., 2001) on a data matrix containing all common taxa (species >1.5% in at least one sample) using the Pearson similarity index and the unweighted pair-group (UPGMA) algorithm. Detrended Correspondence Analysis (DCA) was carried out to further analyze the results derived from clustering and to investigate the relationship between foraminifera and environmental variables (Hammer & Harper, 2005). For further paleoenvironmental assessment, the longitudinal axis of the species *Bulimina elongata* was measured (15 to 57 measures per sample) using an Olympus SC50 camera and Stream Basic software.

3.5. Calcareous Nannofossils

A total of 46 samples was analyzed between 81.18 and 65.20 mbsf with a variable sample resolution that increases up to 10–20 cm from 74.50 to 70.50 mbsf and results in a time resolution of 8 and 33 Kyr, respectively. Standard smear slides were processed following the routine method described in Bown and Young (1998). Preliminary qualitative estimate of the abundance and preservation state of calcareous nannofossil assemblages was performed for all samples. Samples were examined under a Zeiss light microscope at 1,250X magnification. The taxonomy adopted is that of Perch-Nielsen (1985) and Agnini et al. (2014). The adopted biostratigraphic schemes are those of Martini (1971), Okada and Bukry (1980), and Agnini et al. (2014). Counts on selected taxa were performed on a given area (1 mm^2; Backman & Shackleton, 1983) for biostratigraphical and paleoecological aims. The number of specimens on a fixed area in a truly pelagic depositional setting provides an estimation of the productivity of the taxa examined even if the variable amount of sediment could bias the absolute number, but previous studies have shown that the standard deviation on different replicas is always <2–5% (Agnini et al., 2016). Biohorizon nomenclature follows that given by Agnini et al. (2014): base (B), base common (Bc), top (T), and top common (Tc).

3.6. Accummulation Rates

Linear sedimentation rate and dry bulk density data from the shipboard report (Ciesielski & Kristoffersen, 1988) were extrapolated to calculate benthic foraminiferal (BFAR; Herguera & Berger, 1991) and coarse fraction (CFAR) accumulation rates (ARs). BFAR values are considered as a proxy for total organic matter flux reaching the seafloor (Gooday, 2003; Jorissen et al., 2007), and CFAR values are an approximation of planktonic foraminiferal ARs (Diester-Haass, 1995).

ARs were also calculated according to the sedimentation rates calculated with the age model derived from correlation with Site 1263, although the trends are very similar to the ARs calculated with the linear sedimentation rate from shipboard data.

4. Results

4.1. Stable Isotope Trends

Results from stable O and C isotope analyses performed on bulk carbonate follow the trends observed by Bohaty et al. (2009) but now resolve Hole 702B record at much higher resolution (every 5 to 10 cm), revealing cyclic variations throughout (Figure S3).

Oxygen isotope values of bulk sediment ($\delta^{18}O_{bulk}$) vary between 0.65‰ and −0.34‰ (maximum amplitude 0.99‰; Figure 3). The lowermost part of the section (from 81.00 to 75.20 mbsf) shows consistently high

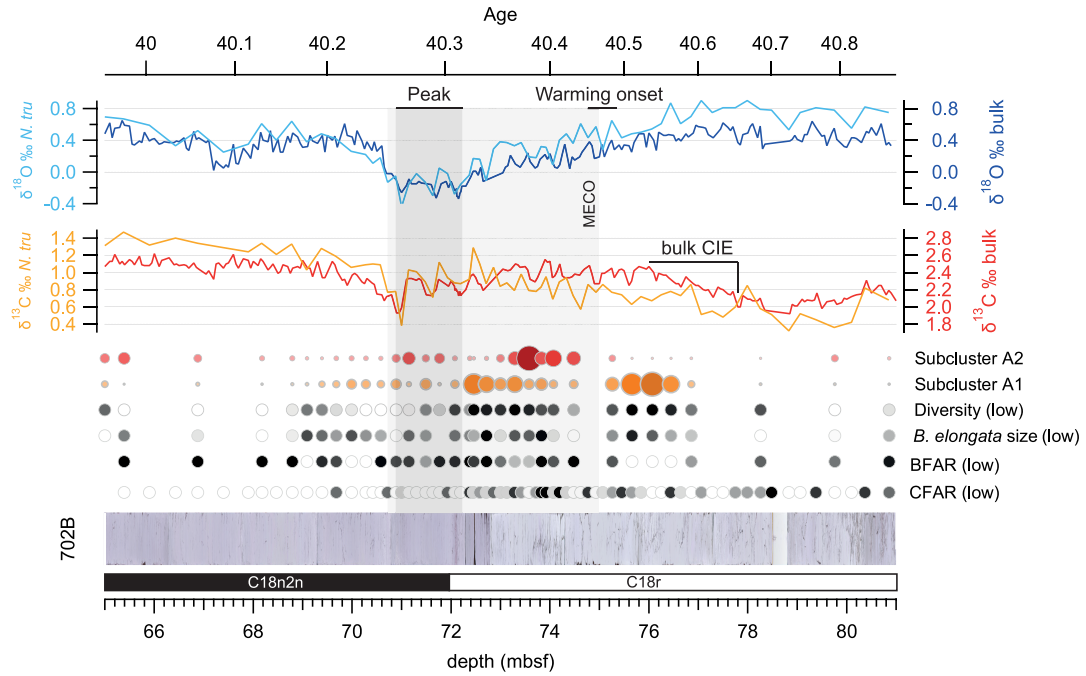

Figure 3. Bulk (darker lines) and benthic (*Nuttallides truempyi*, lighter lines) isotopic data from Site 702 plotted against depth (mbsf). Visual representation of relative abundances of benthic Subclusters A1 (red dots) and A2 (orange dots), benthic foraminifera diversity (Fisher-α), *B. elongata* maximum test size, benthic foraminifera accumulation rates (BFARs) and coarse fraction accumulation rates (CFARs) (darker dots represent lower values). Age derived from this study.

values (>0.20‰). A gradual decreasing trend is recorded between 75 and 72.15 mbsf, where the minimum $\delta^{18}O_{bulk}$ value is recorded. Negative $\delta^{18}O_{bulk}$ values are concentrated within 73.05 and 70.60 mbsf and shows three distinct negative peaks at 72.15, 71.70, and 71.00 mbsf (MECO OIE peak conditions), and this pattern is also present in the other O and C isotopic records. The last peak is followed by a very rapid +0.59‰ increase in $\delta^{18}O_{bulk}$ within a 0.4 m interval (between 71.00 and 70.60 mbsf). $\delta^{18}O_{bulk}$ recover to preexcursion values toward the top of the studied interval, interrupted by a short-term decrease to ~0‰ $\delta^{18}O_{bulk}$ between 67.70 and 67.20 mbsf.

Overall, oxygen isotope values measured on *N. truempyi* ($\delta^{18}O_{benthic}$) parallel the trend observed in $\delta^{18}O_{bulk}$ (Figure 3), showing a slightly larger variability from 0.90‰ in the lower part of the studied interval to −0.44 ‰ (maximum amplitude 1.35‰) in the middle part. While the negative excursion of the $\delta^{18}O_{benthic}$ record starting at 74.50 mbsf has a similar excursion rate (−0.56‰ across ~3 m) than the $\delta^{18}O_{bulk}$ record, the second part of the excursion (72.86 to 71.00 mbsf) shows a higher excursion rate in the $\delta^{18}O_{benthic}$ record: a −0.74‰ drop within a 1.86 m interval. The three negative peaks observed in $\delta^{18}O_{bulk}$ are also recorded in $\delta^{18}O_{benthic}$, which display minimum values at the third peak (71 mbsf). Similar to the $\delta^{18}O_{bulk}$ trend, the recovery in $\delta^{18}O_{benthic}$ values is recorded within a short interval (+0.87‰ increase between 71 and 69.67 mbsf), but the length of the recovery interval is twice as long in $\delta^{18}O_{benthic}$ compared to $\delta^{18}O_{bulk}$ (~0.40 m). Post-excursion $\delta^{18}O_{benthic}$ values are lower than preexcursion values by −0.2‰.

Carbon isotope values of bulk sediment ($\delta^{13}C_{bulk}$) range between 2.62‰ and 1.92‰ (maximum amplitude 0.69‰; Figure 3). A gradual increasing trend in $\delta^{13}C_{bulk}$ is observed from the lower to the middle part of the studied interval, between 78.35 (1.96‰) and 76.00 mbsf (2.47‰), followed by an interval of relatively constant high $\delta^{13}C_{bulk}$ values ranging between 2.25‰ and 2.47‰. A decreasing trend in $\delta^{13}C_{bulk}$ values starts ~73.00 mbsf, and three minor, negative peaks are distinguished at 72.20, 71.60, and 70.95 mbsf, the last one being more significant. They coincide with the three negative excursions in $\delta^{18}O_{bulk}$ and $\delta^{18}O_{benthic}$ values. Recovery to preexcursion values is recorded within a 1.2 m thick interval (between 70.90 and 69.70 mbsf), and $\delta^{13}C_{bulk}$ values remain relatively constant (>2.32‰) above the recovery interval. A few, below-average $\delta^{13}C_{bulk}$ values are recorded in coincidence with relatively low $\delta^{18}O_{bulk}$ values at ~67.20 mbsf.

Benthic carbon isotope values ($\delta^{13}C_{benthic}$) fluctuate between 1.47‰ and 0.32‰, showing a larger variability (max. amplitude 1.14‰) than $\delta^{13}C_{bulk}$ values (Figure 3). Despite minor differences between $\delta^{13}C_{benthic}$ and $\delta^{13}C_{bulk}$ records, they show similar trends, with minimum values in the lower part of the study interval and higher values in the uppermost part. Short-term trends in the $\delta^{13}C_{benthic}$ record are difficult to assess due to the larger variability and lower sampling resolution. However, the gradual increase in $\delta^{13}C_{benthic}$ values is interrupted across interval 72.37–70.57 mbsf, and a three-peaked negative excursion (approximately −0.6‰) can be distinguished. The three negative peaks in $\delta^{13}C_{benthic}$ (at 72.19, 71.48, and 71.00 mbsf) coincide with those identified in $\delta^{13}C_{bulk}$, $\delta^{18}O_{bulk}$, and $\delta^{18}O_{benthic}$ values, with the latter peak recording the most prominent negative excursion.

Cross-plots of $\delta^{18}O$ versus $\delta^{13}C$ values are useful to assess the correlation between these two proxies. A linear regression comprising all samples within the MECO event shows a positive correlation between $\delta^{18}O_{bulk}$ and $\delta^{13}C_{bulk}$ values (Figure S4a). No correlation is observed during the pre-MECO interval, where increasing $\delta^{13}C$ values are recorded while $\delta^{18}O$ values remain high. The MECO linear regression of the $\delta^{18}O_{bemthic}$ versus $\delta^{13}C_{benthic}$ cross-plot (Figure S4b) shows a less pronounced slope. In this case, the number of samples ($n = 72$) could partially account for the poor linear regression fit and different slope result compared to the bulk record ($n = 238$). Benthic MECO regression line is plotted against the regression lines of other Eocene warming events for comparison (Figure S4c).

4.2. Rock Magnetism and Paleomagnetism

The maximum IRM after, magnetization with 0.7 T inducing field, is between 0.3 and 0.4 mA/m. In all samples, 77% to 85% of the maximum IRM is reached within a magnetizing field of 100 mT (Figure S5a), indicating that the magnetic mineralogy is dominated by a low coercivity phase, likely consisting of magnetite. This result supports the reliability of the presented paleomagnetic data set, because the ChRM directions were isolated by AF demagnetization up to a peak field of 100 mT.

The intensity of the NRM ranges around 10^{-5} and 10^{-4} A/m. We obtained ChRM directions suitable for magnetic polarity stratigraphy from 17 samples out of 23 (74%). Of these 17, 11 have been obtained by linear interpolation of vector end points (Kirschvink, 1980). On six specimens, the vector end points are found to decay toward the demagnetization axes origin without a clear linear pattern, and the ChRM directions have been estimated by calculating the Fisher (1953) mean of the vector end points themselves, an approach already successfully used in analyses of paleomagnetic data (Tauxe et al., 2012) (Figure S5c and Table S3). The directional data set is organized in two modes, whereby seven directions have negative inclination while 10 have positive inclination. The sampled stratigraphic interval straddles two cores, namely, 702B-8X and 702B-9X. Due to the lack of declination control (in particular between the two cores), we estimated the average direction of the two modes, and of the whole data set, using the inclination-only approach of McFadden and Reid (1982; Figure S5d).

The inclination data are plotted together with the inclination of the continuous archive halves measurement (Clement, 1991). There is a substantial agreement between the two data sets in the interval from 70 to 72.3 mbsf. Our new discrete-sample based magnetostratigraphy constrains at 71.99 mbsf, the depth of the magnetic polarity reversal that was originally interpreted as the C18n.2n-C18r Chron boundary (Clement & Hailwood, 1991; Figure 2 and S6). Shipboard measurements are characterized by a gap between 72.25 and 74.35 mbsf, limiting the reliability of the position originally proposed for the Chron boundary (Clement & Hailwood, 1991). Our new data clearly show consistent positive ChRM inclination below 71.99 mbsf (i.e., reversed magnetic polarity).

4.3. Benthic Foraminiferal Assemblages

Benthic foraminifera are strongly dominated by calcareous taxa (98% of the assemblages) matching the continuously high (~80%) $CaCO_3$ content recorded. Diversity (Fisher-α index) ranges between 10.8 (minimum at 73.29 mbsf) and 18.2 (maximum at 66.88 mbsf) (Figure 4). Low diversity values (below average Fisher-α 14.3) are mostly recorded between 78.26 and 72.08 mbsf. In contrast, dominance oscillates, showing the highest (above average 0.20) but also the lowest values between 79.76 and 72.46 mbsf.

Assemblages show changes in relative abundance of species across the studied interval. A classical hierarchical cluster analysis of species ($n = 33$) shows two main clusters (A and B) and four subclusters (A1, A2, B1,

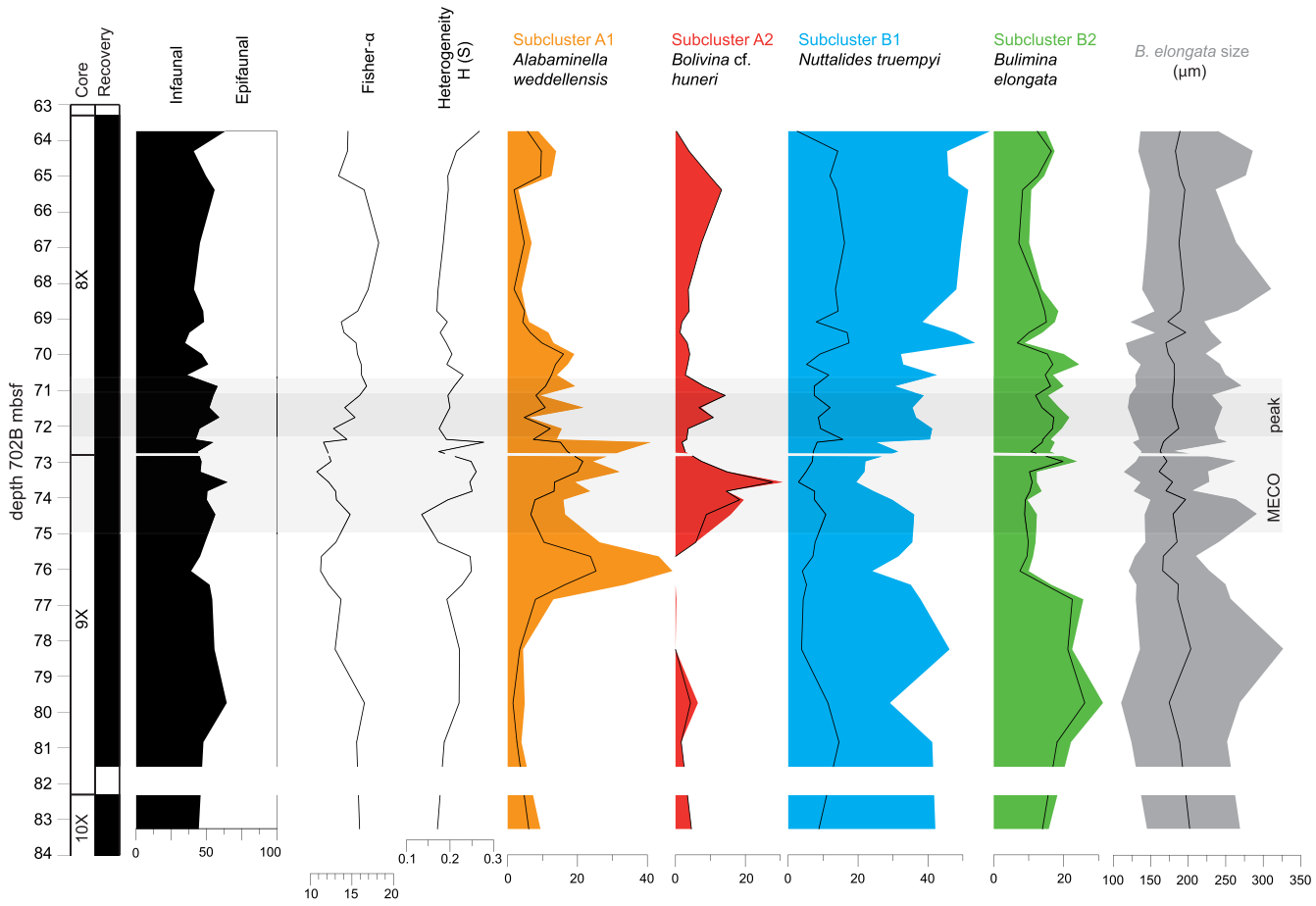

Figure 4. Benthic foraminifera quantitative analysis at Site 702. Morphotypes (infaunal/epifaunal ratio), diversity (Fisher-α index), and dominance indices and relative abundance of Subclusters A1 (orange), A2 (red), B1 (blue), and B2 (green), including their most representative species (black lines within each color plot, species names in the figure). The gray plot represents the range of *Bulimina elongata* test sizes (black line = average).

and B2) with similarity <0 (Figure S7). Cluster B contains more species (n = 24) and has a higher relative abundance (up to 72.8% of the assemblages) than Cluster A.

In Subcluster A1, the main component is *Alabaminella weddellensis*, followed by *Caucasina* sp. and *Epistominella exigua*. These taxa have flattened trochospiral tests and an inferred epifaunal habitat. Infaunal taxa (e.g., *Buliminella grata* and *Buliminella beaumonti*) are a minor component of Subcluster A1 (<2.25%). The relative abundance of this subcluster strongly varies across the studied interval from 3.07% to 47.19%, with the largest changes and highest values recorded between 76.86 and 69.39 mbsf (highest value at 76.07 mbsf) (Figure 4). Subcluster A2 only includes two species, *Bolivina* cf. *huneri* and *Fursenkoina* sp. 2, the former being the main component. Both species are believed to have had an infaunal mode of life, and they show substantial ornamentation on their tests (Figure S2). The relative abundance of Subcluster A2 increases between 74.48 and 70.89 mbsf (maximum at 73.58 mbsf). Both subclusters are scarce in the lower part of the studied interval, and their relative abundances show a negative correlation in the middle and upper part of the investigated section.

Subcluster B1 is the most diverse one, including 19 species. *Nuttallides truempyi* is the most abundant species, followed by *Globocassidulina subglobosa*, *Cibicidoides micrus*, *Oridorsalis umbonatus*, *Bulimina alazanensis*, and *Cibicidoides praemundulus* (each of them >5% in relative abundance). The lowest values of this subcluster (average < 37.26%) are recorded between 76.45 and 72.46 mbsf (Figure 4). Subcluster B2 shows the smallest changes in relative abundance across the study interval, and unlike the other subclusters, it is more abundant in the lower part (between 83.29 and 76.45 mbsf). It is dominated by *Bulimina elongata*, while the other four species forming this subcluster show relative abundances <5%. Due to the different

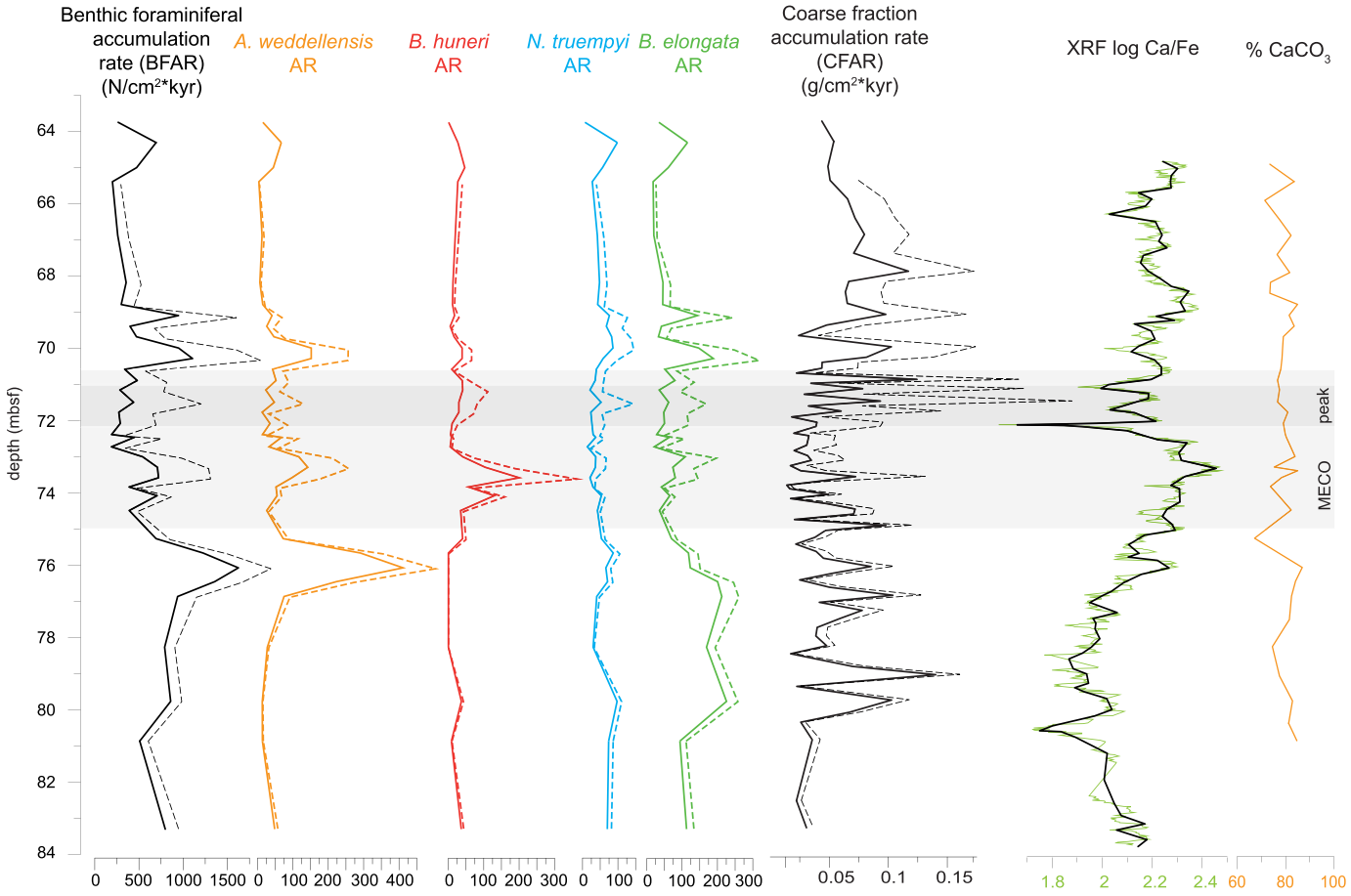

Figure 5. Accumulation rates (ARs), XRF, and $CaCO_3$ %. Solid lines represent ARs calculated with the linear sedimentation rate from shipboard data. Dashed lines are ARs calculated with sedimentation rates derived from Site 702 age model (this study).

abundance trend of *B. elongata* as compared to other species, the length of this taxon was measured across the study interval. Average values (181.91 μm) and minimum values do not show any significant changes (Figure 4), but maximum test sizes have lower values between 76.07 to 68.79 mbsf (lowest at 72.72 mbsf).

In order to better understand and interpret the paleoecological changes related to subcluster abundance fluctuations, a DCA analysis was performed on the same data set as the cluster analysis (with species >1.5% in relative abundance; Figure S8). Species from Cluster A fall within positive values of Axis 1, while Cluster B shows Negative Axis 1 values except for one outlier. Species from Subcluster A2 show high positive values along Axis 2, while Subcluster A1 values are negative along Axis 2. Cluster B shows Intermediate Axis 2 values, ranging between 25 and −40.

4.4. Benthic foraminifera and Coarse Fraction Accumulation Rates

BFARs and species-specific ARs have been calculated for the dominant species of each subcluster. Calculations were made with assumed constant sedimentation rates (Ciesielski & Kristoffersen, 1988) and with sedimentation rates derived from Site 702 age model; however, both calculations show similar overall trends and range of values (Figure 5).

BFARs show average values in the lower part of the study interval, shifting to lower values between 72.72 and 70.58 mbsf and between 68.79 and 65.00 mbsf. *Alabaminella weddellensis* has low ARs values across the section, showing larger values in the intervals 76.75–75.66, 73.58–73, and 70.28–69.99 mbsf. *Nuttallides truempyi* and *B. huneri* ARs are stable except for a noticeable increase of the latter between 74.07 and 73.19 m. In contrast to the other species, *B. elongata* ARs are higher in the lower part of the

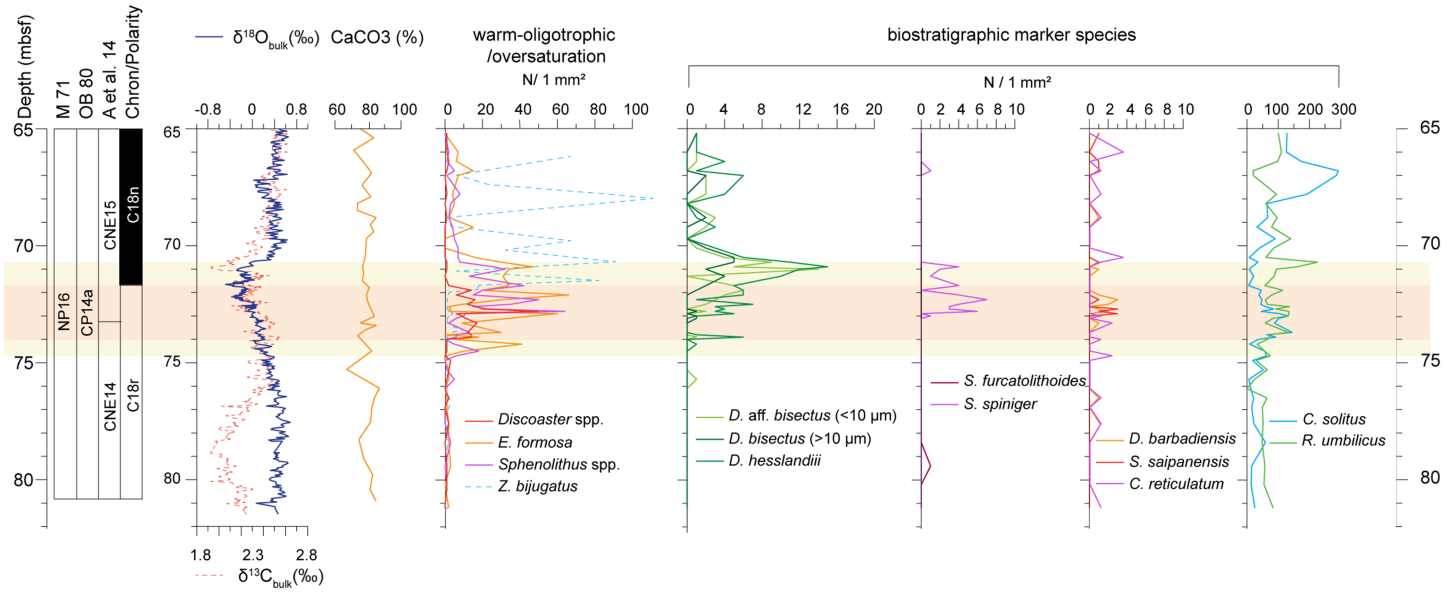

Figure 6. Calcareous nannofossils abundances plotted against depth. Biozones recognized are shown on the left and abundances of relevant biostratigraphic markers on the right. Relative abundance of warm species and the isotopic records are plotted to show correlation across the MECO event (light orange box) and during the warming phase (dark orange box).

interval, between 83.29 and 75.66 mbsf, with two positive peaks between 70.28 and 69.00 mbsf that parallel the general BFAR trend.

Despite the wide range of CFAR values (>63 µm) (Figure 5), there is a short interval with low values between 74.77 and 71.63 mbsf, while above average (>0.5 g * cm^2/Kyr) values are constant in the lower and upper parts of the section. This proxy has been commonly used as an estimation of the planktonic foraminiferal ARs (e.g., Boscolo Galazzo et al., 2014).

4.5. Calcareous Nannofossil Biostratigraphy and Abundance Patterns

Calcareous nannofossil assemblages from Site 702 were previously reported by Pea (2011), but our data provide a biostratigraphic frame based on the semiquantitative abundance patterns of the index species (N/mm^2) used in the biozonations (Figure 6 and Table S4).

4.5.1. Base of *Reticulofenestra umbilicus* (>14 µm)

It marks the base of Subzone CP14a (Okada & Bukry, 1980) and the base of Zone NP16, as the Top of *Blackites gladius*, which was originally proposed to define the base of Zone NP16 (Martini, 1971), has been reported to extend into lower Zone NP17 (e.g., Agnini et al., 2014; Berggren & Aubry, 1984; Wei & Wise, 1989). *Reticulofenestra umbilicus* is present throughout the section with a continuous, relatively common abundance that is lower in the basal part and increases from 74.1 (±0.10) mbsf upward. This abundance pattern indicates that the base of this taxon is positioned below the base of the studied interval.

4.5.2. Base of *Cribrocentrum reticulatum*

It denotes the base of Zone CNE14 (Agnini et al., 2014). This taxon is unevenly distributed and suggests, conversely to what was reported in Pea (2011), that its base is located below the base of the study section. The appearance of *C. reticulatum* shows diachroneity, starting more than 2 Myr before at low-middle latitudes than at high latitudes (Agnini et al., 2014; Villa et al., 2008). This discrepancy and its low abundance at Site 702 are most likely related to the warm/temperate preference suggested for this taxon (e.g., Backman, 1987; Bukry, 1973; Haq & Lohmann, 1976).

4.5.3. Top of *Sphenolithus furcatolithoides*

It has been proposed to define the base of Subzone MNP16B (Fornaciari et al., 2010) at low-middle latitudes. This warm water taxon (e.g., Agnini et al., 2006; Gibbs et al., 2004; Wei & Wise, 1992) is rare at Site 702, and only one specimen was observed at 79.40 mbsf. This finding does not allow us to precisely position this biohorizon, but the specimen lies, as expected, between the base of *R. umbilicus* and the appearance of *Dictyococcites bisectus*.

4.5.4. Base of Common (Bc) and Continuous *Dictyococcites bisectus* (>10 μm)

It marks the base of Zone CNE15 (Agnini et al., 2014) at low-middle latitudes, while it is found to occur more than 2 Myr later in the high latitude Southern Ocean Site 748 (Villa et al., 2008). The taxonomy of *D. bisectus* is complicated, and we follow Agnini et al. (2014), who include forms >10 μm, in order to directly correlate results between Site 702 and low to low-middle latitude sites (i.e., Sites 1051 and 1052 and Alano section). Similar taxa such as *D*. aff. *bisectus* and *D. hesslandii* (see Agnini et al., 2014, for detail on taxonomy) enter or reenter in the record very close to each other in Chron C18r (Pea, 2011; Figure 6). These taxa are rare at Site 702 likely because of their temperate affinity (Haq & Lohmann, 1976; Villa et al., 2008; Wei & Wise, 1990), but they display a relatively continuous presence (Figure 6 and Table S4).

4.5.5. Top Common/Top of *Sphenolithus spiniger*

The top common of *S. spiniger* defines the base of Subzone MNP17A (Fornaciari et al., 2010). This warm water species is virtually absent in the lower part of the study interval at Site 702, and it displays a rare but substantially continuous occurrence from 73.05 (±0.05) mbsf to 70.80 (±0.1) mbsf, where it disappears. A similar trend for the final tail of occurrence of this taxon has been recognized in multiple sections at low-middle latitudes (e.g., Sites 1051, 1052, and 1263 and Alano, Italy; Fornaciari et al., 2010; Toffanin et al., 2011; Agnini et al., 2014).

4.5.6. Top of *Chiasmolithus solitus*

It marks the base of Zone NP17 and Subzone CP14b (Martini, 1971; Okada & Bukry, 1980). This species is continuously present across the study interval at Site 702, and its highest occurrence is located in the upper part. We cannot thus validate the inconsistencies reported in the literature on the relative position of this biohorizon among sequences located at low-middle latitudes and between high and low-middle latitudes sections (Agnini et al., 2014; Marino & Flores, 2002; Villa et al., 2008).

In summary, the simultaneous presence of *R. umbilicus* (>14 μm) and *C. solitus* indicates that the study interval belongs entirely to Subzone CP14a and Zone NP16 (Martini, 1971; Okada & Bukry, 1980). The presence of *C. reticulatum* from the base of the section and the appearance of *D. bisectus* at 73.20 (±0.1) mbsf indicate that the study interval spans the upper part of Zone CNE14 and the basal part of Zone CNE15 (Agnini et al., 2014).

The semiquantitative abundance patterns of selected taxa show major changes in surface waters across the study interval. The total number of forms ascribable to the genus *Sphenolithus*, which includes mainly *S. moriformis* gr., displays a remarkable increase in abundance at 74.80 (±0.10) mbsf and remains relatively high up to 70.80 (±0.10) mbsf, where it returns to the background values observed in the lower part. Similarly, the abundance of forms belonging to *Ericsonia formosa*, the only representative of its genus, increases exactly in the same interval. Within this interval but across a shorter period (from 73.95 ± 0.05 to 71.80 ± 0.10 mbsf), the genus *Discoaster* also shows an increase from virtually zero to a peak value of 50 specimens per mm^2 recorded at 72.80 mbsf. An anomalous and highly variable increase in abundance of *Zyghrablithus bijugatus* starts at 71.15 ± 0.15 mbsf, but the abundance pattern is characterized by a high variance of the signal ($1\sigma = 36$; Figure 6).

5. Discussion

5.1. Finding MECO

The MECO event has been defined by a negative bulk OIE, followed by a peak interval of lowest $\delta^{18}O$ values that ends with a rapid recovery to preexcursion values. This pattern is recurrent in records from different latitudes and ocean basins (Bohaty et al., 2009; Giorgioni et al., 2019; Jovane et al., 2007; Spofforth et al., 2010). At Site 702 in the South Atlantic Ocean, our high-resolution isotopic analyses follow the same overall trend. $\delta^{18}O$ profiles show a manifest decrease starting at 75 mbsf, followed by three relative minimum values at 72.15, 71.70, and 71 mbsf, ending in a rapid recovery (+0.6‰ $\delta^{18}O_{bulk}$ within 0.4 m) after the last minimum peak (Figure 3). Overall, the $\delta^{18}O_{bulk}$ pattern is paralleled by the $\delta^{18}O_{benthic}$ record, although the benthic record presents a positive excursion in the lower part of the studied interval, before the beginning of the OIE (Figure 3).

The driving mechanisms of the MECO are still largely unknown; however, the $\delta^{18}O_{bulk}$ versus $\delta^{13}C_{bulk}$ cross-plot suggests that these mechanisms were weaker or absent in surface waters before and after the

warming. Samples from the pre- and post-MECO periods show no correlation, while samples comprising the MECO event have a positive linear correlation (Figure S4a). Similarly, the $\delta^{18}O_{benthic}$ versus $\delta^{13}C_{benthic}$ cross-plot show no correlation in samples from the pre- and post-MECO interval (Figure S4b), suggesting that MECO driving mechanisms were weaker or absent before and after the MECO also in the deep sea. The positive correlation between $\delta^{18}O$ and $\delta^{13}C$ supports a constant linear relationship between temperature ($\delta^{18}O$) and carbon release ($\delta^{13}C$) across the MECO, as observed in older hyperthermal events (Lauretano et al., 2015, 2018; Stap et al., 2010; Westerhold et al., 2018). The linear regression calculated with benthic isotope samples across the MECO (dashed line Figure S4b) is less steep than those calculated for other early Eocene hyperthermals (Figure S4c; Westerhold et al., 2018), which suggests a different carbon signature and heavier carbon source of the MECO (Lauretano et al., 2015).

Comparison of our high-resolution stable isotope record with that from Site 1263 suggests a total duration of ~270 Kyr for the MECO (between the onset of the bulk OIE at 75 mbsf and the recovery to the same $\delta^{18}O_{bulk}$ values at 70.60 mbsf) (Figure 3). Site 1263, on which our age model is based, experienced some dissolution during the MECO peak, which may have led to slight overestimations of sedimentation rates across this interval. However, it seems very likely that the total duration of the MECO did not exceed 300 Kyr at Site 702. Conversely, if the duration of the MECO is calculated using the linear sedimentation rate data from the shipboard report (1.224 cm/Kyr across the study interval), its duration is >700 Kyr.

5.2. Paleoenvironmental Interpretation: Benthic Foraminiferal Response

Benthic foraminifera reveal short, transient changes in the assemblages that point to a temporary shift in environmental conditions at the seafloor across the study interval.

The species with larger relative abundance shifts belong to subcluster A1, which is mainly composed of phytodetritus exploiting taxa (PET; e.g., *A. weddellensis*, *Caucasina* sp., and *E. exigua*) and shows higher abundances in the middle of the studied interval, between 76.86 and 69.39 mbsf (Figure 4). PET taxa have been related to seasonality (Boscolo Galazzo et al., 2015, and references therein) and probably to an opportunistic life strategy and rapid reproduction due to their small size. Across this interval with high abundance of species from Subcluster A1, there are peaks in relative abundance of *B. huneri* (the main component of Subcluster A2; Figure 4), a species that has been associated with seasonality and input of refractory (low quality) organic matter (e.g., D'haenens et al., 2012). The interval with peaks in PET taxa and *B. huneri* (~76.5–69 mbsf) probably represents a period of stronger seasonality, with changes in the type of organic matter flux to the seafloor. High percentages of Subclusters A1 and A2 coincide with high $\delta^{13}C$ values (Figure 3), pointing to a change in the organic carbon source. The negative correlation between the abundance of Subclusters A1 and A2 may be related to their different ecological preferences, with species from Subcluster A1 adapted to feeding on phytodetritus and those from Subcluster A2 preferentially feeding on refractory organic matter. These results support fluctuations in the organic carbon flux across this interval.

Subclusters B1 and B2 decrease in relative abundance coinciding with the interval of increased percentage of Subclusters A1 and A2 (between ~76.5 and 72.5 mbsf; Figure 4). While subcluster B1 recovers to previous (and even higher) relative abundance values after this interval, subcluster B2 does show consistently low values. In addition, the ARs of *N. truempyi* (main component of Subcluster B1) show no significant changes across the studied interval and point to a decrease in relative-—but not in absolute—abundance (Figure 5). This nonspecialist, cosmopolitan epifaunal species and other Eocene lower bathyal species of Subcluster B1 (e.g., *Globocassidulina subglobosa*, *Oridorsalis umbonatus*, and *Bulimina alazanenesis*) might have adapted better than *B. elongata* to the inferred changes in organic matter flux, whose ARs notably fluctuate.

DCA analysis confirms differences among subclusters (Figure S8). Axis 1 may be controlled by the type of organic matter reaching the seafloor, with species from Cluster A (which thrived during the period of inferred changes in organic matter flux, 76.86–69.39 mbsf) showing positive values, and species from Cluster B, which dominated during the pre- and post-event, showing negative values. The interpretation of Axis 2 is more complex, but it might be related to changes in temperature. Species from Cluster A2, which is more abundant during the OIE (MECO warming phase), show high Axis 2 values, while the rest of the species have low or negative values along this axis.

The main limiting factors for deep-sea benthic foraminifera are oxygen concentration and the amount and type of food (e.g., Gooday, 2003; Murray, 2006). No evidence for low oxygenation has been found at Site 702 (e.g., species tolerant to low-oxygen conditions and dark sediments); thus, oxygen was not likely a significant factor driving the benthic turnover at this site. Assemblages are composed of mixed infaunal and epifaunal taxa, and the morphogroups ratio does not show any significant trends (Figure 4). Together with the assemblage composition (Figure S7), they point to fairly steady oligo-mesotrophic conditions at the seafloor. Continuously high (>80%) $CaCO_3$ content (Figure 5), the strong dominance of calcareous (>98%) over agglutinated benthic foraminifera, and the overall good preservation of the foraminiferal tests and the nannofossil assemblages (Pea, 2011; this study) indicate that Site 702 was well above the CCD across the MECO, as suggested by Bohaty et al. (2009).

No extinctions have been recorded across the MECO at Site 702 (Table S2) in contrast to the extinction of almost half of deep-sea benthic foraminiferal species across the PETM (e.g., Alegret et al., 2009, b, 2018; Arreguín-Rodríguez et al., 2018; Miller et al., 1987; Thomas, 1998, 2003, 2007; Tjalsma & Lohmann, 1983). Similarly, no benthic foraminiferal extinctions have been recorded across the MECO in other locations from different latitudes and basins (Boscolo Galazzo et al., 2013; Moebius et al., 2014, 2015) nor across some Paleocene (e.g., Alegret et al., 2016; Deprez et al., 2017) and Eocene smaller hyperthermal events (e.g., Arreguín-Rodríguez et al., 2016; Arreguín-Rodríguez & Alegret, 2016).

5.3. Paleoenvironmental Interpretation: Surface Waters

Previous studies on the paleoenvironmental affinities of calcareous nannofossil taxa have documented that *Discoaster* (e.g., Haq & Lohmann, 1976; Haq, Lohmann, & Sherwood, 1977; Haq, Premoli-Silva, Lohmann, 1977; Wei & Wise, 1990; Pospichal & Wise, 1990; Agnini et al., 2006), *Sphenolithus* (e.g., Agnini et al., 2007; Aubry, 1998; Bralower, 2002; Gibbs et al., 2004; Wei & Wise, 1990), and *Ericsonia* (e.g., Haq & Lohmann, 1976; Haq, Lohmann et al., 1977; Wei & Wise, 1990; Aubry, 1992; Wei & Wise, 1992; Kelly et al., 1996; Bralower, 2002; Agnini et al., 2007) preferentially thrive in warm waters and oligotrophic conditions. The virtual absence of these taxa in the lower and upper parts of the study interval, combined with their abundance peaks between 74.80 and 70.80 mbsf, suggest that they were ecologically excluded before and after the MECO because of the cool sea-surface temperatures at Site 702. Coinciding with the beginning of surface water warming and the OIE that marks the MECO, *Discoaster*, *Sphenolithus*, and *Ericsonia* extended their biogeographical distribution. Their abundance peaks suggest that the increase in surface-water temperature was sufficient to surmount their ecological thresholds. Anomalous warming allowed these taxa to survive within their thermal optimum but outside their natural biogeographical domain, while the disappearance of these species is related to decreased temperatures and increased nutrient availability. More interestingly, the biochronology of the appearances and disappearances of the marker species of standard zonations show that Site 702 was located at the transition between high and low-middle latitudes and could in fact represent the ideal link between these two apparently unconnected paleoecological domains. Understanding the different responses of calcareous nannofossils to the MECO at different latitudes is fundamental, as it could shed light on the appearance of *D. bisectus* and the evolution of sphenoliths at low-middle latitudes, as well as on the expansion of temperate taxa toward high latitudes (Toffanin et al., 2011; Villa et al., 2008, 2014). Site 702 records the expansion of warm water taxa and temperate taxa toward higher latitudes across the MECO, suggesting that a strong global teleconnection exists between these different geographical areas.

The peak of *Z. bijugatus* in the post-MECO interval may be related to a change in water chemistry rather than to temperature changes. Warming during the MECO should have favored the arrival and proliferation of this species, as documented for other warm water/oligotrophic taxa (Agnini et al., 2007). However, its increase during the post-MECO at Site 702 points to an intermittent carbonate oversaturation of sea surface waters, triggered by increased alkalinity due to accelerated terrestrial chemical weathering, as suggested for the PETM (Dickens et al., 1997; Penman & Zachos, 2018; Zeebe & Zachos, 2013). The record of these changes well after the climax of the MECO contributes to the MECO conundrum (Sluijs et al., 2013). Indeed, the extremely fragile structure of *Z. bijugatus* holococcolith is easily dissolved in the early stage of the sedimentation process, but the enhanced availability of carbonate in the seawaters might have favored the preservation of the very delicate crystallites forming the holococcolith.

5.4. Accummulation Rates and the Ocean Organic Carbon Budget

An increase in metabolic rates has been previously invoked to explain lower foraminiferal ARs across hyperthermal events (e.g., Boscolo Galazzo et al., 2015; Arreguín-Rodríguez et al., 2016). Higher temperatures increase the metabolic rates of heterotroph organisms such as planktonic and benthic foraminifera, requiring a higher nutrient intake (e.g., John et al., 2013; Laws et al., 2000). If the food demand increase is not compensated (e.g., by an increase in primary productivity), it could result in an overall decrease in heterotroph productivity (Boscolo Galazzo et al., 2014). Additionally, increased respiration rates throughout the water column may have contributed to decreasing organic carbon reaching the seafloor. Oligotrophic settings are more likely to display this mechanism and register lower benthic and planktonic foraminifera ARs across a warming period, as nutrient availability is already low and primary productivity is not able to cope with the increasing demand. This mechanism has been suggested for oligotrophic Site 1263 (Boscolo Galazzo et al., 2015), where low BFARs and CFARs are recorded during the MECO peak and might also explain the decreased BFARs and CFARs recorded at Site 702.

Our records show low CFARs values between 74.77 and 71.63 mbsf, coinciding with the duration of the MECO $\delta^{18}O_{bulk}$ excursion (Figure 3). Similarly, BFAR shows relatively low values from 74.42 mbsf upward, but it is between 72.72 mbsf and 70.58 where minimum values are reached. This period of low BFARs overlaps with the highest isotopic excursion rate of the $\delta^{18}O_{benthic}$ record (−0.74‰ in 1.86 m), during the later stage of MECO warming. Hence, CFAR and BFAR values at Site 702 seem to be coupled with $\delta^{18}O_{bulk}$ and $\delta^{18}O_{benthic}$ excursions, respectively, happening first in surface waters (CFAR values start to decrease at 74.77 mbsf) and right after in the deep sea (BFAR decreasing at 74.42 mbsf).

BFARs have been largely used as a proxy for delivery of organic matter to the seafloor (e.g., Diester-Haass & Faul, 2019). Low BFARs values have been recorded across MECO warming at Site 702 (this study) and during MECO peak conditions at Site 1263 (Boscolo Galazzo et al., 2015), suggesting less organic matter arriving to the seafloor in oligo-mesotrophic settings. This mechanism could have played a significant role as a positive feedback in the ocean carbon budget in the short term. If export productivity decreased during MECO warming (as reported by low CFARs) and less organic matter arrived at the seafloor (as reported by low BFARs), the organic carbon pump was likely less efficient during this warming period. As a consequence, less organic carbon was being buried at the seafloor (Diester-Haass & Faul, 2019); hence, this oceanic region would have been less efficient or slower taking up carbon from the atmosphere and favoring CO_2 accumulation in the ocean during warming. Although this mechanism accounts for the observed faunal changes at Sites 702 and 1263 and the decreased export productivity registered at Equatorial Atlantic ODP Site 959 (Cramwinckel et al., 2019), it does not apply to eutrophic settings (e.g., Site 1051, North Atlantic Ocean) where BFARs and CFARs increased during MECO peak conditions (Moebius et al., 2015). Further AR estimates, accompanied by revised sedimentation rates (calculated with robust age models), are needed to accurately assess foraminiferal ARs and their role in the ocean organic carbon budget during MECO warming.

5.5. Disentangling MECO Environmental Signal

Carbon stable isotopes have been challenging to interpret across the MECO due to the different trends revealed at several sites (Bohaty et al., 2009). At Site 702, the $\delta^{13}C_{bulk}$ record shows similarities with the $\delta^{18}O_{bulk}$ trend, in particular the three-peaked values at 72.15, 71.70, and 71 mbsf (Figure 3). This suggests a correlated mechanism during peak conditions for both isotope records, as shown by cross-plot linear regressions (Figure S4). Interestingly, a positive $\delta^{13}C_{bulk}$ excursion happening before the MECO OIE overlaps with the main shifts recorded in the benthic fauna. The start of the positive $\delta^{13}C_{bulk}$ excursion at 78.35 mbsf coincides with decreasing diversity of benthic assemblages (78.26 mbsf) (Figure 3). These shifts predate by 1.76 m (~150 Kyr) the start of the $\delta^{18}O_{bulk}$ excursion, which has traditionally marked the start of the MECO event. Sharp abundance increases of PET benthic taxa (Subcluster A1) as well as even lower diversity values are particularly noticeable between 76.86 and 72.46 mbsf, a period across which $\delta^{13}C_{bulk}$ reach higher values (Figure 2). As discussed in section 5.2, this period is likely associated with a change in the flux of organic matter, especially between 76.45–75.26 and 73.83–72.46 mbsf, which significantly affected the benthos (low diversity, high dominance, and maximum abundance of Subcluster A1). The relative and absolute abundance of *B. elongata* (main component of Subcluster B2) decrease across these two intervals (Figures 4 and 5) and its maximum length values decrease (Figure 4), suggesting that this species (and

likely the other species from Subcluster B2) was disadvantaged by changes in the type of food supply to the seafloor. Our results document that the significant ecological changes recorded by the benthic foraminifera assemblages, occurring ~150 Kyr before the start of the OIE, are coupled with a positive CIE. Carbon isotopic changes are hence likely related to changes in the organic carbon flux to the seafloor, as evidenced by benthic assemblages.

Regarding the oxygen isotope signal, warming started synchronously in both surface and bottom waters, similarly to Site 1263 records (Boscolo Galazzo et al., 2014) but contrasting with data at Site 738, where warming is recorded earlier at the bottom than at the surface (Bohaty et al., 2009). The extent of warming during MECO peak conditions appears to have lasted longer in surface waters than in the deep sea in the Indian sector of Southern Ocean Site 738 (Bohaty et al., 2009). Instead, our O isotope records from Site 702 show tightly coupled variations in bulk and benthic values across MECO peak conditions (Figure 3), suggesting a similar warming pace in both surface and bottom waters, mirroring the records at Site 1263 (Boscolo Galazzo et al., 2014). Environmental effects of the MECO at Site 702 were more similar to low latitude Atlantic Sites (Site 1263) than other sites at similar latitudes (e.g., Site 738) in the Southern Ocean (Indian sector). Calcareous nannofossil data support this hypothesis, suggesting that Site 702 temporarily became part of the low-middle latitude domain during the MECO. High-resolution records at other southern high latitude sites are needed to verify if warming started earlier in bottom waters in the western part of the Southern Ocean and to assess the duration of MECO peak conditions in surface and bottom waters.

6. Conclusions

New high-resolution carbon and oxygen isotopic records in bulk carbonate and monospecific benthic foraminifera at ODP Site 702 yield a ~300 Kyr duration of the MECO event in the South Atlantic. The mechanisms driving coupled changes in $\delta^{18}O$ and $\delta^{13}C$ isotope values were weaker or absent before and after the event according to linear regression analysis of the $\delta^{18}O$ versus $\delta^{13}C$ cross-plots.

We document the expansion of warm and temperate calcareous nannofossil taxa toward higher latitudes during the MECO at Site 702, suggesting a strong global teleconnection between these different biogeographical areas. In the deep sea, changes in the benthic fauna predate by ~150 Kyr the start of the warming and correlate with a positive $\delta^{13}C$ excursion, pointing to a change in the type of organic matter reaching the seafloor prior to MECO warming. Planktonic and BFARs decline during warming, which could have act as a positive feedback during MECO warming due to decreased export productivity and decreased organic carbon burial at Site 702 and other ocean oligotrophic ocean settings.

Acknowledgments
We thank M. Cramwinckel, V. Luciani, and Associate Editor P. Lippert for their thoughtful comments that helped improving this manuscript. We also thank Henning and his team for isotope analyses at MARUM, Holger and Alex for sampling assistance at BCR, and Cristina for SEM imaging at Servicio General de Apoyo a la Investigación-SAI, Universidad de Zaragoza. Samples and data used in this research were provided by the International Ocean Discovery Program (IODP), which is sponsored by the U.S. National Science Foundation (NSF) and participating countries. L. R. C. and L. A. financial support provided by the Spanish Ministry of Economy and Competitiveness (Project CGL 2017-84693-R), IUCA (Instituto Universitario de Investigación en Ciencias Ambientales de Aragón), and Aragon government (Reference Group E33_17R) co-financed with Feder 2014-2020 "Building Europe from Aragon." E. D. and T. W. are supported by the Deutsche Forschungsgemeinschaft DFG Grants DA 1757/2-1 and WE 5479/3. Data reported are tabulated in the supporting information and archived in Pangaea database (https://doi.org/10.1594/PANGAEA.908747). This research is part of the PhD thesis of the first author.

References

Agnini, C., Fornaciari, E., Raffi, I., Catanzariti, R., Pälike, H., Backman, J., & Rio, D. (2014). Biozonation and biochronology of Paleogene calcareous nannofossils from low and middle latitudes. *Newsletters on Stratigraphy*, *47*(2), 131–181. https://doi.org/10.1127/0078-0421/2014/0042

Agnini, C., Fornaciari, E., Rio, D., Tateo, F., Backman, J., & Giusberti, L. (2007). Responses of calcareous nannofossil assemblages, mineralogy and geochemistry to the environmental perturbations across the Paleocene/Eocene boundary in the Venetian Pre-Alps. *Marine Micropaleontology*, *63*(1–2), 19–38. https://doi.org/10.1016/j.marmicro.2006.10.002

Agnini, C., Muttoni, G., Kent, D. V., & Rio, D. (2006). Eocene biostratigraphy and magnetic stratigraphy from Possagno, Italy: The calcareous nannofossil response to climate variability. *Earth and Planetary Science Letters*, *241*(3–4), 815–830. https://doi.org/10.1016/j.epsl.2005.11.005

Agnini, C., Spofforth, D. J. A., Dickens, G. R., Rio, D., Pälike, H., Backman, J., et al. (2016). Stable isotope and calcareous nannofossil assemblage record of the late Paleocene and early Eocene (Cicogna section). *Climate of the Past*, *12*(4), 883–909. https://doi.org/10.5194/cp-12-883-2016

Alegret, L., Ortiz, S., Arreguín-Rodríguez, G. J., Monechi, S., Millán, I., & Molina, E. (2016). Microfossil turnover across the uppermost Danian at Caravaca, Spain: Paleoenvironmental inferences and identification of the latest Danian event. *Palaeogeography, Palaeoclimatology, Palaeoecology*, *463*, 45–59. https://doi.org/10.1016/j.palaeo.2016.09.013

Alegret, L., Ortiz, S., & Molina, E. (2009). Extinction and recovery of benthic foraminifera across the Paleocene–Eocene Thermal Maximum at the Alamedilla section (Southern Spain). *Palaeogeography, Palaeoclimatology, Palaeoecology*, *279*(3–4), 186–200. https://doi.org/10.1016/j.palaeo.2009.05.009

Alegret, L., Ortiz, S., Orue-Etxebarria, X., Bernaola, G., Baceta, J. I., Monechi, S., et al. (2009). The Paleocene-Eocene Thermal Maximum: New data on microfossil turnover at the Zumaia Section, Spain. *PALAIOS*, *24*(5), 318–328. https://doi.org/10.2110/palo.2008.p08-057r

Alegret, L., Reolid, M., & Vega Pérez, M. (2018). Environmental instability during the latest Paleocene at Zumaia (Basque-Cantabric Basin): The bellwether of the Paleocene-Eocene Thermal Maximum. *Palaeogeography, Palaeoclimatology, Palaeoecology*, *497*, 186–200. https://doi.org/10.1016/j.palaeo.2018.02.018

Arndt, S., Jørgensen, B. B., LaRowe, D. E., Middelburg, J. J., Pancost, R. D., & Regnier, P. (2013). Quantifying the degradation of organic matter in marine sediments: A review and synthesis. *Earth-Science Reviews*, *123*, 53–86. https://doi.org/10.1016/j.earscirev.2013.02.008

Arreguín-Rodríguez, G. J., & Alegret, L. (2016). Deep-sea benthic foraminiferal turnover across early Eocene hyperthermal events at Northeast Atlantic DSDP Site 550. *Palaeogeography, Palaeoclimatology, Palaeoecology*, *451*, 62–72. https://doi.org/10.1016/j.palaeo.2016.03.010

Arreguín-Rodríguez, G. J., Alegret, L., & Thomas, E. (2016). Late Paleocene-middle Eocene benthic foraminifera on a Pacific seamount (Allison Guyot, ODP Site 865): Greenhouse climate and superimposed hyperthermal events: Benthic Foraminifera on Pacific seamount. *Paleoceanography*, *31*(3), 346–364. https://doi.org/10.1002/2015PA002837

Arreguín-Rodríguez, G. J., Thomas, E., D'haenens, S., Speijer, R. P., & Alegret, L. (2018). Early Eocene deep-sea benthic foraminiferal faunas: Recovery from the Paleocene Eocene Thermal Maximum extinction in a greenhouse world. *PLoS ONE*, *13*(2), e0193167. https://doi.org/10.1371/journal.pone.0193167

Aubry, M.-P. (1992). Late Paleogene calcareous nannoplankton evolution: A tale of climatic deterioration. In D. R. Prothero & W. A. Berggren (Eds.), *Eocene-Oligocene climatic and biotic evolution* (pp. 272–309). New Jersey: Princeton University Press. https://doi.org/10.1515/9781400862924.272

Aubry, M.-P. (1998). Early Paleogene calcareous nannoplankton evolution: A tale of climatic amelioration. In M.-P. Aubry, S. G. Lucas, & W. A. Berggren (Eds.), *Late Paleocene–early Eocene biotic and climatic events in the marine and terrestrial records* (pp. 158–201). New York: Columbia University Press.

Backman, J. (1987). Quantitative calcareous nannofossil biochronology of Middle Eocene through Early Oligocene sediment from DSDP Sites 522 and 523. In *Abhandlungen der Geologischen Bundesanstalt* (Vol. 39, pp. 21–31).

Backman, J., & Shackleton, N. J. (1983). Quantitative biochronology of Pliocene and early Pleistocene calcareous nannoplankton from the Atlantic, Indian and Pacific Oceans. *Marine Micropaleontology*, *8*, 141–170. https://doi.org/10.1016/0377-8398(83)90009-9

Berggren, W. A., & Aubry, M.-P. (1984). Rb-Sr glauconite isochron of the Eocene Castle Hayne Limestone, North Carolina: Further discussion. *Geological Society of America Bulletin*, *95*, 364–370. https://doi.org/10.1130/0016-7606(1984)95<364:rgiote>2.0.co;2

Berggren, W. A., & Pearson, P. N. (2005). A revised tropical to subtropical Paleogene planktonic foraminiferal zonation. *The Journal of Foraminiferal Research*, *35*(4), 279–298. https://doi.org/10.2113/35.4.279

Bijl, P. K., Houben, A. J. P., Schouten, S., Bohaty, S. M., Sluijs, A., Reichart, G.-J., et al. (2010). Transient Middle Eocene Atmospheric CO_2 and Temperature Variations. *Science*, *330*(6005), 819–821. https://doi.org/10.1126/science.1192534

Bohaty, S. M., & Zachos, J. C. (2003). Significant Southern Ocean warming event in the late middle Eocene. *Geology*, *31*(11), 1017–1020. https://doi.org/10.1130/G19800.1

Bohaty, S. M., Zachos, J. C., Florindo, F., & Delaney, M. L. (2009). Coupled greenhouse warming and deep-sea acidification in the middle Eocene. *Paleoceanography*, *24*(2), PA2207. https://doi.org/10.1029/2008PA001676

Bornmalm, L. (1997). *Taxonomy and paleoecology of late Neogene benthic foraminifera from the Caribbean Sea and eastern equatorial Pacific Ocean*. Oslo: Scandinavian Univ. Press.

Boscolo Galazzo, F., Giusberti, L., Luciani, V., & Thomas, E. (2013). Paleoenvironmental changes during the Middle Eocene Climatic Optimum (MECO) and its aftermath: The benthic foraminiferal record from the Alano section (NE Italy). *Palaeogeography, Palaeoclimatology, Palaeoecology*, *378*, 22–35. https://doi.org/10.1016/j.palaeo.2013.03.018

Boscolo Galazzo, F., Thomas, E., Pagani, M., Warren, C., Luciani, V., & Giusberti, L. (2014). The middle Eocene climatic optimum (MECO): A multiproxy record of paleoceanographic changes in the southeast Atlantic (ODP Site 1263, Walvis Ridge): MECO repercussions in the SE Atlantic. *Paleoceanography*, *29*(12), 1143–1161. https://doi.org/10.1002/2014PA002670

Bown, P., & Young, J. (1998). Techniques. In P. R. Bown (Ed.), *Calcareous nannofossil biostratigraphy* (pp. 16–28). Cambridge: Chapman & Hall.

Bralower, T. J. (2002). Evidence of surface water oligotrophy during the Paleocene-Eocene thermal maximum: Nannofossil assemblage data from Ocean Drilling Program Site 690, Maud Rise, Weddell Sea. *Paleoceanography*, *17*(2), 1029–1042. https://doi.org/10.1029/2001PA000662

Bukry, D. (1973). Low-latitude coccolith biostratigraphic zonation. In N. T. Edgar, & J. B. Saunders (Eds.), *Proceedings of the Ocean Drilling Program, Initial Reports* (Vol. 15, pp. 685–703). College Station, Texas: Ocean Drilling Program. https://doi.org/10.2973/dsdp.proc.15.1973

Ciesielski, P. F., & Kristoffersen, Y. (1988). *Proceedings of the Ocean Drilling Program, Initial Reports* (Vol. 114). College Station, Texas: Ocean Drilling Program.

Ciesielski, P. F., & Kristoffersen, Y. (1991). *Proceedings of the Ocean Drilling Program, Scientific Results* (Vol. 114). College Station, Texas: Ocean Drilling Program.

Clement, B. M., & Hailwood, E. A. (1991). Magnetostratigraphy of sediments from Sites 701 and 702. In P. F. Ciesielski, & Y. Kristoffersen (Eds.), *Proceedings of the Ocean Drilling Program, Scientific Results* (Vol. 114, pp. 359–366). https://doi.org/10.2973/odp.proc.sr.114.1991

Corliss, B. H. (1991). Morphology and microhabitat preferences of benthic foraminifera from the northwest Atlantic Ocean. *Marine Micropaleontology*, *17*(3–4), 195–236. https://doi.org/10.1016/0377-8398(91)90014-W

Corliss, B. H., & Chen, C. (1988). Morphotype patterns of Norwegian Sea deep-sea benthic foraminifera and ecological implications. *Geology*, *16*(8), 716–719. https://doi.org/10.1130/0091-7613

Cramwinckel, M. J., van der Ploeg, R., Bijl, P. K., Peterse, F., Bohaty, S. M., Röhl, U., et al. (2019). Harmful algae and export production collapse in the equatorial Atlantic during the zenith of Middle Eocene Climatic Optimum warmth. *Geology*, *47*, 247–250. https://doi.org/10.1130/G45614.1

Deprez, A., Jehle, S., Bornemann, A., & Speijer, R. P. (2017). Differential response at the seafloor during Palaeocene and Eocene ocean warming events at Walvis Ridge, Atlantic Ocean (ODP Site 1262). *Terra Nova*, *29*(1), 71–76. https://doi.org/10.1111/ter.12250

D'haenens, S., Bornemann, A., Stassen, P., & Speijer, R. P. (2012). Multiple early Eocene benthic foraminiferal assemblage and δ13C fluctuations at DSDP Site 401 (Bay of Biscay—NE Atlantic). *Marine Micropaleontology*, *88–89*, 15–35. https://doi.org/10.1016/j.marmicro.2012.02.006

Dickens, G. R., Castillo, M. M., & Walker, J. C. G. (1997). A blast of gas in the latest Paleocene: Simulating first-order effects of massive dissociation of oceanic methane hydrate. *Geology*, *25*(3), 259–262. https://doi.org/10.1130/0091-7613(1997)025%3C0259:ABOGIT%3E2.3.CO;2

Diester-Haass, L. (1995). Middle Eocene to early Oligocene paleoceanography of the Antarctic Ocean (Maud Rise, ODP Leg 113, Site 689): Change from a low to a high productivity ocean. *Palaeogeography, Palaeoclimatology, Palaeoecology*, *113*(2–4), 311–334. https://doi.org/10.1016/0031-0182(95)00067-V

Diester-Haass, L., & Faul, K. (2019). Paleoproductivity reconstructions for the Paleogene Southern Ocean: A direct comparison of geochemical and micropaleontological proxies. *Paleoceanography and Paleoclimatology*. https://doi.org/10.1029/2018PA003384

Edgar, K. M., Wilson, P. A., Sexton, P. F., Gibbs, S. J., Roberts, A. P., & Norris, R. D. (2010). New biostratigraphic, magnetostratigraphic and isotopic insights into the Middle Eocene Climatic Optimum in low latitudes. *Palaeogeography, Palaeoclimatology, Palaeoecology*, *297*(3–4), 670–682. https://doi.org/10.1016/j.palaeo.2010.09.016

Edgar, K. M., Wilson, P. A., Sexton, P. F., & Suganuma, Y. (2007). No extreme bipolar glaciation during the main Eocene calcite compensation shift. *Nature*, *448*(7156), 908–911. https://doi.org/10.1038/nature06053

Fisher, R. (1953). Dispersion on a sphere. *Proceedings of the Royal Society A: Mathematical, Physical and Engineering Sciences*, *217*(1130), 295–305. https://doi.org/10.1098/rspa.1953.0064

Fontanier, C., Jorissen, F. J., Licari, L., Alexandre, A., Anschutz, P., & Carbonel, P. (2002). Live benthic foraminiferal faunas from the Bay of Biscay: Faunal density, composition, and microhabitats. *Deep Sea Research Part I: Oceanographic Research Papers*, *49*(4), 751–785. https://doi.org/10.1016/S0967-0637(01)00078-4

Fornaciari, E., Agnini, C., Catanzariti, R., Rio, D., Bolla, E. M., & Valvasoni, E. (2010). Mid-Latitude calcareous nannofossil biostratigraphy and biochronology across the middle to late Eocene transition. *Stratigraphy*, *7*, 229–264. EID: 2-s2.0-79953076907

Galazzo, F. B., Thomas, E., & Giusberti, L. (2015). Benthic foraminiferal response to the Middle Eocene Climatic Optimum (MECO) in the South-Eastern Atlantic (ODP Site 1263). *Palaeogeography, Palaeoclimatology, Palaeoecology*, *417*, 432–444. https://doi.org/10.1016/j.palaeo.2014.10.004

Gibbs, S., Shackleton, N., & Young, J. (2004). Orbitally forced climate signals in mid-Pliocene nannofossil assemblages. *Marine Micropaleontology*, *51*(1–2), 39–56. https://doi.org/10.1016/j.marmicro.2003.09.002

Giorgioni, M., Jovane, L., Rego, E. S., Rodelli, D., Frontalini, F., Coccioni, R., et al. (2019). Carbon cycle instability and orbital forcing during the Middle Eocene Climatic Optimum. *Scientific Reports*, *9*(1), 9357. https://doi.org/10.1038/s41598-019-45763-2

Gooday, A. J. (2003). Benthic foraminifera (protista) as tools in deep-water palaeoceanography: Environmental influences on faunal characteristics. *Advances in Marine Biology*, *46*. https://doi.org/10.1016/S0065-2881(03)46002-1

Gooday, A. J., & Rathburn, A. E. (1999). Temporal variability in living deep-sea benthic foraminifera: A review. *Earth-Science Reviews*, *46*(1–4), 187–212. https://doi.org/10.1016/S0012-8252(99)00010-0

Gordon, A. L., Georgi, D. T., & Taylor, H. W. (1977). Antarctic polar front zone in the Western Scotia Sea—Summer 1975. *Journal of Physical Oceanography*, *7*, 309–328. https://doi.org/10.1175/1520-0485(1977)007<0309:apfzit>2.0.co;2

Gradstein, F. M., Ogg, J. G., Schmitz, M., & Ogg, G. (2012). *The geologic time Scale 2012 2-Volume set*. Elsevier Science. https://doi.org/10.1016/C2011-1-08249-8

Gross, O. (2000). Influence of temperature, oxygen and food availability on the migrational activity of bathyal benthic foraminifera: Evidence by microcosm experiments. In G. Liebezeit, S. Dittmann, & I. Kröncke (Eds.), *Life at interfaces and under extreme conditions* (pp. 123–137). Dordrecht: Springer Netherlands. https://doi.org/10.1007/978-94-011-4148-2_12

Hammer, Ø., & Harper, D. (2005). *Paleontological data analysis*. Oxford: Blackwell Publishing.

Hammer, Ø., Harper, D. A. T., & Ryan, P. D. (2001). PAST: Paleontological statistics software package for education and data analysis. *Paleontologia Electronica*, *4*(1), 9. https://palaeo-electronica.org/2001_1/past/issue1_01.htm

Haq, B. U., & Lohmann, G. P. (1976). Early Cenozoic calcareous nannoplankton biogeography of the Atlantic Ocean. *Marine Micropaleontology*, *51*, 119–194. https://doi.org/10.1016/0377-8398(76)90008-6

Haq, B. U., Premoli-Silva, I., & Lohmann, G. P. (1977). Calcareous plankton paleobiogeographic evidence for major climatic fluctuations in the early Cenozoic Atlantic Ocean. *Journal of Geophysical Research*, *82*(27), 3861–3876. https://doi.org/10.1029/JC082i027p03861

Haq, B. U., Lohmann, G. P., & Sherwood, W. W. Jr. (1977). Calcareous nannoplankton biogeography and its paleoclimate implications: Cenozoic of the Falkland Plateau (DSDP Leg 36) and Miocene of the Atlantic Ocean. In P. F. Barker & I. W. D. Dalziel (Eds.), *Proceedings of the Ocean Drilling Program, Scientific Results* (Chap. 14, Vol. 36). College Station, Texas: Ocean Drilling Program. https://doi.org/10.2973/dsdp.proc.36.1977

Hayward, B. W., Kawagata, S., Sabaa, A., Grenfell, H., Van Kerckhoven, L., Johnson, K., & Thomas, E. (2012). *The last global extinction (Mid-Pleistocene) of deep-sea benthic foraminifera (Chrysalogoniidae, Ellipsoidinidae, Glandulonodosariidae, Plectofrondicularіidae, Pleurostomellidae, Stilostomellidae), their Late Cretaceous-Cenozoic history and taxonomy* (Vol. 43). Cushman Foundation for Foraminiferal Research Special Publication.

Herguera, J. C., & Berger, W. H. (1991). Paleoproductivity from benthic foraminifera abundance: Glacial to postglacial change in the west-equatorial Pacific. *Geology*, *19*, 1173–1176. https://doi.org/10.1130/0091-7613(1991)019<1173:PFBFAG>2.3.CO;2

Hilting, A. K., Kump, L. R., & Bralower, T. J. (2008). Variations in the oceanic vertical carbon isotope gradient and their implications for the Paleocene-Eocene biological pump. *Paleoceanography*, *23*(3). https://doi.org/10.1029/2007PA001458

Holbourn, A., Henderson, A. S., & MacLeod, N. (2013). *Atlas of benthic foraminifera*. Natural History Museum, London: Wiley-Blackwell.

Ivany, L. C., Lohmann, K. C., Hasiuk, F., Blake, D. B., Glass, A., Aronson, R. B., & Moody, R. M. (2008). Eocene climate record of a high southern latitude continental shelf: Seymour Island, Antarctica. *Geological Society of America Bulletin*, *120*(5–6), 659–678. https://doi.org/10.1130/B26269.1

John, E. H., Pearson, P. N., Coxall, H. K., Birch, H., Wade, B. S., & Foster, G. L. (2013). Warm ocean processes and carbon cycling in the Eocene. *Philosophical Transactions of the Royal Society A: Mathematical, Physical and Engineering Sciences*, *371*(2001), 20130099–20130099. https://doi.org/10.1098/rsta.2013.0099

Jones, R. W., & Charnock, M. A. (1985). "Morphogroups" of agglutinated foraminifera. Their life positions and feeding habits and potential applicability in (paleo)ecological studies. *Revue de Paléobiologie*, *4*(2), 311–320.

Jorissen, F. J. (1999). Benthic foraminiferal microhabitats below the sediment-water interface. In B. K. Sen Gupta (Ed.), *Modern foraminifera* (pp. 161–179). Dordrecht: Springer Netherlands. https://doi.org/10.1007/0-306-48104-9_10

Jorissen, F. J., de Stigter, H. C., & Widmark, J. G. (1995). A conceptual model explaining benthic foraminiferal microhabitats. *Marine Micropaleontology*, *26*(1–4), 3–15. https://doi.org/10.1016/0377-8398(95)00047-X

Jorissen, F. J., Fontanier, C., & Thomas, E. (2007). Chapter seven: Paleoceanographical proxies based on deep-sea benthic foraminiferal assemblage characteristics. In *Developments in marine geology* (Vol. 1, pp. 263–325). Elsevier. https://doi.org/10.1016/S1572-5480(07)01012-3

Jovane, L., Florindo, F., Coccioni, R., Dinares-Turell, J., Marsili, A., Monechi, S., et al. (2007). The middle Eocene climatic optimum event in the Contessa Highway section, Umbrian Apennines, Italy. *Geological Society of America Bulletin*, *119*(3–4), 413–427. https://doi.org/10.1130/B25917.1

Kelly, D. C., Bralower, T. J., Zachos, J. C., Silva, I. P., & Thomas, E. (1996). Rapid diversification of planktonic foraminifera in the tropical Pacific (ODP Site 865) during the late Paleocene thermal maximum. *Geology*, *24*, 423–426. https://doi.org/10.1130/0091-7613(1996)024<0423:RDOPFI>2.3.CO;2

Kirschvink, J. L. (1980). The least-squares line and plane and the analysis of palaeomagnetic data. *Geophysical Journal International*, *62*(3), 699–718. https://doi.org/10.1111/j.1365-246X.1980.tb02601.x

Laskar, J., Fienga, A., Gastineau, M., & Manche, H. (2011). La2010: A new orbital solution for the long term motion of the Earth. *Astronomy & Astrophysics*, *532*, A89. https://doi.org/10.1051/0004-6361/201116836

Lauretano, V., Littler, K., Polling, M., Zachos, J. C., & Lourens, L. J. (2015). Frequency, magnitude and character of hyperthermal events at the onset of the Early Eocene Climatic Optimum. *Climate of the Past*, *11*(10), 1313–1324. https://doi.org/10.5194/cp-11-1313-2015

Lauretano, V., Zachos, J. C., & Lourens, L. J. (2018). Orbitally paced carbon and deep-sea temperature changes at the peak of the early Eocene climatic optimum. *Paleoceanography and Paleoclimatology*, *33*, 1050–1065. https://doi.org/10.1029/2018PA003422

Laws, E. A., Falkowski, P. G., Smith, W. O., Ducklow, H., & McCarthy, J. J. (2000). Temperature effects on export production in the open ocean. *Global Biogeochemical Cycles*, *14*, 1231–1246. https://doi.org/10.1029/1999GB001229

Loeblich, A. R. Jr., & Tappan, H. (1987). *Foraminiferal genera and their classification* (Vol. 1-2). Van Nostrand Reinhold Company.

Luciani, V., Giusberti, L., Agnini, C., Fornaciari, E., Rio, D., Spofforth, D. J. A., & Pälike, H. (2010). Ecological and evolutionary response of Tethyan planktonic foraminifera to the middle Eocene climatic optimum (MECO) from the Alano section (NE Italy). *Palaeogeography, Palaeoclimatology, Palaeoecology*, *292*, 82–95. https://doi.org/10.1016/j.palaeo.2010.03.029

Lurcock, P. C., & Wilson, G. S. (2012). PuffinPlot: A versatile, user-friendly program for paleomagnetic analysis. *Geochemistry, Geophysics, Geosystems*, *13*, 1–6. https://doi.org/10.1029/2012GC004098

Lyle, M., Lyle, A. O., Backman, J., & Tripati, A. K. (2005). Biogenic sedimentation in the Eocene equatorial Pacific—The stuttering greenhouse and Eocene carbonate compensation depth. *Proceedings. Ocean Drilling Program. Scientific Results*, *199*, 1–35. https://doi.org/10.2973/odp.proc.sr.199.219.2005

Marino, M., & Flores, J.-A. (2002). Data report: Calcareous nannofossil data from the Eocene to Oligocene, Leg 177, Hole 1090B. In R. Gersonde, D. A. Hodell, & P. Blum (Eds.), *Proceedings of the Ocean Drilling Program, Scientific Results* (Chap. 8, Vol. 177). College Station, Texas: Ocean Drilling Program. https://doi.org/10.2973/odp.proc.sr.177.2003

Martini, E. (1971). Standard Tertiary and Quaternary calcareous nannoplankton zonation. In *Paper presented at 2nd International Conference Planktonic Microfossils, Rome, Italy* (pp. 739–785).

McFadden, P. L., & Reid, A. B. (1982). Analysis of palaeomagnetic inclination data. *Geophysical Journal International*, *69*, 307–319. https://doi.org/10.1111/j.1365-246X.1982.tb04950.x

Miller, K. G., Fairbanks, R. G., & Mountain, G. S. (1987). Tertiary oxygen isotope synthesis, sea level history, and continental margin erosion. *Paleoceanography*, *2*(1), 1–19. https://doi.org/10.1029/PA002i001p00001

Moebius, I., Friedrich, O., Edgar, K. M., & Sexton, P. F. (2015). Episodes of intensified biological productivity in the subtropical Atlantic Ocean during the termination of the Middle Eocene Climatic Optimum (MECO): Intensified productivity during the MECO. *Paleoceanography*, *30*(8), 1041–1058. https://doi.org/10.1002/2014PA002673

Moebius, I., Friedrich, O., & Scher, H. D. (2014). Changes in Southern Ocean bottom water environments associated with the Middle Eocene Climatic Optimum (MECO). *Palaeogeography, Palaeoclimatology, Palaeoecology*, *405*, 16–27. https://doi.org/10.1016/j.palaeo.2014.04.004

Mullender, T. A. T., Frederichs, T., Hilgenfeldt, C., de Groot, L. V., Fabian, K., & Dekkers, M. J. (2016). Automated paleomagnetic and rock magnetic data acquisition with an in-line horizontal "2G" system. *Geochemistry, Geophysics, Geosystems*, *17*, 1–14. https://doi.org/10.1002/2016GC006436

Müller-Merz, E., & Oberhänsli, H. (1991). Eocene bathyal and abyssal benthic foraminifera from a South Atlantic transect at 20–30 S. *Palaeogeography, Palaeoclimatology, Palaeoecology*, *83*(1–3), 117–171. https://doi.org/10.1016/0031-0182(91)90078-6

Murray, J. W. (1991). *Ecology and paleoecology of benthic foraminifera*. Longman.

Murray, J. W. (2006). *Ecology and applications of benthic foraminifera*. Cambridge University Press.

Okada, H., & Bukry, D. (1980). Supplementary modification and introduction of code numbers to the low-latitude coccolith biostratigraphic zonation (Bukry, 1973; 1975). *Marine Micropaleontology*, *5*, 321–325. https://doi.org/10.1016/0377-8398(80)90016-X

Ortiz, S., & Thomas, E. (2006). Lower-middle Eocene benthic foraminifera from the Fortuna section (Betic Cordillera, southeastern Spain). *Micropaleontology*, *52*(2), 97–150. https://doi.org/10.2113/gsmicropal.52.2.97

Pea, L. (2011). *Eocene-Oligocene paleoceanography of the subantarctic South Atlanctic: Calcareous nannofossil reconstructions of temperature, nutrient, and dissolution history*. University of Parma.

Penman, D. E., & Zachos, J. C. (2018). New constraints on massive carbon release and recovery processes during the Paleocene-Eocene Thermal Maximum. *Environmental Research Letters*, *13*(10), 105008. https://doi.org/10.1088/1748-9326/aae285

Perch-Nielsen, K. (1985). Cenozoic calcareous nannofossils. In H. M. Bolli, J. B. Saunders, & K. Perch-Nielsen (Eds.), *Plankton stratigraphy* (pp. 427–554). Cambridge University Press.

Pospichal, J. J., & Wise, S. W. Jr. (1990). Paleocene to middle Eocene calcareous nannofossils of ODP Sites 689 and 690, Maud Rise, Weddell Sea. In *Proceedings of the Ocean Drilling Program, Scientific Results* (Vol. 113, pp. 613–638). College Station, Texas: Ocean Drilling Program.

Reid, J. L., Nowlin, W. D. J., & Patzert, W. C. (1977). On the characteristics and circulation of the Southwestern Atlantic Ocean. *Journal of Physical Oceanography*, *7*, 62–91. https://doi.org/10.1175/1520-0485(1977)007<0062:otcaco>2.0.co;2

Sexton, P. F., Wilson, P. A., & Norris, R. D. (2006). Testing the Cenozoic multisite composite $\delta^{18}O$ and $\delta^{13}C$ curves: New monospecific Eocene records from a single locality, Demerara Rise (Ocean Drilling Program Leg 207). *Paleoceanography*, *21*(2), PA2019. https://doi.org/10.1029/2005PA001253

Sluijs, A., Zeebe, R. E., Bijl, P. K., & Bohaty, S. M. (2013). A middle Eocene carbon cycle conundrum. *Nature Geoscience*, *6*(6), 429–434. https://doi.org/10.1038/ngeo1807

Spofforth, D. J. A., Agnini, C., Pälike, H., Rio, D., Fornaciari, E., Giusberti, L., et al. (2010). Organic carbon burial following the middle Eocene climatic optimum in the central western Tethys. *Paleoceanography*, *25*(3), PA3210. https://doi.org/10.1029/2009PA001738

Stap, L., Lourens, L. J., Thomas, E., Sluijs, A., Bohaty, S., & Zachos, J. C. (2010). High-resolution deep-sea carbon and oxygen isotope records of Eocene Thermal Maximum 2 and H2. *Geology*, *38*, 607–610. https://doi.org/10.1130/G30777.1

Takata, H., Nomura, R., Tsujimoto, A., Khim, B.-K., & Chung, I. K. (2013). Abyssal benthic foraminifera in the eastern equatorial Pacific (IODP EXP 320) during the middle Eocene. *Journal of Paleontology*, *87*(06), 1160–1185. https://doi.org/10.1666/12-107

Tauxe, L., Stickley, C. E., Sugisaki, S., Bijl, P. K., Bohaty, S. M., Brinkhuis, H., et al. (2012). Chronostratigraphic framework for the IODP Expedition 318 cores from the Wilkes Land Margin: Constraints for paleoceanographic reconstruction. *Paleoceanography*, *27*, PA2214. https://doi.org/10.1029/2012PA002308

Thomas, E. (1998). The biogeography of the Late Paleocene benthic foraminiferal extinction. In M. P. Aubry, S. Lucas, & W. A. Berggren (Eds.), *Late Paleocene-Early Eocene biotic and climatic events in the marine and terrestrial records* (pp. 214–243). New York: Columbia University Press.

Thomas, E. (2003). Extinction and food at the seafloor: A high-resolution benthic foraminiferal record across the initial Eocene thermal maximum, Southern Ocean site 690. In *Special Paper 369: Causes and consequences of globally warm climates in the early Paleogene* (Vol. 369, pp. 319–332). Geological Society of America. https://doi.org/10.1130/0-8137-2369-8.319

Thomas, E. (2007). Cenozoic mass extinctions in the deep sea: What perturbs the largest habitat on Earth? In *Special Paper 424: Large Ecosystem Perturbations: Causes and Consequences* (Vol. 424, pp. 1–23). Geological Society of America. Retrieved from http://special-papers.gsapubs.org/cgi/doi/10.1130/2007.2424(01)

Tjalsma, R. C., & Lohmann, G. P. (1983). Paleocene-Eocene bathyal and abyssal benthic foraminifera from the Atlantic Ocean. *Micropaleontology*, Special Edition, *4*, 89.

Toffanin, F., Agnini, C., Rio, D., Acton, G., & Westerhold, T. (2013). Middle Eocene to early Oligocene calcareous nannofossil biostratigraphy at IODP Site U1333 (equatorial Pacific). *Micropaleontology*, *59*, 69–82. https://www.jstor.org/stable/24413317

Toffanin, F., Agnini, C., Fornaciari, E., Rio, D., Giusberti, L., Luciani, V., et al. (2011). Changes in calcareous nannofossil assemblages during the Middle Eocene Climatic Optimum: Clues from the central-western Tethys (Alano section, NE Italy). *Marine Micropaleontology*, *81*(1–2), 22–31. https://doi.org/10.1016/j.marmicro.2011.07.002

Tripati, A. (2005). Deep-sea temperature and circulation changes at the Paleocene-Eocene Thermal Maximum. *Science*, *308*(5730), 1894–1898. https://doi.org/10.1126/science.1109202

Van Morkhoven, F. P. C. M., Berggren, W. A., & Edwards, A. S. (1986). *Cenozoic cosmopolitan deep-water benthic foraminifera*. Elf-Aquitaine.

Villa, G., Fioroni, C., Pea, L., Bohaty, S., & Persico, D. (2008). Middle Eocene–late Oligocene climate variability: Calcareous nannofossil response at Kerguelen Plateau, Site 748. *Marine Micropaleontology*, *69*(2), 173–192. https://doi.org/10.1016/j.marmicro.2008.07.006

Villa, G., Fioroni, C., Persico, D., Roberts, A. P., & Florindo, F. (2014). Middle Eocene to Late Oligocene Antarctic glaciation/deglaciation and Southern Ocean productivity. *Paleoceanography*, *29*(3), 223–237. https://doi.org/10.1002/2013PA002518

Wade, B. S., & Kroon, D. (2002). Middle Eocene regional climate instability: Evidence from the western North Atlantic. *Geology*, *30*, 1011–1014. https://doi.org/10.1130/0091-7613(2002)030<1011:MERCIE>2.0.CO;2

Wei, W., & Thierstein, H. R. (1991). Upper Cretaceous and Cenozoic calcareous nannofossils of the Kerguelen Plateau (South Indian Ocean) and Prydz Bay (East Antarctica). In J. Barron, B. Larsen, et al. (Eds.), *Proceedings of the Ocean Drilling Program, Scientific Results* (Chap. 26, Vol. 119). College Station, Texas: Ocean Drilling Program. https://doi.org/10.2973/odp.proc.sr.119.1991

Wei, W., & Wise, S. W. J. (1989). Paleogene calcareous nannofossil magnetobiochronology: Results from South Atlantic DSDP Site 516. *Marine Micropaleontology*, *14*(1–3), 119–152. https://doi.org/10.1016/0377-8398(89)90034-0

Wei, W., & Wise, S. W. J. (1990). Biogeographic gradients of middle Eocene-Oligocene calcareous nannoplankton in the South Atlantic Ocean. *Palaeogeography, Palaeoclimatology, Palaeoecology*, *79*(1–2), 29–61. https://doi.org/10.1016/0031-0182(90)90104-F

Wei, W., & Wise, S. W. J. (1992). Eocene-Oligocene calcareous nannofossil magnetobiochronology of the Southern Ocean. *Newsletters on Stratigraphy*, *26*(2–3), 119–132. https://doi.org/10.1127/nos/26/1992/119

Westerhold, T., Röhl, U., Donner, B., & Zachos, J. C. (2018). Global extent of Early Eocene hyperthermal events—A new Pacific benthic foraminiferal isotope record from Shatsky Rise (ODP Site 1209). *Paleoceanography and Paleoclimatology*, *33*(6), 626–642. https://doi.org/10.1029/2017PA003306

Westerhold, T., Röhl, U., Frederichs, T., Agnini, C., Raffi, I., Zachos, J. C., & Wilkens, R. H. (2017). Astronomical calibration of the Ypresian timescale: Implications for seafloor spreading rates and the chaotic behavior of the solar system? *Climate of the Past*, *13*, 1129–1152. https://doi.org/10.5194/cp-13-1129-2017

Westerhold, T., Röhl, U., Frederichs, T., Bohaty, S. M., & Zachos, J. C. (2015). Astronomical calibration of the geological timescale: Closing the middle Eocene gap. *Climate of the Past*, *11*(9), 1181–1195. https://doi.org/10.5194/cp-11-1181-2015

Westerhold, T., Röhl, U., Pälike, H., Wilkens, R., Wilson, P. A., & Acton, G. (2014). Orbitally tuned timescale and astronomical forcing in the middle Eocene to early Oligocene. *Climate of the Past*, *10*(3), 955–973. https://doi.org/10.5194/cp-10-955-2014

Zachos, J. C. (2001). Trends, rhythms, and aberrations in global climate 65 Ma to present. *Science*, *292*(5517), 686–693. https://doi.org/10.1126/science.1059412

Zeebe, R. E., & Zachos, J. C. (2013). Long-term legacy of massive carbon input to the Earth system: Anthropocene versus Eocene. *Philosophical Transactions of the Royal Society A: Mathematical, Physical and Engineering Sciences*, *371*, 20120006. https://doi.org/10.1098/rsta.2012.0006

Zijderveld, J. D. A. (1967). A.C. demagnetization of rocks: Analysis of results. In D. W. Collinson, K. M. Creer, & S. K. Runcorn (Eds.), *Methods in paleomagnetism* (pp. 254–286). New York: Elsevier.

4.1 Benthic foraminiferal turnover across Eocene climatic events

4.1.3. Eocene (Bartonian) benthic foraminifera and paleoenvironmental changes in the Western Tethys

Lucía Rivero-Cuesta, Eustoquio Molina & Laia Alegret, 2018

Palaeogeography, Palaeoclimatology, Palaeoecology 503, 102-111

Supplementary material of this article can be found in Appendix IV

Palaeogeography, Palaeoclimatology, Palaeoecology 503 (2018) 102–111

Contents lists available at ScienceDirect

Palaeogeography, Palaeoclimatology, Palaeoecology

journal homepage: www.elsevier.com/locate/palaeo

Eocene (Bartonian) benthic foraminifera and paleoenvironmental changes in the Western Tethys

L. Rivero-Cuesta*, E. Molina, L. Alegret

Departamento de Ciencias de la Tierra & Instituto Universitario de Ciencias Ambientales IUCA, Universidad de Zaragoza, Zaragoza, Spain

ARTICLE INFO

Keywords:
Tethys Ocean
Middle Eocene
Enhanced current activity
Torre Cardela
Betic cordillera
Carbon isotopes

ABSTRACT

The Eocene was a period of intense climate variability and the response of deep-sea biota is still poorly understood, especially across certain understudied intervals from the middle Eocene. We present new benthic foraminiferal data from a Bartonian marine sequence deposited in the western Tethys Ocean (Torre Cardela section, Spain), and determine the biotic and paleoenvironmental turnover. The assemblages indicate a middle to lower bathyal depth of deposition, and they contain allochthonous taxa (e.g. asterigerinids) that were transported from shallower settings. A Detrended Correspondence Analysis (DCA) performed on the total assemblage differentiates the autochthonous and allochthonous taxa, supporting the idea of different provenience. We suggest that the latter were likely transported downslope by currents. Quantitative analyses of the autochthonous assemblages show a strong dominance of calcareous infaunal taxa, mainly bolivinids, which point to a high flux of organic matter to the seafloor. *Bolivinoides crenulata*, the most common species, is associated with inputs of refractory organic matter and high-energy environments. Five intervals were differentiated based on changes in the relative abundance of taxa. Two intervals (B and D) show the highest percentages of allochthonous taxa and *B. crenulata*. We suggest that enhanced current activity not only transported allochthonous taxa, but also brought in refractory organic matter to the seafloor, which was consumed by opportunistic taxa during these two intervals. We conclude that benthic foraminiferal assemblages at Torre Cardela were strongly controlled by the amount and type of organic matter reaching the seafloor, which were in turn affected by sedimentary and, ultimately, by climatic factors.

1. Introduction

The Eocene was a critical time in the Earth's climate evolution during the Cenozoic. This epoch started with a pronounced warming event at the Paleocene-Eocene boundary superimposed on a global greenhouse climate that persisted during the Eocene (Zachos et al., 2008), and a gradual cooling trend is recorded towards the Eocene-Oligocene transition (Coxall et al., 2005). These long-term climatic trends were punctuated by several hyperthermal events, or transient perturbations of the global C cycle associated with global warming (Thomas and Zachos, 2000; Zachos et al., 2010; Kirtland Turner et al., 2014). Most of these events were short-lived (< 200 kyr), but there are records of a longer-lived event named Middle Eocene Climatic Optimum (MECO; (Bohaty and Zachos, 2003; Bohaty et al., 2009; Sluijs et al., 2013). With an estimated duration of ~500 kyr, the MECO entails an increase in atmospheric pCO_2 (Bijl et al., 2010), shoaling of the carbonate compensation depth (Bohaty et al., 2009; Pälike et al., 2012), and a 4–6 °C increase in surface and deep waters (Bohaty and Zachos, 2003; Bohaty et al., 2009; Edgar et al., 2010) at ~40 Ma. The stable isotopic signature of the MECO suggests that the driver mechanism was different from other Eocene hyperthermal events (Bohaty and Zachos, 2003; Lunt et al., 2011; Sluijs et al., 2013), suggesting that the consequences might also have been different.

Benthic foraminifera are one of the most abundant, diverse and widely distributed groups at the seafloor and they are an excellent tool to reconstruct the paleoenvironmental evolution through periods of climate change (Jorissen et al., 2007). Variations in benthic foraminiferal assemblages mainly indicate changes in water depth, organic matter flux to the seafloor, oxygenation and temperature (e.g., Van der Zwaan et al., 1999; Gooday, 2003; Murray, 2006; Van der Zwaan et al., 1999). Many authors consider that the amount, quality and seasonality of the flux of organic matter from the sea surface are key factors controlling the assemblage composition (Gooday, 1994; Loubere, 1998; Den Dulk et al., 2000). Oxygen also plays an important role, being a limiting resource when the flux of organic matter is high (Jorissen et al., 1995). The benthic foraminiferal assemblage turnover across the MECO

* Corresponding author at: Área de Paleontología, Departamento de Ciencias de la Tierra, Universidad de Zaragoza, Pedro Cerbuna 12, 50009 Zaragoza, Spain.
E-mail address: lrivero@unizar.es (L. Rivero-Cuesta).

https://doi.org/10.1016/j.palaeo.2018.05.003
Received 11 January 2018; Received in revised form 24 April 2018; Accepted 1 May 2018
Available online 03 May 2018
0031-0182/

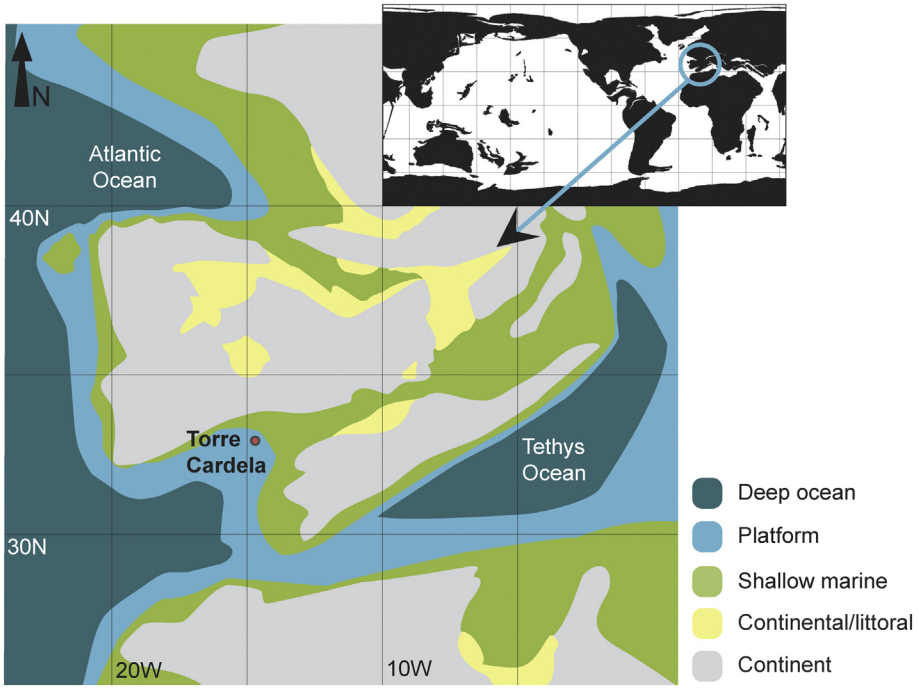

Fig. 1. Paleogeographic reconstruction (40 Ma) showing the location of Torre Cardela section. Modified from ODSN Plate Tectonics Reconstruction Service and Andeweg (2002).

interval has been documented in the Atlantic Ocean (Boscolo Galazzo et al., 2014; Moebius et al., 2015), in the South Indian Ocean (Moebius et al., 2014), in the Equatorial Pacific (Takata et al., 2013) and in the central Tethys Ocean (Boscolo Galazzo et al., 2013). However, further studies in different oceans and latitudes are needed to understand the response of benthic foraminifera to the MECO, to unravel the nature and specifically the aftermath of this event, and to better understand the Eocene climate variability in a global scale.

So far, the Torre Cardela section in the Betic Cordillera (southern Spain, Fig. 1) is the only land-based section from the western Tethys Ocean where the interval immediately following the MECO has been documented (Gonzalvo and Molina, 1996). The stratigraphic continuity, high sedimentation rates and abundance and diversity of foraminiferal tests suggest that this section is appropriate for micropaleontological studies, but the analysis of benthic foraminifera was missing. Here we report on the benthic foraminiferal assemblage changes across the Bartonian in the Torre Cardela section, and determine the paleoenvironmental evolution to evaluate the impact of the variable Eocene climate in this area from the Western Tethys.

2. Geological setting

The Torre Cardela section is located in the southern part of the Iberian Peninsula (coordinates 37° 29′ 02.4″ N, 3° 20′ 43.8″ W). This area lies in the Subbetic realm (External Zones) of the Betic Cordillera, which represents the most occidental edge of the Alpine Orogeny. The studied sedimentary succession belongs to the Cañada Formation, a 500 m-thick sequence of hemipelagic marls with interbedded turbiditic sandstones (Comas, 1978) that was deposited during the Eocene in the western part of the Tethys Ocean (Fig. 1). The Torre Cardela section is a 145 m-thick sequence composed of a rhythmic series of 25 to 35 cm-thick sandy carbonate (calcarenite) layers interbedded with 1 to 20 m-thick grey silty-marly intervals. These levels contain abundant calcareous microfossils that reveal a middle to late Eocene age (Gonzalvo and Molina, 1996). No evidence for bed amalgamation nor any large-scale vertical re-arrangement of beds was observed in the Torre Cardela section, as it did not suffer important tectonic disturbances during the middle Eocene (Andeweg, 2002).

3. Material and methods

3.1. Benthic foraminiferal studies

Quantitative studies of benthic foraminifera were carried out in 25 samples selected from the same set of samples that Gonzalvo and Molina (1996) used to establish the planktonic foraminiferal biozonation at Torre Cardela. All samples were collected from lithologically similar, marly intervals and are evenly distributed throughout the lowermost 100 m of the section (Fig. 2). A standard procedure was followed to extract microfossils: the sediment was disaggregated in water with diluted H_2O_2, washed through a 63 μm sieve and dried at 50 °C. The residue was studied under a binocular microscope, showing that the preservation of benthic foraminiferal tests was variable but in general adequate to detect diagnostic morphological features. Two samples (90 and 92.5) were not suitable for quantitative analysis due to the scarce material available, and they were excluded from the study.

Quantitative analyses of benthic foraminifera were based on representative splits of approximately 300 specimens of the > 63 μm fraction, obtained with a modified Otto micro-splitter. The taxonomic identification of the assemblages follows Loeblich Jr. and Tappan (1987) for genera identification except for uniserial forms, which follows Hayward et al. (2012). Identification to species level was possible in many cases, mainly following Tjalsma and Lohmann (1983), Grünig (1985), Van Morkhoven et al. (1986), Bolli et al. (1994), Alegret and Thomas (2001), Katz et al. (2003), Holbourn et al. (2013), Ortiz and Thomas (2006), Alegret et al. (2008), Fenero et al. (2012) and Arreguín-Rodríguez et al. (2018). Original descriptions of species were checked in the Ellis & Messina Online Catalogue of Foraminifera, and holotype images were obtained from the Smithsonian Paleobiology Collections when available for comparison with our specimens.

The data matrix produced was standardized by converting count data into relative abundance (percentages) for each sample (Supplementary Data 1). In addition, many species were grouped into genera and morphogroups. A total number of 117 taxa (114 calcareous

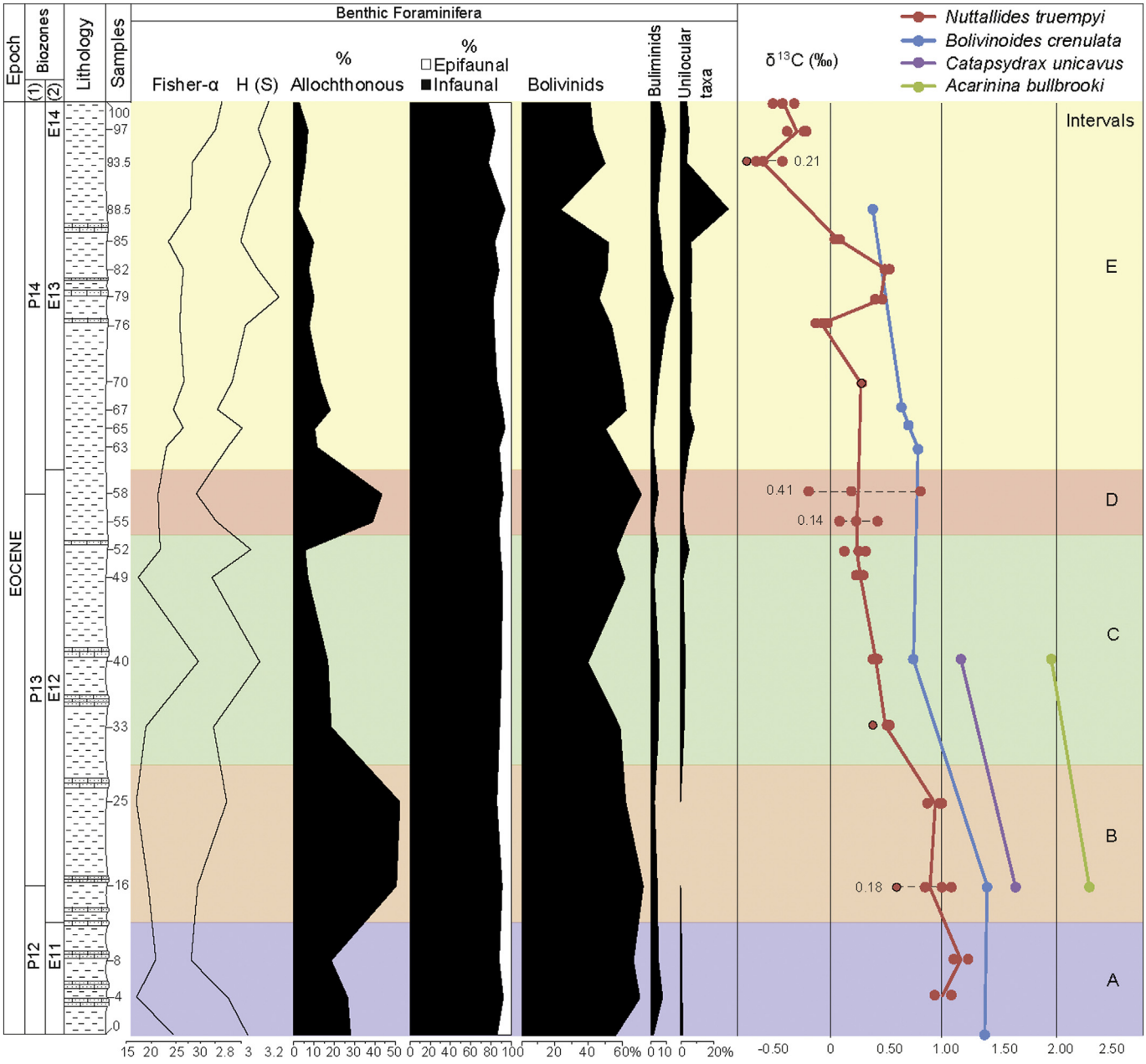

Fig. 2. Benthic foraminiferal indices (based on the autochthonous assemblages only): Fisher-α diversity index, Shannon-Weaver H(S) heterogeneity index, and relative abundance of infaunal morphogroups at the Torre Cardela section. Percentages of significant benthic foraminiferal groups, and species-specific carbon stable isotope data. Dashed lines in the $\delta^{13}C$ data represent standard deviation; red circles with a black ring represent "rusty" specimens (see text). Planktonic foraminiferal biozones (1) Gonzalvo and Molina (1996) and (2) this work. (For interpretation of the references to colour in this figure legend, the reader is referred to the web version of this article.)

and 3 agglutinated) were identified, and the relevant and best-preserved specimens are illustrated in Fig. 3. The images were obtained by SEM (scanning electron microscope) imaging at the University of Zaragoza. Due to the high number of species identified, Fig. 4 only includes species whose relative abundance is higher than 1% in at least one sample.

Morphogroup analysis was performed, and the most probable microhabitat preferences and environmental parameters (bottom water oxygen and organic flux levels) were inferred following Corliss (1985), Jones and Charnock (1985), Corliss and Chen (1988), Murray (2006) and Jorissen et al. (2007). The Fisher-α and H(S) Shannon–Weaver indices were calculated as proxies for diversity and heterogeneity of the assemblages, respectively (Murray, 2006). Paleobathymetry assignments were based on the occurrence and relative abundances of depth-dependent species. This is based on their upper-depth limits (Van Morkhoven et al., 1986; Alegret and Thomas, 2001; Ortiz and Thomas, 2006; Fenero et al., 2012) and on comparisons with benthic foraminiferal assemblages whose paleodepths can be derived independently by back-tracking (Grünig and Herb, 1980; Ingle Jr., 1980; Tjalsma and Lohmann, 1983; Thomas, 1990; Speijer, 1994; Bignot, 1998; Katz et al., 2003).

A hierarchical cluster analysis was performed with the PAST package (Hammer et al., 2001) using the Pearson similarity index and the unweighted pair-group average (UPGMA) algorithm. R-mode and Q-mode analyses were performed on a data matrix including all the studied samples and selected species that showed relative abundance > 2% in at least one sample. Detrended Correspondence Analysis (DCA) was carried out in order to further analyse the results derived

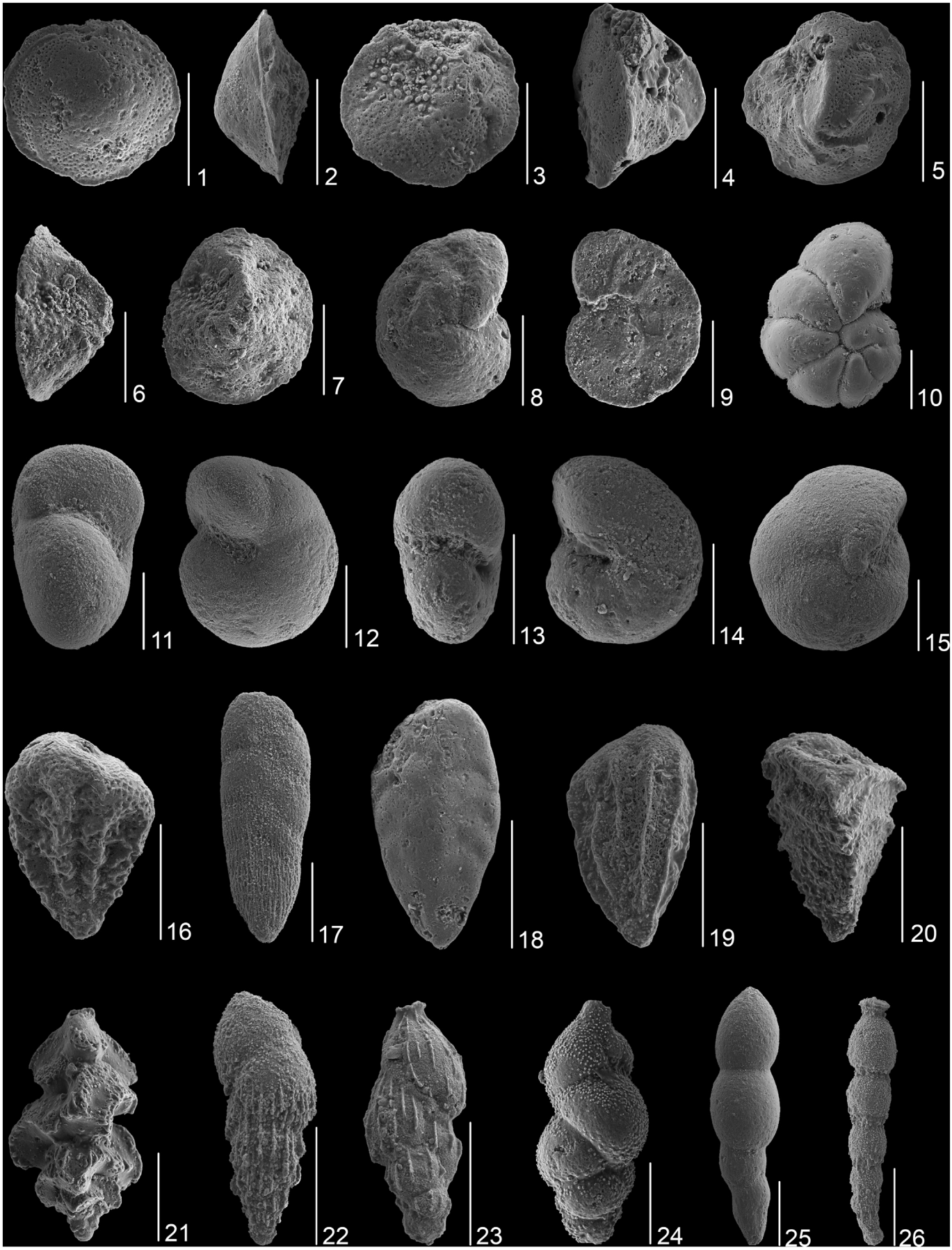

(caption on next page)

Fig. 3. Scanning electron micrographs of selected benthic foraminiferal species at Torre Cardela. All scale-bars represent 100 μm. 1–3, *Asterigerinata* sp. A (0 m); 4, 5, *Asterigerina* sp. (16 m); 6, 7, *Asterigerina* sp. B (0 m); 8, 9, *Cibicides laurisae* (0 m); 10, *Lobatula lobatula* (16 m); 11, 12, *Gyroidinoides* sp. (33 m); 13, 14, *Anomalinoides capitatus* (0 m); 15, *Pullenia* sp. (33 m); 16, *Bolivinoides crenulata* (0 m); 17, *Bolivina nobilis-gracilis* (52 m); 18, *Brizalina* sp. (16 m); 19, *Bulimina alazanensis* (4 m); 20, *Reusella terquemi* (0 m); 21, *Angulogerina muralis* (0 m); 22, *Fursenkoina* sp. A (52 m); 23, *Uvigerina longa* (65 m); 24, *Uvigerina elongata* (0 m); 25, *Nodosarella* sp. (49 m); 26, *Siphonodosaria* sp. (49 m).

from clustering, as they contribute to investigate the relationship between benthic foraminifera and environmental variables (Hammer and Harper, 2005).

3.2. Stable isotopes analyses

Species-specific C and O stable isotope analyses were performed at the Leibniz Laboratory for Radiometric Dating and Stable Isotope Research (Kiel University, Germany) using a Kiel IV carbonate preparation device connected to a MAT 253 mass spectrometer from ThermoScientific. During preparation the carbonates were reacted with 100% phosphoric acid (H_3PO_4) under vacuum at 75 °C, and the evolved carbon dioxide was analysed eight times for each individual sample. All values are reported in the Vienna Pee Dee Bee notation (VPDB) relative to NBS19. Precision of all different laboratory internal and international standards (NBS19 and IAEA-603) is < 0.05‰ for $\delta^{13}C$ and < 0.09‰ for $\delta^{18}O$ values.

Twelve specimens of *Nuttallides truempyi* were extracted from each sample where specimens were sufficiently abundant, and used for triplicate isotope analyses (except for samples 4 and 8). The analysed material is moderately preserved, less than half of the specimens show broken edges and chambers, and they are infilled with very fine-grained material. Sutures are visible, and the central boss is made of clear shell material. Size (diameter) ranges from 200 μm (juvenile specimens mostly) up to 500 μm. The, largest, best-preserved and most complete specimens were selected for isotope analyses. *Bolivinoides crenulata* (50 specimens) were extracted from samples that did not yield enough specimens of *N. truempyi* (samples 0, 63, 65, 67 and 88.5). Two additional samples (16 and 40) were selected as control samples, where both benthic (*N. truempyi* and *B. crenulata*) and planktonic species (*Acarinina bullbrooki* and *Catapsydrax unicavus*) were analysed.

3.3. Biostratigraphy and sedimentation rates

The biozones recognised at the Torre Cardela section by Gonzalvo and Molina (1996) include the upper part of planktonic foraminiferal Zone P12 and Zones P13 and P14 (Berggren and Miller, 1988), mostly Bartonian in age. In order to update this biozonation to a more recent one (Berggren and Pearson, 2005), as shown in Fig. 2, we revised the slide collection used by Gonzalvo and Molina (1996). Most of the biostratigraphic concepts used by these authors are in line with more recent ones (Berggren and Pearson, 2005), however there are a few exceptions. The Last Occurrence (LO) of *Morozovelloides crassatus* occurs within E12 Zone, instead of reaching the top of Zone E13. This species marks the transition between Zones E13/E14 (Berggren and Pearson, 2005). We used the LO of *M. crassatus* as the top of Zone E13, as it has been suggested to coincide with the same horizon as the extinction of the *Morozovelloides* lineage (Wade, 2004). This decision was also based on the First Occurrence (FO) of *Globigerinatheka semiinvoluta*, which is close to, but younger than, the LO of *M. spinulosa* (Wade, 2004).

Jovane et al. (2010) proposed to place the Lutetian/Bartonian boundary at the top of Chron C19r. Due to the lack of magnetostratigraphic data at Torre Cardela, and since the original section has been covered by road works, we analysed the planktonic foraminiferal biostratigraphy data to determine the proximity to the L/B boundary. The FO of *Turborotalia pomeroli* is present at Torre Cardela, but associated younger bioevents (e.g., the FO of *T. cerroazulensis*; Jovane et al., 2010) have not been identified in this section. On the other hand, the LO of *Acarinina bullbrooki* should be located above the L/B boundary and below the FO of *Orbulina beckmanni* (marker of Zone E12). Surprisingly, this species has been identified within Zone E13 (85 m at Torre Cardela), well above Zone E11 where its LO has been reported from other sites of similar latitudes (Jovane et al., 2010; Wade et al., 2011). Given the discrepancies about the aforementioned planktonic foraminiferal events, we cannot be certain that the lowermost part of the Torre Cardela section includes the L/B boundary. The extinction of large muricate planktonic foraminifera (large *Acarinina* and *Morozovelloides*) has been defined as the marker of the middle - late Eocene transition (Agnini et al., 2011). These genera disappear in the uppermost part of the section (95 m) at Torre Cardela, suggesting the location of the Middle–Late Eocene transition.

Sedimentation rates across the studied interval have been estimated based on the revised biozones at Torre Cardela. According to the duration of the planktonic foraminiferal biozones (calibrated astronomically by Pälike et al., 2006 and Wade et al., 2011), sedimentation rates are 8.4 cm/kyr within Zone E12, and 1.95 cm/kyr within Zone E13. These are the only biozones that appear to be complete at Torre Cardela. Caution should be taken, however, as discrepancies were observed among planktonic foraminiferal events, but these results point to a much higher sedimentation rate in the lower half of the section.

4. Results

4.1. Paleobathymetry: autochthonous versus allochthonous taxa

Benthic foraminiferal assemblages contain common bathyal and middle bathyal to abyssal species (*Bulimina alazanensis*, *Bulimina semicostata*, *Cibicidoides eocaenus*, *Cibicidoides micrus*, *Cibicidoides praemundulus*, *Globocassidulina subglobosa*, *Oridorsalis umbonatus*; Tjalsma and Lohmann, 1983; Van Morkhoven et al., 1986; Bignot, 1998; Thomas, 1990; Alegret and Thomas, 2001; Katz et al., 2003; Ortiz and Thomas, 2006; Fenero et al., 2013; Holbourn et al., 2013). Other species that have been reported from lower bathyal Paleogene biofacies (*Anomalinoides pompilioides*, *Nuttallides truempyi*, *Pleurostomella paleocenica*; Ingle Jr., 1980) are also present. *Nuttallides truempyi* and *Bulimina semicostata* have an upper depth limit (UDL) of 600 m (Van Morkhoven et al., 1986), although the former has been recorded in shallower waters in the southern Tethys during the Paleocene (Speijer and Schmitz, 1998). *Aragonia aragonensis* has been recorded from middle bathyal environments (600–1000 m paleodepth) of Eocene age (Grünig and Herb, 1980; Bignot, 1998) and potentially at shallower depths (Deprez et al., 2015), although it ranges from bathyal to abyssal depths (Van Morkhoven et al., 1986; Alegret et al., 2009; Arreguín-Rodríguez et al., 2018).

Due to the wide paleobathymetric ranges of many of these species, we compared the composition of the assemblages and relative abundance of taxa at Torre Cardela with other sections deposited in the same basin during the middle Eocene to early Oligocene, namely the Fuente Caldera section (lower bathyal, planktonic biozones P15-P17; Molina et al., 2006) and the Zarabanda section (1000 m, middle-lower bathyal; planktonic biozones O5-O7; Fenero et al., 2013). The similarity of these assemblages with ours (including abundant *Bolivinoides crenulata*), together with the paleodepth preferences of the identified species, suggests a similar middle to lower bathyal depth of deposition at Torre Cardela. Benthic foraminiferal assemblages across the MECO interval in the middle bathyal (600–1000 m) Alano di Piave section (north-eastern Italy, central-western Tethys; Agnini et al., 2011) also contain common

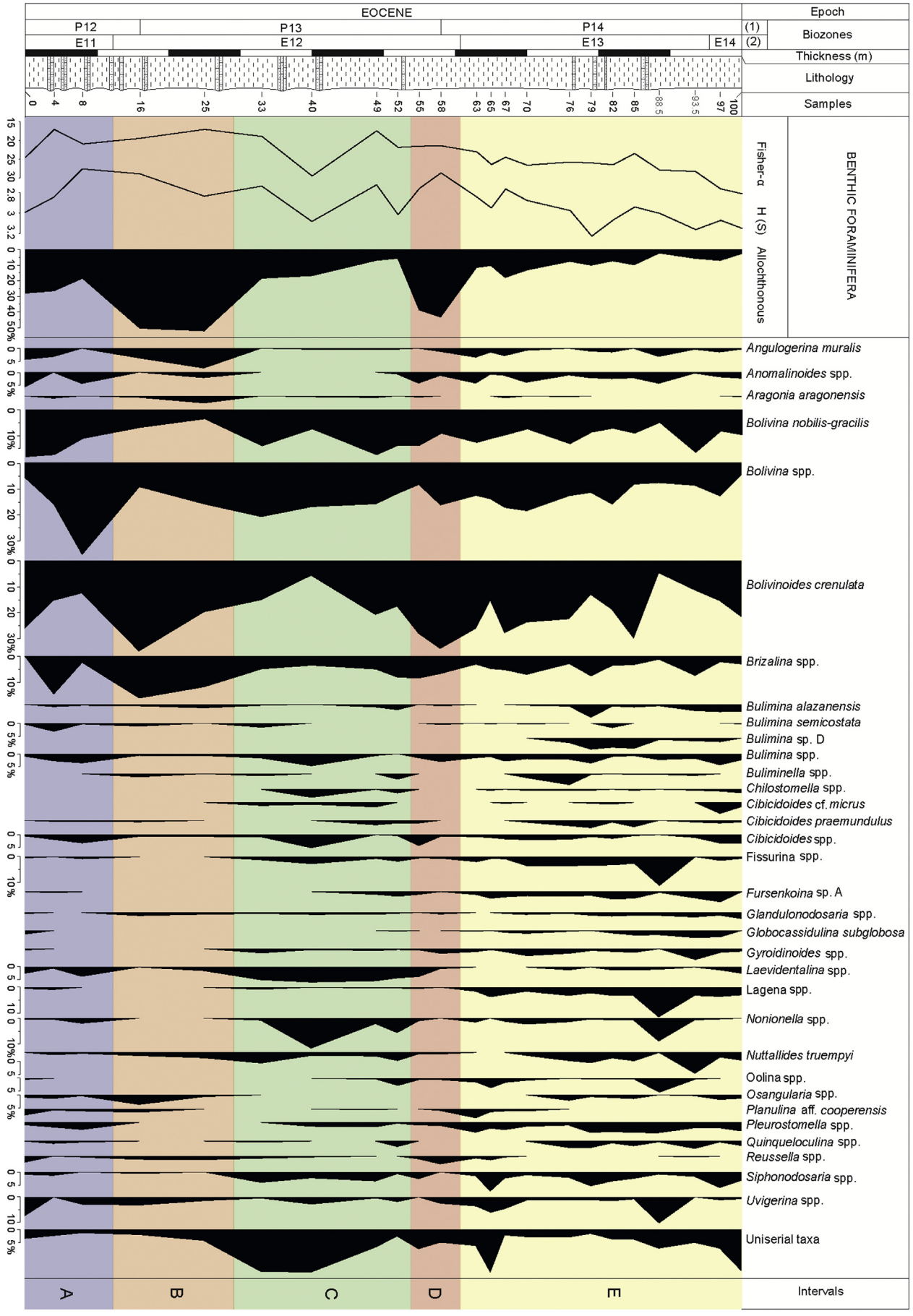

(caption on next page)

Fig. 4. Benthic foraminiferal diversity indices and relative abundance of significant benthic foraminiferal taxa at Torre Cardela (based on autochthonous assemblages only). Planktonic foraminiferal biozones (1) Gonzalvo and Molina (1996) and (2) this work.

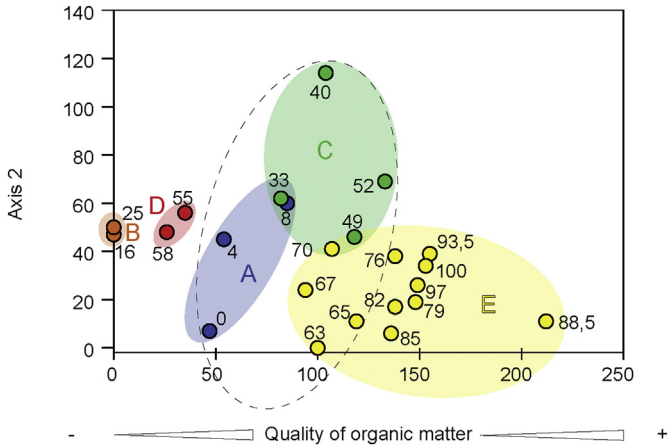

Fig. 5. Q-mode DCA analysis of samples from Torre Cardela. Coloured ellipses group samples from the same intervals, as interpreted from relative abundance of benthic foraminifera. Low values along axis 1 (intervals B and D) indicate low quality of organic matter, high values (samples from interval E) are linked to a high quality, and the dashed ellipse includes samples with intermediate values.

infaunal, bi- and triserial taxa (including *Bolivinoides crenulata*) (Boscolo Galazzo et al., 2013), showing close similarities with the assemblages at Torre Cardela.

Neritic taxa such as *Cibicides laurisae*, *Lobatula lobatula* and several species of *Asterigerina* and *Asterigerinata* (Fenero et al., 2012, 2013) are also present throughout the studied section. This group, which strongly fluctuates between < 5% and 50% of the total assemblages, was interpreted by Fenero et al. (2012, 2013) as allochthonous taxa that were transported from the shelf towards deeper parts of the slope. DCA analysis on the total assemblage dataset differentiates these shallow-water taxa (low values on Axis 1; Suppl. Fig. 1) from the lower-middle bathyal autochthonous assemblages, supporting this hypothesis.

In order to elucidate the environmental conditions that prevailed at the seafloor in this western Tethys location, we describe the allochthonous and autochthonous assemblages separately. Total assemblage refers to autochthonous plus allochthonous assemblages; assemblage refers to autochthonous taxa only (total assemblage minus the allochthonous taxa).

4.2. Autochthonous benthic foraminifera

Autochthonous assemblages are strongly dominated by calcareous taxa, and agglutinated species make up < 2% of the assemblages. Infaunal morphogroups dominate over epifaunal ones, making up to 75% of the assemblages.

Assemblages are generally diverse, with 40 to 80 species recognised per sample. Diversity slightly increases upwards in the section (Fig. 2), reaching its maximum values in the uppermost two samples. Heterogeneity shows a similar upward increasing trend, reaching its lowest value in sample 8 and the maximum value in sample 79.

Among calcareous taxa, assemblages are strongly dominated by bolivinids, including several species of the genera *Bolivina*, *Bolivinoides* and *Brizalina*. This group is more dominant in the lower half of the section (0–60 m), where it constitutes > 50% of the assemblages (except for sample 40). *Bolivinoides crenulata* is the species with the highest relative abundance, ranging from 8.86% to 34.16%. Other common calcareous taxa include *Anomalinoides*, *Fursenkoina*, *Gyroidinoides*, *Nonionella* and *Pleurostomella*, as well as uniserial (e.g. *Siphonodosaria*) and unilocular morphogroups. Uniserial taxa were difficult to determine at the genus level due to high fragmentation of their tests. The unilocular group includes *Fissurina*, *Lagena* and *Oolina*, and its relative abundance increases towards the upper part of the section, showing a pronounced peak in sample 88.5.

Based on the analysis of the autochthonous assemblages and on the relative contribution of allochthonous taxa, five intervals (A to E, Fig. 4) were recognised across the studied section:

Interval A (0–12 m): assemblages are strongly dominated by bolivinids (mainly *Bolivina* spp., *Bolivina nobilis-gracilis* and *Bolivinoides crenulata*). Buliminids, *Pleurostomella* spp. and *Uvigerina* spp. are also common. Diversity of the assemblages slightly decreases upwards.

Interval B (12–29 m): this interval contains the highest percentage of allochthonous taxa (~50% of the total assemblage) across the studied section, and the autochthonous assemblage is characterised by the highest relative abundance of bolivinids (mainly *Bolivinoides crenulata*) and the common occurrence of *Angulogerina muralis* and *Osangularia* spp. Fisher-α diversity index reaches the minimum values of the studied section.

Interval C (29–53.5 m): the percentage of bolivinids decreases, mainly due to the decrease in relative abundance of *Bolivinoides crenulata*, while the percentage of uniserial forms (particularly laevidentalinids) increases. The increase in relative abundance of *Nonionella* spp. and *Cibicidoides* spp. coincides with an increase in diversity in sample 40.

Interval D (53.5–60.5 m): it is characterised by an increase in the abundance of allochthonous taxa, and autochthonous assemblages are strongly dominated by *Bolivinoides crenulata*, as in interval B. Species of *Anomalinoides* and *Cibicidoides* are common.

Interval E (60.5–100 m): the dominance of bolivinids gradually decreases, but this group still makes up to 40% of the autochthonous assemblages. Uniseral and unilocular taxa are common, and the percentage of buliminids and various *Pleurostomella* species increases towards the upper part of the section. This interval contains one sample (88.5) with a higher relative abundance of unilocular taxa, *Nonionella* spp. and *Uvigerina* spp., and lowest percentage of bolivinids.

The five intervals are differentiated in the Q-mode DCA plot (Fig. 5), where samples with a higher contribution of allochthonous taxa (intervals B and D) show the lowest values along Axis 1, intervals immediately below these (intervals A and C) show higher values along this axis, and samples from the upper half of the studied section (interval E) show the highest values along the Axis 1.

4.3. Stable isotope analysis

Results from species-specific $\delta^{13}C$ analyses (Fig. 2) on *N. truempyi* show a decreasing trend of > 1.50‰ from the lower part of the section towards the upper part. In addition to standard analyses on moderately preserved tests, some poorly preserved, "rusty" specimens of *N. truempyi* covered with an orange-yellow patina were analysed in four samples to assess the preservation bias. Remarkably, these rusty specimens did not show significantly different values than the better-preserved specimens, especially in sample 76, where the "rusty" specimens yielded the same result as regular specimens. Standard deviation, calculated from triplicate analyses performed on every sample (except samples 4 and 8), is particularly high in sample 58 (interval D), possibly due to the presence of reworked specimens from adjacent, shallower areas.

The $\delta^{13}C$ and $\delta^{18}O$ values do not show a strong correlation (see Suppl. Fig. 5), and correlation value is low ($p = 0.064$). Control samples for which planktonic and benthic taxa were analysed (samples 16 and 40) show differences depending on the ecology of the species: *Acarinina bullbrooki* (encrusted mixed-layer symbiotic) yields higher $\delta^{13}C$ values

than deep-dweller *Catapsydrax unicavus*. Benthic species show lower $\delta^{13}C$ values than both planktonic species. These data suggest that general $\delta^{13}C$ trends are preserved, even though $\delta^{13}C$ absolute values may not be primary signals.

4.4. Paleoenvironmental reconstruction and interpretation

Benthic foraminiferal assemblages contain species with different paleobathymetric ranges, and reveal that allochthonous taxa are remarkably abundant at the Torre Cardela section. The autochthonous assemblage indicates a middle to lower bathyal depth of deposition, while the allochthonous assemblage contains species typical from neritic environments. Some of these allochthonous species are believed to have had epiphytic lifestyles (Alegret et al., 2008; Fenero et al., 2013), living attached to animals, plants or hard substrates that were likely transported as floating material into pelagic environments, as reported by Fenero et al. (2012). The significant changes in relative abundance of this group suggest that transport of shallower material towards deeper parts of the basin was more intense in intervals B and D, possibly related to enhanced current activity, as suggested in the nearby Zarabanda and Fuente Caldera sections. The analysis of benthic foraminifera in the Fuente Caldera section showed abundant reworked neritic taxa and epiphytic species during the early Oligocene (Alegret et al., 2008; Fenero et al., 2012). Similarly, the identification of shallow-water benthic foraminifera in the bathyal Zarabanda section was attributed to transport by turbidity currents after erosion of a shallow platform, possibly due to the destabilization of the outer ramp sediment (Fenero et al., 2013).

The second most remarkable feature of the benthic assemblages at Torre Cardela refers to the strong dominance by bolivinids. This group is considered as indicative of a high input of organic matter to the seafloor (e.g. (Gooday, 1994; Bernhard and Sen Gupta, 1999; Murray, 2006). *Bolivinoides crenulata* is the most dominant species within the bolivinids group and the autochthonous assemblage. This species has been suggested to proliferate during periods of enhanced input of low-quality, refractory organic matter to the seafloor (Agnini et al., 2009; Ortiz et al., 2011; D'haenens et al., 2012; Boscolo Galazzo et al., 2013), and is considered as an opportunistic species related to high-energy environments. The relative abundance of *B. crenulata* shows a positive correlation with the percentage of allochthonous taxa, especially in intervals B and D, and may indicate increased current activity and downslope transport of low-quality organic matter together with shallow-water benthic foraminifera. We argue that *B. crenulata* was able to feed on this type of organic matter that was not easily digested by other taxa, thus dominating the assemblages during these intervals. Decreasing abundance of shallow-water and opportunistic taxa in the same intervals could be explained by reduced supply of refractory organic matter and less downslope transport, likely caused by weakened current activity.

Abundant bolivinids and other bi-triserial taxa related to a high nutrient supply have also been reported from other Eocene Tethyan sections (Alegret et al., 2008; Molina et al., 2006; Agnini et al., 2009; Boscolo Galazzo et al., 2013; Fenero et al., 2013). Although high food availability is commonly associated with decreasing oxygen levels (TROX model; Jorissen et al., 1995), we did not find any evidence for anoxic conditions such as laminated sediments or dark, organic levels. In addition, bolivinids have also been reported from environments with well-oxygenated bottom waters (Fontanier et al., 2005; Jorissen et al., 2007). We suggest that benthic foraminifera at Torre Cardela were more strongly controlled by the amount and type of organic matter rather than by oxygenation at the seafloor.

The high dominance of bolivinids in interval A may indicate a high nutrient flux to the seafloor. Intervals B and D show lower diversity than adjacent intervals and a sharp increase in the percentage of allochthonous taxa and *Bolivinoides crenulata*. This is likely related to enhanced current activity and downslope transport of shallow-water taxa and sediments to the bathyal realm. The decrease in the percentage of allochthonous taxa in intervals C and E suggests less intense current activity. The percentage of bolivinids decreased as well, but the overall abundance of infaunal morphogroups did not significantly change because the percentage of uniserial taxa and other infaunal morphotypes such as *Nonionella* spp. increased, possibly indicating a change in the type (quality) of food rather than in its amount.

Sample 88.5 contains an anomalous assemblage with higher relative abundance of unilocular morphologies (Fig. 2 and Suppl. Fig. 2) that might indicate well-oxygenated, oligotrophic conditions possibly related to changes in deep-water currents, as documented in the upper part of Zone E13 in the Alano section (Boscolo Galazzo et al., 2013). The lack of a higher-resolution sampling across this interval however, precludes further investigation to test this hypothesis at Torre Cardela.

5. Discussion

Assemblages from Torre Cardela bear similarities with those reported from the Cap Breton canyon (Bay of Biscay), where the abundance of shallow infaunal bolivinids and other taxa that are able to feed on low-quality organic matter have been associated with the dynamics of sedimentary processes (Hess and Jorissen, 2009). Despite the high nutrient flux, no dysoxic conditions were reported at the seafloor in the canyon, possibly because refractory organic matter may have been fully consumed by the benthic population before it could degrade. Similarly, there is no evidence for oxygen deficiency of sea-bottom waters at Torre Cardela, and we hypothesize that sedimentary processes may have strongly influenced benthic foraminifera, controlling the flux and quality of organic matter input to the seafloor.

Intervals B and D at Torre Cardela include the base and the top of planktonic foraminiferal biozone E12. This biozone is defined by the total range of the species *Orbulinoides beckmanii* (Berggren and Pearson, 2005), which is considered as a marker for the MECO (Edgar et al., 2010). In the Tethys Ocean, the E12 biozone has been well identified in the Alano section (Spofforth et al., 2010), where two positive $\delta^{13}C$ excursions have been recorded right after the MECO peak, in coincidence with two organic-rich events (ORG1 and ORG 2; Spofforth et al., 2010). Benthic assemblages across these events (Boscolo Galazzo et al., 2013) show similar characteristics to assemblages B and D at Torre Cardela (dominance of infaunal morphogroups, especially bolivinids). The Alano section was deposited in a very similar (middle bathyal, high-productivity) environment, and stress-tolerant taxa (bi- and triserial taxa; e.g. *Bolivina* spp., *B. crenulata*, *Uvigerina* spp.) dominated across intervals ORG1 and ORG2, as observed in intervals B and D at Torre Cardela. In Alano, deposition of both organic-rich events seems to have been controlled by variations in surface productivity, where the increase in organic carbon flux led to low oxygen conditions at the seafloor, followed by a rapid recovery to well-oxygenated waters (Boscolo Galazzo et al., 2013). The lack of evidence for decreased oxygenation across intervals B and D at Torre Cardela may be related to differences in the depositional setting, and local sedimentary disturbances seem to have influenced the assemblages at this site.

Despite the different parameters shaping benthic foraminiferal assemblages, one might speculate that increased weathering resulting from an intensification of the hydrological cycle during Eocene hyperthermal events (Nicolo et al., 2007) may have led to more runoff, higher sedimentation rates (as estimated for the lower part of Torre Cardela section, intervals B to D) and enhanced transport of nutrients and sediments to the basin, thus increasing productivity. In addition, high burial rates of organic carbon in marine shelves may have led to decreased atmospheric pCO_2, consistent with global cooling following MECO (Bohaty et al., 2009; Spofforth et al., 2010; Sluijs et al., 2013). We acknowledge that the organic events at Alano section occur after the peak climatic conditions of the MECO (Spofforth et al., 2010), which we have not been able to clearly identify at Torre Cardela. A higher-resolution age model would be of great interest to confirm this

correlation, but further studies are not feasible at present because the original section has been covered by road works. With the available data, we conclude that benthic foraminiferal assemblages at Torre Cardela were strongly controlled by the amount and type of organic matter reaching the seafloor, which are in turn affected by sedimentary and, ultimately, climatic factors.

6. Conclusions

1. The analysis of benthic foraminifera from the Torre Cardela section provides the first insights into the effects of middle Eocene climate variations on the deep-water marine ecosystems of the western Tethys Ocean. The studied interval encompasses planktonic foraminiferal biozones E11 to E14 (including the post-MECO interval) and corresponds to the Bartonian Stage.
2. Five intervals were differentiated based on changes in the relative abundance of benthic foraminiferal taxa. Two of them contain higher percentages of allochthonous taxa, and indicate enhanced downslope transport of sediment and shallow-water taxa to middle-lower bathyal settings.
3. The abundance of bolivinids points to a high nutrient flux, and the dominance of *Bolivinoides crenulata* is possibly linked to a higher input of low-quality, refractory organic matter in a high-energy, well-oxygenated environment, especially in the same intervals (B and D) where allochthonous taxa are most abundant.
4. The amount and type of food reaching the seafloor, possibly controlled by current activity, are here interpreted as the main parameters controlling benthic foraminiferal assemblages at Torre Cardela.

Declarations of interest

None.

Acknowledgments

The authors thank S. D'haenens, D. Peryt and M. Boukhary for their constructive reviews. This work was supported by the Spanish Ministry of Economy and Competitiveness and FEDER funds [project numbers CGL 2014-58794 and CGL2017-84693-R, and predoctoral grant number BES-2015-075140]; and Aragón Government with European Social Fund [Consolidated Research Group E05]. Authors would like to acknowledge the use of Servicio General de Apoyo a la Investigación-SAI, Universidad de Zaragoza, and Cristina Gallego for the SEM imaging. We are grateful to Nils Andersen (Kiel University) for isotope analyses. This research is part of the PhD thesis of the first author.

Appendix A. Supplementary data

Supplementary data to this article can be found online at https://doi.org/10.1016/j.palaeo.2018.05.003.

References

Agnini, C., Macrì, P., Backman, J., Brinkhuis, H., Fornaciari, E., Giusberti, L., Luciani, V., Rio, D., Sluijs, A., Speranza, F., 2009. An early Eocene carbon cycle perturbation at ~52.5 Ma in the Southern Alps: chronology and biotic response. Paleoceanography 24 (PA2209).

Agnini, C., Fornaciari, E., Giusberti, L., Grandesso, P., Lanci, L., Luciani, V., Muttoni, G., Pälike, H., Rio, D., Spofforth, D.J., 2011. Integrated biomagnetostratigraphy of the Alano section (NE Italy): a proposal for defining the middle-late Eocene boundary. Geol. Soc. Am. Bull. 123, 841–872.

Alegret, L., Thomas, E., 2001. Upper Cretaceous and lower Paleogene benthic foraminifera from northeastern Mexico. Micropaleontology 47, 269–316.

Alegret, L., Cruz, L.E., Fenero, R., Molina, E., Ortiz, S., Thomas, E., 2008. Effects of the Oligocene climatic events on the foraminiferal record from Fuente Caldera section (Spain, western Tethys). Palaeogeogr. Palaeoclimatol. Palaeoecol. 269, 94–102.

Alegret, L., Ortiz, S., Molina, E., 2009. Extinction and recovery of benthic foraminifera across the Paleocene-Eocene thermal maximum at the Alamedilla section (southern Spain). Palaeogeogr. Palaeoclimatol. Palaeoecol. 279, 186–200.

Andeweg, B., 2002. Cenozoic Tectonic Evolution of the Iberian Peninsula: Effects and Causes of Changing Stress Fields. VU University of Amsterdam.

Arreguín-Rodríguez, G.J., Thomas, E., D'haenens, S., Speijer, R.P., Alegret, L., 2018. Early Eocene deep-sea benthic foraminiferal faunas: recovery from the Paleocene Eocene thermal maximum extinction in a greenhouse world. PLoS One 13, e0193167.

Berggren, W.A., Miller, K.G., 1988. Paleogene tropical planktonic foraminiferal biostratigraphy and magnetobiochronology. Micropaleontology 34, 362.

Berggren, W.A., Pearson, P.N., 2005. A revised tropical to subtropical Paleogene planktonic foraminiferal zonation. J. Foraminifer. Res. 35, 279–298.

Bernhard, J.M., Sen Gupta, B.K., 1999. Foraminifera of oxyen-depleted environments. In: Modern Foraminifera. Kluwer Academic Publishers, pp. 201–216.

Bignot, G., 1998. Middle Eocene benthic foraminifers from holes 960A and 960C, Central Atlantic Ocean. In: Mascle, J., Lohmann, G.P., Moullade, M. (Eds.), Proceedings of the Ocean Drilling Program, Scientific Results. Texas A&M University, pp. 433–444.

Bijl, P.K., Houben, A.J.P., Schouten, S., Bohaty, S.M., Sluijs, A., Reichart, G.-J., Damsté, J.S.S., Brinkhuis, H., 2010. Transient middle Eocene atmospheric CO_2 and temperature variations. Science 330, 819–821.

Bohaty, S.M., Zachos, J.C., 2003. Significant Southern Ocean warming event in the late middle Eocene. Geology 31, 1017–1020.

Bohaty, S.M., Zachos, J.C., Florindo, F., Delaney, M.L., 2009. Coupled greenhouse warming and deep-sea acidification in the middle Eocene. Paleoceanography 24, PA2207.

Bolli, H.M., Beckmann, J.-P., Saunders, J.B., 1994. Benthic Foraminiferal Biostratigraphy of the South Caribbean Region. Cambridge University Press, pp. 408.

Boscolo Galazzo, F., Giusberti, L., Luciani, V., Thomas, E., 2013. Paleoenvironmental changes during the Middle Eocene Climatic Optimum (MECO) and its aftermath: the benthic foraminiferal record from the Alano section (NE Italy). Palaeogeogr. Palaeoclimatol. Palaeoecol. 378, 22–35.

Boscolo Galazzo, F., Thomas, E., Pagani, M., Warren, C., Luciani, V., Giusberti, L., 2014. The middle Eocene climatic optimum (MECO): a multiproxy record of paleoceanographic changes in the southeast Atlantic (ODP Site 1263, Walvis Ridge): MECO repercussions in the SE Atlantic. Paleoceanography 29, 1143–1161.

Comas, M.C., 1978. Sobre la geología de los Montes orientales: sedimentación y evolución paleogeográfica desde el Jurásico al Mioceno inferior (Zona Subbética, Andalucía). PhD Thesis, University of Bilbao, pp. 332.

Corliss, B.H., 1985. Microhabitats of benthic foraminifera within deep-sea sediments. Nature 314, 435–438.

Corliss, B.H., Chen, C., 1988. Morphotype patterns of Norwegian Sea deep-sea benthic foraminifera and ecological implications. Geology 16, 716–719.

Coxall, H.K., Wilson, P.A., Pälike, H., Lear, C.H., Backman, J., 2005. Rapid stepwise onset of Antarctic glaciation and deeper calcite compensation in the Pacific Ocean. Nature 433, 53–57.

Den Dulk, M., Reichart, G.-J., Van Heyst, S., Zachariasse, W.J., Van der Zwaan, G.J., 2000. Benthic foraminifera as proxies of organic matter flux and bottom water oxygenation? A case history from the northern Arabian Sea. Palaeogeogr. Palaeoclimatol. Palaeoecol. 161, 337–359.

Deprez, A., Tesseur, S., Stassen, P., D'haenens, S., Steurbaut, E., King, C., Claeys, P., Speijer, R.P., 2015. Early Eocene environmental development in the northern Peri-Tethys (Aktulagay, Kazakhstan) based on benthic foraminiferal assemblages and stable isotopes (O, C). Mar. Micropaleontol. 115, 59–71.

D'haenens, S., Bornemann, A., Stassen, P., Speijer, R.P., 2012. Multiple early Eocene benthic foraminiferal assemblage and δ13C fluctuations at DSDP site 401 (Bay of Biscay — NE Atlantic). Mar. Micropaleontol. 88–89, 15–35.

Edgar, K.M., Wilson, P.A., Sexton, P.F., Gibbs, S.J., Roberts, A.P., Norris, R.D., 2010. New biostratigraphic, magnetostratigraphic and isotopic insights into the Middle Eocene Climatic Optimum in low latitudes. Palaeogeogr. Palaeoclimatol. Palaeoecol. 297, 670–682.

Fenero, R., Thomas, E., Alegret, L., Molina, E., 2012. Oligocene benthic foraminifera from the Fuente Caldera section (Spain, western Tethys): taxonomy and paleoenvironmental inferences. J. Foraminifer. Res. 42, 286–304.

Fenero, R., Cotton, L., Molina, E., Monechi, S., 2013. Micropalaeontological evidence for the late Oligocene Oi-2b global glaciation event at the Zarabanda section. Spain. Palaeogeogr. Palaeoclimatol. Palaeoecol. 369, 1–13.

Fontanier, C., Jorissen, F.J., Chaillou, G., Anschutz, P., Grémare, A., Griveaud, C., 2005. Live foraminiferal faunas from a 2800 m deep lower canyon station from the Bay of Biscay: faunal response to focusing of refractory organic matter. Deep Sea Res. Part Oceanogr. Res. Pap. 52, 1189–1227.

Gonzalvo, C., Molina, E., 1996. Bioestratigrafía y cronoestratigrafía del tránsito Eoceno Medio-Eoceno Superior en la Cordillera Bética. Rev. Esp. Micropaleontol. XXVIII 25–44.

Gooday, A.J., 1994. The biology of Deep-Sea foraminifera: a review of some advances and their applications in paleoceanography. PALAIOS 9, 14.

Gooday, A.J., 2003. Benthic foraminifera (protista) as tools in deep-water Palaeoceanography: environmental Infuences on faunal characteristics. Adv. Mar. Biol. 46.

Grünig, A., 1985. Systematical description of Eocene Benthic Foraminifera of Possagno (northern Italy), Sansoain (northern Spain) and Biarritz (Aquitaine, France). In: Memorie Degli Instituti Di Geologia e Mineralogia Dell'Università Di Padova, pp. 251–302.

Grünig, A., Herb, R., 1980. Paleoecology of late Eocene benthonic foraminifera from Possagno (Treviso-northern Italy). Cushman Found. Spec. Publ. 19, 68–85.

Hammer, Ø., Harper, D., 2005. Paleontological Data Analysis. Blackwell Publishing, Oxford.

Hammer, Ø., Harper, D.A.T., Ryan, P.D., 2001. PAST: paleontological statistics software package for education and data analysis. Paleontol. Electron. 4 (1), 9.

Hayward, B.W., Kawagata, S., Sabaa, A., Grenfell, H., Van Kerckhoven, L., Johnson, K., Thomas, E., 2012. The Last Global Extinction (Mid-Pleistocene) of Deep-Sea Benthic Foraminifera (Chrysalogoniidae, Ellipsoidinidae, Glandulonodosariidae, Plectofrondicularíidae, Pleurostomellidae, Stilostomellidae), their Late Cretaceous-Cenozoic History and Taxonomy. Cushman Foundation for Foraminiferal Research Special Publication.

Hess, S., Jorissen, F.J., 2009. Distribution patterns of living benthic foraminifera from Cap Breton canyon, Bay of Biscay: faunal response to sediment instability. Deep Sea Res. Part Oceanogr. Res. Pap. 56, 1555–1578.

Holbourn, A., Henderson, A.S., MacLeod, N., 2013. Atlas of Benthic Foraminifera, Natural History Museum (ed). Wiley-Blackwell, pp. 642.

Ingle Jr., J.C., 1980. Cenozoic paleobathymetry and depositional history of selected sequences within the southern California Continental Borderland. Cushman Found. Spec. Publ. 19, 163–195.

Jones, R.W., Charnock, M.A., 1985. "Morphogroups" of agglutinated foraminifera. Their life positions and feeding habits and potential applicability in (paleo)ecological studies. Rev. Palèobiologie 4 (2), 311–320.

Jorissen, F.J., de Stigter, H.C., Widmark, J.G., 1995. A conceptual model explaining benthic foraminiferal microhabitats. Mar. Micropaleontol. 26, 3–15.

Jorissen, F.J., Fontanier, C., Thomas, E., 2007. Chapter seven: Paleoceanographical proxies based on Deep-Sea benthic foraminiferal assemblage characteristics. In: Developments in Marine Geology. Elsevier, pp. 263–325.

Jovane, L., Sprovieri, M., Coccioni, R., Florindo, F., Marsili, A., Laskar, J., 2010. Astronomical calibration of the middle Eocene Contessa Highway section (Gubbio, Italy). Earth Planet. Sci. Lett. 298, 77–88.

Katz, M.E., Tjalsma, R.C., Miller, K.G., 2003. Oligocene bathyal to abyssal benthic foraminifera of the Atlantic Ocean. Micropaleontology 49, 1–45.

Kirtland Turner, S., Sexton, P.F., Charles, C.D., Norris, R.D., 2014. Persistence of carbon release events through the peak of early Eocene global warmth. Nat. Geosci. 7, 748–751.

Loeblich Jr., A.R., Tappan, H., 1987. Foraminiferal Genera and Their Classification. Van Nostrand Reinhold Company, pp. 970 (ed.).

Loubere, P., 1998. The impact of seasonality on the benthos as reflected in the assemblages of deep-sea foraminifera. Deep Sea Res. Part Oceanogr. Res. Pap. 45, 409–432.

Lunt, D.J., Ridgwell, A., Sluijs, A., Zachos, J.C., Hunter, S., Haywood, A., 2011. A model for orbital pacing of methane hydrate destabilization during the Palaeogene. Nat. Geosci. 4, 775–778.

Moebius, I., Friedrich, O., Scher, H.D., 2014. Changes in Southern Ocean bottom water environments associated with the Middle Eocene Climatic Optimum (MECO). Palaeogeogr. Palaeoclimatol. Palaeoecol. 405, 16–27.

Moebius, I., Friedrich, O., Edgar, K.M., Sexton, P.F., 2015. Episodes of intensified biological productivity in the subtropical Atlantic Ocean during the termination of the Middle Eocene Climatic Optimum (MECO): intensified productivity during the MECO. Paleoceanography 30, 1041–1058.

Molina, E., Gonzalvo, C., Ortiz, S., Cruz, L.E., 2006. Foraminiferal turnover across the Eocene–Oligocene transition at Fuente Caldera, southern Spain: no cause–effect relationship between meteorite impacts and extinctions. Mar. Micropaleontol. 58, 270–286.

Murray, J.W., 2006. Ecology and applications of benthic foraminifera. Cambridge University Press, pp. 426.

Nicolo, M.J., Dickens, G.R., Hollis, C.J., Zachos, J.C., 2007. Multiple early Eocene hyperthermals: their sedimentary expression on the New Zealand continental margin and in the deep sea. Geology 35, 699.

Ortiz, S., Thomas, E., 2006. Lower-middle Eocene benthic foraminifera from the Fortuna section (Betic Cordillera, southeastern Spain). Micropaleontology 52, 97–150.

Ortiz, S., Alegret, L., Payros, A., Orue-Etxebarria, X., Apellaniz, E., Molina, E., 2011. Distribution patterns of benthic foraminifera across the Ypresian–Lutetian Gorrondatxe section, Northern Spain: response to sedimentary disturbance. Mar. Micropaleontol. 78, 1–13.

Pälike, H., Norris, R.D., Herrle, J.O., Wilson, P.A., Coxall, H.K., Lear, C.H., Shackleton, N.J., Tripati, A.K., Wade, B.S., 2006. The heartbeat of the Oligocene climate system. Science 314, 1894–1898.

Pälike, H., Lyle, M.W., Nishi, H., Raffi, I., Ridgwell, A., Gamage, K., Klaus, A., Acton, G., Anderson, L., Backman, J., Baldauf, J., Beltran, C., Bohaty, S.M., Bown, P., Busch, W., Channell, J.E.T., Chun, C.O.J., Delaney, M., Dewangan, P., Dunkley Jones, T., Edgar, K.M., Evans, H., Fitch, P., Foster, G.L., Gussone, N., Hasegawa, H., Hathorne, E.C., Hayashi, H., Herrle, J.O., Holbourn, A., Hovan, S., Hyeong, K., Iijima, K., Ito, T., Kamikuri, S., Kimoto, K., Kuroda, J., Leon-Rodriguez, L., Malinverno, A., Moore Jr., T.C., Murphy, B.H., Murphy, D.P., Nakamura, H., Ogane, K., Ohneiser, C., Richter, C., Robinson, R., Rohling, E.J., Romero, O., Sawada, K., Scher, H., Schneider, L., Sluijs, A., Takata, H., Tian, J., Tsujimoto, A., Wade, B.S., Westerhold, T., Wilkens, R., Williams, T., Wilson, P.A., Yamamoto, Y., Yamamoto, S., Yamazaki, T., Zeebe, R.E., 2012. A Cenozoic record of the equatorial Pacific carbonate compensation depth. Nature 488, 609–614.

Sluijs, A., Zeebe, R.E., Bijl, P.K., Bohaty, S.M., 2013. A middle Eocene carbon cycle conundrum. Nat. Geosci. 6, 429–434.

Speijer, R.P., 1994. Extinction and Recovery Patterns in Benthic Foraminiferal Paleocommunities across the Cretaceous/Paleogene and Paleocene/Eocene Boundaries. Universiteit Utrecht, Utrecht, Geologica Ultraiectina. Faculteit Aardwetenschappen, pp. 191.

Speijer, R.P., Schmitz, B., 1998. A benthic foraminiferal record of Paleocene Sea level and trophic/redox conditions at Gebel Aweina. Egypt. Palaeogeogr. Palaeoclimatol. Palaeoecol. 137, 79–101.

Spofforth, D.J.A., Agnini, C., Pälike, H., Rio, D., Fornaciari, E., Giusberti, L., Luciani, V., Lanci, L., Muttoni, G., 2010. Organic carbon burial following the middle Eocene climatic optimum in the central western Tethys. Paleoceanography 25, PA3210.

Takata, H., Nomura, R., Tsujimoto, A., Khim, B.-K., Chung, I.K., 2013. Abyssal benthic foraminifera in the eastern equatorial Pacific (IODP EXP 320) during the middle Eocene. J. Paleontol. 87, 1160–1185.

Thomas, E., 1990. Late Cretaceous through neogene deep-sea benthic foraminifers (Maud Rise, Weddell Sea, Antarctica). In: Barker, P., Kennett, J.P. (Eds.), Proceedings of the Ocean Drilling Program. Scientific Reports, Ocean Drilling Program, pp. 571–594.

Thomas, E., Zachos, J.C., 2000. Was the late Paleocene thermal maximum a unique event? GFF 122, 169–170.

Tjalsma, R.C., Lohmann, G.P., 1983. Paleocene - Eocene Bathyal and Abyssal Benthic Foraminifera from the Atlantic Ocean (Micropaleontology Special Edition). pp. 89.

Van der Zwaan, G.J., Duijnstee, I.A.P., Den Dulk, M., Ernst, S.R., Jannink, N.T., Kouwenhoven, T.J., 1999. Benthic foraminifers: proxies or problems?: a review of paleocological concepts. Earth-Sci. Rev. 46, 213–236.

Van Morkhoven, F.P.C.M., Berggren, W.A., Edwards, A.S., 1986. Cenozoic Cosmopolitan Deep-Water Benthic Foraminifera, Bull. Centres Rech. Explor.-Prod. Elf-Aquitaine, pp. 421.

Wade, B.S., 2004. Planktonic foraminiferal biostratigraphy and mechanisms in the extinction of Morozovella in the late middle Eocene. Mar. Micropaleontol. 51, 23–38.

Wade, B.S., Pearson, P.N., Berggren, W.A., Pälike, H., 2011. Review and revision of Cenozoic tropical planktonic foraminiferal biostratigraphy and calibration to the geomagnetic polarity and astronomical time scale. Earth-Sci. Rev. 104, 111–142.

Zachos, J.C., Dickens, G.R., Zeebe, R.E., 2008. An early Cenozoic perspective on greenhouse warming and carbon-cycle dynamics. Nature 451, 279–283.

Zachos, J.C., McCarren, H., Murphy, B., Röhl, U., Westerhold, T., 2010. Tempo and scale of late Paleocene and early Eocene carbon isotope cycles: implications for the origin of hyperthermals. Earth Planet. Sci. Lett. 299, 242–249.

4.1 Benthic foraminiferal turnover across Eocene climatic events

4.1.4. Paleoenvironmental and ecological changes during the Eocene-Oligocene transition based on foraminifera from the Cap Bon Peninsula in North East Tunisia

Chaima Grira, Narjess Karoui-Yaakoub, Mohamed Hési Negra, Lucía Rivero-Cuesta & Eustoquio Molina, 2018

Journal of African Earth Sciences 143, 145-161

Journal of African Earth Sciences 143 (2018) 145–161

Contents lists available at ScienceDirect

Journal of African Earth Sciences

journal homepage: www.elsevier.com/locate/jafrearsci

Paleoenvironmental and ecological changes during the Eocene-Oligocene transition based on foraminifera from the Cap Bon Peninsula in North East Tunisia

Chaima Grira [a], Narjess Karoui-Yaakoub [a], Mohamed Hédi Negra [b], Lucia Rivero-Cuesta [c], Eustoquio Molina [c, *]

[a] Département des Sciences de la Terre, Faculté des Sciences de Bizerte, Université Carthage, Jarzouna, Bizerte 7021, Tunisia
[b] Unité de Recherche: Petrologíe Sédimentaire et Cristaline, Falculté des Sciences de Tunis, Université Tunis El Manar, Tunisia
[c] Departamento de Ciencias de la Tierra and IUCA, Universidad de Zaragoza, E-50009 Zaragoza, Spain

ARTICLE INFO

Article history:
Received 29 July 2017
Received in revised form
24 January 2018
Accepted 19 February 2018
Available online 19 March 2018

Keywords:
Foraminifera
Eocene/oligocene
Extinction
Paleoenvironment
Tunisia

ABSTRACT

Biostratigraphic analysis of the Eocene-Oligocene transition (E-O) at the Menzel Bou Zelfa and Jhaff composite section in the Cap Bon Peninsula (North East Tunisia) allowed us to recognize a continuous planktic foraminiferal biozonation: E14 *Globigerinatheka semiinvoluta* Zone, E15 *Globigerinatheka index* Zone, E16 *Hantkenina alabamensis* Zone and O1 *Pseudohastigerina naguewichiensis* Zone. A quantitative study of benthic and planktic foraminifera assemblages was carried out and the richness and diversity of foraminifera allowed us to reconstruct the paleoenvironmental evolution from marine to terrestrial environments. From the Eocene E14 Zone, the foraminiferal association characterizes a relatively warm climate with considerable oxygen content and a dominance of keeled and spinose planktic foraminifera, which became extinct at the E/O boundary, possibly due to cooling of the planktic environment. Nevertheless, the small benthic foraminifera do not show an extinction event at the Eocene/Oligocene (E/O) boundary, indicating that the benthic environment was not significantly affected. In the basal Oligocene O1 Zone, the benthic environment changes to a shallower setting due to cooling of the climate. These changes generated a remarkable dominance of globular forms in the planktic environment. Small benthic foraminifera apparently have a gradual extinction event, or more likely a gradual pattern of local disappearances, that could have been caused by the Oi1 glaciation.

1. Introduction

The E-O transition, around 34 Ma, was a pivotal time in Earth's evolution as the climate shifted from Early Cenozoic greenhouse to glacial conditions with significant permanent ice sheets on Antarctica (Shackleton and Kennett, 1976; Zachos et al., 1996; Wade et al., 2012; Ortiz and Kaminski, 2012). This was associated with a cooling of the regions of low, medium and high latitudes (Coxall and Pearson, 2007; Lear et al., 2008).

As the world shifted from warm Eocene climate to colder Oligocene climate, there were major changes in ecology, productivity, chemistry and also probably within the vertical structure of the water column. This major change under the climatic conditions is reflected by similar progressive changes in the oxygen and carbon isotopes of the benthic foraminifera from deep waters (Coxall et al., 2005; Coxall and Wilson, 2011) as well as in the lithology of the pelagic sediments (Pälike et al., 2012), reflecting the cooling of the oceans and the development of large ice sheets in Antarctica (Shackleton and Kennett, 1976; Zachos et al., 1996; DeConto and Pollard, 2003; Coxall et al., 2005; Lear et al., 2008). These climate changes were associated with a reduction of atmospheric carbon dioxide (Pearson et al., 2009; Pagani et al., 2011), the extinction of many species of phytoplankton and zooplankton (Funakawa et al., 2006; Pearson et al., 2008) a deepening of the calcite compensation depth (CCD), a fall in sea level increased ocean alkalinity (Coxall et al., 2005), and the tectonic changes that have opened Oceanic gateways of flows around the Antarctic (Exon et al., 2004; Stickley et al., 2004; Barker et al., 2007).

Planktic foraminifera suffered extinction across the E/O boundary (Martínez-Gallego and Molina, 1975; Molina, 1980, 1986;

* Corresponding author.
E-mail address: emolina@unizar.es (E. Molina).

https://doi.org/10.1016/j.jafrearsci.2018.02.013
1464-343X/

Molina et al., 1986, 1988; 1993, 2006; Nocchi et al., 1988; Gonzalvo and Molina, 1992; Farouk et al., 2013, 2015; Pearson and Wade, 2015; Karoui-Yaakoub et al., 2017). Planktic foraminifera suffered a rapid but gradual extinction event, which is characterized by the extinction of the hantkeninids and turborotalids (*Hantkenina primitiva, Hantkenina compressa, Hantkenina alabamensis, Hantkenina nanggulanensis*, *Cribohantkenina lazzarii, Turborotalia cocoaensis and Turborotalia cunialensis*). Furthermore, the larger *Pseudohastigerina micra* s. str. also seems to have gone extinct. These species gradually became extinct in about 0.04 Myr and account for 31% of the planktic assemblages (Molina, 2015). The E/O boundary was defined at the Massignano section, coinciding with the extinction of the hantkeninids (Premoli Silva and Jenkins, 1993).

Larger foraminifera living in shallow platforms had a turnover (Orabi et al., 2015), but did not suffer extinction coinciding with the E/O boundary (Molina et al., 2016), although the magnitude of this turnover is not yet well known. Small benthic foraminifera, living in bathyal and abyssal environments, are not so well studied as planktic and their pattern of extinction at the E/O boundary is not yet known in detail. Deep-sea benthic foraminifera underwent a mass but gradual extinction from the late Eocene-early Oligocene, with modern type assemblages becoming established (Kaminski et al., 1989; Thomas, 1992; Thomas and Gooday, 1996; Kaminski and Gradstein, 2005; Thomas and Via, 2007).

The aim of this work is to study the paleoenvironmental changes across the E/O boundary in North East Tunisia, based on the quantitative analyses of small benthic and planktic foraminiferal assemblages at the Menzel bou Zelfa and Jhaff composite section. The richness of planktic foraminiferal species reflects the climatic stability of the water, and therefore, varies depending on ocean circulation being greatest where redistribution of hot water masses is promoted (Wade and Pearson, 2008). This causes a variety of ecological habitats where the various species of life grow and proliferate. The planktic foraminiferal extinction event is known to coincide with the E/O boundary, but little is known about what happened at the sea bottom. Our study therefore, focuses on small benthic foraminifera in order to investigate the nature and timing of the benthic foraminiferal turnover and to ascertain whether the benthic extinctions coincided with the E/O boundary and the beginning of the Oi1 glaciation.

2. Geological and geographical setting

The 54 m thick Menzel Bou Zelfa (MBZ) section is located in the north-eastern of Tunisia in the Cap Bon peninsula. Section sampling was carried out on the NE flank of the anticline Jebel Abderrahmane. The stratigraphic series is essentially composed of marls, limestones and sands ranging in age from the middle Eocene to Quaternary (Fig. 1). However, in some places the E/O boundary interval was covered with Quaternary deposits, for which reason it was decided to merge two separate sections into a single composite one. It was necessary to carry out detailed sampling across the E/O boundary, which is why a better exposed section in the same area about 1 km to the south was chosen, located between the coordinate points 36° 42′16.44″N and 10°41′42.5800E. This interval of the composed section is named Jhaff (J6-J13). This detailed interval was located between MBZ 26 and MBZ 25 (Fig. 2).

This section is composed of light grey marls occasionally interbedded with centimetric argillaceous reddish limestone beds, rich in iron oxide and is called Unit 1. From sample Jhaff 11 it comprises a sandy limestone bed rich in iron oxide and is called Unit 2. This sample marks a transition to a new facies characterized by grey sandy marls. This facies is overlaid by dark grey marls intersected at the top by a centimetric bed of indurated marl with ferruginous concretions. The units 1 and 2 are marine and belong to the Tellien Domain. The top of the section is formed by light grey marl, sometimes intercalated with yellowish to brownish rust, overlaid with a sandstone bed with yellow limestone cement known as Unit 3. This upper unit is terrestrial and belongs to the Numidian Flysch (Boukhalfa et al., 2009).

3. Materials and methods

In the field it was possible to select a complete section, which was accessible and presented the best outcrop. An initial scatter sampling was performed during the first visit to identify the location of the boundaries, followed by a second more detailed sampling to further characterize them.

The marly samples were washed in the laboratory. Each sample was soaked in tap water for few days, adding diluted H_2O_2 for some very compacted samples. These samples were then washed through a column of three interlocking sieves, with meshes 250 μm, 150 μm and 63 μm. The washed residue was collected in Petri dishes and dried in a stove at a temperature of 50 °C.

The residues were sorted and observed under a binocular microscope in order to identify the foraminifera. The quantitative and taxonomic studies were based on representative splits of >300 specimens of the 63 and 150-μm fraction combined, obtained with an Otto microsplitter and the rest of the sample was scanned to look for rare species. Relative abundance of common taxa was calculated, together with faunal indices commonly used in ecology and paleoenvironmental reconstruction. The most representative taxa were photographed using the Scanning Electron Microscope at the ETAP (Tunisian National Oil Company).

The biostratigraphy of this section was previously studied and published by the present authors (Karoui-Yaakoub et al., 2017) with planktic foraminifera biozonation based on Pearson et al. (2006). The last occurrence (LO) of the index taxon *Globigerinatheka semiinvoluta* was used to recognize E14, the LO of *Globigerinatheka index* to mark E15, the LO of *Hantkenina alabamensis* to locate the E16/O1 boundary, and the LO of *Pseudohastigerina naguewichiensis* to mark the first biozone of the Rupelian (Fig. 2).

Benthic fauna occupies numerous and diverse ecological niches. Indeed, it yields a considerable amount of information about the conditions of the bottom of the ocean and has played an important role over the years in interpreting these conditions. Furthermore, determining the micro-habitat of benthic foraminifera is fundamental as it allows us to specify the ecological requirements of each species. This work has used quantitative analysis based primarily on the nature of foraminifera tests, whether calcitic, agglutinated or porcelaneous (Fontanier, 2003).

4. Results

In this work the association of planktic foraminifera in the middle and upper Eocene sediments reflects a considerable number of individuals (about 500 individuals), belonging to around 25 species. This number of planktic foraminifera is relatively small compared to the number of species of benthic foraminifera (see below). Major turnovers of planktic foraminifera occur across the E/O boundary; the quantitative analysis revealed that planktic foraminifera are very numerous but not very diversified (about 7 species). Furthermore, it showed low diversity of benthic foraminifera (about 15 species) and represented by a relatively small number of individuals (Fig. 2).

The planktic foraminifera are present in all samples of the middle Eocene to the lower Oligocene succession interval and show a variation of the assemblage composition and relative abundance. A faunal turnover occurred during the E/O transition interval and includes major extinctions of some species such as the extinction of

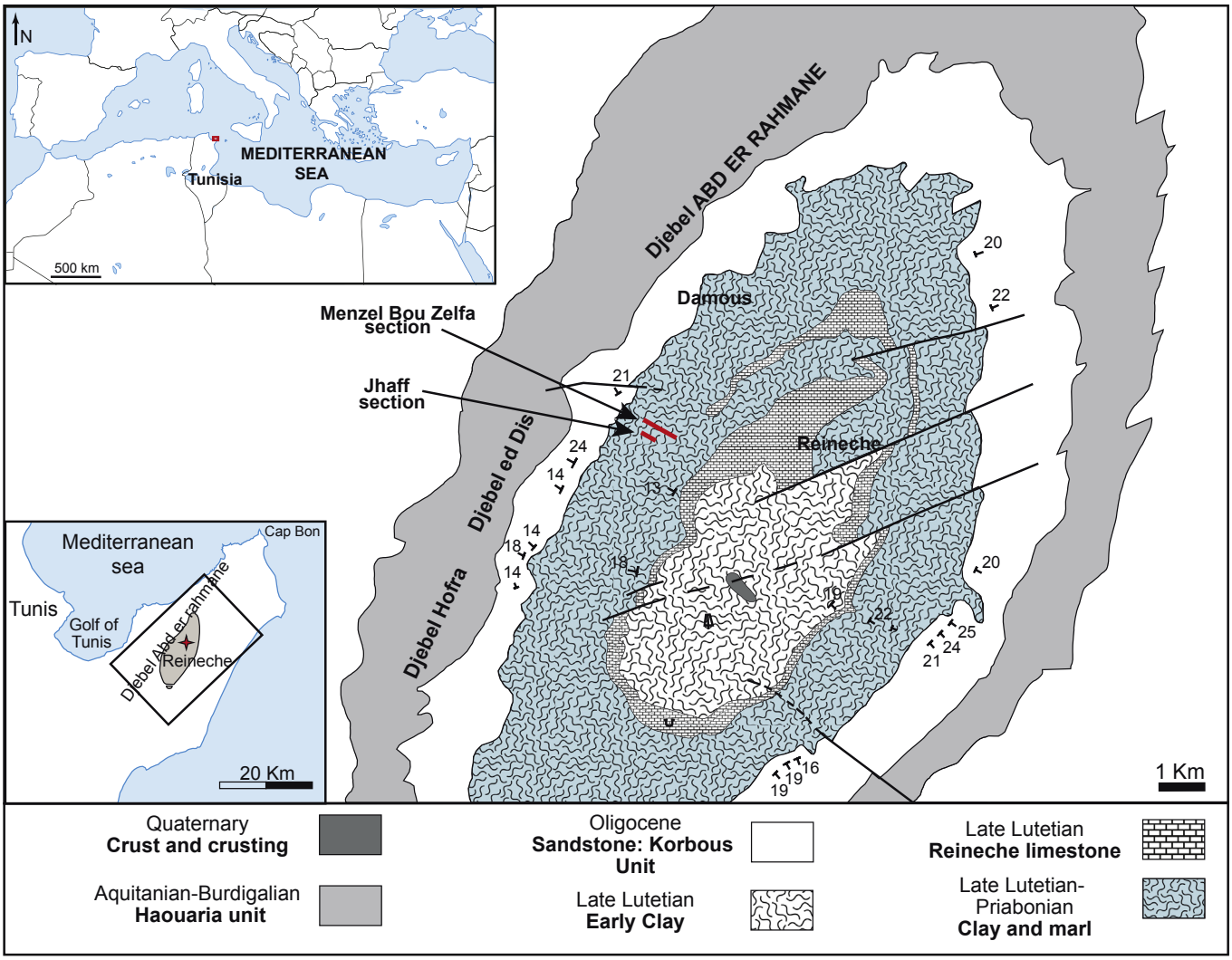

Fig. 1. Geographical and geological location of the Menzel Bou Zelfa and Jhaff sections.

all species of the genus *Hantkenina* and three species of *Turborotalia* (*T. cerroazulensis* Cole, *T. cocoaensis* Cushman, *T. cunialensis* Toumarkine and Bolli). At the same time, species such as *Pseudohastigerina micra* Cole, *P. naguewichiensis* Myatliuk, *Chilguembelina ototara* Finlay, *Streptochilus martini* Pijpers, and *Tenuitella praegemma* Li dominate the assemblages.

Above the E/O boundary, there is a gradual decrease in the influence of pelagic realm signaled by a decreased number of planktic foraminifera and a micro-faunistic undiversified association announced by a low value of species richness, 10 to 15 species per sample. According to Wade and Pearson (2008), a minor change in temperature can have an important effect on planktic foraminifera as their niches are closely grouped together and depend on the stratification of the water column.

Benthic foraminiferal species richness varies from 30 to 50 species per sample, represented mainly by calcitic test species such as *Bolivinoides floridana* Cushman, *Brizalina antegressa* Subbotina, *Globocassidulina subglobosa* Brady, *Cibicidoides mundulus* Brady, Parker and Jones, *C. praemundulus* Berggren and Miller, *Oridorsalis umbonatus* Reuss and *Gyroidina girardana* Reuss. Indeed, the extinction of only two species (*Nuttallides truempyi* Nuttall and *Angulogerina muralis* Terquem) was observed across the E/O transition interval.

The dominance of the benthic foraminifera especially with the calcitic test, is recorded throughout the section (Fig. 3), such as *B. floridana, Br. antegressa* Subbotina, *Gl. Subglobosa* Brady, *C. mundulus* Brady, *C. praemundulus* Berggren and Miller, *O. umbonatus* Reuss, *G. girardana* Reuss, *C. eocaenus* Gümbel, *C. mexicanus* Nuttall, and representative species of tri-serial tests groups such as *Bulimina jarvisi* Cushman and Parker, *Bu. macilenta* Cushman and Parker, *Bu. jacksonensis* Cushman, *Bu. thanetensis* Cushman and Parker and *Bu. secaensis* Cushman and Stainforth.

On the other hand, the agglutinated test forms are less abundant (around 10%) and are represented by the species *Reticulophragmium amplectens* Gzybowski, *Valvulina peruviana* Cushman and Stainforth, *Rhadbamina samunica* Berry, *Ammodiscus* sp., *Karrierella* sp. The Miliolidae with porcelaneous tests are represented mainly by Spiroloculinidae and are very rare throughout the section.

5. Discussion

As foraminifera constitute the major protists in many marine ecosystems (Murray, 1991), we will discuss their role in the reconstruction of the paleoenvironment. Their potential for fossilization makes them good indicators of the physicochemical

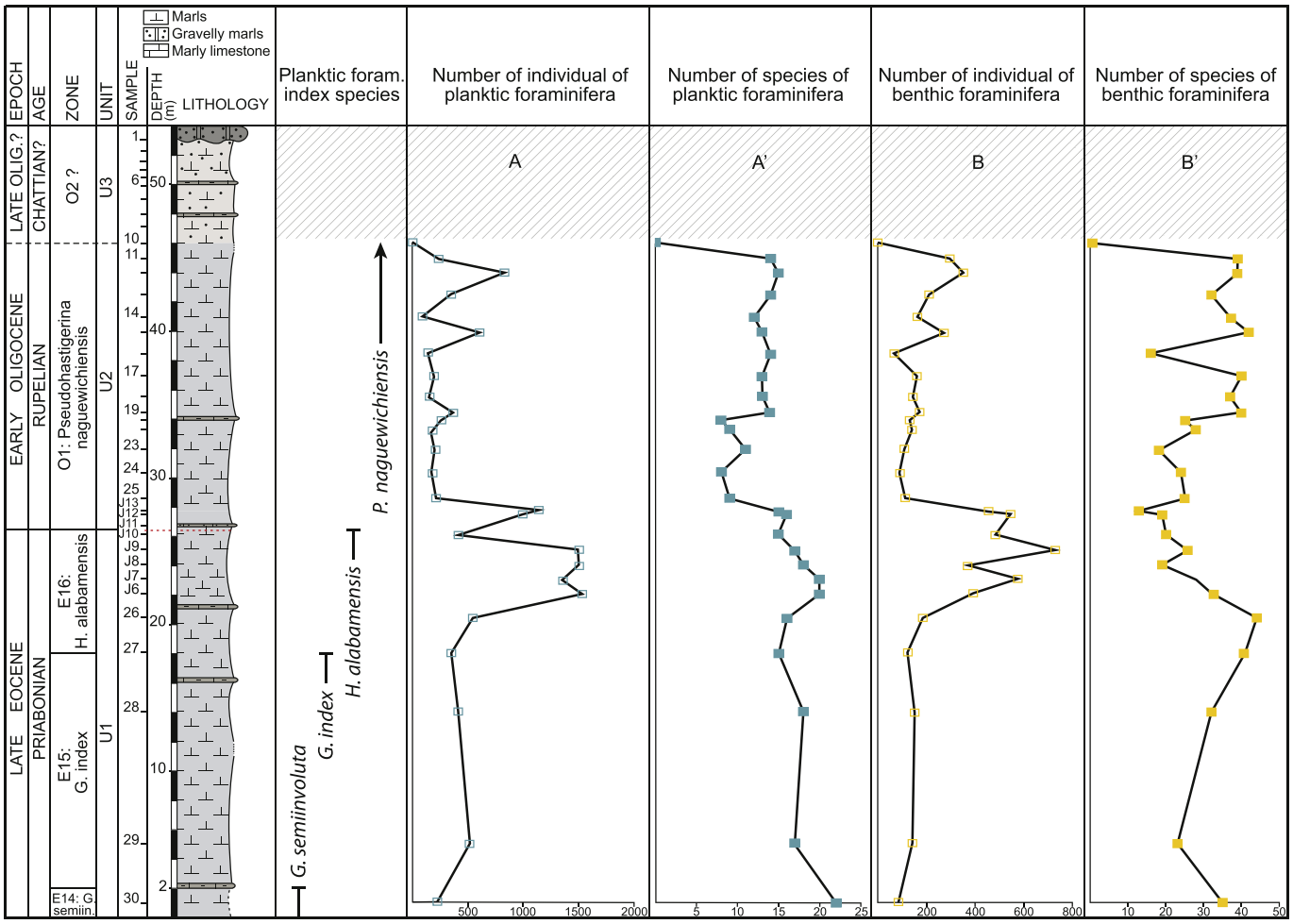

Fig. 2. Planktic foraminiferal biostratigraphy and specific richness of foraminifera.

conditions of deposition environment where they were buried. Changes in relative abundances and diversity have been used to infer changes in carbonate saturation state, oxygenation and food supply (Gooday, 2003).

The calcitic test assemblages found are typical of bathyal and abyssal environments; generally, the Bolivinidae, Buliminidae, Uvigerinidae and Cibicidoidae genera require bathyal environments (Holbourn et al., 2013). On the contrary, Gyroidinoidinae indicates an abyssal domain. We also noticed the coexistence of several species such as *C. mexicanus* Nuttall, *Bu. Jarvisi* Cushman and Parker, *C. grimsdalei* Nuttall, indicators of a low to median bathyal environment (Holbourn et al., 2013) (Fig. 3).

Furthermore, we identified cosmopolitan species which thrive in deep sea basins such as *Nuttallides umboniferus* rarely found on the Oligocene sediment, *Epistominella exigua* which was also rarely found on the Eocene and Oligocene sediment, and *Cibicidoides wuellerstorfi* which are distributed all along the section (Jorissen et al., 2007). However, below the E/O boundary we recorded the LO of the species *Nuttallides truempyi* which is proposed to reflect fluctuations in organic matter flux to the seafloor (meso-to eutrophic) under oxygenated bottom-water conditions. Indeed, it is one of the dominant lower bathyal-abyssal taxa with an age range of Late Cretaceous (Maastrichtian) to latest Eocene, which was reported in Molina et al. (2006), Berggren and Miller (1989) and Holbourn et al. (2013). *Angulogerina muralis,* which refer to the Eocene (Ortiz and Thomas, 2006; Molina et al., 2006) was also found in this section and we marked the LO close to the E/O which was also reported in the Fuente Caldera section in Spain (Molina et al., 2006) (Fig. 3a).

The assemblages of small benthic foraminifera in Menzel Bou Zelfa and Jhaff sections are very diverse. Species with calcitic test are significantly the most dominant and have a very high frequency ranging from 85.63 to 100%. This percentage reflects sedimentation above the CCD. The quantitative study of benthic foraminifera species immediately below the E/O boundary (Fig. 4) shows the abundance of bathyal forms, the most important among them being *Br. antegressa* (around 8%) and *B. floridana* (around 6%). Moreover, we cannot exclude the presence of some foraminifera with calcitic test but typical of neritic environment such as Lagenidae and Lenticulininae (around 0.1–0.7%). Their presence is interpreted as the result of erosion of the shallow levels and thus transport from the platform to the bathyal environment. On the other hand, we noticed the presence of some agglutinated forms mostly represented by clavulinids, *Ammodiscus*, *Karrierella*, vulvulinids, and *Plectina* such as *Cyclamina cancellata, Ammodiscus incertus* and *Reticulophragmium amplectens,* which coincide with Alano section NE Italy (Agnini et al., 2011). These forms show relatively small percentages (about 0.05%).

Approaching the E/O boundary, the abundance of these agglutinated forms shows a slight increase, particularly of the species *Cyclammina cancellata*, which shows a maximum value 0.68% (Table 1). This increase is negligible compared to percentages of

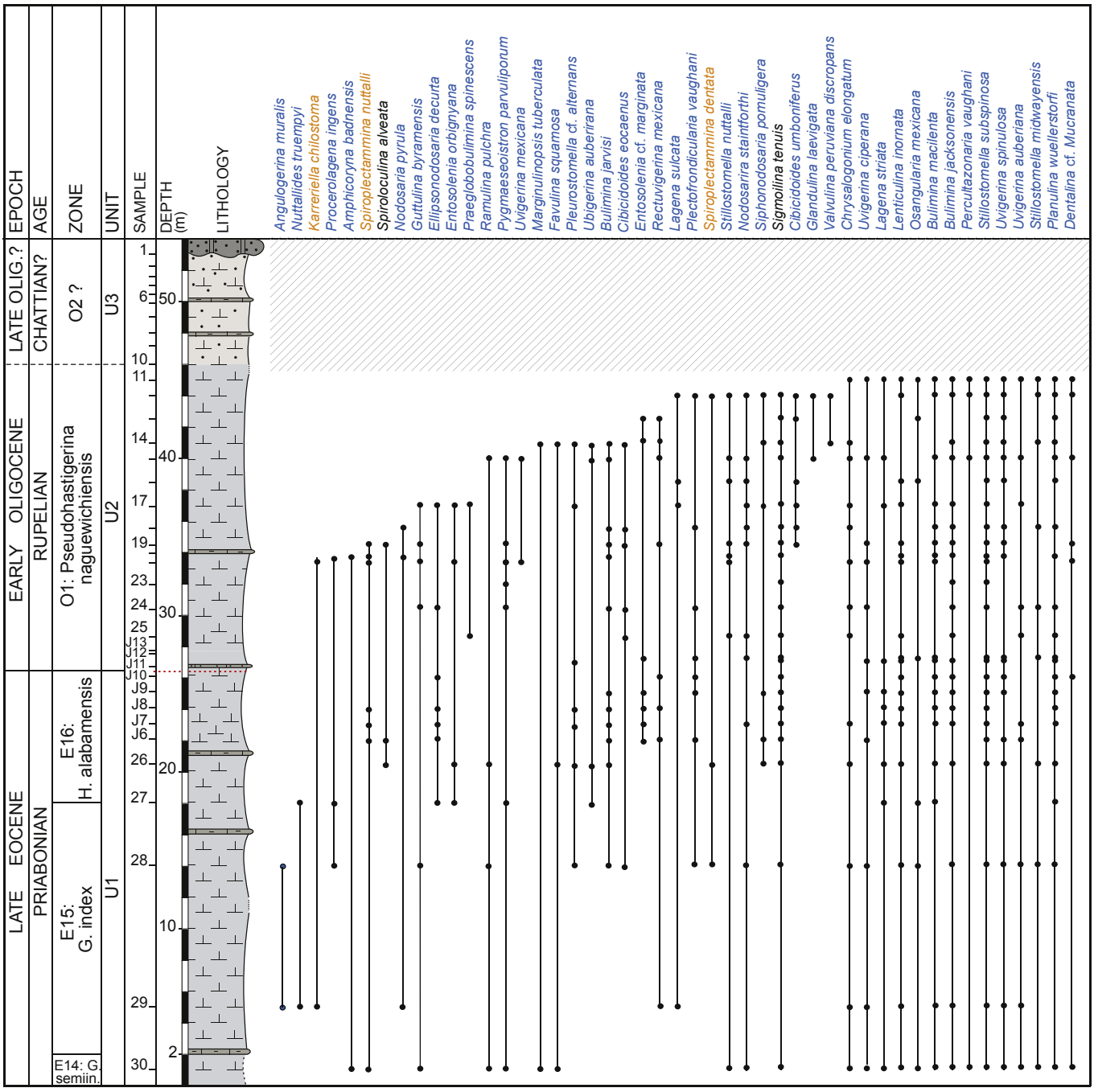

Fig. 3a. Stratigraphic distribution of benthic foraminifera species.

forms of hyaline tests that showed considerable ability to survive and thrive during the limit. While the frequency of species with hyaline tests increased steadily up to the upper part of the O1 Zone reaching a high frequency of around 98.3%.

This mixture of foraminifera, comprising 3 types of test, could be indicative of a decrease in sea level and an increase in erosion that caused the transport of certain non-native species from the platform to the bathyal domain. This decrease could be linked to the cooling and global glaciation characterizing the E-O transition (Molina et al., 2006). Approaches based on micro-organisms for the estimation of paleo-depth have been developed by determining the index of oceanity which normally increases with depth (Bellier et al., 2010). The density of planktic foraminifera is therefore maximal in open marine environments. Moreover, we have also used some species of benthic foraminifera considered to be indicator species for paleobathymetry (Nyong and Olsson, 1984; Van Morkhoven et al., 1986; Culver, 2003; Alegret and Thomas, 2004).

The index of oceanity shows values close to 80% (Fig. 5) at the base of the series, decreasing to 40% at sample Jhaff 10. Indeed, the index marks some fluctuations in the last 30 m (from sample MBZ 26). The percentages of around 80% recorded at the base of the series indicate sedimentation in nearby bathymetries 200 m and more precisely the upper bathyal domain. This is confirmed by the presence of an association of planktic foraminifera typical of the surface dwellings and intermediate environments (Molina et al., 2006) such as *T. cunialensis*, *T. cocoaensis*, *Cr. inflata*, *H.*

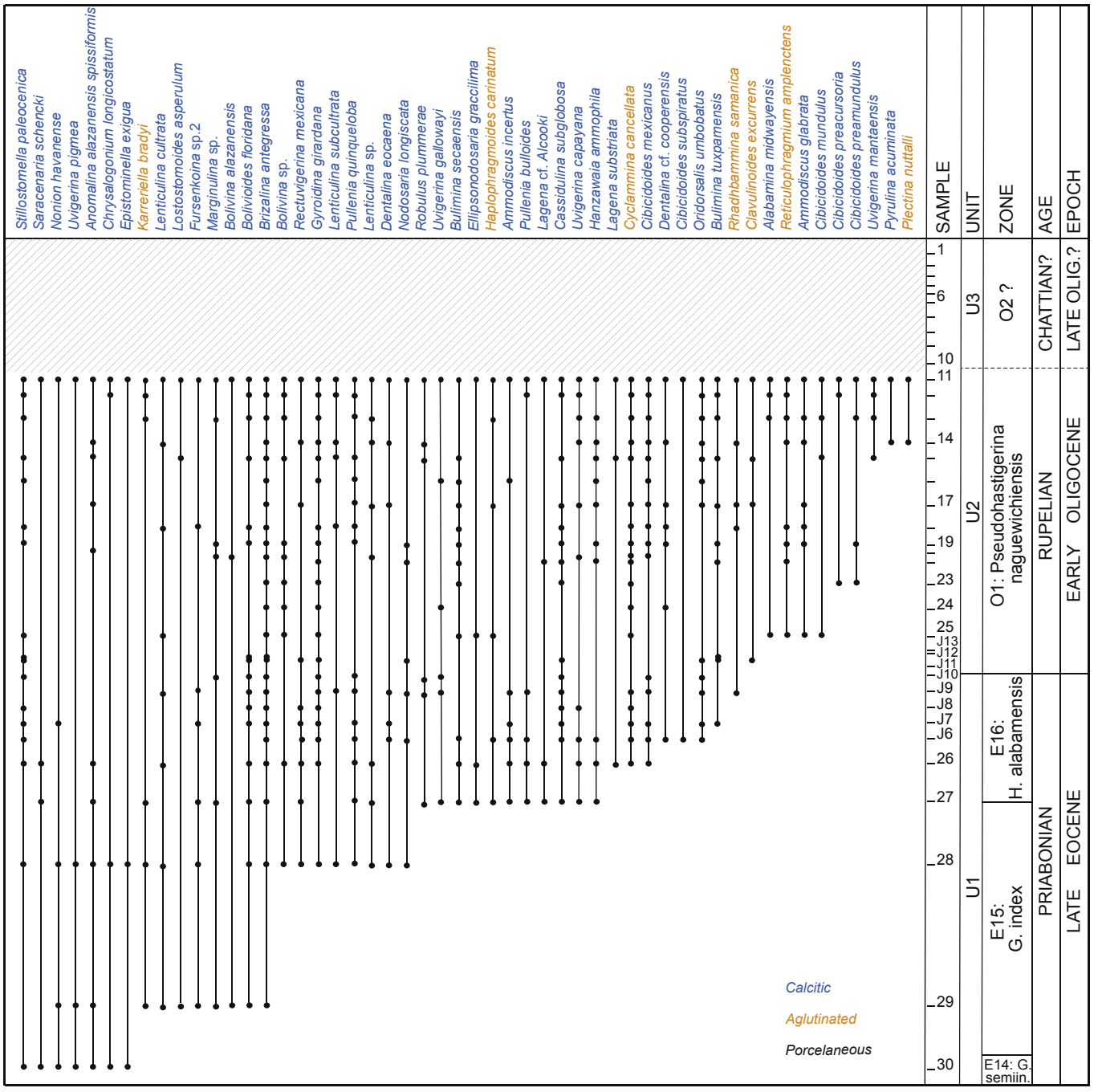

Fig. 3b. Stratigraphic distribution of benthic foraminifera species.

alabamensis, S. linaperta, S. corpulenta, S. eocaena that showed a relative abundance at the base of this series (Fig. 5). However, it should be noted that values below 80% indicating low bathymetries are probably related to a fall in the number of planktic foraminifera and therefore the state of preservation of these microorganisms. This reflects a disturbance of stratification of the water column caused by the decline in sea level. Moreover, the upheaval in the behavior of foraminifera is essentially due to the disappearance of the latest keeled forms and therefore a fall in the index of oceanity at the E/O boundary. However, this change is followed by the development of typical forms of deep dwellings such as *D. pseudovenezuelana, D. tripartita, C. unicavus, Gl. suteri*. At the same time, we note that the assemblages of benthic foraminifera are dominated by the calcitic test forms of the upper bathyal domain such as *B. floridana, Br. antegressa, Gl. subglobosa, C. mundulus, O. umbonatus.*

The abundance of benthic forms is continuous throughout the series, causing the decrease of the index of oceanity, showing the eustatic variation during the late Eocene and the base of Oligocene. The relative fall of this index at the E/O boundary could indicate a decrease in sea level, from the decline of the sea spawned during global cooling.

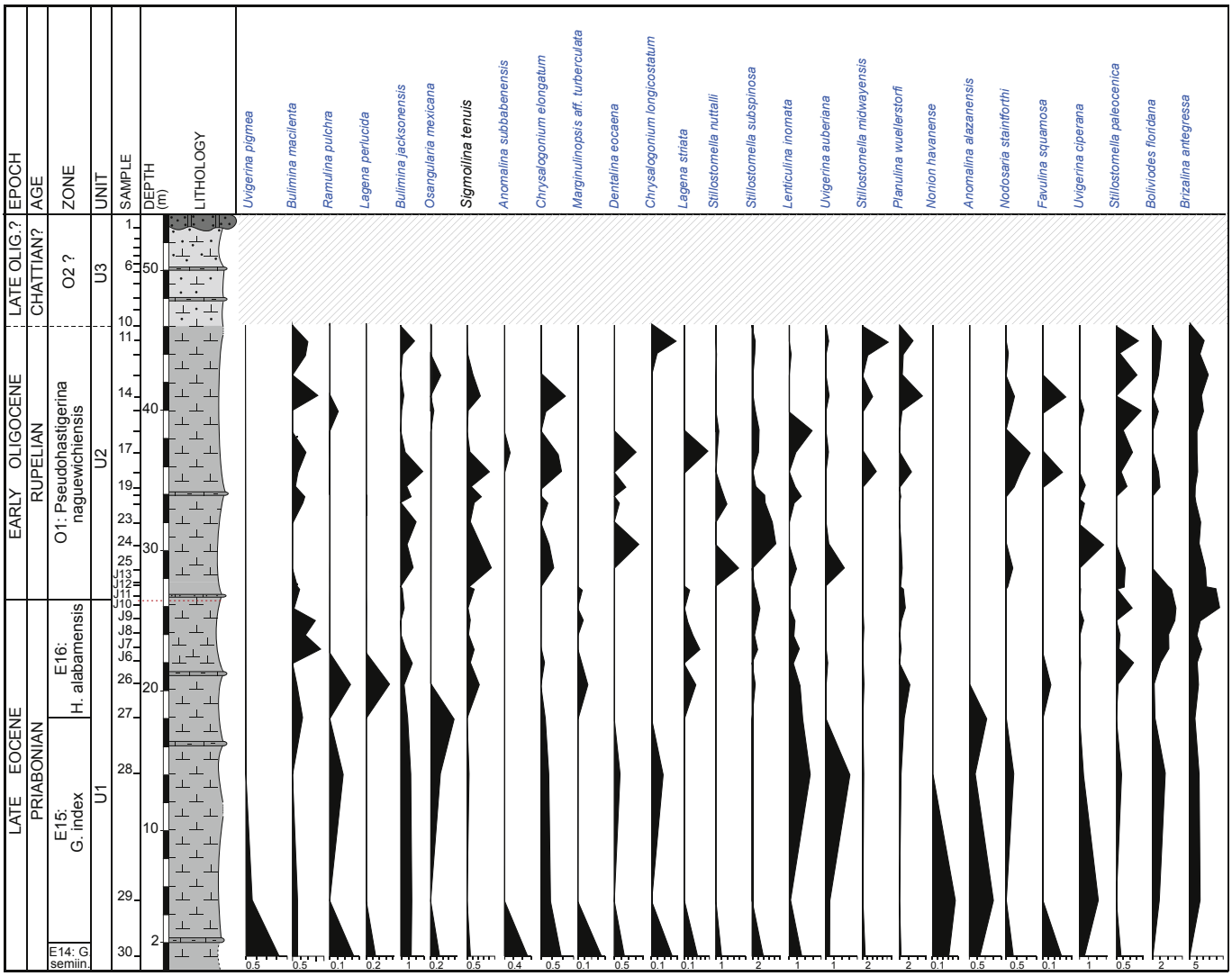

Fig. 4a. Relative abundances of the most common benthic foraminifera species.

Foraminifera have a rapid adaptation to environmental changes, a potential for fossilization and a strong correlation with the latitudinal distributions of surface temperatures, and the use of approaches based on the morphology of their test could provide an estimation of the paleotemperature and paleobathymetry (Murray, 1991). The change in the water column structure is mainly due to the variation of the thermocline, which is defined as the depth where we find the highest temperature transition. Even in the general case, the warm surface waters or deep thermocline favors the establishment of shallow dwellings with warm waters. However, the reduction in depth of the thermocline favors deep niches and forms that thrive in cold waters (Wade and Pearson, 2008).

In the section of Menzel Bou Zelfa and Jhaff, planktic foraminifera present a well-preserved test in all samples. At the base of the section, precisely in the E14, E15 biozones of *Gl. semiinvoluta* and *Gl. index,* we notice a major faunal change in the history of the evolution of planktic foraminifera, which involves paleoenvironmental implications in determining the Bartonian/Priabonian boundary (Fig. 5). These changes are manifested by the absence of keeled forms such as *Morozovelloides* and *Acarinina* that are abundant in low and middle latitudes (Agnini et al., 2011). In fact, these forms normally record the low values of $\delta^{18}O$ and the greatest values of $\delta^{13}C$ and are typical of warm waters (Pearson et al., 1993, 2001; Norris, 1996). The absence of these typical forms of surface water, with no disruption of those living in deeper waters, generally reflects a drop in temperature or more precisely the cooling of surface waters.

According to Wade (2004), the extinction of these keeled forms may result from the destruction of their dwellings, due initially to sudden cooling of the thermocline. In addition, the drop in temperature is accompanied mainly by a decrease in the depth of the thermocline. These forms are therefore disturbed by the installation of a low temperature zone, meaning an inability to adapt to these conditions caused their major extinction. This structural change in the water column may also have impacts on the reproductive side of foraminifera, leading to a gradually decreasing frequency. This change was followed by the invasion of the mixed level by the genera *Hantkenina, Turborotalia* and *Subbotina* at the reduced level of the thermocline, and thus the change in the depth of their niches (Wade, 2004).

This extinction can be associated with several factors including the main cause, which is the inability of *acarininids* to overcome this temperature decrease. A small increase in the number of keeled forms on the upper Eocene at samples (J6, J7, J8, J9, MBZ 26, MBZ27,

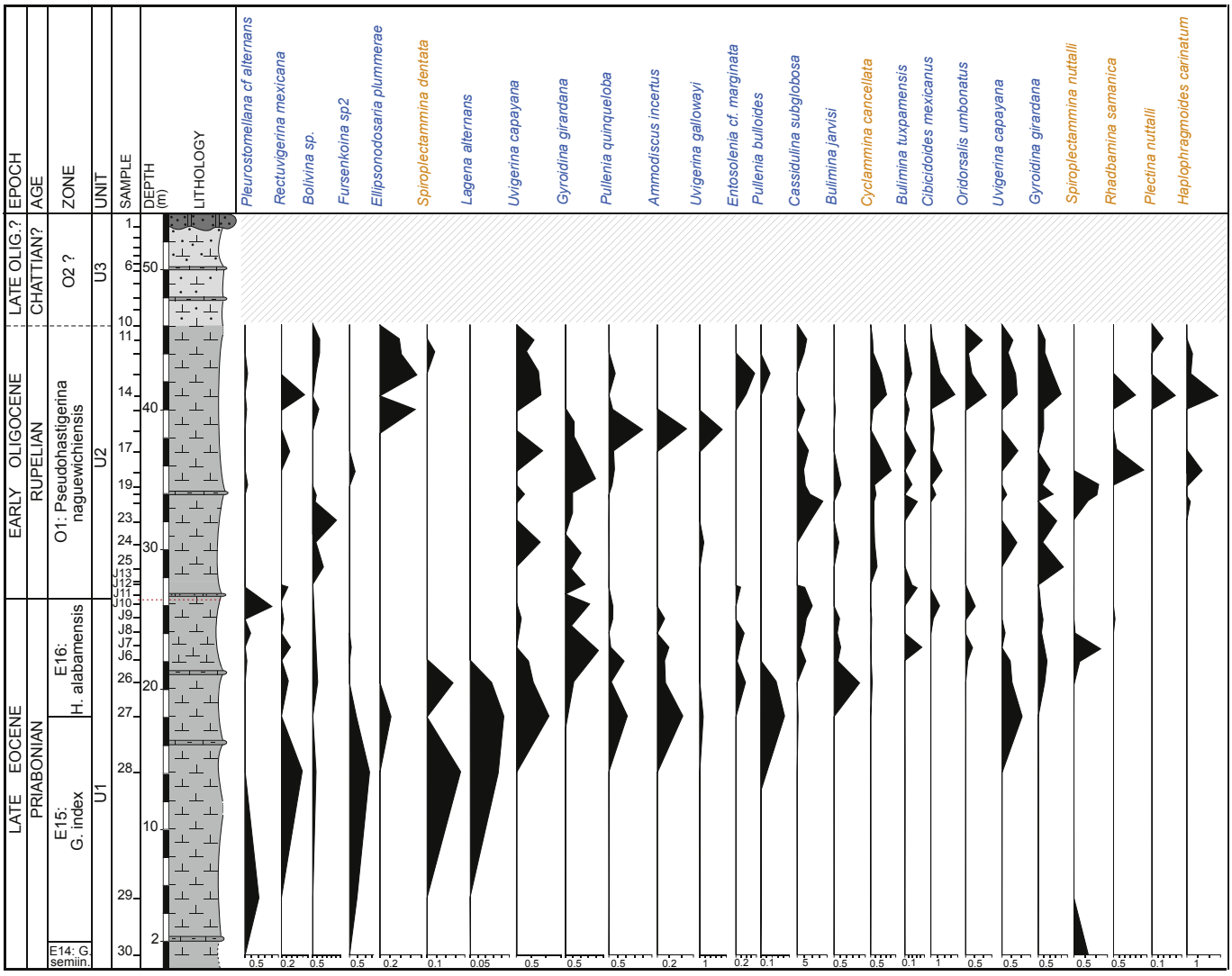

Fig. 4b. Relative abundances of the most common benthic foraminifera species.

MBZ28, MBZ 29) could be explained by a particular abundance of the species: *T. cunialensis, T. cocoaensis T. cerroazulensis, H. primitiva, H. compressa.*

The top of the Eocene, precisely the top of the E16 zone, is characterized by the last appearance of five species of the genus *Hantkenina,* typical of surface dwellings; *H. compressa, H. primitiva, H. nanggulanensis, H. alabamensis* and *Cribrohantkenina lazzarii,* is associated with the extinction of *T. cerroazulensis T. cunialensis* and *T. cocoaensis*. According to Coxall and Pearson (2007), these species require the establishment of a warm climate with considerable oxygen levels, which explains their development during the Middle to Upper Eocene. In addition, Molina et al. (2006) pointed out that these species would be linked to a lower rate of $\delta^{18}O$ and a high rate of $\delta^{13}C$, belonging to the group of low and middle latitudes reflecting a mixed level of warm water. Thus, the species which survived the beginning of the cooling would subsequently be affected by this event.

From the boundary, this extinction of tropical and subtropical forms is followed by an increase in the number of species belonging to the families Globigerinidae, Globoquadrinidae and the species *T. ampliapertura*. However, at the base of the Oligocene the species *S. corpulenta* and *S. eocaena* and the Globoquadrinidae *Dentoglobigerina galavisi*, *Dentoglobigerina pseudovenezuelana* constantly increase in number. According to Wade and Pearson (2008), these species show high values of $\delta^{18}O$ which reflect dwellings belonging to a deep cold thermocline. It should be noted that *Catapsydrax unicavus* which appears on the lower Eocene is one of the species that has shown a considerable abundance after the E/O boundary and is considered a good indicator of deep, cold environments (sub thermocline) (Pearson et al., 2001). Based on these data, some species are indicators of cold deep water. These species have survived despite the crisis by adapting to the new way of life; the others were not able to survive and underwent a major extinction.

However, we noticed the existence of a third group of foraminifera that was affected by this crisis but was able to adapt to these conditions, these are the *Pseudohastigerina* group. According to Wade and Pearson (2008), the species *Ps. naguewichiensis* is associated with values depleted in $\delta^{18}O$, indicating that it has been calcified in the mixed levels. Indeed we notice the existence of this species in the samples above the E/O boundary, but in the fractions less than 150 μm, meaning it suffered an actual reduction in size. Furthermore, the species *Ps. micra* has been able also adapt to these conditions using a different strategy. Indeed, they are smaller than

Table 1
Percentages of small benthic foraminifera.

	Uvigerina pigmea	*Bulimina macilenta*	*Ramulina pulchra*	*Lagena perlucida*	*Bulimina jacksonensis*	*Osangularia mexicana*	*Sigmoilina tenuis*	*Anomalina subbadenensis*	*Chrysalogonium elongatum*	*Marginulinopsis aff. tuberculata*	*Dentalina eocaena*	*Lagena striata*	*Spiroplectammina nuttalli*	*Stillostomella nuttalli*	*Stillostomella subspinosa*
MBZ1	0	0	0	0	0	0	0	0	0	0	0	0	0	0	0
MBZ2	0	0	0	0	0	0	0	0	0	0	0	0	0	0	0
MBZ3	0	0	0	0	0	0	0	0	0	0	0	0	0	0	0
MBZ4	0	0	0	0	0	0	0	0	0	0	0	0	0	0	0
MBZ5	0	0	0	0	0	0	0	0	0	0	0	0	0	0	0
MBZ6	0	0	0	0	0	0	0	0	0	0	0	0	0	0	0
MBZ7	0	0	0	0	0	0	0	0	0	0	0	0	0	0	0
MBZ8	0	0	0	0	0	0	0	0	0	0	0	0	0	0	0
MBZ9	0	0	0	0	0	0	0	0	0	0	0	0	0	0	0
MBZ10	0	0	0	0	0	0	0	0	0	0	0	0	0	0	0
MBZ11	0	0,95	0	0	1,71	0	0	0	0	0	0	0	0	0	1,14
MBZ12	0	0,84	0	0	0,25	0	0,08	0	0	0	0	0	0	0,08	1,09
MBZ13	0	0,00	0	0	0	0,35	0,53	0	0	0	0	0	0	0	0,35
MBZ14	0	1,58	0	0	0,39	0	1,18	0	1,18	0	0	0	0	0	0,39
MBZ15	0	0,00	0,11	0	0,11	0,11	0,11	0	0,22	0	0	0	0	0	1,02
MBZ16	0	0,00	0	0	0	0	0	0	0	0	0	0	0	0,48	2,42
MBZ17	0	0,84	0	0	0,55	0	0,27	0,27	0,83	0	1,4	0,55	0	0,27	2,23
MBZ18	0	0,34	0	0	2,72	0	2041	0	1,02	0	0	0	0	0	0,34
MBZ19	0	0,18	0	0	0,73	0	0,37	0	0	0	0,74	0	1,1	0,92	1,29
MBZ21	0	0,77	0	0	1,27	0	1,27	0	0	0	0	0	1,02	1,53	4,34
MBZ22	0	0,64	0	0	0	0	0,64	0	0,32	0	0,32	0	0,64	1,92	4,5
MBZ23	0	0,00	0	0	1,93	0	0,32	0	0	0	0	0	0	0	7,09
MBZ24	0	0,00	0	0	0,77	0	1,16	0	0,38	0	1,56	0	0	0	8,17
MBZ25	0	0,00	0	0	1,53	0	2,15	0	0,61	0	0	0	0	4	0
Jhaff13	0	0,31	0	0	0	0	0,18	0	0	0	0	0	0	0	0,81
Jhaff12	0	0,45	0	0	0,19	0	0,64	0	0	0,06	0	0,13	0	0	1,23
Jhaff10	0	0,11	0	0	0,44	0	0,11	0	0	0	0	0	0	0	2,78
Jhaff9	0	1,57	0	0	0	0	0,31	0	0	0,09	0	0,09	0	0	2,02
Jhaff8	0	0,83	0	0	0,05	0	0,16	0	0	0	0	0,22	0,05	0	0,88
Jhaff7	0	1,87	0	0	0,62	0	0,67	0	0	0	0	0,41	1,19	0	2,08
Jhaff6	0	0,00	0	0	1,19	0	0,25	0	0,15	0,05	0	0	0,25	0	0
MBZ26	0	0,27	0,27	0,82	0,41	0	1,09	0	0	0,13	0	0,27	0	0	1,09
MBZ27	0	0,64	0	0	0,85	0,85	0	0	0,21	0	0	0	0	0	0
MBZ28	0	0,00	0,17	0	1,24	0,35	0,17	0	0,35	0	0,36	0	0	0	0
MBZ29	0,3	0,30	0	0	1,36	0	0	0	0,45	0	0	0	0	0	0
MBZ30	1,61	0,32	0,32	0,32	1,29	0,32	0,32	1,29	0,96	0,32	0,65	0,32	0,64	0,96	3,87

	Lenticulina inornata	*Uvigerina auberiana*	*Stillostomella midwayensis*	*Planulina wuellerstorfi*	*Nonion havanense*	*Anomalina alazanensis*	*Nodosaria stainforthi*	*Favulina squamosa*	*Uvigerina ciperana*	*Stillostomella paleocenica*	*Brizalina antegressa*	*Bolivioides floridana*	*Pleurostomellana* cf. *alternans*	*Rectuvigerina mexicana*	*Fursenkoina* sp2	*Ellipsonodosaria plummerae*	*Bolivina* sp	*Spiroplectammina dentata*
MBZ1	0	0	0	0	0	0	0	0	0	0	0	0	0	0	0	0	0	0
MBZ2	0	0	0	0	0	0	0	0	0	0	0	0	0	0	0	0	0	0
MBZ3	0	0	0	0	0	0	0	0	0	0	0	0	0	0	0	0	0	0
MBZ4	0	0	0	0	0	0	0	0	0	0	0	0	0	0	0	0	0	0
MBZ5	0	0	0	0	0	0	0	0	0	0	0	0	0	0	0	0	0	0
MBZ6	0	0	0	0	0	0	0	0	0	0	0	0	0	0	0	0	0	0
MBZ7	0	0	0	0	0	0	0	0	0	0	0	0	0	0	0	0	0	0
MBZ8	0	0	0	0	0	0	0	0	0	0	0	0	0	0	0	0	0	0
MBZ9	0	0	0	0	0	0	0	0	0	0	0	0	0	0	0	0	0	0
MBZ10	0	0	0	0	0	0	0	0	0	0	0	0	0	0	0	0	0	0
MBZ11	0	0,38	10,27	3,04	0	0	0	0	0	1,52	10,5	2,47	0	0	0	0,38	0,76	0
MBZ12	0,25	0	2,10	0,84	0	0	0,08	0	0	0,25	7,66	2,35	0	0	0	0,42	0,76	0,08
MBZ13	0	0	0	0,53	0	0	0	0	0	1,43	13,4	1,61	0,18	0	0	0,71	0,36	0
MBZ14	0	0,39	3,95	5,13	0	0	0,4	0,39	0	0	8,7	0	0	0,79	0	0	0	0
MBZ15	0	0	0	0,56	0	0	0,23	0	0,56	1,70	9,9	1,59	0,11	0	0	0,68	0,68	0
MBZ16	2,91	0	0	0	0	0	0	0	0	0,48	5,34	0	0	0	0	0	0	0
MBZ17	0,84	0,27	0	0	0	0	1,12	0	0	1,11	5,87	0	0	0,28	0	0	0	0
MBZ18	0	0	5,44	2,72	0	0	0,68	0,34	0	0,34	5,78	1,70	0	0	0,34	0	0	0
MBZ19	0,74	0	0	0	0	0	0,37	0	0,73	0,73	4,07	2,03	0,18	0	0	0	0,37	0
MBZ21	1,53	0	0	0,25	0	0	0	0	0	0	3,84	0	0	0	0	0	0,26	0
MBZ22	0,64	0	0	0	0	0	0	0	0,64	0	4,5	0	0	0	0	0	2,57	0
MBZ23	0	0	0	0	0	0	0	0	0	0	8,06	0	0	0	0	0	0,32	0
MBZ24	0	0,38	0,38	0,38	0	0	0	0	3,11	0	7	0	0	0	0	0	1,17	0

(*continued on next page*)

Table 1 (*continued*)

	Lenticulina inornata	*Uvigerina auberiana*	*Stillostomella midwayensis*	*Planulina wuellerstorfi*	*Nonion havanense*	*Anomalina alazanensis*	*Nodosaria stainforthi*	*Favulina squamosa*	*Uvigerina ciperana*	*Stillostomella paleocenica*	*Brizalina antegressa*	*Bolivioides floridana*	*Pleurostomellana* cf. *alternans*	*Rectuvigerina mexicana*	*Fursenkoina* sp2	*Ellipsonodosaria plummerae*	*Bolivina* sp	*Spiroplectammina dentata*
MBZ25	0,92	2,46	0	0,61	0	0	0,31	0	0	0,61	11,4	0	0	0	0	0	0	0
Jhaff13	0,13	0	0,06	0,25	0	0	0,13	0	0	0,56	12,5	4,32	0	0	0	0	0	0
Jhaff12	0,13	0	0	0,9	0	0	0	0	0,06	0,06	19,6	5,45	0	0,26	0	0	0	0
Jhaff10	0,11	0	0	1,33	0	0	0	0	0	1,11	22	6,68	2,12	0	0	0	0	0
Jhaff9	0,81	0	0	0,49	0	0	0	0	0,53	0	8,67	7,00	0	0	0	0	0	0
Jhaff8	0,61	0	0	0,05	0	0	0	0	0	0,27	5,61	4,73	0,44	0,06	0	0	0	0
Jhaff7	1,35	0,05	0	0,41	0	0	0,05	0	0	0,2	9,37	4,94	0	0,36	0,15	0	0	0
Jhaff6	0,41	0,2	0	0	0	0	0	0	0,10	0,98	4,67	1,86	0,1	0	0	0	0	0
MBZ26	1,37	0	0,41	2,32	0	0	0	0,13	0	0,13	6,44	0,41	0	0,27	0	0	0,55	0,27
MBZ27	1,72	0	0	1,07	0	1,07	0	0	0	0	3,86	0,64	0	0	0,42	0,21	0	0
MBZ28	2,66	3,19	0,35	0,35	0	0,36	0,36	0	0,53	0,35	6,93	3,55	0	0,71	1,24	0	0,36	0,36
MBZ29	0,15	0,45	0	0	0,45	1,52	0	0	2,42	0	7,59	1,82	1,06	0	0,45	0	0	0
MBZ30	1,61	0,32	0,96	0,32	0,32	0,65	0,32	0,32	0,64	0,32	0	0	0	0	0	0	0	0

	Lagena alternans	*Pullenia quiqueloba*	*Ammodiscus incertus*	*Uvigerina gallowayi*	*Pullenia bulloides*	*Cassidulina subglobosa*	*Bulimina jarvisi*	*Cyclammina cancellata*	*Bulimina tuxpamensis*	*Cibicidoides mexicanus*	*Rhadbammina samanica*	*Oridorsalis umbonatus*	*Entosolenia* cf. *marginata*	*Plectina nuttali*	*Uvigerina capayana*	*Gyroidina girardana*	*Haplophragmoides carinatum*
MBZ1	0	0	0	0	0	0	0	0	0	0	0	0	0	0	0	0	0
MBZ2	0	0	0	0	0	0	0	0	0	0	0	0	0	0	0	0	0
MBZ3	0	0	0	0	0	0	0	0	0	0	0	0	0	0	0	0	0
MBZ4	0	0	0	0	0	0	0	0	0	0	0	0	0	0	0	0	0
MBZ5	0	0	0	0	0	0	0	0	0	0	0	0	0	0	0	0	0
MBZ6	0	0	0	0	0	0	0	0	0	0	0	0	0	0	0	0	0
MBZ7	0	0	0	0	0	0	0	0	0	0	0	0	0	0	0	0	0
MBZ8	0	0	0	0	0	0	0	0	0	0	0	0	0	0	0	0	0
MBZ9	0	0	0	0	0	0	0	0	0	0	0	0	0	0	0	0	0
MBZ10	0	0	0	0	0	0	0	0	0	0	0	0	0	0	0	0	0
MBZ11	0	0	0	0	0	6,46	0	0,19	0	0,19	0	0,95	0	0,19	0,57	0,57	0
MBZ12	0	0	0	0	0,17	4,88	0	0,25	0,08	0,75	0	0,16	0	0	0,33	0,58	0
MBZ13	0	0,36	0	0	0	0	0	1,07	0,17	1,43	0	0,35	0,71	0	0,71	1,25	0
MBZ14	0	0	0	0	0	0	0	1,58	0	3,55	1,97	1,18	0,39	0,39	0,79	1,97	0
MBZ15	0	0,23	0	0	0	5,23	0,11	0,22	0,11	0,11	0	0	0	0	0	0,45	0
MBZ16	0	1,94	0,49	4,36	0	0	0	0	0	0,48	0	0	0	0	0	0,48	0
MBZ17	0	0,28	0	0	0	7,54	0	1,11	0,27	0,27	0,27	0	0	0	0,83	0	0
MBZ18	0	0,34	0	0	0	4,42	0,34	2,04	0	1,7	2,72	0	0	0	0	1,02	0
MBZ19	0	0,18	0	0	0	5,54	0,55	0,37	0,18	0,18	0	0	0	0	0	0,36	0
MBZ21	0	0	0	0	0	8,69	0,25	0,512	0	0,76	0	0	0	0	0,25	1,27	0
MBZ22	0	0	0	0	0	17,0	0	0,32	0,32	0	0	0	0	0	0	0	0
MBZ23	0	0	0	0	0	9,03	0	0,32	0	0	0	0	0	0	0	1,61	0
MBZ24	0	0	0	0,77	0	0	0,38	0,38	0	0	0	0	0	0	0,77	0,38	0
MBZ25	0	0	0	0	0	0	0	0,61	0	0	0	0	0	0	0	2,15	0,31
Jhaff13	0	0	0	0	0	8,46	0	0	0,18	0	0	0	0,18	0	0	0	0
Jhaff12	0	0	0	0	0	5,19	0	0	0,32	0	0	0,06	0	0	0	0,06	0
Jhaff10	0	0,22	0	0	0	10,13	0	0	0	1,33	0	0,55	0	0	0	0,22	0
Jhaff9	0	0,22	0,13	0	0,22	6,73	0,49	0,09	0	0,4	0,13	0	0,35	0	0	0,449	0
Jhaff8	0	0	0	0	0	4,89	0,27	0,05	0	0	0	0	0,16	0	0,16	0,27	0
Jhaff7	0	0,1	0,21	0	0	2,34	0,57	0,05	0,46	0	0	0,41	0,05	0	0	0,57	0
Jhaff6	0	0,73	0,1	0	0	4,76	0,25	0,05	0	0	0	0,1	0,31	0	0,36	0,62	0,16
MBZ26	0,14	0,14	0,14	0	0,27	0	2,05	0,13	0	0	0	0	0	0	0,54	0,54	0
MBZ27	0,21	1,07	0,43	0,64	0,43	0,64	0	0	0	0	0	0	0	0	1,07	0	0
MBZ28	0,18	0	0	0	0	0	0	0	0	0	0	0	0	0	0	0	0
MBZ29	0	0	0	0	0	0	0	0	0	0	0	0	0	0	0	0	0
MBZ30	0	0	0	0	0	0	0	0	0	0	0	0	0	0	0	0	0

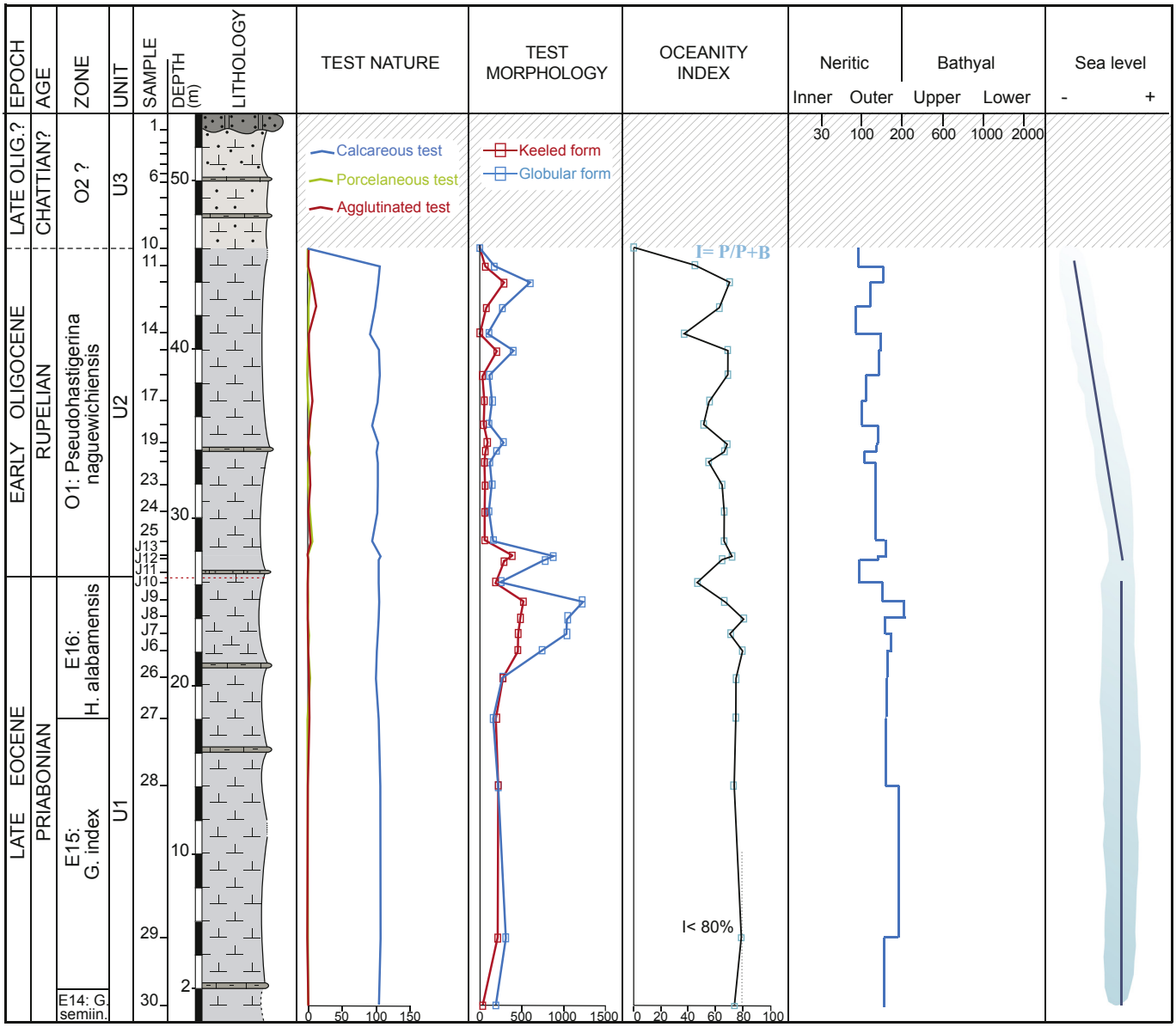

Fig. 5. Relative abundance of muricate and globular taxa, calcareous, agglutinated and porcelaneous taxa and the oceanity index.

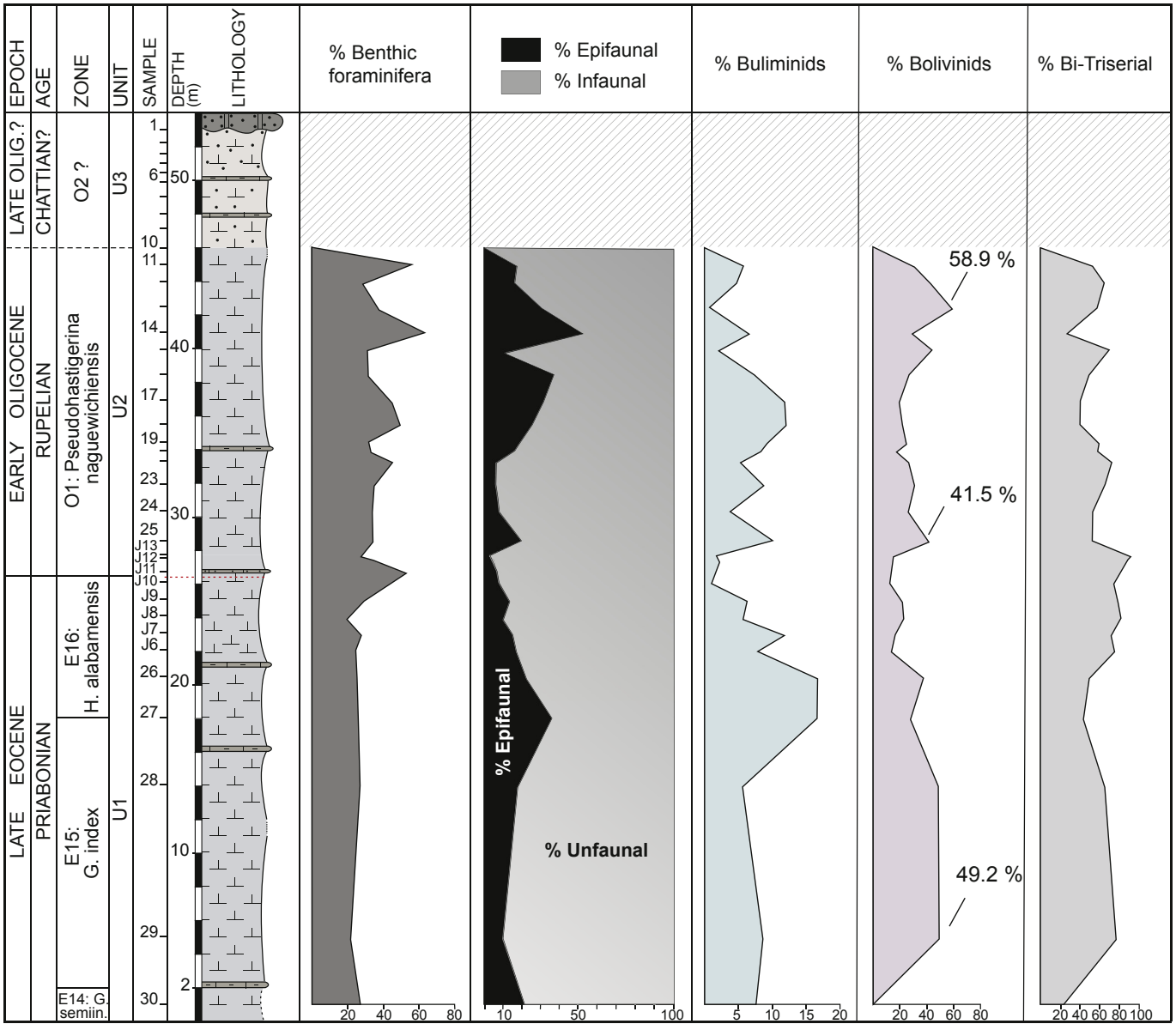

Fig. 6. Relative abundance of infaunal and epifaunal morphogroups.

150 μm and are considered *Pseudohastigerina* cf. *micra* (see Plate 1).

In conclusion, we can note a remarkable dominance of globular forms during the late Eocene to the Oligocene, adapting to the cold climate (Fig. 6). This can be explained by the instability of the environment in the tropical zones caused mainly by the decrease in temperature and thus the paleoecological changes of the foraminiferal habitat. These changes would likely be in conjunction with the predominance of glaciation in the high latitudes and a change in the circulation of deep waters (Wade and Pearson, 2008).

Due to their lifestyle, their ubiquity and richness in marine environments as well as their potential fossilization, benthic foraminifera are good markers of paleo-depth due to their ability to rapidly respond to environmental parameters. Based on the results obtained, it is noted that the benthic foraminifera assemblages reflect the variations in their relative abundances along the section, reacting to the cooling which starts at the upper Eocene. Below the boundary, there is a dominance of infaunal species characterized by percentage around 80%, due particularly to the high frequency of Buliminids and Bolivinids. Their high abundance could be related to a significant transfer of the organic matter to the bottom of the sea as they proliferate in these environments (Molina et al., 2006; Alegret et al., 2008; Fenero et al., 2012) (see Plate 2).

As we approach to the E/O boundary, we notice that the diversity of the assemblages decline, reaching the lowest values. This decrease is partly due to a decline in relative abundance of rectilinear species with complex apertures (Pleurostomella, Buliminidae, etc.) (Thomas and Via, 2007; Bordiga et al., 2015). We noticed also a temporary decrease in abundance of buliminids reaching 1.03%, also reported by Miller et al. (1985), Thomas (1992), and Coccioni and Galeotti (2003) in the Massignano section.

The presence of infauna increases after the boundary, reaching a maximum value of about 89%. This abundance of infauna is due to the proliferation of the Bi and Tri-serial forms (Fig. 6). Therefore, we interpret a high relative abundance of the infaunal, triserial

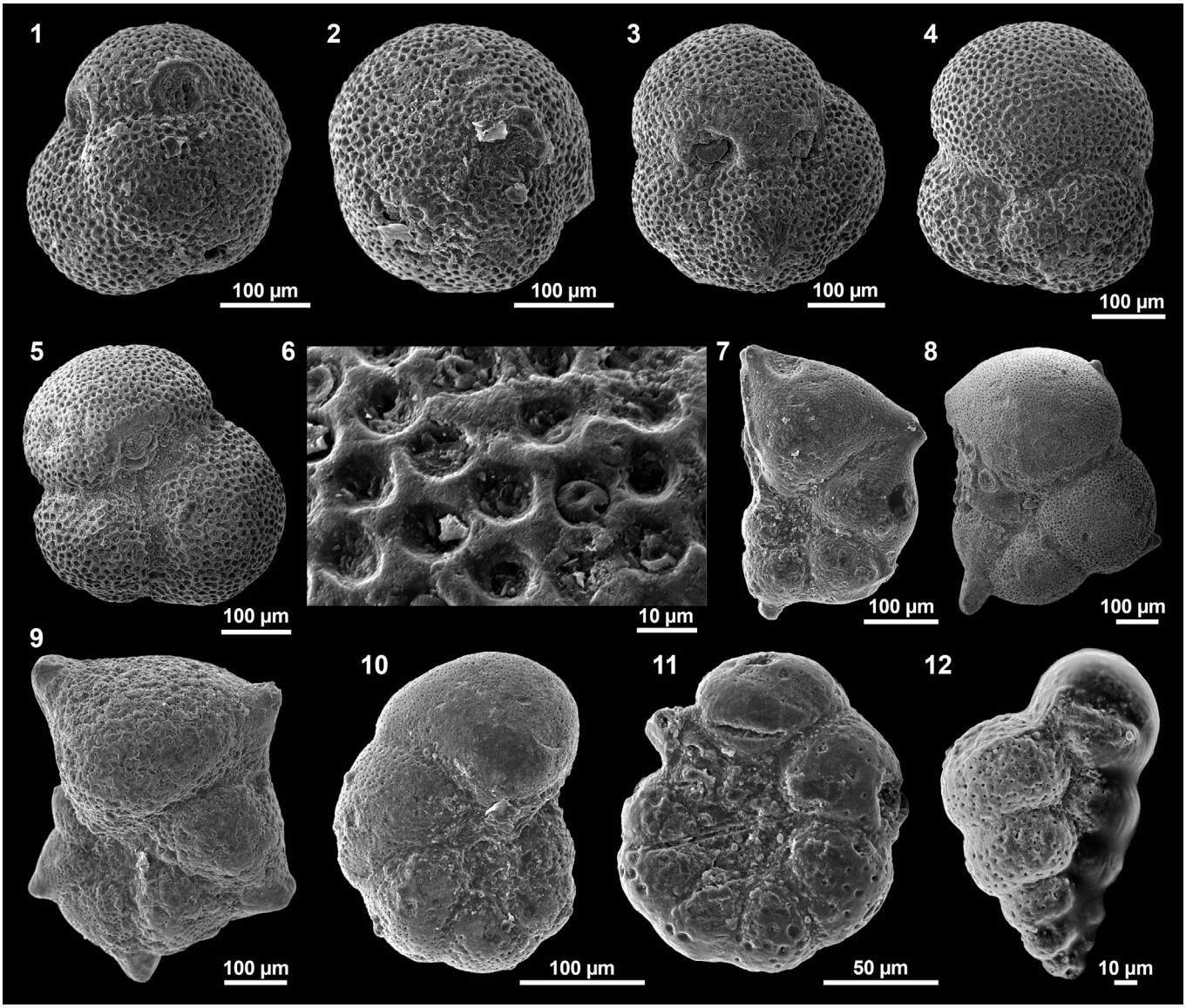

Plate 1. 1–3: *Globigerinatheka semiinvoluta* KEIJZER. Zone E14. Sample MBZ30. 4–5: *Globigerinatheka index* FINLAY. Sample MBZ29. Zone E15. 6: *Globigerinatheka index* FINLAY. Sample MBZ29. Zone E15. 7: *Hantkenina alabamensis* CUSHMAN. Sample MBZ 27. Zone E16. 8: *Cribrohantkenina inflata* HOWE. Sample MBZ 27. Zone E16. 9: Cribrohantkenina lazzarii. Sample Jhaff 8. Zone E16. 10: *Pseudohastigerina micra* COLE. Sample MBZ 12. Zone O1. 11: *Pseudohastigerina naguewichiensis* MYATLIUK. Sample MBZ 12. Zone O1. 12: *Streptochilus martini* PIJPERS. Sample MBZ 27. Zone E16.

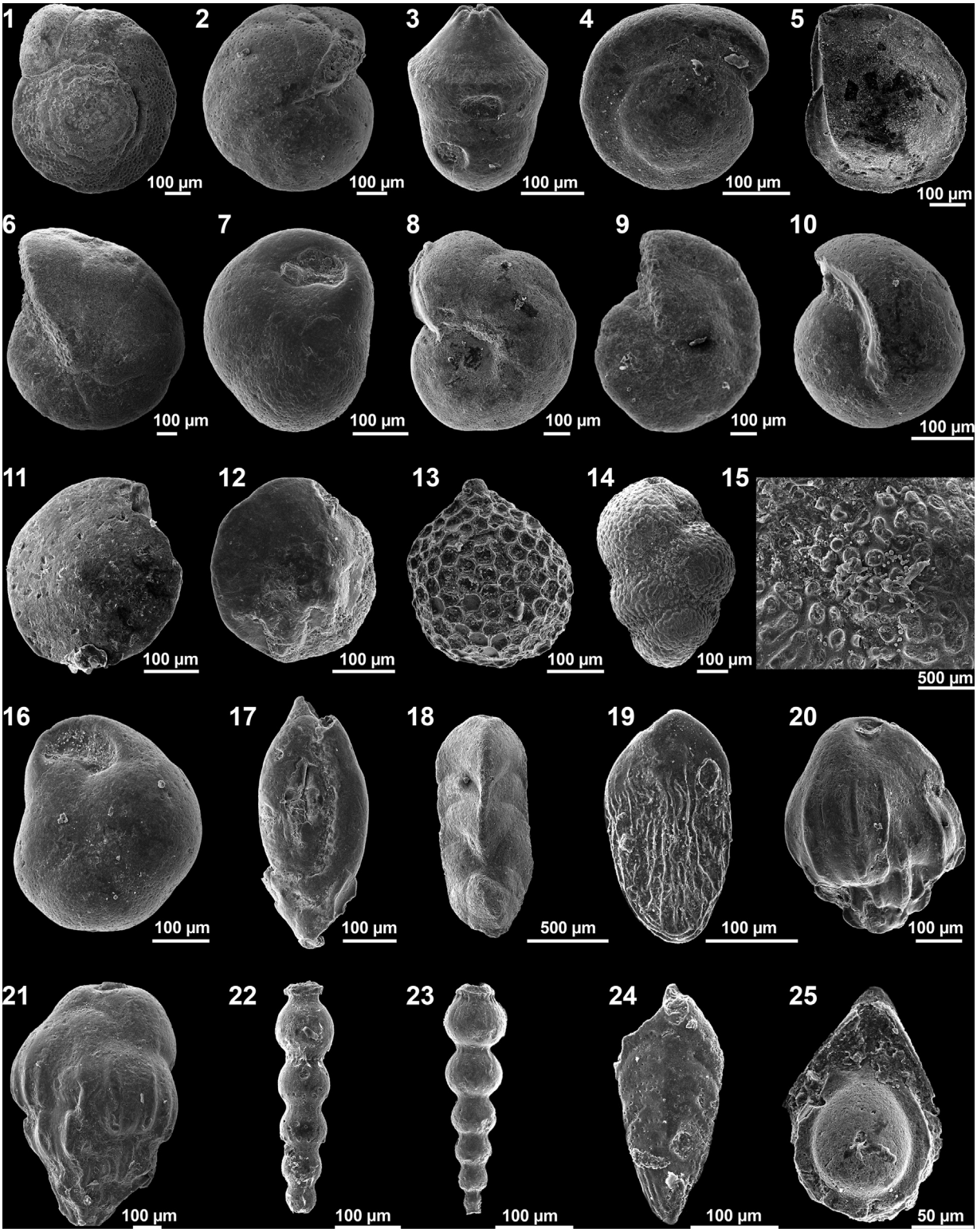

Plate 2. 1–2: *Cibicidoides mexicanus* NUTTALL. Sample MBZ15. Zone O1. 3:*Pseudoglandulina manifesta* REUSS. Sample MBZ29. Zone E15. 4: *Gyroidina girardana* REUSS. Sample MBZ29. Zone E15. 5: *Lenticulina inornata* D'ORBIGNY. Sample J12. Zone O1. 6: *Cyclammina cancellata* BRADY. Sample MBZ14. Zone O1. 7: *Globocassidulina subglobosa* BRADY. Sample MBZ16. Zone O1. 8: *Planulina wuellerstorfi* SCHWAGER. Sample J12. Zone O1. 9: *Reticulophragmium amplectens* GRZYBOWSKI. Sample MBZ12. Zone O1. 10: *Pullenia quinqueloba* REUSS. Sample MBZ28. Zone E15. 11–12: *Oridorsalis umbonatus* REUSS Cole. Sample J12. Zone O1. 13: *Favulina squamosa* MONTAGU. Sample MBZ30. Zone E14. 14: Plectina nuttalli CUSHMAN & STAINFORTH. Sample MBZ11. Zone O1. 15: *Plectina nuttalli* CUSHMAN & STAINFORTH. Sample MBZ11. Zone O1. 16: *Cassidulina caudriae* CUSHMAN & STAINFORTH. Sample MBZ13. Zone O1. 17: *Sigmoilina tenuis* CZJZEK. Sample J7. Zone E16. 18: *Clavulinoides eucarinatus* CUSHMAN & BERMUDEZ. Sample MBZ17. Zone O1. 19: *Coryphostoma midwayensis* CUSHMAN. Sample MBZ22. Zone O1. 20: *Bulimina macilenta* CUSHMAN & PARKER. Sample J12. Zone O1. 21: *Bulimina secaensis* CUSHMAN & STAINFORTH. Sample MBZ27. Zone E15. 22: *Stilostomella subspinosa* CUSHMAN. Sample MBZ22. Zone O1. 23: *Stilostomella paleocenica* CUSHMAN & TODD. Sample MBZ19. Zone O1. 24: *Brizalina antegressa* SUBBOTINA. Sample MBZ24. Zone O1. 25: *Entosolenia flintiana* CUSHMAN. Sample J8. Zone E16.

buliminids as indicative of a high food supply (Gooday, 2003; Bordiga et al., 2015). They are represented mainly by small size forms and smooth test or lightly ornamented by longitudinal costae, which generally explains a significant transfer of the potent supply to the bottom of the sea. Indeed, two peaks (around 50%) of Bolivinidae are recorded during the upper Eocene and at the E/O boundary. These peaks in fact correspond to an increase in the percentage of the species *Br. antegressa* and *B. floridana,* which are representative of bathyal domain. We suggest that this remarkable increase in the percentage of bolivinids is the response of benthic foraminifera to a local increase in the flux of organic matter to the sea floor. In parallel with the dominance of the infaunal group recorded throughout the section, we notice the presence of some epifaunal species also characteristic of bathyal domain such as *C. eocaenus, C. mexicanus, Planulina wuellerstorfi* and *Alabamina dissonata.*

This high influence of infaunal species typical of bathyal domains, markers of the environments with minimum oxygen and an important flow of organic matter (Gooday, 2003) such as *Bu. macilenta, Bu. jacksonensis, Bu. jarvisi, Br. antegressa, B. floridana, U. spinulosa* and *Glo. subglobosa* associated with a small percentage of epifaunal foraminifera (about 20%), undoubtedly indicates a bathyal environment with eutrophic conditions.

The assemblages of the benthic foraminifera found are the result of an accumulation of autochthonous and allochthonous forms, the latter being typical of neritic domains towards the deeper levels such *L. inornata, La. sulcata, Si. tenuis,* as well as the distribution of the organic substances in the bathyal zone. This mixture of forms could be related to the decrease in sea level at the beginning of the Oi1 glaciation, facilitating the transport of this shallow species towards deeper environments. The retreat of the sea is also accompanied by an increase in detrital elements observed from the sample MBZ 12.

Small benthic foraminifera do not show an extinction event at the E/O boundary, indicating that the benthic environment was not significantly affected. The extinction of *N. truempyi* is similarly not recorded up to the boundary, although it was considered a marker for the E/O boundary (Molina et al., 2006), possibly because the environment was not yet enough deep for this species to live in the section studied.

In the basal Oligocene O1 Zone, the small benthic foraminifera shows an apparently gradual pattern of extinction, which more likely could be a pattern of local disappearances caused by the decrease in temperature and depth. This pattern was not previously reported (Bolli et al., 1994; among others), although Hayward et al. (2010) suggested that it could be a benthic faunal turnover after the rapid E-O cooling event. The maximum glacial conditions occurred about 200 k.y. after the E/O boundary (Pearson et al., 2008). Consequently, this pattern of extinctions or disappearances could be caused by the Oi1 glaciation.

6. Conclusions

The detailed micropaleontological study of the samples of the Menzel Bou Zelfa and Jhaff section allowed us to establish different characteristics of the planktic and benthic associations of foraminifera, which meant we could reconstruct the paleoenvironment and highlight the global and regional eustatic changes.

The exploitation of all the micropaleontological data for planktic foraminifera led us to establish a regional scale of biozonation which we used to highlight the biological events recorded in the deposits of the E-O transition in accordance with the differential behavior of planktic and benthic foraminifera. In the biostratigraphic paper, we were able to recognize in the of Menzel Bou Zelfa and Jhaff section the following zones: E14. *Globigerinatheka semiinvoluta*, E15. *Globigerinatheka index,* E16. *Hantkenina alabamensis* for the late Eocene and zone O1. *Pseudohastigerina naguewichiensis* for the lower Oligocene.

Based on a quantitative analysis and paleoecological preferences for planktic and benthic foraminifera, we have established a general paleoenvironment reconstruction during the Eocene. From the base to the top of the Menzel Bou Zelfa and Jhaff section, these analyses revealed that the associations of foraminifera are characteristic of a relatively warm climate with considerable oxygen content during the middle to late Eocene, whereas at base of Oligocene the data indicates a cooling of the climate.

The diversity of foraminifera reveals that the top of the Eocene is marked by a massive extinction event of a distinctive group of planktic foraminifera, probably caused by the decrease in temperature, bathymetry and reduction in depth of the thermocline. Nevertheless, the small benthic foraminifera do not show an extinction event at the E/O boundary, indicating that the benthic environment was not significantly affected. Similarly, the extinction of *N. truempyi*, which is considered a marker for the E/O boundary, is recorded at the boundary due to bathymetry.

In the basal Oligocene a clear dominance of infaunal morphotypes with calcitic test, especially the bolivinids, indicates bathyal domains with cold-water, eutrophic seas and oxygen minimum. In the basal Oligocene O1 Zone, the benthic environment is apparently affected by a gradual extinction event that could be caused by the Oi1 glaciation. The small benthic foraminifera show a gradual pattern of extinction, which more likely could be local disappearances caused by the decrease in temperature and depth. Consequently, further studies are necessary to confirm whether this pattern is a global extinction event or just a local pattern of disappearances.

Acknowledgements

We would like to thank the research unit team “Petrologie sedimentaire et crystalline” of the Faculty of Sciences of Tunis and the team of the Electronic Microscopy Scanning laboratory of the Tunisian Petroleum Development Company (ETAP). This study received financial support and assistance through Project CGL2014-58794P from the Spanish Ministry of Science and Technology (FEDER funds) and Consolidated Group E05 from the Government of Aragón. We are grateful to Silvia Ortiz (PetroStrat, UK) for her helpful review that significantly improved the manuscript and to Paul Smith for correcting the English text. Furthermore, we would like to thank Orabi H. Orabi for reviewing the manuscript and Moncef Saïd Mtimed for help in the field and laboratory.

References

Agnini, C., Fornaciari, E., Giusberti, L., Grandesso, P., Lanci, L., Luciani, V., Muttoni, G., Pälike, H., Rio, D., Spofforth, D.J.A., Stefani, C., 2011. Integrated biomagnetostratigraphy of the Alano section (NE Italy): a proposal for defining the middle-late Eocene boundary. GSA Bulletin 123 (5/6), 841–872.

Alegret, L., Thomas, E., 2004. Benthic foraminifera and environmental turnover across the cretaceous/paleogene boundary at blake nose (ODP hole 1049C, Northwestern Atlantic). Palaeogeogr. Palaeoclimatol. Palaeoecol. 208, 59–83.

Alegret, L., Cruz, L.E., Fenero, R., Molina, E., Ortiz, S., Thomas, E., 2008. Effects of the Oligocene climatic events on the foraminiferal record from Fuente Caldera section (Spain, western Tethys). Palaeogeogr. Palaeoclimatol. Palaeoecol. 269, 94–102.

Barker, S., Broecker, W., Clark, E., Hajdas, I., 2007. Radiocarbon age offsets of foraminifera resulting from differential dissolution and fragmentation within the sedimentary bioturbated zone. Paleoceanography 22 (2). PA2205.

Bellier, J.-P., Mathieu, R., Granier, B., 2010. Short treatise on foraminiferology (essential on modern and fossilForaminifera) (Court traité de foraminiférologie (L'essentiel sur les foraminifères actuels et fossiles)). Carnets Géol. 1–104 [Notebooks on Geology].

Berggren, W.A., Miller, K.G., 1989. Cenozoic bathyal and abyssal calcareous benthic foraminiferal zonation. Micropaleontology 35, 308–320.

Bolli, H.M., Beckmann, J.P., Saunders, J.B., 1994. Benthic Foraminiferal

Biostratigraphy of the South Caribbean Region. Cambridge University Press.
Bordiga, M., Henderiks, J., Tori, F., Monechi, S., Fenero, R., Legarda-Lisarri, A., Thomas, E., 2015. Microfossil evidence for trophic changes during the Eocene Oligocene transition in the south Atlantic (ODP site 1263, Walvis Ridge). Clim. Past 11, 1249–1270.
Boukhalfa, K., Ben Ismail-Lattrache, K., Riahi, S., Soussi, M., Khomsi, S., 2009. Analyse biostratigraphique et sédimentologique des serieséoóligocènes et miocènes de la Tunisie septentrionale: implications stratigraphiques et géodynamiques. C. R. Geoscience 341, 49–62.
Coccioni, R., Galeotti, S., 2003. Deep-water benthic foraminiferal events from the Massignano eocene/oligocene boundary stratotype, Central Italy. In: Prothero, D.R., Ivany, L., Nesbitt, E. (Eds.), From Greenhouse to Icehouse: the Marine Eocene–oligocene Transition. Columbia University Press, pp. 438–452.
Coxall, H.K., Pearson, P.N., 2007. The eocene–oligocene transition. In: Haywood, W.M., et al. (Eds.), Deep-time Perspectives on ClimateChange: Marrying the Signal from Computer Models and Biological Proxies. The Micropalaeontological Society,Special Publications. The Geological Society, London, pp. 351–387.
Coxall, H.K., Wilson, P.A., 2011. Early Oligocene glaciation and productivity in the eastern equatorial Pacific: insights into global carbon cycling. Paleoceanography 26. PA2221.
Coxall, H.K., Wilson, P.A., Pälike, H., Lear, C.H., Backman, J., 2005. Rapid stepwise onset of Antarctic glaciation and deeper calcite compensation in the Pacific Ocean. Nature 433, 53–57.
Culver, S.J., 2003. Benthic foraminifera across the Cretaceous–Tertiary (K–T) boundary: a review. Mar. Micropaleontol. 47, 177–226.
DeConto, R.M., Pollard, D., 2003. Rapid Cenozoic glaciation of Antarctica induced by declining atmospheric CO2. Nature 421, 245–249.
Exon, N.F., Brinkhuis, H., Robert, C.M., Kennet, J.P., Hill, P.J., Macphail, M.K., 2004. Tectono-sedimentary history of uppermost Cretaceous through Oligocene sequences from the Tasmanian region, a temperate Antarctic margin. In: Exon, N.F., Kennett, J.P., Malone, M.J. (Eds.), The Cenozoic Southern Ocean: Tectonics, Sedimentation, and Climate Change between Australia and Antarctica. American Geophysical Union, Geophysical Monograph Series, vol. 151, pp. 319–344.
Farouk, S., Ahmad, F., Smadi, A.A., 2013. Stratigraphy of the middle eocene-lower Oligocene successions in northwestern and eastern Jordan. J. Asian Earth Sci. 73, 396–408.
Farouk, S., Faris, M., Ahmad, F., Powell, J.H., 2015. New microplalnktonic biostratigraphy and depositional sequences across the Middle-Late Eocene and Oligocene boundaries in eastern Jordan. GeoArabia 20 (3), 145–172.
Fenero, R., Thomas, E., Alegret, L., Molina, E., 2012. Oligocene benthic foraminifera from the Fuente Caldera section (Spain, western Tethys): taxonomy and paleoenvironmental inferences. J. Foraminifer. Res. 42 (4), 286–304.
Fontanier, C., 2003. Ecologie des foraminifères benthiques du Golf du Gascogne: Étude de la variabilité spatiale et temporelle des faunes de foraminifères benthiques et de la composition isotopique ($\delta^{18}O$, $\delta^{13}C$) de leurs tests. Thèse doctorale. Université Bordeaux.
Funakawa, S., Nishi, H., Moore, T.C., Nigrini, C.A., 2006. Late eocene–early Oligocene radiolarians, ODP leg 199 holes 1218A, 1219A, and 1220A, central pacific. In: Wilson, P.A., Lyle, M., Firth, J.V. (Eds.), Proc. ODP, Sci. Results, vol. 199, pp. 1–74.
Gonzalvo, C., Molina, E., 1992. Bioestratigrafía y cronoestratigrafía del tránsito Eoceno-Oligoceno en Torre Cardela y Massignano (Italia). Rev. Esp. Palaontol. 7, 109–126.
Gooday, A.J., 2003. Benthic foraminifera (Protista) as tools in deep water palaeoceanography: environmental influences on faunal characteristics. Adv. Biol. 46, 1–90.
Hayward, B.W., Johnson, K., Sabaa, A.T., Kawagata, S., Thomas, E., 2010. Cenozoic record of elongate, cylindrical, deep-sea benthic foraminifera in the North Atlantic and equatorial Pacific Oceans. Mar. Micropaleontol. 74, 75–95.
Holbourn, A., Henderson, A.S., Macleod, N., 2013. Atlas of Benthic Foraminifera. Natural History Museum.
Jorissen, F.J., Fontanier, C., Thomas, E., 2007. Paleoceanographical proxies based on Deep-sea benthic foraminiferal assemblage characteristics. In: Hillaire-Marcel, C., de Vernal, A. (Eds.), Proxies in Late Cenoczoic Paleoceanography 1, Developments in Marine Geology, pp. 263–313.
Kaminski, M.A., Gradstein, F.M., 2005. Atlas of Paleogene Cosmopolitan Deep-water Agglutinated Foraminifera. Kraków, 8, pp. 237–255. Grzybowski Fundation Special Publication.
Kaminski, M.A., Gradstein, F.M., Scott, D.B., Mackinnon, K.D., 1989. Benthic Foraminifera of the Baffin Bay and Labrador Sea. PANGAEA. https://doi.org/10.1594/PANGAEA.743960.
Karoui-Yaakoub, N., Grira, C., Mtimet, M.S., Negra, M.H., Molina, E., 2017. Planktic foraminiferal biostratigraphy, paleoecology and chronostratigraphy across the Eocene/Oligocene boundary in northern Tunisia. J. Afr. Earth Sci. 125, 126–136.
Lear, C.H., Bailey, T.R., Pearson, P.N., Coxall, H.K., Rosenthal, Y., 2008. Cooling and ice growth across the Eocene-Oligocene transition. Geology 36, 251–254.
Martínez-Gallego, J., Molina, E., 1975. Estudio del tránsito Eoceno-Oligoceno con foraminíferos planctónicos al Sur de Torre Cardela (Provincia de Granada, Zona Subbética). Cuadernos de Geología 6, 177–195.
Miller, K.G., Curry, W.B., Ostermann, D.R., 1985. Late paleogene (Eocene to Oligocene) benthic foraminiferal oceanography of the goban Spur region, deep sea drilling Project leg 80. In: Graciansky, P.C., Poag, C.W., et al. (Eds.), Initial Reports of the Deep Sea Drilling Project80, pp. 505–538.
Molina, E., 1980. Oligoceno-Mioceno inferior por medio de foraminíferos planctónicos en el sector central de las Cordilleras Béticas (España). Tesis doctoral. Publicación Universidades de Granada y Zaragoza.
Molina, E., 1986. Description and biostratigraphy of the main reference section of the Eocene/Oligocene boundary in Spain: Fuente Caldera section. Dev. Paleontol. Stratigr. 9, 53–63.
Molina, E., 2015. Evidence and causes of the main extinction events in the Paleogene based on extinction and survival patterns of foraminifera. Earth Sci. Rev. 140, 166–181.
Molina, E., Monaco, P., Nocchi, M., Parisi, G., 1986. Biostratigraphic correlation between the central Subbetic (Spain) and umbro-marchean (Italy) pelagic sequences at the eocene/oligocene boundary using foraminifera. Dev. Paleontol. Stratigr. 9, 75–85.
Molina, E., Keller, G., Madile, M., 1988. Late Eocene to Oligocene events: molino de Cobo, Betic Cordillera, Spain. Rev. Espanola Micropaleontol. 20, 491–514.
Molina, E., Gonzalvo, C., Keller, G., 1993. The Eocene-Oligocene planktic foraminiferal transition: extinctions, impacts and hiatuses. Geol. Mag. 130 (4), 483–499.
Molina, E., Gonzalvo, C., Ortiz, S., Cruz, L.E., 2006. Foraminiferal turnover across the Eocene–Oligocene transition at Fuente Caldera, southern Spain: No cause–effect relationship between meteorite impacts and extinctions. Mar. Micropaleontol. 58, 270–286.
Molina, E., Torres-Silva, A., Ćorić, S., Briguglio, A., 2016. Integrated biostratigraphy across the Eocene/Oligocene boundary at Noroña, Cuba, and the question of the extinction of orthophragminids. Newsl. Stratigr. 49 (1), 27–40.
Murray, J.W., 1991. Ecology and Paleoecology of Benthic Foraminifera. Longman Scientific and Technical, Harlow, Essex, England.
Nocchi, M., Monechi, S., Coccioni, R., Madile, M., Monaco, P., Orlando, M., Parisi, G., Premoli Silva, I., 1988. The extinction of Hantkeninidae as a marker for defining the Eocene–Oligocene boundary: a proposal. In: Premoli Silva, I., Coccioni, R., Montanari, A. (Eds.), The Eocene–Oligocene Boundary in the Marche-Umbria Basin (Italy). Ancona, International Subcommission on Paleogene Stratigraphy, pp. 249–252. Special Publication.
Norris, R.D., 1996. Symbiosis as an evolutionary innovation in the radiation of Paleocene planktic foraminifera. Paleobiology 22, 461–480.
Nyong, E.E., Olsson, R.K., 1984. A paleoslope model of campanian to lower maestrichtian foraminifera in the North American basin and adjacent continental margin. Mar. Micropaleontol. 8, 437–477.
Orabi, H., El Beshtawy, M., Osman, R., Gadallah, M., 2015. Larger benthic foraminiferal turnover across the eocene-oligocene transition at Siwa oasis, western desert, Egypt. J. Afr. Earth Sci. 105, 85–92.
Ortiz, S., Thomas, E., 2006. Lower–middle Eocene benthic foraminifera from the Fortuna section (Betic Cordillera, southeastern Spain). Micropaleontology 52 (2), 97–150.
Ortiz, S., Kaminski, A.M., 2012. Record of deep-sea, benthic elongate-cylindrical foraminifera across the Eocene-Oligocene transition in the North Atlantic Ocean (ODP hole 647a). J. Foraminifer. Res. 42 (4), 345–368.
Pagani, M., Huber, M., Liu, Z., Bohaty, S.M., Henderiks, J., Sijp, W., Krishnan, S., DeConto, R.M., 2011. The role of carbon dioxide during the onset of Antarctic Glaciation. Science 334, 1261–1264.
Pälike, H., Lyle, M.W., Nishi, H., Raffi, I., Ridgwell, A., Gamage, K., Klaus, A., Acton, G.D., Anderson, L., Backman, J., Baldauf, J.G., Beltran, C., Bohaty, S.M., Bown, P.R., Busch, W.H., Channell, J.E.T., Chun, C.O.J., Delaney, M.L., Dewang, P., Dunkley, J. Tom, Edgar, K.M., Evans, H.F., Fitch, P., Foster, G.L., Gussone, N., Hasegawa, H., Hathorne, Ed, Hayashi, H., Herrle, Jens O., Holbourn, A., Hovan, S.A., Hyeong, K., Iijima, K., Ito, T., Kamikuri, Shin-Ichi, Kimoto, K., Kuroda, J., Leon-Rodriguez, L., Malinverno, A., Moore, T.C., Murphy, B., Murphy, D.P., Nakamur, H., Ogane, K., Ohneiser, C., Richter, C., Robinson, R.S., Rohling, Eelco J., Romero, Oscar E., Sawada, Ken, Scher, Howie D., Schneider, L., Sluijs, A., Takata, H., Tian, J., Tsujimoto, A., Wade, B.S., Westerhold, T., Wilkens, Roy H., Williams, T., Wilson, P.A., Yamamoto, Y., Yamamoto, S., Yamazaki, T., Zeebe, R.E., 2012. A cenozoic record of the equatorial pacific carbonate compensation depth. Nature 488, 609–614.
Pearson, P.N., Wade, B.S., 2015. Systematic Taxonomy of Exceptionally Well-preserved Planktonic Foraminifera from the Eocene/Oligocene Boundary of Tanzania, 45. Cushman Foundation Special Publication, pp. 1–85.
Pearson, P.N., Shackleton, N.J., Hall, M.A., 1993. The stable isotope paleoecology of middle Eocene planktonic foraminifera and multispecies isotope stratigraphy, DSDP Site 523, South Atlantic. J. Foraminifer. Res. 23, 123–140.
Pearson, P.N., Norris, R.D., Empson, A.J., 2001. Mutabella mirabilis gen. et sp. nov., a Miocene microperforate planktonic foraminifer with an extreme level of intraspecific variability. J. Foraminifer. Res. 31 (2), 120–132.
Pearson, P.N., Olsson, R.K., Huber, B.T., Hemleben, C., Berggren, W.A. (Eds.), 2006. Atlas of Eocene Planktonic Foraminifera. Cushman Foundation for Foraminiferal Research, Fredericksburg.
Pearson, P.N., McMillan, I.K., Wade, B.S., Jones, T.D., Coxall, H.K., Bown, P.R., Lear, C.H., 2008. Extinction and environmental change across the Eocene-Oligocene boundary in Tanzania. Geology 36, 179–182.
Pearson, P.N., Foster, F.L., Wade, B.S., 2009. Atmospheric carbon dioxide through the Eocene-Oligocene climate transition. Nature 461, 1110–1113.
Premoli Silva, I., Jenkins, G., 1993. Decision on the Eocene Oligocene boundary stratotype. Episodes 16 (3), 379–382.
Shackleton, N., Kennett, J.P., 1976. Paleotemperature history of the Cenozoic and the initiation of Antarctic Glaciation: oxygen and carbon isotope analyses in DSDP sites 277, 279, and 281. In: Kennett, J.P.P., Houtz, R.E., et al. (Eds.), Initial Reports of the Deep Sea Drilling Project, vol. XXIX. U.S. Government Printing Office, Washington, D.C, pp. 743–755.

Stickley, C.E., Brinkhuis, H., Schellenberg, S.A., Sluijs, A., Fuller, M.D., Grauert, M., Röhl, U., Warnaar, J., Wiliams, G.L., 2004. Timing and nature of the deepening of the Tasmanian gateway. Paleoceanography 19 (4). PA4026.
Thomas, E., 1992. Middle Eocene–late Oligocene bathyal benthic foraminifera (Weddell Sea): faunal changes and implications for ocean circulation. In: Prothero, D.R., Berggren, W.A. (Eds.), Late Eocene–oligocene Climatic and Biotic Evolution. Princeton University Press, pp. 245–271.
Thomas, E., Gooday, A.J., 1996. Cenozoic deep-sea benthic foraminifers: tracers for changes in oceanic productivity? Geology 24 (4), 355–358.
Thomas, D.J., Via, R.K., 2007. Neogene evolution of Atlantic thermohaline circulation: perspective from Walvis Ridge, southeastern Atlantic ocean. Paleoceanography 22, PA2212.
Van Morkhoven, F.P.C.M., Berggren, W.A., Edwards, A.S., 1986. Cenozoic cosmopolitan deep-water benthic foraminifera. Bull. Cent. Rech. Explor.-Prod. Elf-Aquitaine - Mem. 11 (421 pp.).
Wade, B.S., 2004. Planktonic foraminiferal biostratigraphy and mechanisms in the extinction of Morozovella in the late middle Eocene. Mar. Micropaleontol. 51, 23–38.
Wade, B.S., Pearson, P.N., 2008. Planktonic foraminiferal turnover, diversity fluctuations and geochemical signals across the Eocene/Oligocene boundary in Tanzania. Mar. Micropaleontol. 68, 244–255.
Wade, B.S., Houben, A.J.P., Quaijtaal, W., Chouten, S., Rosenthal, Y., Miller, K.G., Katz, M.E., Wright, J.D., Brinkhuis, H., 2012. Multiproxy record of abrupt sea-surface cooling across the Eocene-Oligocene transition in the Gulf of Mexico. Geology 40 (2), 159–162.
Zachos, J.C., Quinn, T.M., Salamy, K.A., 1996. High resolution (104years) deep-sea foraminiferal stable isotope records of the Eocene-Oligocene climate transition. Paleoceanography 11, 251–266.

4.2 Contribution to the definition of the Bartonian GSSP

4.2.1. Reassessing the Bartonian unit stratotype at Alum Bay (Isle of Wight, UK): an integrated approach.

Laura Cotton, Lucía Rivero-Cuesta, Gloria Franceschetti, Alina Iakovleva, Laia Alegret, Jaume Dinarès-Turell, Jerry Hooker, Chris King, Richard Fluegeman, Stacy Yager & Simonetta Monechi, 2020

Newsletters on Stratigraphy 54/1, 17-42 545,

Newsletters on Stratigraphy, Vol. 54/1 (2021), 17–42 **Article**
Published online July 13, 2020; published in print January 2021

Reassessing the Bartonian unit stratotype at Alum Bay (Isle of Wight, UK): an integrated approach

Laura Cotton[1]*, Lucía Rivero-Cuesta[2], Gloria Franceschetti[3], Alina Iakovleva[4], Laia Alegret[2], Jaume Dinarès-Turell[5], Jerry Hooker[6], Chris King[7], Richard Fluegeman[8], Stacy Yager[8] and Simonetta Monechi[3]

With 13 figures

Abstract. The Global Stratotype Section and Point (GSSP) for the base of the Bartonian, currently remains undefined. The Bartonian unit stratotype is located at the Barton coastal section in the Hampshire Basin, on the South Coast of the UK. The base of the "Barton beds" was originally placed at the lowest occurrence of *Nummulites prestwichianus*, and this is still the basis of the recognition of the unit Bartonian Stage as a formal chronostratigraphic unit of the Paleogene. However, this biostratigraphic marker is not widely applicable elsewhere. The base of the lithostratigraphic unit, the Barton Clay Formation, also extends below this level creating further complication. The parastratotype section is located at Alum Bay, 7 km away, on the Isle of Wight. Despite a number of studies carried out in 1970s and '80s on both sections, global correlation remains problematic. Here we present an integrated (micropalaeontological, stratigraphic, palaeomagnetic) study of the Lutetian-Bartonian transition at Alum Bay, and aim at improving the stratigraphy of this section to better define the base of the Bartonian and contribute towards a decision on the GSSP.

Key words. Lutetian, Bartonian, GSSP, Nummulites, stratotype, biostratigraphy

1. Introduction

The Eocene Epoch is a dynamic period of Earth's history and has been the focus of numerous palaeontological, biostratigraphical, geochemical, magnetostratigraphical and palaeoclimatic studies. However, one of the Eocene stage boundaries remain formally undefined, the Bartonian. At present, the base of the Bartonian stage has no designated Global Stratotype Section and Point (GSSP). Traditionally the Bartonian has been defined by the Bartonian unit stratotype between Highcliffe and Barton-on-Sea (hereafter referred to as Barton), within the Hampshire Basin in the south of the UK, which contains well-preserved Pa-

Authors' addresses:
[1] Corresponding author: Department of Geological Sciences, University of Florida, 241 Williamson Hall, Gainesville, FL32611, U. S. A. Present address: School of Environment, Geosciences and Geography, University of Portsmouth, Burnaby Building, Burnaby Road, Portsmouth PO1 3QL, UK
[2] Departamento de Ciencias de la Tierra, Universidad de Zaragoza, Pedro Cerbuna 12, 50009 Zaragoza, Spain
[3] Dipartimento di Scienze della Terra, Università di Firenze, Via LaPira 4, I-50121 Firenze, Italy
[4] Laboratory of Paleofloristics, Geological Institute, Russian Academy of Sciences, Pyzhevsky pereulok 7, 119017 Moscow, Russia
[5] Istituto Nazionale di Geofisica e Vulcanologia (INGV), Via di Vigna Murata 605, I-00143 Roma, Italy
[6] Department of Earth Sciences, Natural History Museum, Cromwell Road, London SW7 5BD UK
[7] Deceased
[8] Department of Geological Sciences, Ball State University, Muncie, IN 47306-0475
* Corresponding author: laura.cotton@port.ac.uk

www.borntraeger-cramer.de
DOI: 10.1127/nos/2020/0563 0078-0421/2020/0563 $ 6.50

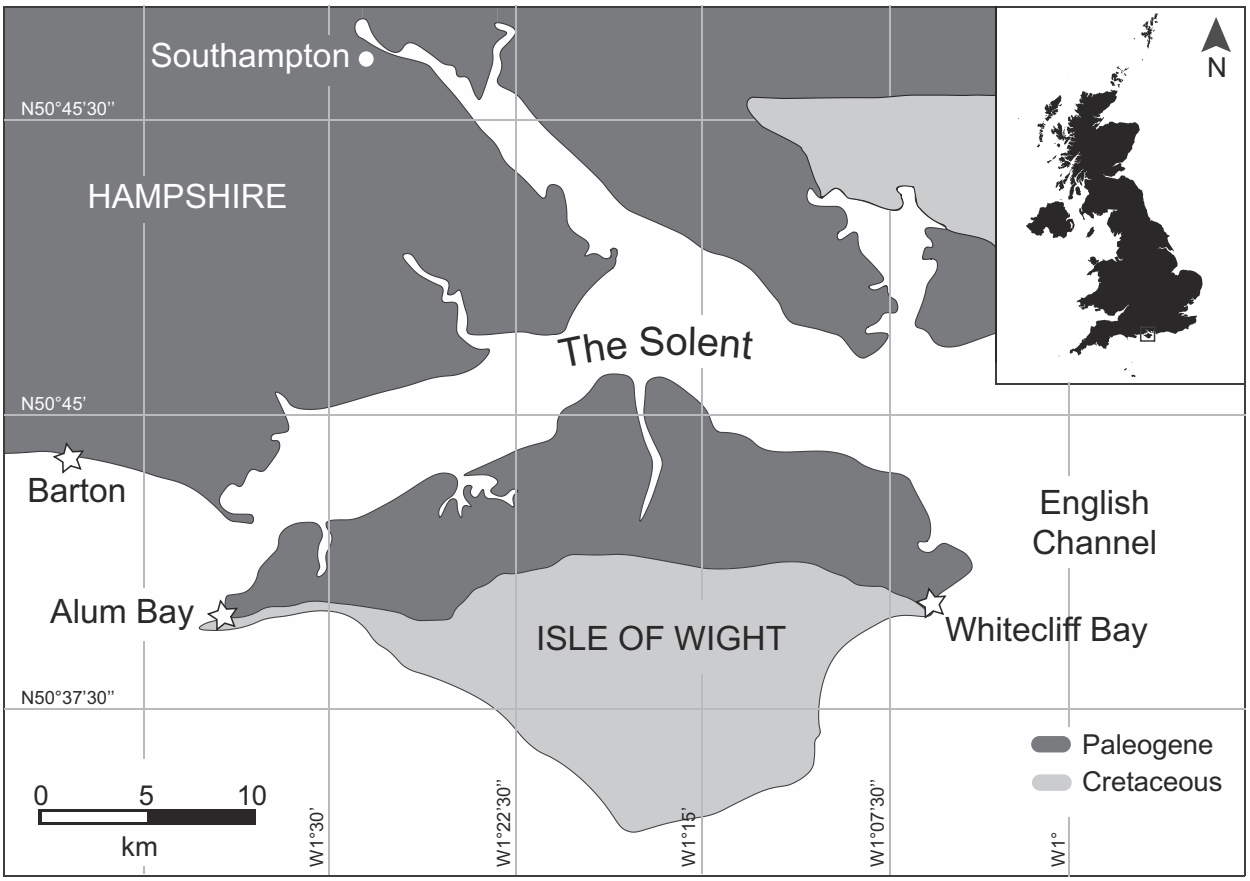

Fig. 1. Location map showing the extent of the Paleogene sediments on the in the Hampshire Basin and location of the Alum Bay, Whitecliff Bay and Barton-on-Sea sections.

leogene sedimentary sequences. Continuity of the section has been and is still being disrupted by sea-defences, although most beds can still be accessed to a limited extent. Keeping (1887) placed the base of the "Barton beds" at the lowest occurrence of the large foraminiferan "*Nummulites prestwichianus*". The Barton Clay of Prestwich (1847) is a lithostratigraphic unit, which extends beneath the *Nummulites prestwichianus* bed and is now defined as a formation (Hooker 1986). The biostratigraphically defined "Barton Beds" are still the basis of the recognition of the Bartonian Stage as a formal chronostratigraphic unit of the Paleogene (Berggren 1972, Curry 1981).

The parastratotype section for the Bartonian is located 7 km away at Alum Bay on the Isle of Wight and is better exposed, although the beds are steeply dipping and there is some tectonic disturbance, which is probably responsible for doubling the thickness of cycle 4 compared to that at Barton. It may also be responsible for differing thicknesses reported by previous authors (Hooker & King 2018). Despite numerous studies since the 1970s and '80s, correlation of both Barton and Alum Bay to global stratigraphy has been challenging owing to a lack of studies combining stratigraphic methods, and a lack of clear global turnover events around this level (Hooker & King 2018).

As outlined above, the boundary has frequently been placed at the *Nummulites prestwichianus* bed. However, this species is not widely correlatable outside the Hampshire Basin. The geographic range of *N. prestwichianus* only extends as far as France, and larger benthic foraminifera (LBF) are well known to be restricted to shallow platform environments and facies dependent, therefore this is a limited marker. In addition, King (2016, fig.154) showed a series of *N. prestwichianus*–like forms with morphological differences to the species description of *N. prestwichianus s. s.*, found in and around the base of the stratotype level, further clouding correlations. The taxonomy of British *Nummulites* will therefore be addressed in detail in a later publication. Only a single, long-ranged,

planktonic foraminifer has been identified, *Dipsidripella danvillensis*, and so correlation of this bed with planktonic foraminiferal biostratigraphy has not been possible. A number of dinoflagellate cyst investigations in the south of England have been carried out since the 1960s (Davey et al. 1966, Gruas-Cavagnetto 1970, Downie et al. 1971, 1976, Eaton 1971a, b, 1976, Gruas-Cavagnetto 1976, Costa and Downie 1976, Costa et al. 1978, Bujak 1976, 1979, Bujak et al. 1980, Islam 1981, 1983a, b, 1984, Jolly 1996, Jolley and Spinner 1989, 1991) which include the palynological study of the Alum Bay. The Eocene Dinoflagellate cyst zonation for southern England proposed by Bujak et al. (1980), was later based on the stratigraphic distribution of dinoflagellate cysts from the Whitecliff Bay and Alum Bay key-outcrop sections. The dinoflagellates do show a taxonomic turnover close to the base Bartonian stratotype with *Rhombodinium draco* occurring a few centimeters above the level of the *N. prestwichianus* bed at several localities in the Hampshire Basin. However, this is not consistent outside of this region. Previous studies on calcareous nannofossils from the site showed they were relatively impoverished, with NP zones being largely recognized by secondary markers. The occurrence of *Reticulofenestra umbilicus*, which is a primary marker of CP14a, within the CP zonation (Okada and Bukry 1980) was recognised by Aubry (1983, 1986) suggesting further correlation potential for calcareous nannoplankton in the section. Palaeomagnetic studies have also been carried out at the Alum Bay section. Hardenbol and Berggren (1978) placed the base Bartonian within magnetic polarity chron C19n. Subsequent Paleogene numerical time scales (Harland et al. 1982, Berggren et al. 1985, Harland et al. 1989, Berggren et al. 1995, Luterbacher et al. 2004, Vandenberghe et al. 2012) continued to associate the base of the Bartonian with magnetic polarity Chron 19n. In keeping with this, Jovane et al. (2010) and Fluegeman (2007) suggested the Top and Base, respectively, of C19n as alternative potential primary events for the base of the Bartonian Stage to guide future GSSP designation. Recently, Dawber et al. (2011) identified C18n indicating the *Nummulites prestwichianus* bed as being within the underlying reversed interval at Alum Bay.

Whilst a large number of previous studies on Alum Bay have been carried out, the majority outlined here

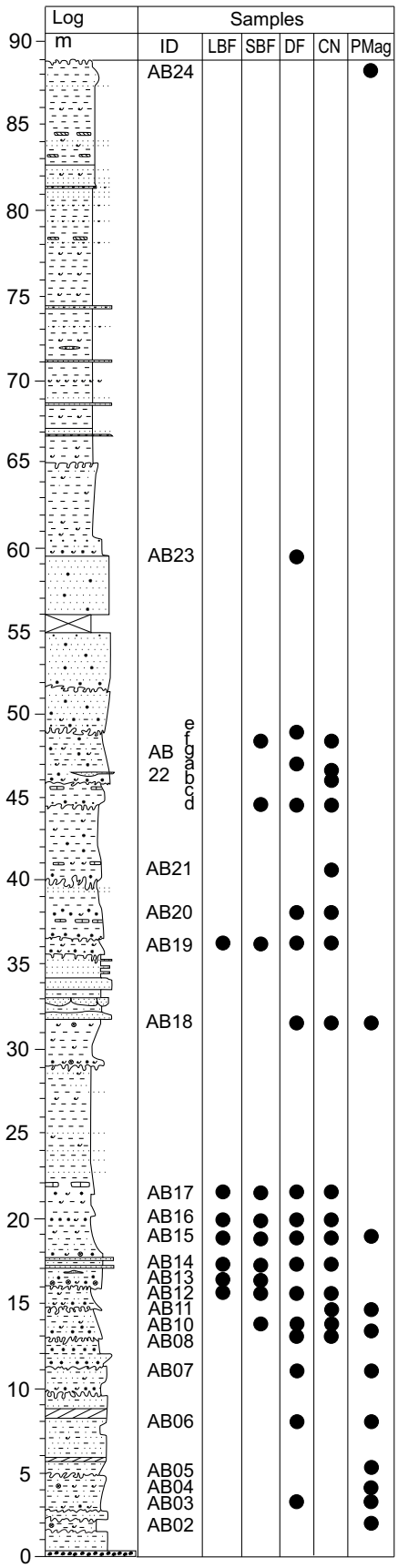

Fig. 2. Stratigraphic log of section showing sampled levels and sample types. Full written lithological description for the log is given in the supplementary information.

focus on one or two stratigraphic techniques. In order to resolve the correlation potential of the base of the Bartonian, we re-examine the Alum Bay section using integrated nannofossil, dinoflagellate, LBF, small benthic foraminifera and magnetostratigraphy to assess potential correlations and placements for boundaries. In particular, we aim to address the occurrences of new nannofossil zonal indicators of the Agnini et al. (2014) mid-latitude zonation and the occurrence of key taxa of dinoflagellate cysts as *Areoligera sentosa, A. tauloma* and *Rhombodinium draco* against the sequence stratigraphy and palaeomagnetism of King (2016). The base of the dinoflagellate *Distatodinium paradoxum* is re-examined for its correlation with strata below the *N. prestwichianus* bed within the Barton Clay as shown in Eaton (1976), as an additional potential biostratigraphic marker. Likewise, the range of *R. draco* is examined to determine whether the Base (of *R. draco*) falls within the C19n interval 2–5 m above the base of the Barton Clay, as recorded in SW Siberia (Iakovleva 2017). Improvement in the stratigraphy of the interval is essential to better define this interval and contribute towards a decision for the GSSP.

2. Geological setting

Alum Bay is situated within the Hampshire Basin, which consists of an asymmetric syncline within the larger Anglo – Paris – Belgian Basin (Fig. 1). The sediments were deposited in a series of transgressive and regressive cycles during the Paleogene, and consist of various near-shore shelf sediments. The Barton Clay Formation spans the upper Lutetian to upper Bartonian, and is overlain by the Becton Sand Formation in the upper Bartonian. According to the Bartonian unit stratotype definition, the Lutetian – Bartonian transition should lie within the Barton Clay Formation. At Alum Bay the Barton Clay succession comprises a series of glauconitic and non-glauconitic clays and sands, with the lower beds showing a clear abundance of LBF. There are two models for the deposition of this formation (see Hooker and King (2018) for detailed discussion), the first indicates that the base of the Barton Clay is a timeline, onlapping in a westwards direction over the underlying Boscombe Sand Formation (King 2016). Alternatively, a number of authors (e. g. Hooker 1986, Bristow et al. 1991) interpreted the succession as five cycles that transgress progressively westwards, with the Boscombe Sands being the more proximal shoreface facies and the Barton Clay the more distal offshore facies. The larger benthic foraminifera near the base of the Barton Clay however do indicate that these lowermost beds were deposited within the photic zone and therefore not deeper than ~100 m water depth. The south of the UK also represents the most northerly extent of the range of *Nummulites* (LBF) during the Paleogene at a palaeolatitude of ~40 degrees North and temperatures in keeping with this.

3. Methods

The Alum Bay section was visited in 2015 by members of the Bartonian Working Group, part of the Subcommission of Paleogene Stratigraphy, as part of an effort to formally constrain the base of the Bartonian Stage. The section comprises a coastal outcrop with near vertical bedding and, although some parts are obscured by a chair lift and intermittent slumps, the section is largely accessible. A total of 32 levels were collected for the study across an almost 100 m transect section, with samples taken at intervals from 50 cm to 6 m, through the Barton Clay Formation and therefore including the base of the unit Bartonian Stage.

3.1. Smaller benthic foraminifera

A set of twenty-five samples was collected to study small benthic foraminiferal assemblages. Samples were soaked in water for 24 hours to help disaggregation, wet sieved over a 63 μm sieve and the collected residue was oven-dried at less than 50 °C for 24 hours. Quantitative analyses of benthic foraminiferal assemblages were based on representative splits of 300 individuals per sample. Picked specimens were identified to species level whenever possible; when the preservation was poor or the test was fragmented, determination was at the genus or higher level. The relative abundance (given as percentage) of each species, the percentage of agglutinated and calcareous-walled taxa, diversity (Fisher-α index), heterogeneity (Shannon-Weaver index) of the assemblages and the planktic/benthic (P/B) ratio were calculated. Additionally, specimens were assigned to infaunal or epifaunal microhabitats (e. g., Jorissen et al. 1995). The sediment from which the 300 specimens were picked was weighed, and used as an approximate estimation of the concentration of foraminifera per gram of sediment.

Only 6 samples out of 25 (AB 12 to AB 17, lower part of the section) contain enough specimens of small benthic foraminifera to perform quantitative analyses (300 specimens) of the assemblages. In order to show a longer record, samples with low concentration of foraminiferal tests (AB 10, AB 19, AB 22d and AB 22f) were also studied. As samples below AB 10 and above AB 22f were barren of small benthic foraminifera, the interpretation given here refers to the lower half of the log. The overall preservation of the tests is good and there are no signs of dissolution, although fragmented tests make up ~20 % of the assemblages.

3.2. Larger benthic foraminifera

Seven of the twenty-five smaller benthic foraminiferal samples contained larger benthic foraminifera (LBF). Samples were picked up to a maximum of 300 specimens. Representative examples of LBF were examined in oriented section, and natural split sections, and traditional measurements of proloculus and deuteroconch size along with successive whorl radii were taken. A total of 18 equatorial sections were used and 2 axial sections.

3.3. Calcareous nannofossils

Twenty-seven samples were collected in the Alum Bay section to study calcareous nannofossil assemblages. Smear slides were prepared from raw material using the technique described by Bown and Young (1998). Qualitative and semi-quantitative analyses were conducted on the light microscope Zeiss Axiophot, at a magnification of 1250x. Two random long traverses were analysed to detect rare key species (i. e. *Chiasmolithus solitus, Sphenolithus furcatolithoides* morphotype *B, S. spiniger, S. obtusus* and *Discoaster distinctus*). Taxonomy follows Perch-Nielsen (1985), Fornaciari et al. (2010) for *Dictyococcites* and Agnini et al. (2014) for *Sphenolithus.* The biostratigraphic schemes adopted are those of Agnini et al. (2014), codified CNE, and Martini (1971) codified NP.

3.4. Palynology

Seventeen samples from the Alum Bay section were analyzed palynologically. Palynomorphs were prepared using the standard palynological techniques of the British Geological Survey (Riding and Kyffin-Hughes 2004) consisting of four main steps: (1) dissolution of carbonates and silicates by HCl and HF acid digestion; (2) sieving between 106 and 10 μm; (3) neutralization with distilled water and centrifugation; (4) staining with Safranin-O. The palynological material is stored within the collections of Zaragoza University (Spain).

Once prepared a quantitative analysis of the samples was carried out. Firstly, a minimum 200 palynomorphs were counted and grouped into 6 broad categories as dinoflagellate cysts, reworked dinoflagellate cysts (mostly Mesozoic), acritarchs, prasinophytes, conifers and foraminiferal linings, but finally prasinophytes, conifers and foraminiferal linings were represented only by few specimens and did not achieve 1 %. Secondly, a minimum of 200 dinoflagellate cysts were counted; the remaining material was scanned for rare dinoflagellate cysts taxa. For palaeoenvironmental reconstructions we followed the approach of Sluijs and Brinkhuis (2009) in using a grouping of morphologically/ecologically related dinoflagellate cyst taxa and assigned cysts to 12 groups: wetzelielloids; *Phthanoperidinium*; other peridinioids; *Homotryblium*–group (mostly *Homotryblium*, plus *Lingulodinium*, *Heteraulacacysta*, *Polysphaeridium*); *Areoligera*–group (*Areoligera*, *Glaphyrocysta*, *Adnatosphaeridium*, *Membranophoridium*); *Enneadocysta*/*Areosphaeridium*; *Distatodinium*; *Cordosphaeridium*–group (*Cordosphaeridium*, *Fibrocysta*, *Araneosphaera araneosa*); *Hystrichokolpoma*; *Spiniferites*–group (*Spiniferites*, *Achomosphaera*, *Hystrichosphaeropsis*, *Hystrichostrogylon*, *Rottnestia borussica*); other gonyaulacoids; gonyaulacoids indet.

3.5. Palaeomagnetism

The palaeomagnetic sampling at Alum Bay was conducted along about 85 m of a Barton Clay Formation stratigraphic section with the meter 0 established at the base of the Formation. A total of 15 stratigraphic levels were sampled corresponding to equivalent biostratigraphic samples. The lower 20 m of the section studied was sampled in more detail (average sampling of about 2 m) whereas wider-spaced sampling was performed along the upper part in this pilot study. Samples consisted of either hand-samples or cubic plastic boxes (2 x 2 x 2 cm) that were pressed on a soft clay cut surface on the outcrop. Both sample types were oriented in-situ with a magnetic compass. The hand-samples were cut in regular standard block samples in the laboratory before palaeomagnetic measurements. Natural remanent magnetization (NRM) and remanence through demagnetization were measured on a

2G Enterprises DC SQUID high-resolution pass-through cryogenic magnetometer (manufacturer noise level of 10^{-12} Am^2) operated in a shielded room at the Istituto Nazionale di Geofisica e Vulcanologia in Rome, Italy. A Pyrox oven in the shielded room was used for thermal demagnetizations and alternating field (AF) demagnetization was performed with three orthogonal coils installed in line with the cryogenic magnetometer. Progressive stepwise AF demagnetization was routinely used and applied after a single heating step to 150 °C. AF demagnetization included 14 steps (4, 8, 13, 17, 21, 25, 30, 35, 40, 45, 50, 60, 80, 100 mT). Characteristic remanent magnetizations (ChRM) were computed by least-squares fitting (Kirschvinkc 1980) on the orthogonal demagnetization plots (Zijderveld 1967). The ChRM declination and inclination were used to derive the latitude of the virtual geomagnetic pole (VGP) of each sample. This parameter was taken as an indicator of the original magnetic polarity, normal polarity being indicated by positive VGP latitudes and reverse polarity by negative VGP latitudes.

4. Results

4.1. Smaller benthic foraminifera

Diversity of the smaller benthic foraminiferal assemblages is low, with an average of 20 species per sample. The Fisher-α diversity index ranges from 2.8 to 6.8, and the Shannon-Weaver H (S) heterogeneity index ranges from 1.31 to 2.13. Both indices show their highest values between meters 14 and 22 (samples AB 10 to AB 17), and subsequently decrease and remain relatively constant towards the uppermost sample containing benthic foraminifera at 48 m. The P/B ratio, which shows a positive correlation with the number of benthic foraminifera per gram, yields percentages below 5 %, probably indicating a shallow setting close to the coastline.

Calcareous taxa dominate the benthic assemblages, and only one agglutinated and two miliolid taxa were identified. Epifaunal morphogroups clearly dominate over infaunal ones (<10 %). The genus *Cibicides* is the most abundant epifaunal taxon, making up to >70 % of the assemblages in all samples. Less abundant but commonly occurring genera include *Bolivina, Brizalina, Buccella, Buliminella, Discorbis, Globulina, Melonis, Nonion*, *Pullenia*, *Quinqueloculina, Robertina* and *Rosalina* (Fig. 3).

Fig. 3. SEM and light microscopy images of common Bartonian benthic foraminiferal species at Alum Bay. All scale bars represent 100 µm, except for 1a and 1b that represent 500 µm. 1) *Nummulites prestwichianus* (sample AB14), equatorial (1a) and axial (1b) section; 2) *Protelphidium* sp. (AB14); 3) *Cibicides ungenianus* (AB22b), dorsal (3a) and ventral (3b) view; 4) *Cibicides pygmeus* (AB19), apertural (4a) and ventral (4b) view; 5) *Cibicides fortunatus* (AB14), dorsal (5a) and ventral (5b) view; 6) *Bucella propingua* (AB14), dorsal (6a) and ventral (6b) view; 7) *Bolivina cookei* (AB14)

The quantitative analysis of the assemblages allowed us to differentiate three intervals (see Fig. 4):

Interval A: 14 to 20.5 m (samples AB 10 to AB 16). The genus *Cibicides* strongly dominates the assemblages (up to 87 %), with the species *Cibicides pygmeus* and *Cibicides ungerianus* together making up ~50 % of the assemblages. The percentage of *Buccella propingua* ranges between 6 % and 12 %. Other species that are present but make up less than 10 % of the assemblages include *Anomalinoides ypresiensis, Bolivina cookei, Cibicides fortunatus, Discorbis perplexa, Globulina gibba* and *Protelphidium* sp. The highest diversity values (Fisher-α = 6.8 and H(S) = 2.13) and the highest percentage of infaunal morphogroups (up to 9.28 %) across the whole succession have been recorded across this interval. Sample AB 16 yields the highest diversity, and a 100 fold increase in number of foraminifera per gram.

Interval B: 20.5 to 40.5 m (samples AB 17 to AB 19). Within the genus *Cibicides*, the species *C. pygmeus* dominates over *C. ungerianus*. The relative decrease in the percentage *C. ungerianus* is coupled with a decrease in *Buccella propingua* and *Protelphidium* sp. and a small increase in the percentage of *Rosalina* sp. Diversity and the percentage of infaunal morphogroups are lower than in interval A. There are no data available from the middle part of this interval as sample AB18 is barren of foraminifera. However, assemblages from its lower and upper parts are very similar, and slightly differ in the lower number of fragments of *Cibicides* sp. and higher percentage of *Rosalina* sp. towards the upper part of interval B.

Interval C: 40.5 to 48 m (samples AB 22d to AB 22e). The genus *Cibicides* reaches its maximum abundance (90 % of the assemblages) with a strong dominance of *C. ungerianus* (> 50 %) over *C. pygmeus*. The percentages of *Buccella propingua, Cibicides fortunatus, Globulina gibba* and *Nonion laeve* are higher than in the previous interval B. Diversity of

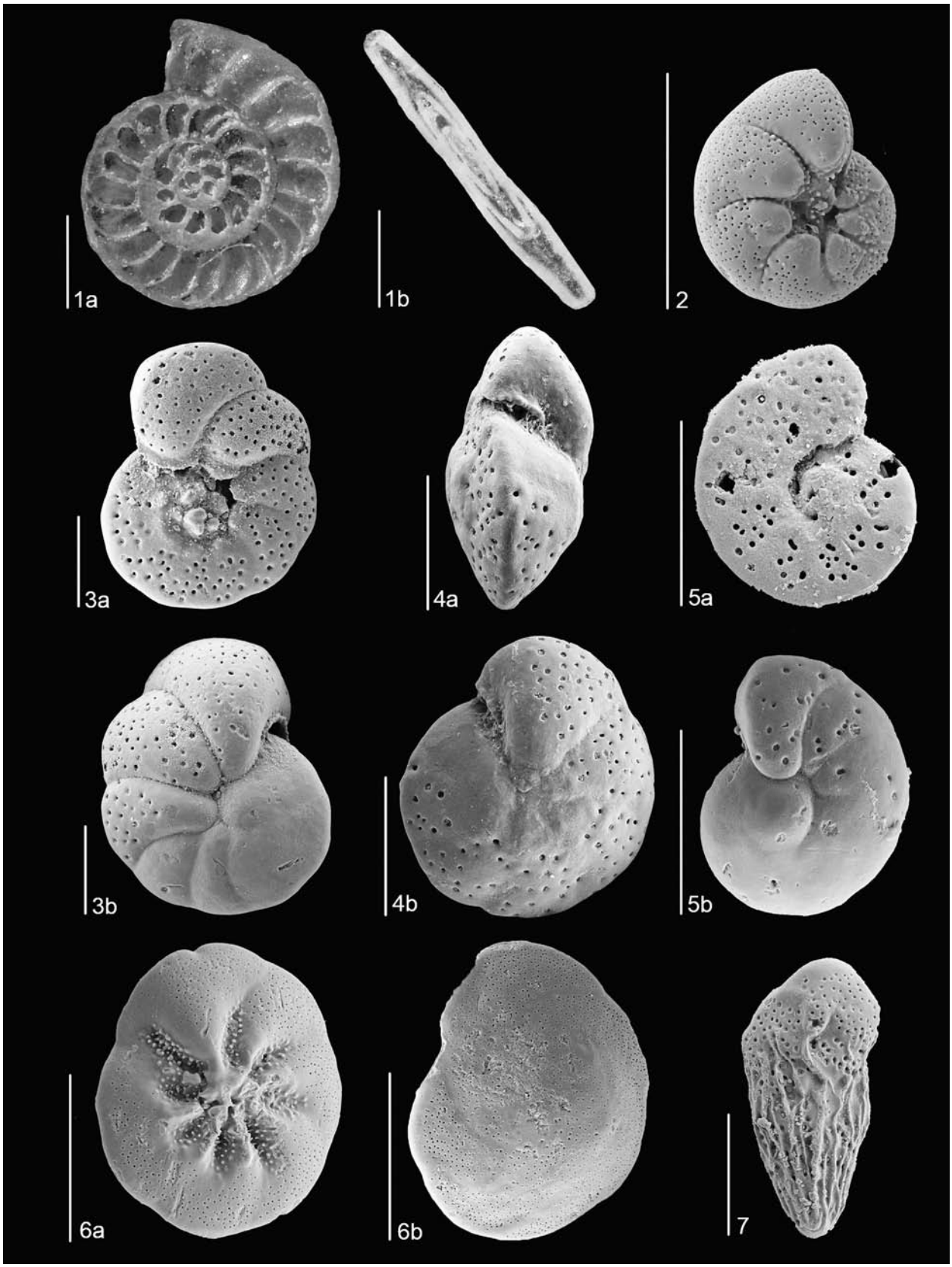
1a
1b
2
3a
4a
5a
3b
4b
5b
6a
6b
7

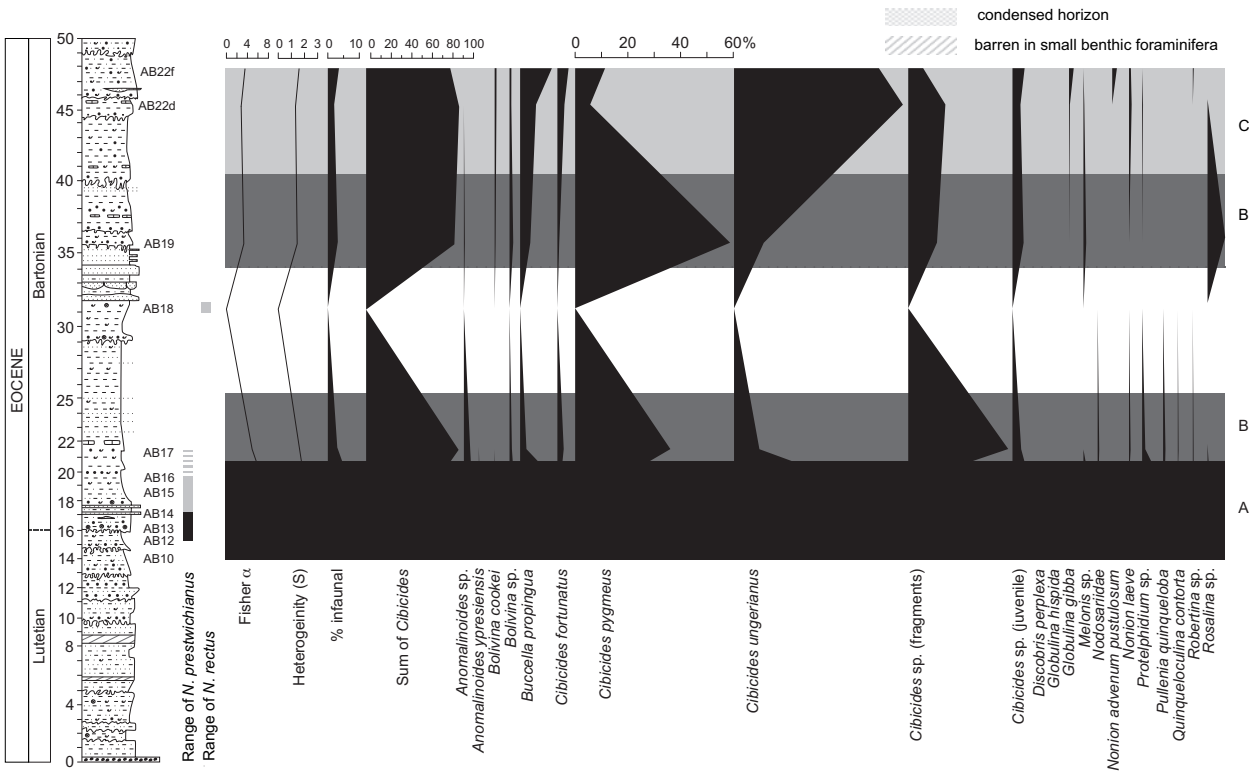

Fig. 4. Abundances and occurrences of smaller benthic foraminiferal and larger benthic foraminiferal taxa, with sampled levels shown on the log. For larger benthic foraminifera black represents abundant (>200 specimens) and grey present (1–50 specimens). Assemblage zones are shown in bands A–C.

Fig. 5. Plate of most abundant and/or diagnostic nannofossils. 1) *Sphenolithus obtusus* Bukry 1971. view at 0°, Sample AB10, cross-polarized light (XPL); 2) *Sphenolithus obtusus* Bukry 1971. view at 45°, Sample AB10; 3) *Dictyococcites bisectus* >10 μm (Hay, Mohler and Wade) Roth, Sample AB21, XPL; 4) *Reticulofenestra umbilicus* (Levin 1965) Martini and Ritzkowski 1968, Sample AB12, XPL; 5) *Chiasmolithus solitus* (Bramlette and Sullivan 1961) Locker 1968, Sample AB10, XPL; 6) *Sphenolithus furcatolithoides* Locker 1967 morphotype B. view at 0°, Sample AB16, XPL; 7) *Sphenolithus furcatolithoides* Locker 1967 morphotype B. view at 0°, Sample AB15, XPL; 8) *Sphenolithus furcatolithoides* Locker 1967 morphotype B. view at 45°, Sample AB16, XPL; 9) *Reticulofenestra dictyoda* (Deflandre in Deflandre & Fert, 1954), Sample AB11, XPL; 10) *Discoaster distinctus* Martini, 1958, Sample AB16, trasmissed light (IIPL); 11) *Braarudosphaera bigelowii* (Gran and Braarud 1935) Deflandre, 1947, Sample AB23b, XPL; 12) *Neococcolithes dubius* (Deflandre in Deflandre and Fert, 1954) Black, 1967, Sample AB11, XPL; 13) *Helicosphaera compacta* Bramlette and Wilcoxon, Sample AB10, XPL; 14) *Helicosphaera compacta* Bramlette and Wilcoxon, Sample AB10, IIPL; 15) *Blackites inflatus* (Bramlette and Sullivan 1961) Kapellos and Schaub 1973, Sample AB13, XPL; 16) *Blackites inflatus* (Bramlette and Sullivan 1961) Kapellos and Schaub 1973, Sample AB13, IIPL; 17) *Ericsonia formosa* (Kamptner, 1963) Wise, 1973, Sample AB23b, XPL; 18) *Discoaster saipanensis* Bramlette & Riedel 1954, Sample AB12, IIPL; 19) *Discoaster barbadiensis* Tan Sin Hok 1927, Sample AB19, IIPL; 20) *Blackites spinosus* (Deflandre & Fert, 1954) Hay & Towe, 1962, Sample AB23b, XPL.

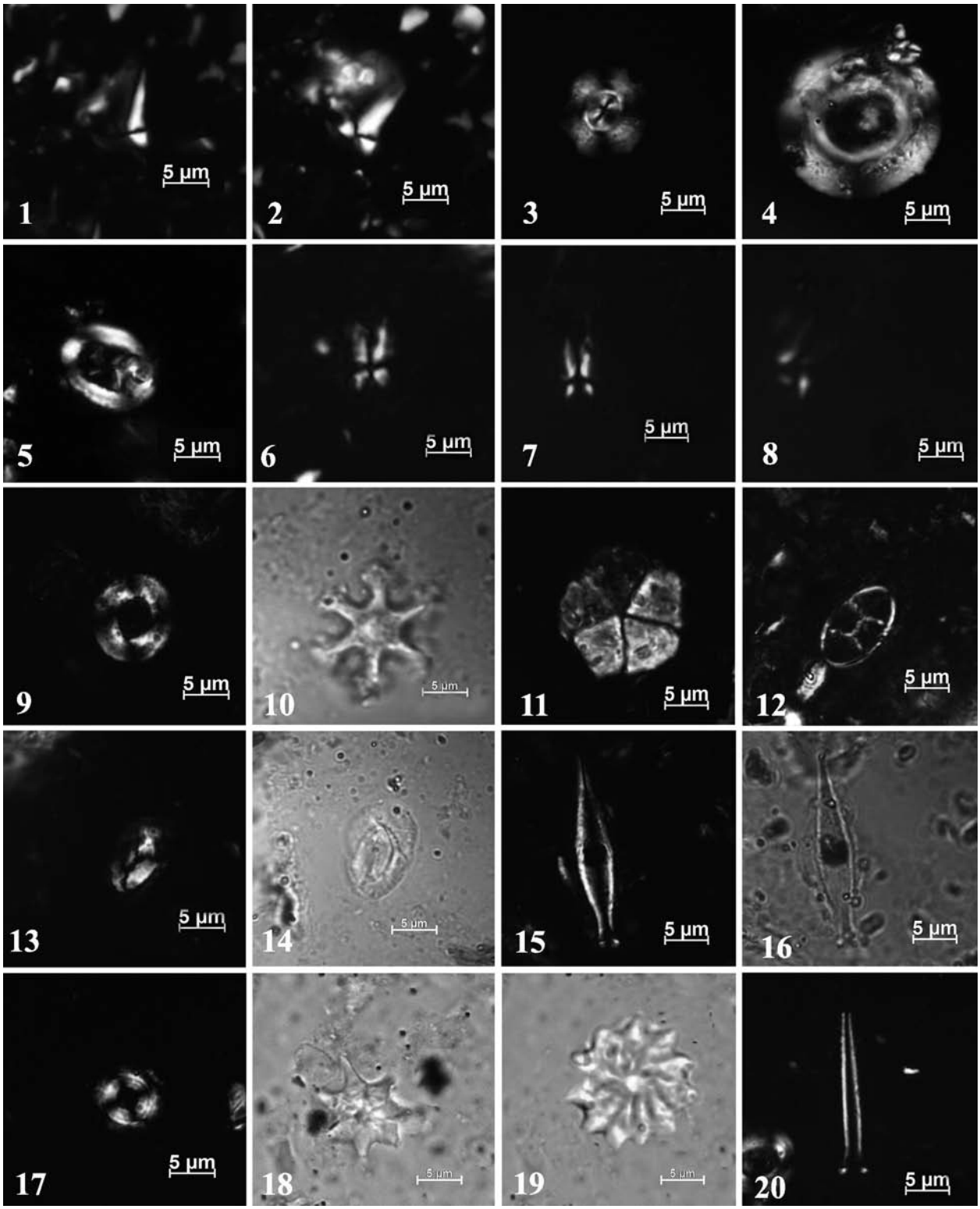
1
5 µm
2
5 µm
3
5 µm
4
5 µm
5
5 µm
6
5 µm
7
5 µm
8
5 µm
9
5 µm
10
5 µm
11
5 µm
12
5 µm
13
5 µm
14
5 µm
15
5 µm
16
5 µm
17
5 µm
18
5 µm
19
5 µm
20
5 µm

the assemblages (Fisher-α = 2.8, H(S) = 1.31) and the percentage of infaunal morphogroups (2 %) show the lowermost values of the section.

4.2. Larger benthic foraminifera

Larger benthic foraminifera, where present, were low in diversity but high in abundance at specific levels (Fig. 4). Preservation of the tests is generally good to excellent although there is some pyritisation. The exception to this is sample AB17 where all specimens are poorly preserved and heavily pyritised. Two taxa were identified, *Nummulites prestwichianus* and *Nummulites rectus*, although assemblages appear monospecific and *N. prestwichianus* was the more abundant of the two taxa. *Nummulites prestwichianus* is characterized by a flattened test with sigmoidal sutures, and loose spiral, following Blondeau (1972), whilst *N. rectus* is more lenticular, with a comparatively tight spiral. Measured specimens of *N. prestwichianus* had a mean proloculus diameter of 93 microns, and range of 65–145 microns. It should be noted that the range of proloculus diameters in sample AB12 was larger than in AB14 and may be linked to taxonomic issues within *N. prestwichianus* which we outline in the discussion. *Nummulites prestwichianus* was abundant in samples AB12–AB14, with ~200 specimens picked from AB12 and >500 in each of AB13 and AB14, thereby indicating the *N. prestwichianus* beds and adjacent levels, utilized in previous studies as the base of the unit Bartonian. Samples AB15 and AB16 contain far fewer specimens. Preservation in sample AB17 was poor and specimens could not be accurately identified to species level. Only two specimens of *N. rectus* were identified and both were within AB18, the highest sample containing LBF.

4.3. Calcareous nannofossils

The nannofossil assemblages consist mainly of *Reticulofenestra umbilicus*, *R. samodurovii*, *Cyclicargolithus floridanus*, *Coccolithus pelagicus* and *Blackites inflatus*. The genus *Discoaster* is rare. However, among discoasterids *D. barbadiensis* is the more frequent. Nannoliths such as *Braarudosphaera bigelowii*, *Lanternithus minutus*, and *Zygrablithus bijugatus* are always present (Fig. 5). Few reworked upper Cretaceous taxa (*Micula murus*, *Watznaueria* and *Prediscosphaera*) are present throughout the section. *Blackites inflatus*, in agreement with Aubry (1983), has been considered reworked since its stratigraphic range is limited to lower Lutetian (NP14–NP15; Perch-Nielsen 1985).

The total abundance varies from rare to common and the preservation from poor to moderate along the section. Generally, the calcareous nannofossil assemblages are moderately diverse throughout the Alum Bay section. Ten samples of twenty-seven are barren of coccoliths, the majority located in the lower part of the section up to 13 m (3 samples) and in the interval between 47 to 72 m (7 samples). Only the sample collected at 72.5 m shows a good preservation and the highest total abundance among the samples studied. Figure 6 gives an overview of nannofossil abundances.

The first sample with calcareous nannofossils is at 13 m (AB8). The total abundance is common, but the richness is low, and only 4 species (*Cribrocentrum reticulatum, R. umbilicus, B. inflatus, B. spinosus*) were recognized. The co-occurrence of *R. umbilicus* and *C. reticulatum*, markers of the base of CNE13 and CNE14 Zones respectively, has been recognized from sample AB8. The co-occurrence suggests, following Agnini et al. (2014), for the lower part of Alum Bay section Zone CNE14 (middle-upper part of Zone NP16).

In the interval from 14 m to 22 m (AB10 to AB17) abundance increases and the preservation is moderate. The assemblages consist of *R. umbilicus, Neococcolithus dubius, C. pelagicus* and *B. bigelowii* and secondarily they contain *D. barbadiensis, D. distinctus, D. saipanensis, L. minutus, C. floridanus, C. reticulatum, S. furcatolithoides* morphotype B, and *R. samodurovi*. Representatives of *Chiasmolithus* are very rare. Only a single specimen of *C. solitus*, marker of the base of NP17 Zone (Martini 1971), has been identified at 13.80 m. *Chiasmolithus solitus* is rare or absent in low latitude sediments, difficult to recognize in poorly preserved material and strongly diachronous at different latitudes (Perch-Nielsen 1985, Wei and Wise 1989, Aubry 1992, Berggren et al. 1995, Marino and Flores 2002a, b, Villa et al. 2008, Fornaciari et al. 2010, Agnini et al. 2014). Owing to the sporadic distribution of this species Perch-Nielsen (1985) suggested to use the Top of *S. furcatolithoides* as an alternative event to the Top of *C. solitus*. Agnini et al. (2014) recognized two different morphotypes of *S. furcatolithoides* A and B. The differences between morphotypes A and B are in the extinction patterns and in the stratigraphic distribution. *Sphenolithus furcatolithoides* morphotype A has its stratigraphic range limited to CNE10 up to lower part of CNE11 Zone, and it corresponds to the middle-upper part of NP15 Zone. On the contrary,

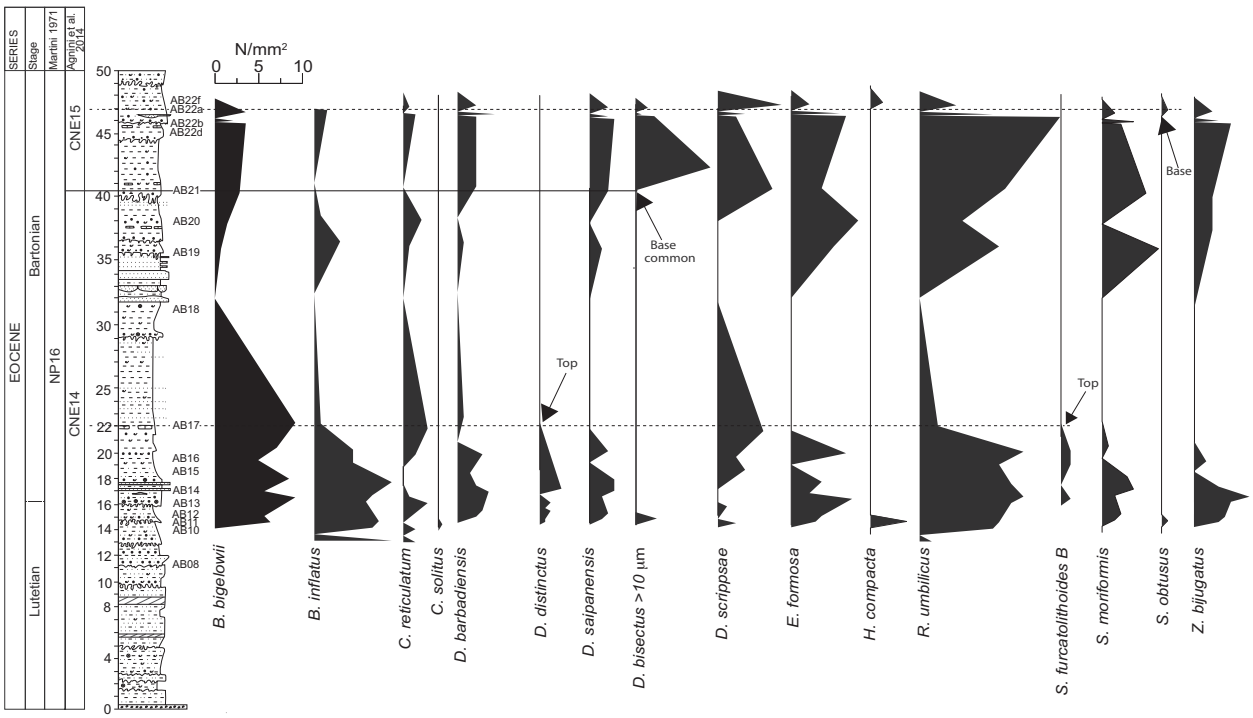

Fig. 6. Abundance pattern of selected nannofossil taxa across the Alum Bay section, expressed as number of specimens per mm2. Biostratigraphic events are indicated with arrows. The Tops of *D. distinctus* and *S. furcatolithoides* are at 22 m, the

S. furcatolithoides morphotype B has a younger stratigraphic distribution from CNE12 to CNE14 Zones (the upper part of NP15 to the upper part of NP16 Zones). Furthermore, Agnini et al. (2011) have correlated the Top of *S. furcatolithoides* B to the upper part of C18r in the Alano section and in ODP Sites 1051 and 1052. In the Alum Bay section only morphotype B of *S. furcatolithoides* has been recognized and the Top has been identified at 22 m (AB17).

According to Martini (1971) the Top of *D. distinctus* could also be used in this area to approximate the NP16/NP17 boundary. *Discoaster distinctus* is continuously present from 14 m up to 22 m (sample AB17) where its Top has been observed. Unfortunately, *D. distinctus* is difficult to identify in poorly preserved material, and according to Dunkley Jones et al. (2009) its range is diachronous, with its highest occurrence up to NP23, thus in the Alum Bay section its uppermost occurrence could not be used as a reliable event. Within the interval from 36 m up to 46 m the calcareous nannofossil assemblages are less abundant and the nannofloral content is similar to the previous interval. The occurrence of *Dictyococcites bisectus* >10 µm, marker of the Base of CNE15 Zone has been identified at 40.5 m (AB21). From this level, these specimens are continuously present. Specimens of *D. bisectus* all specimens <10 µm (usually rare) have been grouped together with *D. scrippsae.*

In the upper part of the section only two (AB22 and AB23b) out of seven studied samples contain calcareous nannofossils. The co-occurrence of *S. obtusus, S. spiniger* (rare) and *D. bisectus* allow us to assign sample AB22 to the lower part of CNE15 Zone (Agnini et al. 2014). The last sample with calcareous nannofossil content has been collected at 73 m (AB23b). This sample shows the highest abundance and an assemblage similar to the previous sample AB22, without the presence of *S. spiniger*. The Top of *S. spiniger* occurs in the lower part of CNE15 Zone slightly above the Base of *S. obtusus* confirming CNE15 Zone (NP 16 Zone) for the upper part of the section.

4.4. Palynology

In general, all 17 palynological samples revealed quantitatively rich palynomorph assemblages with the absolute (80–100 %) dominance of dinoflagellate cysts; acritarchs do not exceed 15 %. The lower part of

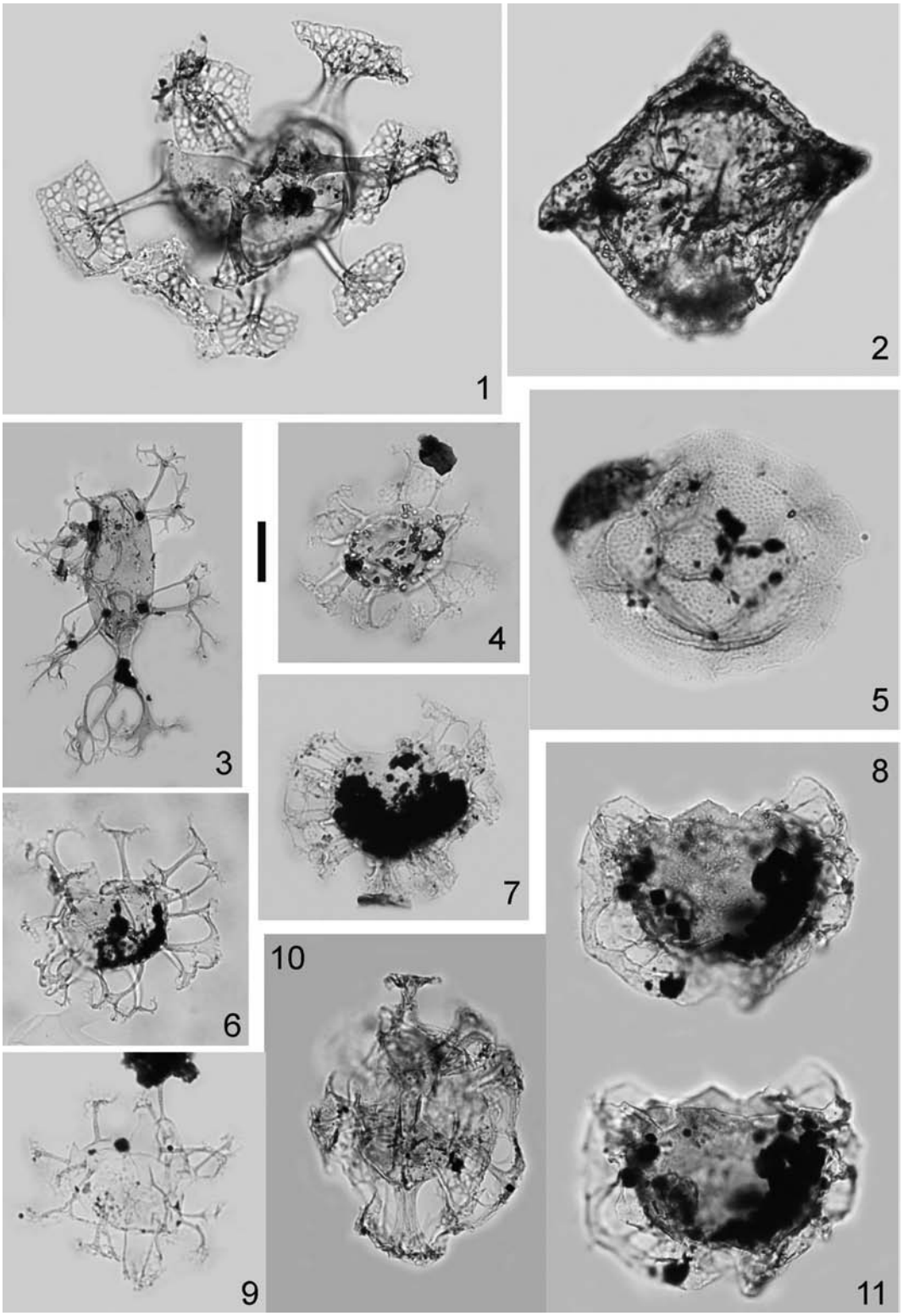

Fig. 7. Dinoflagellate taxa from the Alum Bay section. The scale bar of 20 μm applies to all specimens. 1) *Areosphaeridium diktyoplokum*, Slide AB 17-2; 2) *Rhombodinium draco*, specimen damaged by crystalline particles, Slide AB 18-4; 3) *Distatodinium craterum-biffii* (transitional form), Slide AB22d-2; 4) *Enneadocysta fenestrata*; Slide AB 23-1; 5) *Heteraulacacysta porosa*, Slide AB 19-4; 6) *Enneadocysta pectiniformis*, Slide AB 14-4; 7) *Hemisphaeridium fenestratum*, Slide AB 23-1; 8, 11) *Glaphyrocysta*? *vicina*, Slide AB 20-3; 9) *Enneadocysta fenestrata*; Slide AB 23-1; *Cordosphaeridium cantharellus*, Slide AB 14-4

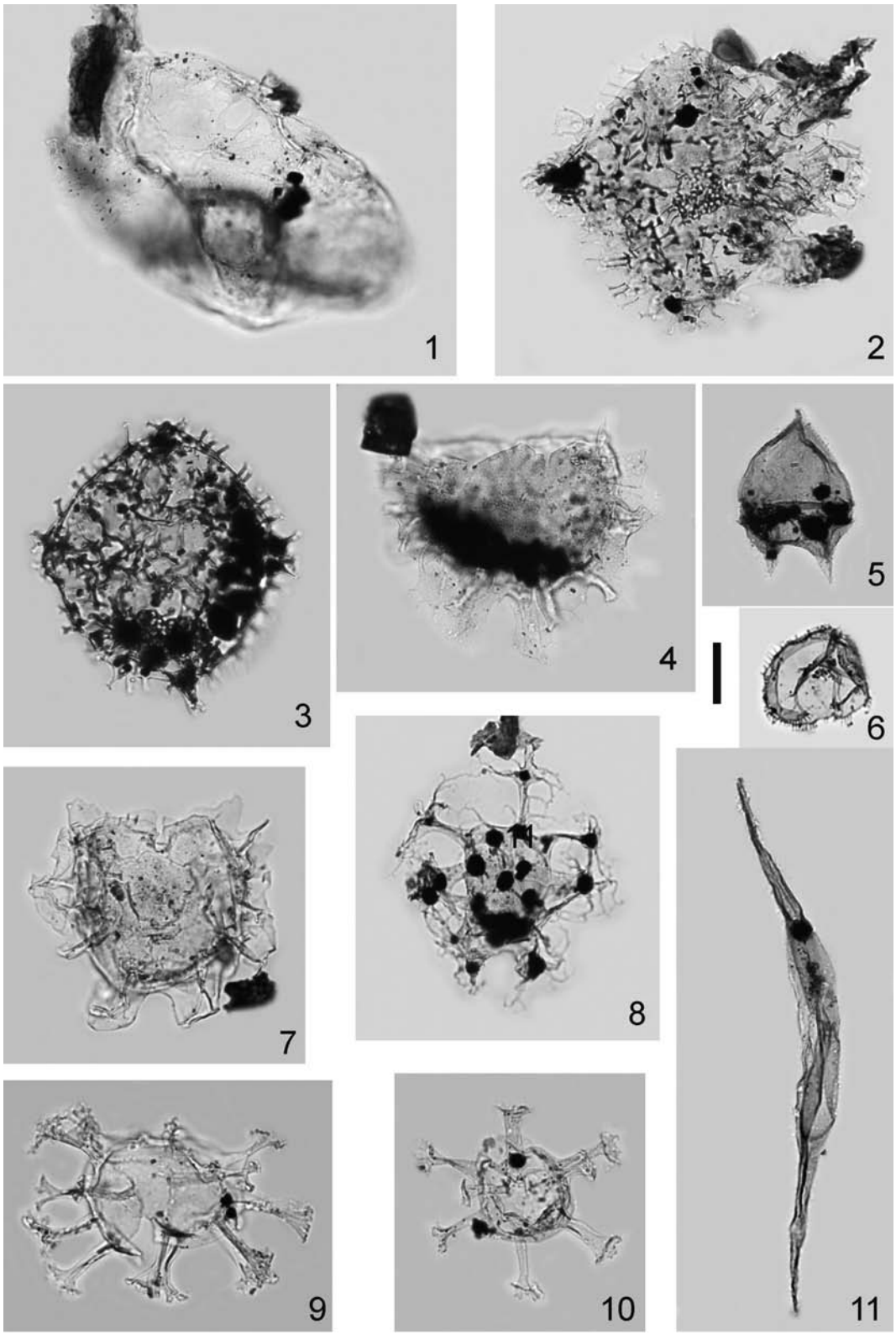

Fig. 8. Dinoflagellate taxa from the Alum Bay section. The scale bar of 20 μm applies to all specimens. 1) *Thalassiphora fenestrata*, Slide AB 10-4; 2) *Wetzeliella* sp.1, archeopyle invisible, Slide AB 10-1; 3) *Wetzeliella* sp. 2, archeopyle invisible; Slide AB 17-1; 4) *Areoligera tauloma*, Slide AB 06-1; 5) *Lentinia serrata*, Slide AB 17-3; 6) *Selenopemphix selenoides*, Slide AB 23-1; 7) *Areoligera undulata*, Slide AB 14-4; 8) *Distatodinium craterum*, Slide AB 14-4; 9) *Homotryblium floripes*, Slide AB 20-3; 10) *Homotryblium tenuispinosum*, Slide AB 06-1; 11) *Palaeocystodinium golzowense*, Slide AB 19-4.

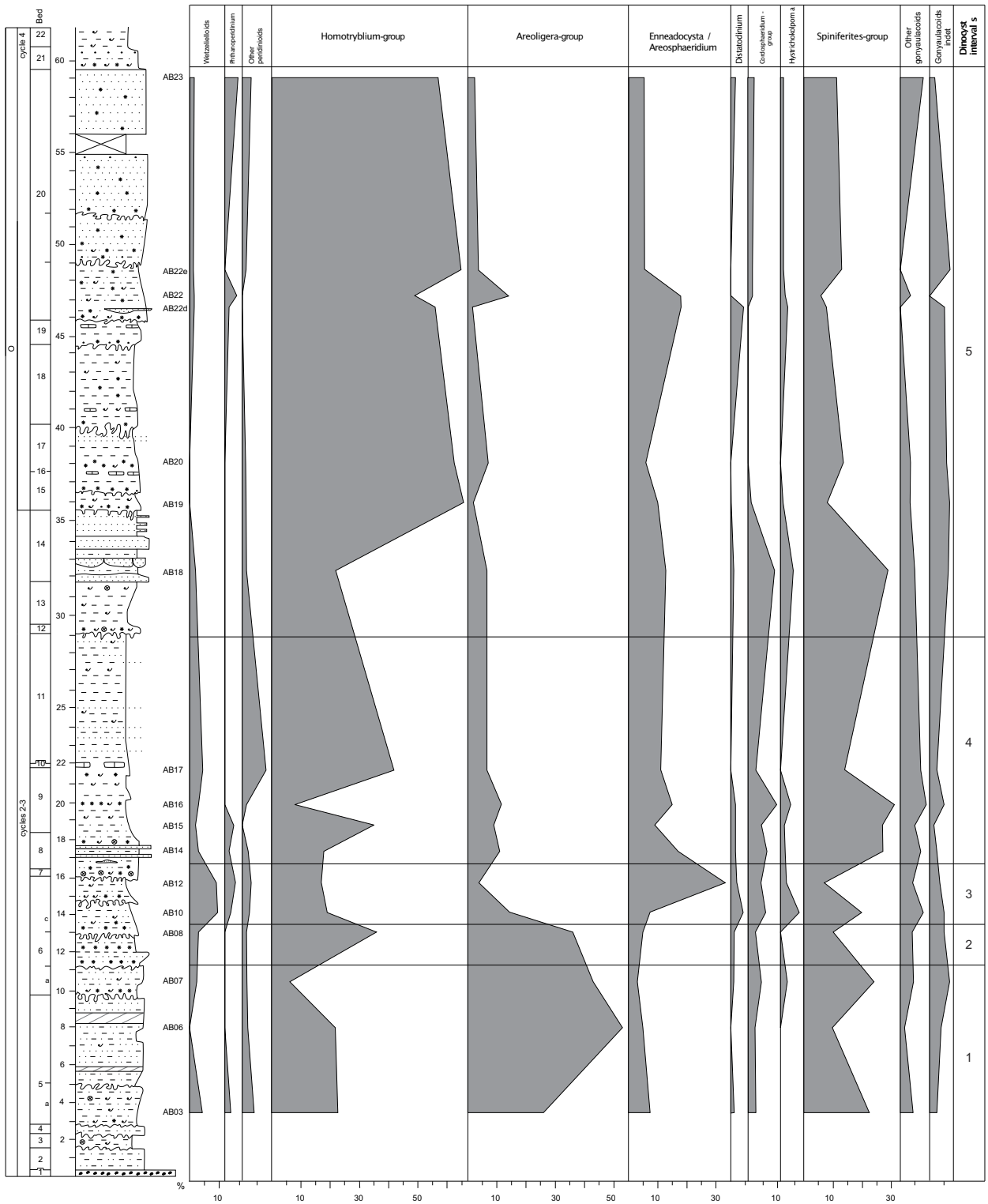

Fig. 9. Distribution of dinoflagellate events in the section and Dinocyst Zones assigned.

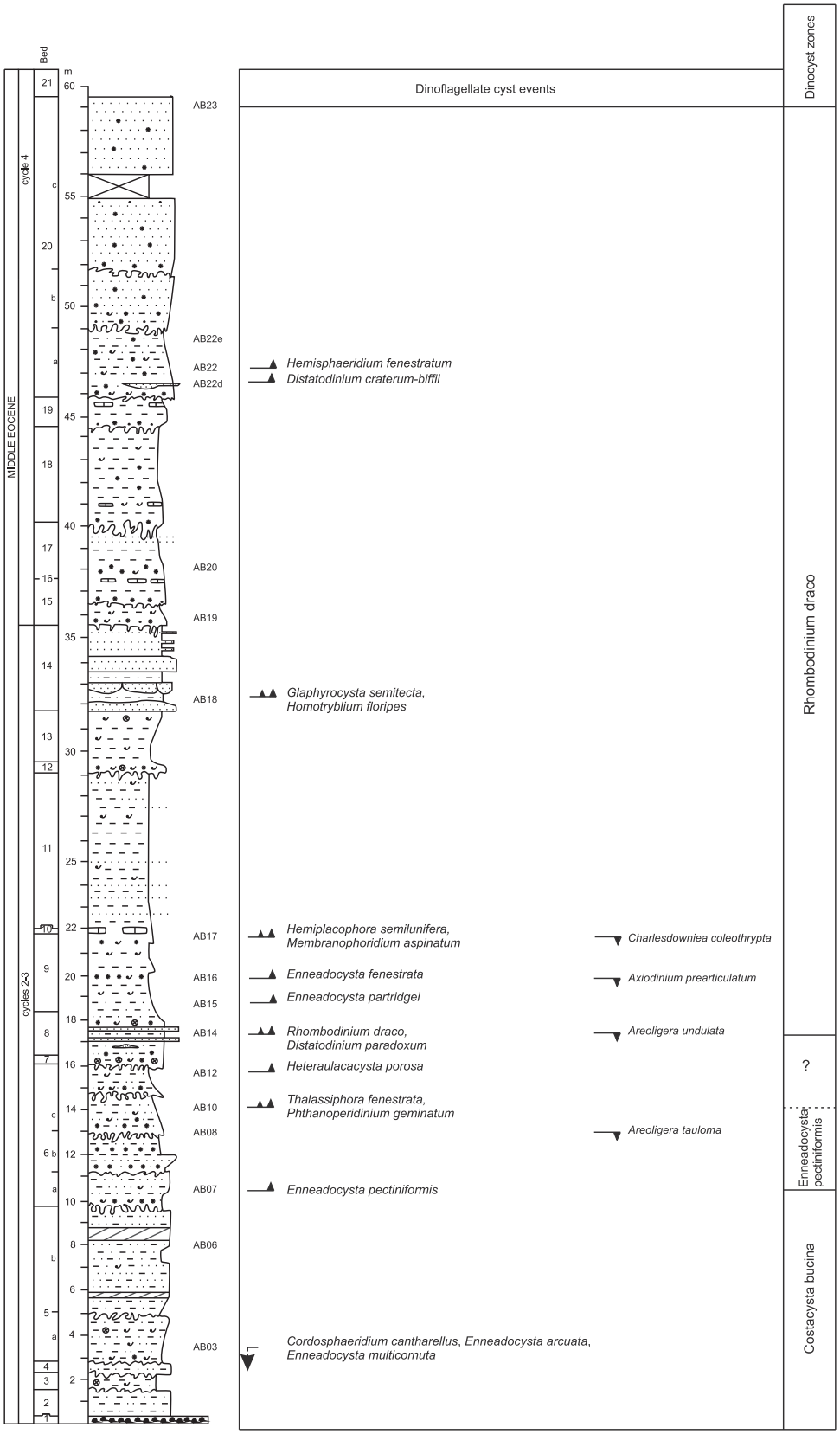

Fig. 10. Distribution and abundances (%) of dinoflagellate eco-groups through the Alum Bay section. Intervals 1 to 5 represent specific assemblage intervals, for full description of each assemblage see section 4.4.

the interval studied is marked by the presence (up to 9 %) of reworked Mesozoic dinoflagellate cysts. Prasinophytes (*Pterospermella*, *Pediastrum*) and pollen grains of conifers represent less than 1 % of the total assemblage. Dinoflagellate cyst assemblages from the studied samples are diversified with moderately well preserved dinoflagellate cysts: in total, ca. 96 dinoflagellate cyst taxa were recognized in the Alum Bay section. The most abundant and stratigraphically significant are shown in Figs. 7 and 8.

The distribution of stratigraphically significant species (Fig. 9) as well as the major changes in relative abundance of different dinoflagellate cysts eco-group fluctuations allowed us to recognize five intervals (Fig. 10).

The lowermost part of the section (samples AB03–AB07) is characterized by the presence from the base of stratigraphically important Lutetian species *Cordosphaeridium cantharellus*, *Enneadocysta arcuata* and *Enneadocysta multicornuta*; species *Distatodinium craterum*, *Selenophemphix nephroides*, *S. selenoides*, *S. armata* and *Glaphyrocysta laciniiforme* are also present. Therefore, this part of the Alum Bay section corresponds to the part of the *Areosphaeridium arcuatum–Cyclonephelium intricatum* Zones interval in southern England (Bujak et al. 1980), the part of the *Enneadocysta arcuata* Zone in Denmark (Heilmann-Clausen 1988), part of the *E. arcuata-E. multicornuta* Subzones in Ukraine (Andreeva-Grigorovich et al. 2011) and the part of the *Costacysta bucina* Zone in eastern Peri-Tethys (Iakovleva 2017). The dinoflagellate cyst assemblage from this part of the section is characterized by the dominance (20–50 %) of the *Areoligera*–group; *Homotryblium*– and *Spiniferites*–groups are very common and attain up to 25 % and 20 % respectively. This may be interpreted as part of a transgressive phase in the inner neritic environments.

The second interval (samples AB07–AB08) revealed the first occurrence of stratigraphically important *Enneadocysta pectiniformis* at ~10.5 m (sample AB07). The Top of *Areoligera tauloma* is noted at ~13.0 m. Consequently, this part of the Alum Bay section may be correlated with the *E. pectiniformis* Zone in eastern Peri-Tethys (Iakovleva 2017). Dinoflagellate cyst assemblage from this interval is characterized by the dominance of *Areoligera* (up to 36 %) and *Homotryblium* (up to 35 %) groups; the *Spiniferites*–group attains 10 %. This may be interpreted as a continuation of the transgressive phase in inner neritic environments.

The third dinoflagellate cyst interval (samples AB10–AB12) is characterized by the lowermost occurrences of *Thalassiphora fenestrata* and *Phthanoperidinium geminatum* at ~14.0 m and of *Heteraulacacysta porosa* at ~15.5 m. It should be noted that previously the Base (LO) of *Th. fenestrata* was often recognized only from the Priabonian (Liengjarern et al. 1980, Bujak and Mudge 1994, Köthe 2012). Now the Base of typical *Th. fenestrata* is known from the *Rhombodinium draco* Zone interval in Denmark (Heilmann-Clausen and Van Simaeys 2005) and eastern Peri-Tethys (Iakovleva 2017), while the Base of specimens recognized as *Th.* cf. *fenestrata* were noted by Heilmann-Clausen and Van Simaeys (2005) from the uppermost Lutetian part of the *E. arcuata* Zone. In the present study, the Base of *Rhombodinium draco* is recognized only from ~17.1 m. Owing to the unfavorable facies characteristics (sandy units with glauconite, pebbles and shells), we cannot exclude the possibility that the true lowermost occurrence of *R. draco* was not represented. In this case, this part of the Alum Bay succession should be tentatively attributed to a part of the *R. draco* Zone. The palynological assemblage from sample AB10 revealed a relative influx of acritarchs and reworked dinoflagellate cysts, indicating a possible transgression. The assemblage from sample AB12 additionally demonstrates a decrease in open-marine *Spiniferites*–group (only 7 %), still common *Homotryblium*–group (7 %) and an increase in *Enneadocysta*–group (33 %); peridinioid taxa attain up to 10 %. This may indicate a more restricted inner-neritic environment.

The fourth dinoflagellate cyst interval (Samples AB14–AB17) revealed the successive occurrences of *Rhombodinium draco* and *Distatodinium paradoxum* at ~17.1 m, *Enneadocysta partridgei* at ~18.5 m, *Enneadocysta fenestrata* at ~19.9 m, *Membranophoridium aspinatum* and *Hemiplacophora semilunifera* at ~21.8 m. The Top (highest occurrence) of *Areoligera undulata* is recognized at ~17.1 m, the Top of *Axiodinium prearticulatum* is noted at ~19.9 m, and the Top of *Charlesdowniea coleothrypta* – at ~21.8 m. Based on the occurrence of stratigraphically important *Rhombodinium draco*, this part of the Alum Bay succession may be attributed to the *R. draco* Zone from the West European zonation of Powell (1992), Ukrainian zonation of Andreeva-Grigorovich et al. (2011), W Siberian zonation of Iakovleva and Aleksandrova (2013) and Peri-Tethyan zonation of Iakovleva (2017). According to nannoplankton data, the recognized Base of *R. draco* in the Alum Bay corresponds to the upper part of the

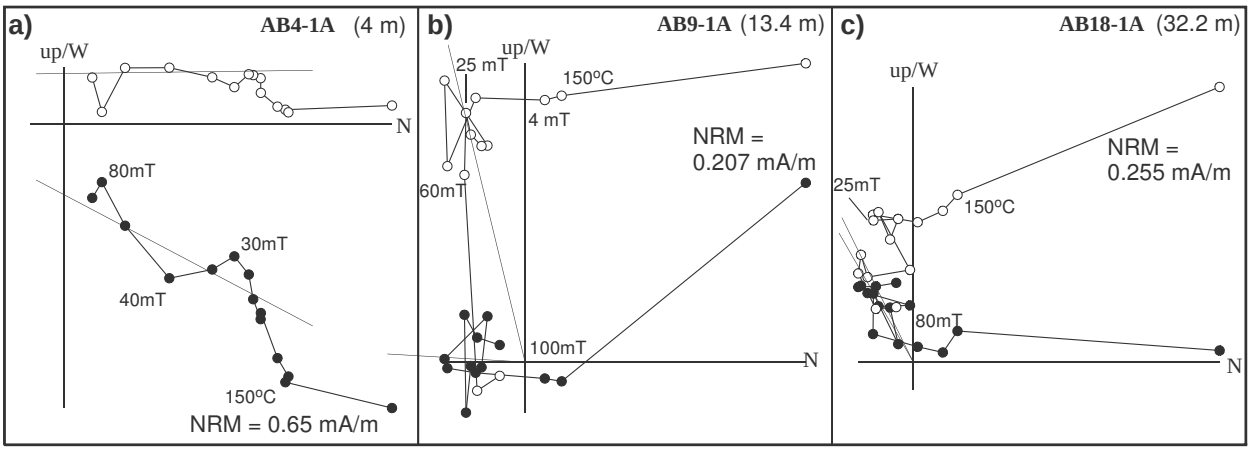

Fig. 11. Representative "class A" normal (a) and reverse (b and c) tilt-corrected (TC) orthogonal demagnetization diagrams from the studied Alum Bay section. The stratigraphic position in meters, the natural remanent magnetization (NRM) intensity and some demagnetization steps are indicated. Open and closed symbols indicate projections onto the upper and lower hemisphere respectively. The computed ChRM direction is shown by a solid grey thick line.

NP16 Zone. Taking into account the questionable attribution of the 3rd dinocyst interval to the *R. draco* Zone, the stratigraphic level of the Base of *R. draco* correlates well with the data from eastern Peri-Tethys, where the Base of *R. draco* is directly calibrated to calcareous nannoplankton and corresponds to the upper part of NP15–NP16 Zone interval (Iakovleva 2017). The dinoflagellate cyst assemblage from this interval is characterized by alternating dominance of open-marine *Spiniferites*–group (up to 30 %), with the low-salinity tolerant *Homotryblium*–group (42 %), indicating a possible transition to the restricted shallow-water environments with reduced salinity.

The fifth dinoflagellate cyst interval (samples AB18–AB23) revealed the lowermost occurrences of the species *Homotryblium floripes* and *Glaphyrocysta intircata* at ~32.4 m, the LO of *Distatodinium craterum-biffii* (transitional form to *D. biffii*) at ~46.5 m and the LO of *Hemisphaeridium fenestratum* at ~47.2 m. Based on the virtual absence of *Rhombodinium porosum* and any other stratigraphically younger taxa, the upper part of the section is still attributed to the *R. draco* Zone interval. The dinoflagellate cyst assemblage is again characterized in the lowermost part of the interval by an increase in the *Spiniferites*–group (28 %) and a relative decrease (21 %) in the *Homotryblium*–group, while most of this interval is marked by a significant increase and dominance of the *Homotryblium*–group, which varies between 49 and 65 %. Such dominance of the *Homotryblium*–group may indicate restricted shallow environments with reduced salinity. A slight influx in the *Areoligera*– and *Enneadocysta*–groups at ~48.0 m may likely reflect a short transgressive pulse.

4.5. Palaeomagnetism

A total of 15 samples have been demagnetized stepwise following the combined thermal and alternating field (AF) protocol outlined above. The NRM intensity generally ranges from 0.2×10^{-3} to 0.6×10^{-3} A/m. with the exception of sample AB2-1A at 2 m that corresponds to a reddish lithology which has an intensity value of 4×10^{-3} A/m. Samples from 11 stratigraphic levels have provided moderately good quality demagnetization data. Samples from 4 stratigraphic levels display scattered demagnetization data preventing the computation of any magnetization components. These later samples are qualified as "class C" samples. Normally, intensity of the samples drops noticeably after the first heating step at 150 °C and proceeds up to about 25–30 mT demagnetizing a component which is usually northerly oriented and steep in *in-situ* (geographic) coordinates (Fig. 11 Z-plots). Above those demagnetizing fields and up to about 80–100 mT demagnetization trajectories trending toward the origin define the characteristic remanent magnetization (ChRM). The ChRM components are either northerly and moderately steeply downward (Fig. 11a) or southerly and upwards (Fig. 11b, c) oriented in bedding corrected coordinates. The fact that the strata are subvertical along the studied sections affirms that

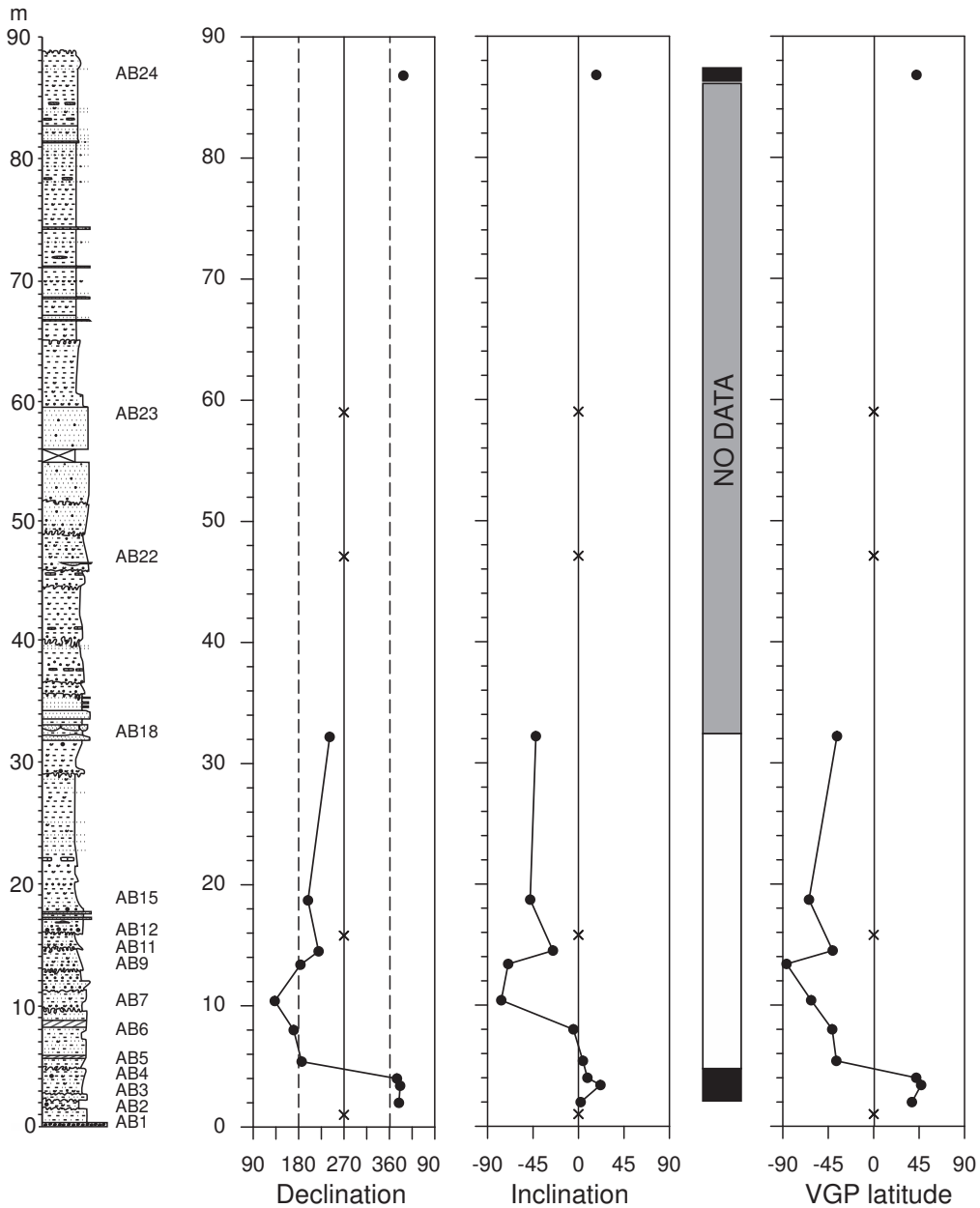

Fig. 12. Magnetic polarity stratigraphy of the Alum Bay section. Crosses indicate "class C" specimens (no data), and closed circles mark "class A and AB" specimens (reliable directions). Magnetostratigraphic interpretation includes normal polarity (black), reverse polarity (white) and undefined polarity (grey) bands.

this component is of pre-tilt origin and likely represents a primary magnetization with dual polarity. The firstly removed low-field component conforms to a recent viscous geomagnetic field direction in geographic coordinates and, thus, represents a secondary overprint. We classify as "class A" samples those where a clear ChRM trajectory including several demagnetization steps trending towards the demagnetization diagram can be retrieved (Fig. 11a–c) or "class AB" when this trajectory is no so well defined. The magnetostratigraphy (Fig. 12) indicates a clear reversal boundary located within the 4.0–5.4 m interval defining a lower normal polarity chron represented by three sample levels and an upper reverse chron that extends up to about 19 m and probably up to 33 m although there is a sampling gap of about 10 m. The interval from 32.2 m up to 86.8 m contains only two sampled stratigraphic levels with "Class C samples"

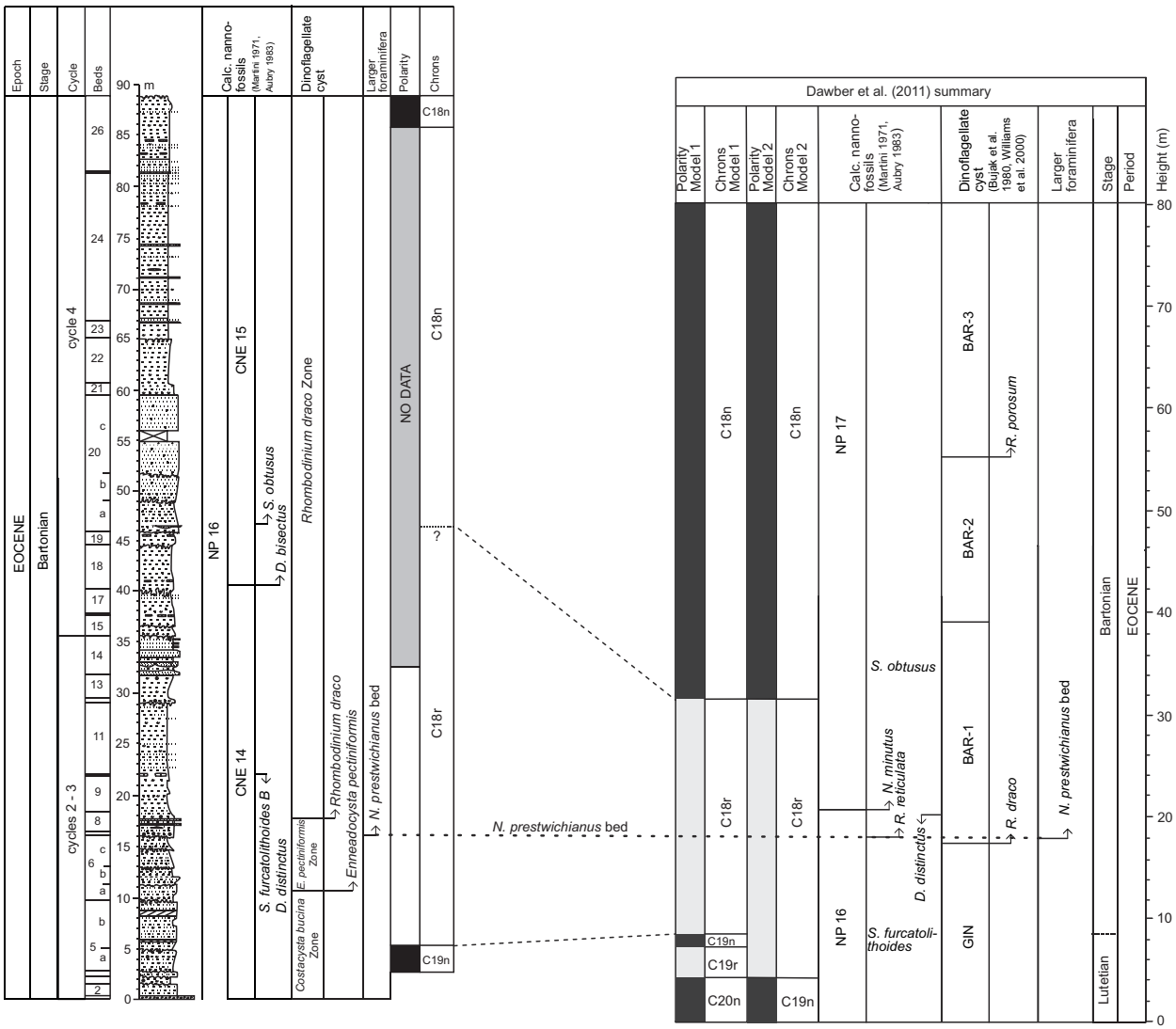

Fig. 13. Summary figure showing biostratigraphy of the Alum Bay section, studied here, magnetic susceptibility, declination and inclination of the interpreted characteristic remanent magnetization, and sampled levels, with comparison to the results of Dawber et al. 2011.

and therefore the polarity of this interval cannot be interpreted with the present dataset. A sample level at the top of the section (86.8 m) presents normal polarity.

5. Interpretation and Discussion

Overall, the biostratigraphic records are in general agreement with each other and show that the Lutetian–Bartonian transition certainly occurs within the section as it is currently defined (Fig. 13). In the absence of a formal Bartonian GSSP, following GTS (Gradstein 2012), the base of the Bartonian has been taken at the C19n/C18r boundary. The Alum Bay section falls largely into CNE14 Zone and the upper part within CNE15. In the scheme of Agnini at al. (2014) the Lutetian/Bartonian boundary is placed at the top of C19n and in the middle of CNE14, so unfortunately its presence cannot be recognised from nannofossil data alone. However, the palaeomagnetic data from the section suggests it is present. The palaeomagnetic data indicate that in the lowermost part of the section (0–5 m) C19n and the C19n/C18r boundary occur, indicating that the Bartonian/Lutetian boundary can be identified approximately between 4.5 m and 5 m. Chrons C18r and C18n have been recognized, but at present it is not possible to determine the C18r/C18n boundary, because in the interval from

32.2 m up to 86.8 m the polarity cannot be interpreted (Fig. 12), although it was recognised by Dawber et al. (2011) (Fig. 13). However, the nannofossil data (Top *S. furcatolithoides, D. bisectus* and *S. obtusus* Base) suggest (as reported by Agnini et al. 2014) that the C18r/C18n could be between 41 m and 47 m. Therefore, additional palaeomagetic sampling would be required to resolve this further.

When nannofossil indicators are compared with Aubry (1983, 1986) and Dawber et al. (2011) using the *Nummulites prestwichianus* bed as a marker, sample 2165 (12.30 m) of Aubry approximately seems to correlate with AB8 at 13 m. The Tops of *S. furcatolithoides* and *D. distinctus* were recognised by Aubry in sample 2171 at 18 m, which correlates with 18.75 m in this study. In our results the Tops of *S. furcatolithoides* and *D. distinctus* are at at meter 20 (AB16) and at 22 m (AB17) respectively, extending their range slightly. In Aubry (1983, 1986) these taxa are used to denote the NP16–NP17 zonal boundary, but more recent works have shown this correlation to be incorrect. Agnini et al. (2014) place the Top of *S. furcatolithoides* B in the middle part of NP16 Zone (upper C18r) and following Dunkley Jones et al. (2009) the range of *D. distinctus* extends to NP23. Additionally, Aubry (1983, 1986) reports the occurrence of *S. obtusus* approximately at 27.2 m, whilst in our results it is at 47 m (AB22). Dawber et al. 2011 also recorded the first occurrence of *Neococcolithites minutus* just 3 m above the *Nummulites prestwichianus* bed (Fig. 13). However, Aubry (1986) just reports in one sentence (p. 299) that she approximated the NP16/17 zonal boundary using the first occurrence in bed E of "a very flattened variety of *Neococcolithites minutes*". Unfortunately Aubry (1983, 1986) did not show the range of this variety in any of the sections studied but only the range of *N. minutus* as a whole; and this taxon extends down to well below the *N. prestwichianus* bed.

Thus, the Base of *N. minutus* is irrelevant, as this species was recorded below *N. prestwichianus* and it is therefore not useful for further refining the stratigraphy.

The nannofossil data and dinoflagellate (*R. draco*) levels appear to be different in our study compared to those reported in Dawber et al. (2011) (from Bujack et al. 1980). Within the palynological data *R. draco* is one of the most biostratigraphically important occurrences. The recognised Base of *R. draco* in Alum Bay corresponds to the topmost part of the NP16 Zone (CNE14) and lower part of C18r. When the third dinoflagellate cyst interval is questionably attributed to the *R. draco* Zone, the stratigraphic occurrence of the Base of *R. draco* correlates well with data from the Eastern Peri-Tethys, where the Base of *R. draco* is directly calibrated to the calcareous nannoplankton occurrences and corresponds to the upper part of the NP16 Zone interval (Iakovleva 2017). It also coincides with the acme of *N. prestwichianus*.

King (2016) shows *Nummulites prestwichianus* as having an upper NP 16 to lower NP 17 Zone range. However, in our study *N. prestwichianus* falls only within the NP 16 Zone. *Nummulites rectus*, the only other larger foraminiferal taxon in the section, is correlated to NP17 Zone and SBZ17 by King (2016). In this study, *N. rectus* was only found in sample AB18 which we assign to the NP16 Zone. Following the ranges given by King (2016) the larger foraminifera would suggest a slightly younger age than the other microfossil studies. However, larger benthic foraminiferal biostratigraphy is challenging owing to factors such as species endemism, dispersals and often lack of independent dating (see Cotton and Pearson 2011, Papazzoni et al 2017). It is therefore more likely that the range of *N. prestwichianus* and *N. rectus* extend into NP16 Zone and their ranges should be updated.

The larger benthic foraminifera comprise of a largely monospecific assemblage, with *Nummulites rectus* only being found in very low numbers at the top of the cycles 2–3, and highest sample containing LBF (AB18). Such assemblages of *Nummulites* are not uncommon and may be linked to the area being at the limits of their range and not a typical oligotrophic shallow carbonate environment. Previous studies have suggested that the *Nummulites prestwichianus* from this region consisted of several morphotypes (King 2016). There is some variation in the proloculus size between the beds, but a full morphological comparison, including other material from the south of the UK is needed to clarify this. All however, closely fit the descriptions of *N. prestwichianus* following Blondeau (1972), and therefore for the purpose of this study we keep them as *N. prestwichianus.* Whilst the beds are certainly distinctive, they have limited use as biostratigraphic marker beds as because of their lateral discontinuity and the potential for diachroneity. Larger benthic foraminifera are well known to be restricted to the oligotrophic, photic zone, and thus only occur during specific intervals in the Alum Bay section, when appropriate environmental conditions are met.

This shallow water environmental interpretation is supported by the smaller benthic foraminifera assem-

blages. Based on benthic foraminifera, Murray and Wright (1974) inferred a near shore shelf depositional setting at Alum Bay, with fine substrate and turbid water for this part of the sequence. Our new study corroborates this interpretation, as in addition to *Cibicides*, the rest of the identified genera at Alum Bay (*Bolivina, Brizalina, Buccella, Buliminella, Discorbis, Nonion*, *Quinqueloculina* and *Rosalina*) are common in inner shelf environments (Murray 2006).

The dominance of a single genus (*Cibicides*) is the most remarkable feature of the small benthic foraminifera assemblages at Alum Bay. This genus is commonly associated with cool waters (Murray 2006). The upper half of the section studied is not only dominated by this one genus, but it also has a strong dominance of one species (>50 % of *C. pygmeus* in interval B, and *C. ungerianus* in interval C), which accounts for the low diversity of the assemblages.

Interval A (14–20.5 m) represents a near shore, shallow shelf setting, possibly partially restricted owing to its low diversity values (Murray 2006). This hypothesis is supported by the occurrence of *Protelphidium*, as this genus is associated with low salinity environments (Murray and Wright 1974). Dinoflagellate assemblages also point towards a restricted-inner neritic environment (sample AB12). The maximum values of diversity, P/B ratio and foraminifera per gram in sample AB16 (19.5 m) of this interval might indicate reduced sedimentation rates and/or changes in sea level.

Interval B (20.5–40.5 m) is dominated by *C. pygmeus*, and it contains one sample barren of foraminifera. Murray and Wright (1974) interpreted barren samples from this part of the log as reflecting intertidal conditions, which might point to variations in sea level and unstable conditions. We argue that *C. pygmeus* may have adapted to environmental instability related to rapidly changing sea level, becoming more abundant in this interval. *Rosalina* spp. has been argued to have a clinging mode of life (attached with organic 'glue' to the seaweeds or hard substrates), indicative of a high-energy environment (Kitazato 1988), supporting a near-shore setting with episodes of intertidal settings.

Interval C (40.5–48 m) is characterised by a strong dominance of *C. ungerianus*, and by a small increase in percentage of species present in interval A such as *Buccella propingua, Cibicides fortunatus and Globulina gibba*. These results point to a return to conditions similar to those inferred from the lower part of the section. However, diversity and the percentage of infaunal morphogroups are lower, possibly due to the proliferation of opportunistic species (*C. ungerianus* and *Buccella propingua*). After the instability recorded in interval B, the assemblages seem to recover and reflect environmental conditions similar to those from interval A.

Our results agree with the interpretation and intervals defined by Murray and Wright (1974) for this part of the section, corresponding to the "Upper Bracklesham Beds" and "Lower Barton Beds". However, the interpretation given by Dawber et al. (2011) for the same section slightly differs from our results. They infer a shallowing-upward trend from the lower part of the section (70–120 m palaeodepth, equivalent to our interval A) to 30–70 m palaeodepth towards our interval B, and 0–30 m towards our interval C. Diversity values are also slightly lower, with Fisher-α ranging from 0 to 5 and H (S) from 0 to 1.5. The trends described by Dawber et al. (2011) do not fit our observations. We do not know the source of these discrepancies, and we cannot evaluate the results in that publication as it does not provide information regarding the methodology followed in the study of benthic foraminifera (e. g., number of specimens counted per sample, permanent record of the picked specimens, taxonomic criteria used in the identification of taxa, etc.), and a table with the benthic foraminiferal counts is missing.

A difference in the preservation was noted when compared to that previously reported by Aubry, with our observations indicating a poor/average preservation compared to Aubry (1983, 1986) in the calcareous nannofossil content. The exception to this is the larger benthic foraminifera in the *Nummulites prestwichianus* bed. Though pyrite is common the preservation of the LBF is often exceptional, owing to their preservation in clay preserving their mineralogy, rather than within shallow water limestones where replacement readily occurs.

6. Conclusion

Integrated stratigraphy combining nannofossil, smaller and larger benthic foraminifera, dinoflagellate and palaeomagnetic studies has been carried out for the first time from Alum Bay, to reassess its potential to define the Lutetian/Bartonian boundary. The Alum Bay section is within nannoplankton Zones CNE14 and CNE15, middle upper part of NP16, the Base of *R. draco* is recognised within the section, which also coincides with the acme of *Nummulites prestwichia-*

nus, both of which are correlated with nannoplankton Zone NP16 which spans the upper Lutetian and lower Bartonian. The palaeomagnetic data indicates C19n and C18r at the base of the section, and C18n at the top, although there is a gap with no data. All analyses therefore support that, on the criterion of the boundary at top C19n the section is largely lower Bartonian in age, with the palaeomagnetic data indicating that the first 5 m of the section also contains the upper Lutetian and that the boundary is therefore within the section. These results largely confirm those from previous individual stratigraphic studies (e. g., Eaton 1971a, b, Aubry 1983, 1986, Dawber et al. 2011). Although notable differences were found in the quality of preservation and distribution in the calcareous nannoplankton, it has also highlighted the potential of LBF from this site for future geochemical work. Higher resolution palaeomagnetic sampling would be needed to further refine the bio- magnetostratigraphy. The results of this study have left many unanswered questions about the stratigraphic succession at Alum Bay. They do, however, provide valuable information on the proposed guide events for the base of the Bartonian (Jovane et al. 2010, Fluegeman 2007). The verification of beds assignable to C19n below the *Nummulites prestwichianus* bed of Keeping (1887) mean that the selection of either the base or the top of C19n as the primary guide event for the base of the Bartonian Stage will not truncate the historical concept of the Bartonian Stage.

Acknowledgements. We thank Mike Kullander of The Needles Landmark Attraction and Mark Larter of Natural England for access to the Alum Bay site. The dinoflagellate cyst research of AI was performed within the framework of the State program no. 0135-2019-0044 (Geological Institute, Russian Acad. Sci.). We acknowledge financial support by the International Commission on Stratigraphy (ICS and IUGS), and by the Spanish Ministry of Economy and Competitiveness and FEDER funds (CGL2017-84693-R).

References

Agnini, C., Fornaciari, E., Giusberti, L., Grandesso, P., Lanci, L., Luciani, V., Muttoni, G., Palike, H., Rio, D., Spofforth, D. J. A., Stefani, C., 2011. Integrated biomagnetostratigraphy of the Alano section (NE Italy): A proposal for defining the middle-late Eocene boundary. Geological Society of America Bulletin 123, 841–872.

Agnini, C., Fornaciari, E., Raffi, I., Catanzariti, R., Pälike, H., Backman, J., Rio, D., 2014. Biozonation and biochronology of Paleogene calcareous nannofossils from low and middle latitudes. Newsletters on Stratigraphy 47 (2), 131–181.

Andreeva-Grigorovich, A. S., Waga, D. D., 2010. Nannofossil biostratigraphy of the Paleogene sediments of the Crimea-Caucasus region (southern Ukraine and Russia). Abstracts of 4th French Congress on Stratigraphy. Strati 2010, 6–8.

Aubry, M.-P., 1983. Biostratigraphie du Paléogène épicontinental de l'Europe du nord-ouest. Étude fondée sur les nannofossiles calcaires. Documents des Laboratoires de Géologie de la Faculté des Sciences de Lyon 89, 1–317.

Aubry, M.-P., 1986. Paleogene calcareous nannoplankton biostratigraphy of northwestern Europe. Palaeogeography, Palaeoclimatology, Palaeoecology 55, 267–334.

Aubry, M.-P., 1992. Late Paleogene nannoplankton evolution: A tale of climatic deterioration. In: Prothero, D. R., Berggren, W. A. (Eds.), Eocene-Oligocene Climatic and Biotic Evolution, Princeton Univ. Press, Princeton, N. J., 272–309.

Berggren, W. A., 1972. A Cenozoic time scale-some implications for regional geology and paleobiogeography. Lethaia 5, 195–215.

Berggren, W. A., Kent, D. V., Flynn, J. J., Van Couvering, J. A., 1985. Cenozoic Geochronology. Geological Society of America Bulletin 96, 1407–1418.

Berggren, W. A., Kent, D. V., Swisher III, C. C., Aubry, M. P., 1995. A revised Cenozoic geochronology and chronostratigraphy. Geochronology timescales and global stratigraphic correlation, SEPM special publication 54, 129–212.

Blondeau, A., 1972. . Les Nummulites Vuibert, Paris, 254 p.

Bown, P. R., Young, J. R., 1998. Techniques. In: Bown, P. R. (Ed.), Calcareous Nannofossil Biostratigraphy, Chapman and Hall, London, 16–28.

Bristow, C. R., Freshney, E. C., Penn, I. E., 1991. The geology of the country around Bournemouth. Memoir of the British Geological Survey, sheet 329 (England and Wales), i–x, 1–116.

Bujak, J. P., 1976. An evolutionary series of Late Eocene dinoflagellate cysts from southern England. Marine Micropaleontology 1, 101–117.

Bujak, J. P., 1979. Proposed phylogeny of the dinoflagellates *Rhombidinium* and *Gochtodinium*. Micropaleontology 25, 308–324.

Bujak, J., Mudge, D., 1994. A high-resolution North Sea Eocene dinocyst zonation. Journal of the Geological Society 151 (3), 449–462.

Bujak, J. P., Downie, C., Eaton, G. L., Williams, G. L., 1980. Dinoflagellate cysts and acritarchs from the Eocene of southern England. Special Papers in Palaeontology 24, 1–100.

Costa, L. I., Dennison, C., Downie, C., 1978. The Paleocene/Eocene boundary in the Anglo-Paris Basin. Journal of the Geological Society 135, 261–264.

Costa, L. I., Downie, C., 1975. The distribution of the dinoflagellate *Wetzeliella* in the Paleogene of North-Western Europe. Palaeontology 19, 591–614.

Cotton, L. J., Pearson, P. N., 2011. Extinction of larger benthic foraminifera at the Eocene/Oligocene boundary. Palaeogeography, Palaeoclimatology, Palaeoecology 311 (3–4), 281–296.

Curry, D., 1981. Bartonian. In: Pomerol, C. (Ed.), Stratotypes of Paleogene stages. Bulletin d'Information des Géologues du Bassin de Paris. Mémoire hors série 2, 23–36.

Davey, R. J., Downie, C., Sarjeant, W. A. S., Williams, G. L., 1966. Fossil dinoflagellate cysts attributed to Baltisphaeridium.. In: Davey, R. J., Downie, C., Sarjeant, W. A. S., Williams, G. L. (Eds.), Studies on Mesozoic and Cainozoic dinoflagellate cysts. Bulletin of the British Museum (Natural History)(Geology) 3, 157–175.

Dawber, C. F., Tripati, A. K., Gale, A. S., MacNiocaill, C., Hesselbo, S. P., 2011. Glacioeustacy during the middle Eocene? Insights from the stratigraphy of the Hampshire Basin, UK. Palaeogeography, Palaeoclimatology, Palaeoecology 300, 84–100.

Downie, C., Hussain, M. A., Williams, G. L., 1971. Dinoflagellate cyst and acritarch associations in the Paleogene of southeast England. Geoscience and Man 3, 29–35.

Dunkley Jones, T., Bown, P. R., Pearson, P. N., 2009. Exceptionally well preserved upper Eocene to lower Oligocene calcareous nannofossils (Prymnesiophyceae) from the Pande Formation (Kilwa Group), Tanzania. Journal of Systematic Palaeontology 7, 359–411.

Eaton, G. L., 1976. Dinoflagellate cysts from the Bracklesham Beds (Eocene) of the Isle of Wight, southern England. Bulletin of the British Museum (Natural History) (Geology) 26, 227–332.

Eaton, G. L., 1971a. A morphogenetic series of dinoflagellate cysts from the Bracklesham Beds of the Isle of Wight, Hampshire, England. In: Farinacci, A. (Ed.), Proceedings of the 2nd Planktonic Conference, Edizioni Tecnoscienza, Rome, 355–379.

Eaton, G. L., 1971b. The use of microplankton in resolving stratigraphical problems in the Eocene of the Isle of Wight. Journal of the Geological Society, London 127, 281–283.

Fluegeman, R. H., 2007. Unresolved issues in Cenozoic chronostratigraphy. Stratigraphy 4 (2–3), 109–116.

Fornaciari, E., Agnini, C., Catanzariti, R., Rio, D., Bolla, E. M., Valvasoni, E., 2010. Mid-latitude calcareous nannofossil biostratigraphy and biochronology across the middle to late Eocene transition. Stratigraphy 7 (4), 229–264.

Gradstein, F., Ogg, J., Smith, A., 2012. A Geologic Timescale, Cambridge University Press, Cambridge, 1176.

Gruas-Cavagnetto, C., 1970. Dinophyceae, Acritarcha et pollens de la Formation de Varengeville (Cuisien, Seine maritime). Revue de Micropaléontologie 15, 63–74.

Gruas-Cavagnetto, C., 1976. Etude palynologique du Paleocene du Sud de l'Angleterre. Cahiers Micropalaeontology 1, 1–49.

Hardenbol, J., Berggren, W. A., 1978. A new Paleogene numerical scale. In: Cohee, G. V., Glaessner, M. F., Hedberg, H. D. (Eds.), Contributions to the geologic time scale. American Association of Petroleum Geologists, Studies in Geology 6, 213–234.

Harland, W. B., Armstrong, R. L., Cox, A. V., Craig, L. E., Smith, A. G., Smith, D. G., 1989. A Geologic Time Scale, Cambridge University Press, Cambridge, 263 p.

Harland, W. B., Cox, A. V., Llewellyn, P. G., Pickton, C. A. G., Smith, A. G., Walters, R., 1982. , Cambridge University Press, Cambridge, 131 p.

Heilmann-Clausen, C., 1988. The Danish Sub-basin, Paleogene dinoflagellates. The north west European Tertiary basin: results of the International Geological Correlation Programme, Project 124, 339–343.

Heilmann-Clausen, C., Van Simaeys, S., 2005. Dinoflagellate cysts from the Middle Eocene to ?lowermost Oligocene succession in the Kysing Research borehole, central Danish Basin. Palynology 29 (1), 143–204.

Hooker, J. J., 1986. Mammals from the Bartonian (middle/late Eocene) of the Hampshire Basin, southern England. Bulletin of the British Museum (Natural History) Geology 39, 191–478.

Hooker, J. J., King, C., 2018. The Bartonian unit stratotype (S. England): Assessment of its correlation problems and potential.. Proceedings of the Geologists' Association 130 (2), 157–169.

Iakovleva, A. I., 2017. Detalization of Eocene dinocyst zonation for Eastern Peritethys. Bulletin of Moscow Society of Naturalists, Geological Series 92, 32–48 (in Russian).

Iakovleva, A. I., Aleksandrova, G. N., 2013. To the question on Dinocyst zonation of Paleocene–Eocene in Western Siberia. Bulletin of the Moscow Society of Naturalists, Geological Section 88 (1), 59–82 (in Russian).

Islam, M. A., 1981. Early and Middle Eocene organic-walled microplankton of the Anglo-Belgian Basin. PhD thesis, University of Sheffield, Sheffield, Great Britain.

Islam, M. A., 1983a. Dinoflagellate cysts from the Eocene cliff sections of the Isle of Sheppey, southeast England. Revue de Micropaléontologie 25, 231–250.

Islam, M. A., 1983b. Dinoflagellate cyst taxonomy and biostratigraphy of the Eocene Bracklesham Group in southern England. Micropaleontology 29, 328–353.

Islam, M. A., 1984. A study of early Eocene palaeoenvironments in the Isle of Sheppey as determined from microplankton assemblage composition. Tertiary Research 6, 11–21.

Jolley, D. W., Spinner, E., 1989. Some dinoflagellate cysts from the London Clay (Palaeocene-Eocene) near Ipswich, Suffolk, England. Review of Palaeobotany and Palynology 60, 361–373.

Jolley, D. W., Spinner, E. G., 1991. Spore-pollen associations from the lower London Clay (Eocene), East Anglia. Tertiary Research 13, 11–25.

Jorissen, F. J., Stigter, H. C., Widmark, J. G., 1995. A conceptual model explaining benthic foraminiferal microhabitats. Marine micropaleontology 26 (1–4), 3–15.

Jovane, L., Sprovieri, M., Coccioni, R., Florindo, F., Marsili, A., Laskar, J., 2010. Astronomical calibration of the middle Eocene Contessa Highway section (Gubbio,

Italy). Earth and Planetary Science Letters 298 (1–2), 77–88.

Keeping, H., 1887. On the discovery of the *Nummulina elegans* Zone at Whitecliff Bay, Isle of Wight. Geological Magazine 3, 70–72.

King, C., 2016. A revised correlation of Tertiary rocks in the British Isles and adjacent areas of NW Europe, Geological Society of London, London, 719 p.

Kirschvink, J. L., 1980. The least-squares line and plane and the analysis of palaeomagnetic data. Geophysical Journal International 62 (3), 699–718.

Kitazato, H., 1988. Ecology of benthic foraminifera in the tidal zone of a rocky shore. Revue de Paléobiologie 2, 815–825.

Köthe, A., 2012. A revised Cenozoic dinoflagellate cyst and calcareous nannoplankton zonation for the German sector of the southeastern North Sea Basin. Newsletters on Stratigraphy 45 (3), 189–220.

Liengjarern, M., Costa, L., Downie, C., 1980. Dinoflagellate cysts from the upper Eocene-lower Oligocene of the Isle of Wight. Palaeontology 23, 475–499.

Luterbacher, H. P., Ali, J. R., Brinkhuis, H., Gradstein, F. M., Hooker, J. J., Monechi, S., Ogg, J. G., Powell, J., Röhl, U, Sanfilippo, A., Schmitz, B., 2004. The Paleogene Period. In: Gradstein, F. M., Ogg, J. M., Smith, A. G. (Eds.), A Geologic Time Scale 2004, Cambridge University Press, Cambridge, 384–408.

Marino, M., Flores, J. A., 2002a. Middle Eocene to early Oligocene calcareous nannofossil stratigraphy at Leg 177 Site 1090. Marine Micropaleontology 45 (3), 383–398.

Marino, M., Flores, J. A., 2002b. Miocene to Pliocene calcareous nannofossil biostratigraphy at ODP Leg 177 Sites 1088 and 1090. Marine Micropaleontology 45 (3), 291–307.

Martini, E., 1971. Standard Tertiary and Quaternary calcareous nannoplankton zonation. Proc. II Planktonic Conference, Roma 1970, Roma, Tecnoscienza 2, 739–785.

Murray, J. W., 2006. Ecology and applications of benthic foraminifera, Cambridge University Press, Cambridge, 426 p.

Murray, J. W., Wright, C. A., 1974. Palaeogene Foraminiferida and palaeoecology, Hampshire and Paris Basins and the English Channel. Special Papers in Palaeontology 14, 1–129.

Norvick, M. S., 1969. An analysis of the microfauna and microflora of the Upper Eocene of the Hampshire Basin. Unpublished PhD thesis, Imperial College, University of London.

Okada, H., Bukry, D., 1980. Supplementary modification and introduction of code numbers to the low-latitude coccolith biostratigraphic zonation (Bukry 1973, 1975). Marine Micropaleontology 5, 321–325.

Papazzoni, C. A., Fornaciari, E., Giusberti, L., Vescogni, A., Fornaciari, B., 2017. Integrating shallow benthic and calcareous nannofossil Zones: the lower Eocene of the Monte Postale section (Northern Italy) SB and CN biozonation in the Eocene of Monte Postale, Italy. Palaios 32 (1), 6–17.

Perch-Nielsen, K., 1985. Mesozoic and Cenozoic calcareous nannofossils. In: Bolli, H. M., Saunders, J. B., Perch-Nielsen, K. (Eds.), Plankton Stratigraphy, Cambridge University Press, Cambridge, 329–554.

Plint, A. G., 1988. Global eustacy and the Eocene sequence in the Hampshire Basin, England. Basin Research 1 (1), 11–22.

Powell, A. J., 1992. Dinoflagellate cysts of the Tertiary System. In: Powell, A. J. (Ed.), A Stratigraphic Index of Dinoflagellate Cysts. British Micropaleontological Society Publication Series, Chapman and Hall, London, 155–251.

Riding, J. B., Kyffin-Hughes, J. E., 2004. A review of the laboratory preparation of palynomorphs with a description of an effective non-acid technique. Revista Brasileira de Paleontologia 7 (1), 13–44.

Sluijs, A., Brinkhuis, H., 2009. A dynamic climate and ecosystem state during the Paleocene-Eocene Thermal Maximum: inferences from dinoflagellate cyst assemblages on the New Jersey Shelf. Biogeosciences 6 (8), 1755–1781.

Vandenberghe, N., Hilgen, F. J., Speijer, R. P., Ogg, J. G., Gradstein, F. M., Hammer, O., Hollis, C. J., Hooker, J. J., 2012. The Paleogene Period. In: Gradstein, F. M., Ogg, J. G., Schmitz, M. (Eds.), The geologic time scale, Cambridge University Press, Cambridge, 855–921.

Villa, G., Fioroni, C., Pea, L., Bohaty, S., Persico, D., 2008. Middle Eocene–late Oligocene climate variability: calcareous nannofossil response at Kerguelen Plateau, Site 748. Marine Micropaleontology 69 (2), 173–192.

Wei, W., Wise JR, S. W., 1989. Paleogene calcareous nannofossil magnetobiochronology: results from South Atlantic DSDP Site 516. Marine Micropaleontology 14 (1–3), 119–152.

Zijderveld, J. D. A., 1967. A. C. demagnetization of rocks: analysis of results. In: Collinson, D. W., Creer, K. M., Runcorn, S. K. (Eds.), Methods in Palaeomagnetism, Elsevier, Amsterdam, 254–286.

Manuscript received: August 08, 2019
Revisions required: September 26, 2019
Revised version received: March 25, 2020
Manuscript accepted: March 25, 2020

Appendix

Sedimentary log and full description of the Alum Bay section:

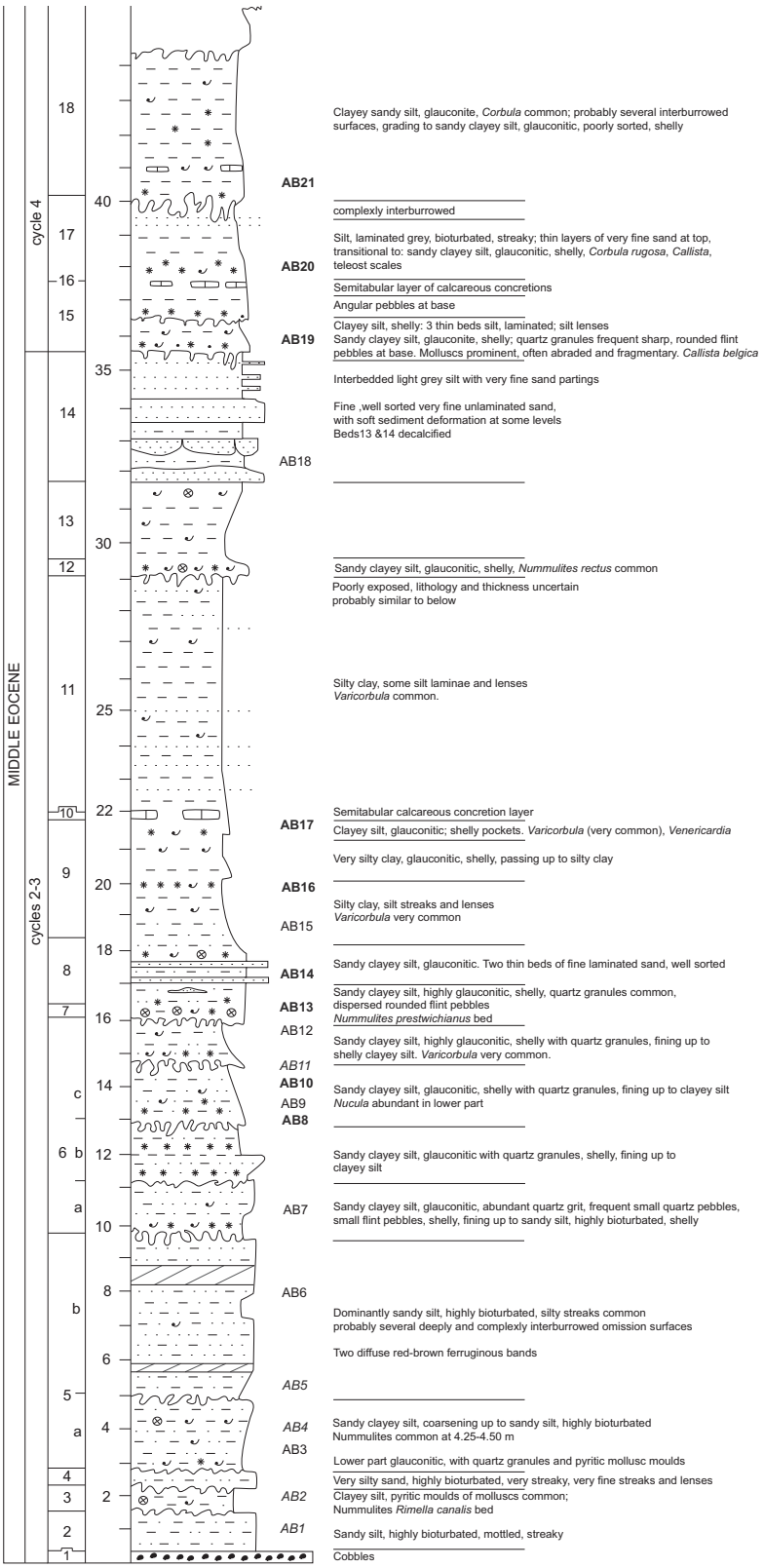

Bold : micropalaeo samples
Italic : palaeomag samples
roman: both

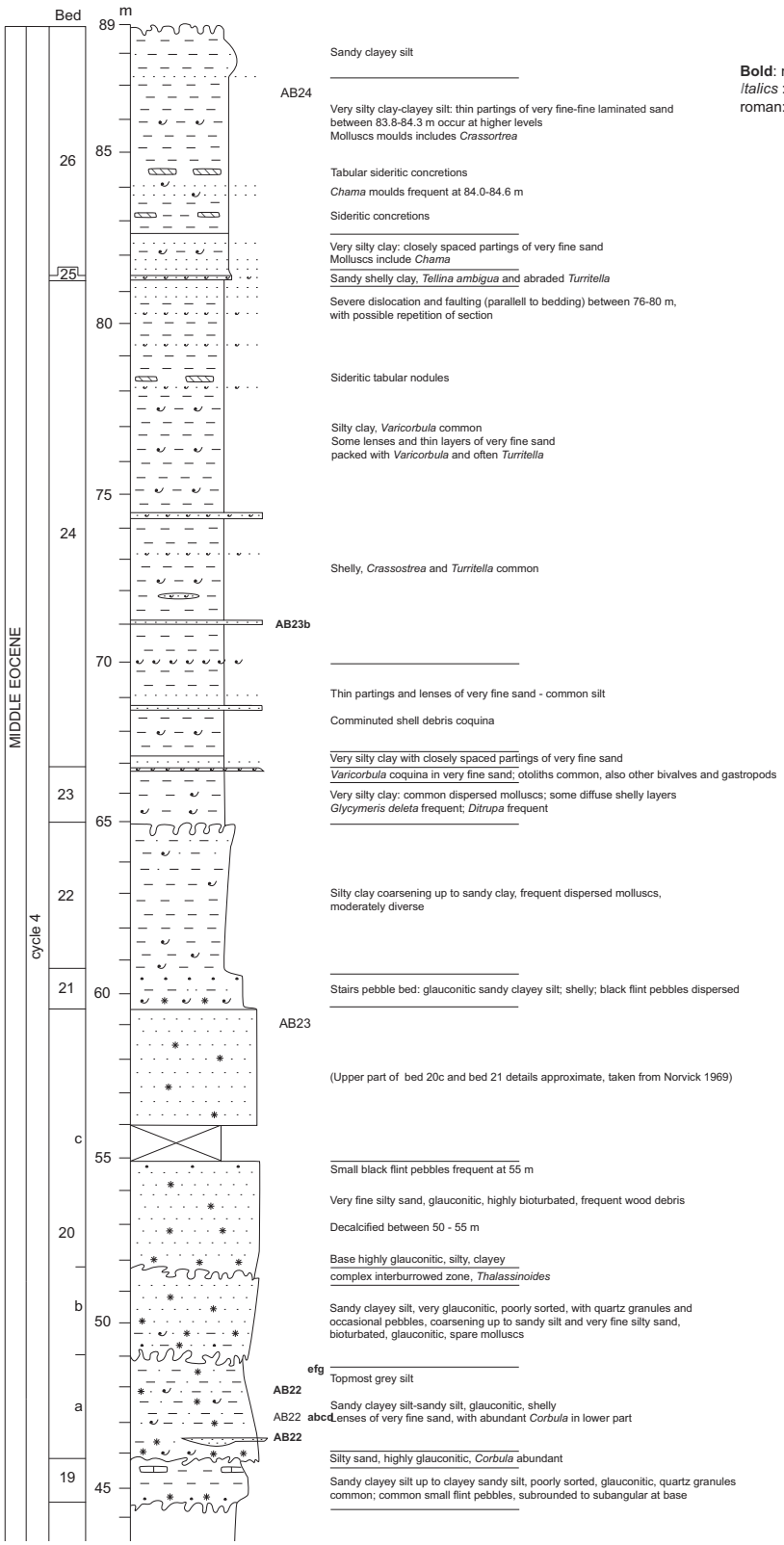

Bold: micropalaeo samples
Italics : palaeomag samples
roman: both

Chapter 5:

Discussion

5.1 Benthic foraminifera response to Eocene climatic events

5.1.1 The Late Lutetian Thermal Maximum

As the first record of benthic foraminifera assemblages across the LLTM, Chapter 4.1.1 (Rivero-Cuesta et al., 2020) reports the foraminiferal turnover across this understudied middle Eocene hyperthermal event, providing valuable paleoecological and paleoenvironmental information at ODP Site 702 (South Atlantic Ocean).

Assemblages are strongly dominated by calcareous taxa throughout the studied interval at Site 702. Both infaunal and epifaunal morphogroups are common, with infaunal taxa slightly dominating the assemblages, pointing to oligo-mesotrophic conditions at the seafloor. No extinctions of benthic foraminifera have been recorded across the study interval, but assemblages show changes in the relative abundance of species.

Cluster analysis reports 3 different clusters of species. The most relevant changes occur between 90.8 and 89.7 mbsf of the study interval (Fig. 4). This interval comprises the LLTM and the pre- and aftermaths of the event according to the isotopic data. Across this interval, the relative abundance of cluster 1 decreases and that of cluster 2 increases. However, the accumulation rates (ARs, hence absolute abundance) of the main species of these clusters show a different trend.

The most common species from cluster 1, *B. elongata* and *C. micrus*, show decreasing ARs across the 90.8 - 89.7 mbsf interval, pointing to a decrease in absolute abundance. On the contrary, *O. umbonatus* and *N. truempyi* (main species from cluster 2) ARs do not vary significantly across the studied interval, indicating that the increase in abundance of species from cluster 2 is only relative and not absolute.

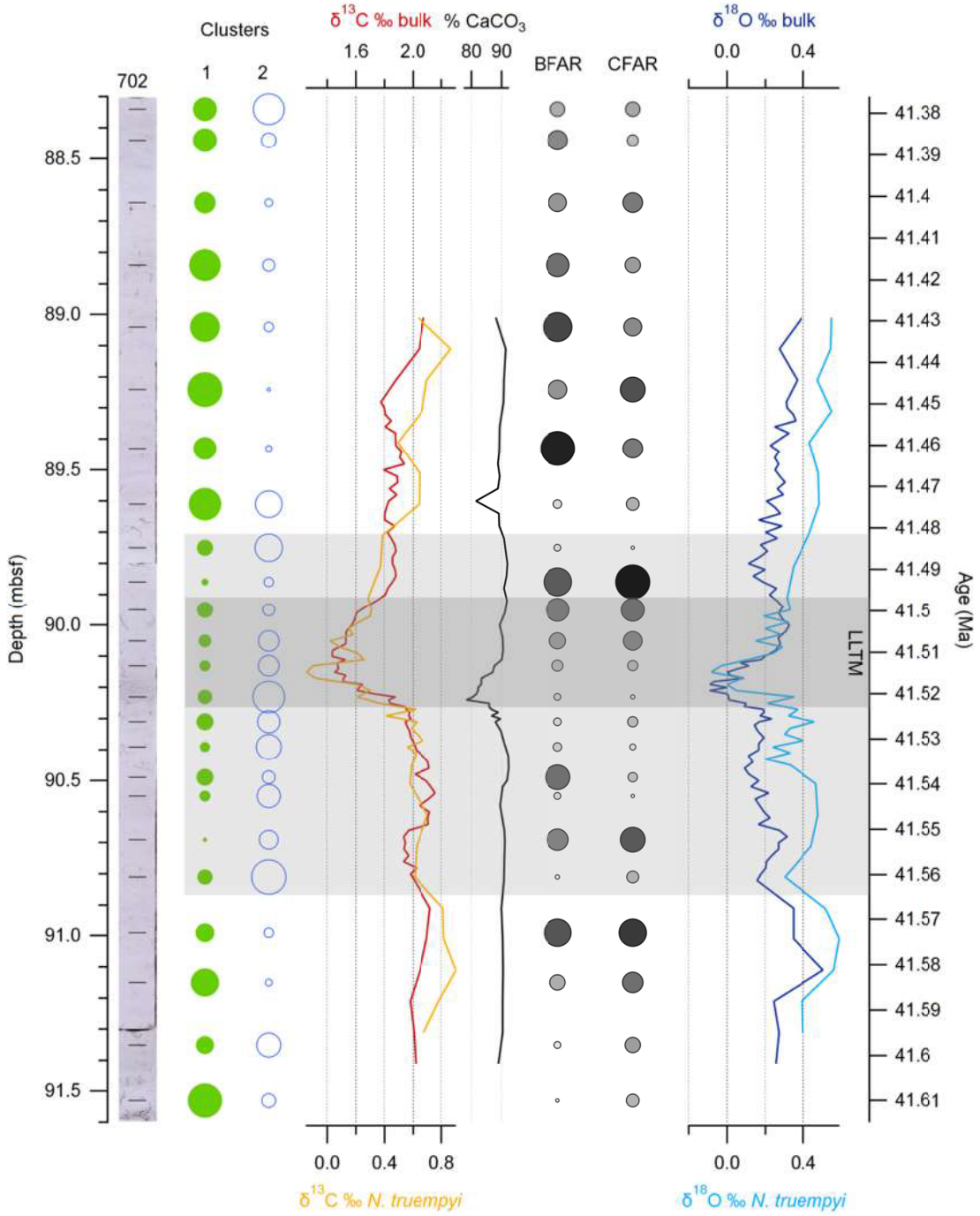

Figure 4. Summary figure from Rivero-Cuesta et al. (2020), illustrating the main results of benthic foraminifera analysis across the LLTM at ODP Site 702 in reference to isotopic data from Westerhold et al. (2018). The dark grey box indicates the position of the LLTM event, and the light grey box indicates the period of environmental instability identified in this study.

Species from cluster 1 seem to have been more affected by the environmental changes related to the LLTM than those of cluster 2. Indeed, cluster 2 species *O. umbonatus* is an extant cosmopolitan species with a broad environmental tolerance (Thomas and Shackleton, 1996; Katz, 1999; Foster et al., 2013) and *N. truempyi* is considered as an indicator of oligotrophic conditions, resistant to $CaCO_3$-corrosive waters (e.g. Tjalsma and Lohmann, 1983; Thomas, 1998; Alegret et al., 2018). Their steady absolute abundance across the studied interval points to a high resilience of these species and those included in cluster 2, being able to cope with the environmental change across the LLTM. This hypothesis is further supported by DCA analysis (Supplementary material in Rivero-Cuesta et al., 2020), where the cosmopolitan, resilient species of cluster 2 species are grouped to the right of axis 1 and the rest of the assemblage, including highly seasonally species from cluster 3 *Alabamina weddellensis* and *Epistominella exigua*, appear on the left part of axis 1.

The decrease in abundance of cluster 1 and particularly its main species *B. elongata* has been attributed to a change in the type of organic matter arriving to the seafloor during the 90.8 - 89.7 mbsf interval, as there is no evidence for large changes in the organic matter flux or oxygenation, which are the main drivers of benthic foraminifera abundance and diversity in the deep sea. There are no specific records on the literature about the food preferences of *B. elongata*, but its turnover at Site 702 suggests this species may have been able to feed on a specific type of organic matter, showing resource partitioning (Murray, 2006 and references therein).

The 90.8 - 89.7 mbsf interval across which *B. elongata* decreases in absolute abundance comprises not only the LLTM but also several kyr before and after the event. This suggests that the environmental effects of the LLTM lasted longer than the associated isotopic excursion. Interestingly, this interval of environmental change coincides with decreased benthic carbon isotope values, suggesting a relation between the decrease in abundance of *B. elongata* and the environmental change reflected by the carbon isotopes in the deep-sea. The paleoecological interpretation of the assemblage turnover, as discussed above, points to a change in the type of organic matter supplied to the seafloor across the LLTM. Further

studies are needed to unravel the nature of this change in type of organic matter flux to the seafloor, and to explore its relation with the carbon isotopic record.

Low CFAR and BFAR values suggest that the production of organic matter at the surface might have decreased during the warming interval of the LLTM. Warming across the LLTM, recorded by oxygen isotopic values, could have led to a decrease in heterotroph biomass (both planktic and benthic foraminifera) according to the metabolic hypothesis (Olivarez Lyle and Lyle, 2006; O'Connor et al., 2009; Boscolo-Galazzo et al., 2014; Arreguín-Rodríguez et al., 2016). Increased temperature accelerates metabolic rates, especially those of heterotroph organisms (Boscolo-Galazzo et al., 2018), which then require a higher food consumption to maintain the same population. In oligo-mesotrophic settings such as Site 702, food availability is a limiting factor, and an increase in food demand would increase competition, eventually leading to a decrease in the heterotroph population. This mechanism might account for the low CFAR and BFAR values (between 90.5 and 90.1 mbsf; Fig. 4) leading to a decrease in the rate of carbon burial at the seafloor, but the role of this possible positive feedback mechanism needs to be further explored.

The slight decrease in $CaCO_3$ content recorded at Site 702 across the LLTM (Westerhold et al., 2018) coincides with a slight increase in corrosion-resistant species (e.g. *O. umbonatus*, *Lenticulina* spp.) and some infaunal taxa (e.g. *Nonion* spp.), suggesting a subtle increase in bottom waters $CaCO_3$ corrosivity, but there are is no evidence for strong $CaCO_3$ dissolution at the seafloor, as inferred from the dominance of calcareous taxa and the good preservation of their tests.

5.1.2 The MECO

The response of benthic foraminifera to the environmental effects across the MECO has been documented from several settings, ocean basins and latitudes yielding different results. Chapter 4.1.2 (Rivero-Cuesta et al., 2019) contributes with new benthic foraminiferal data across the MECO at ODP Site 702 in the south Atlantic.

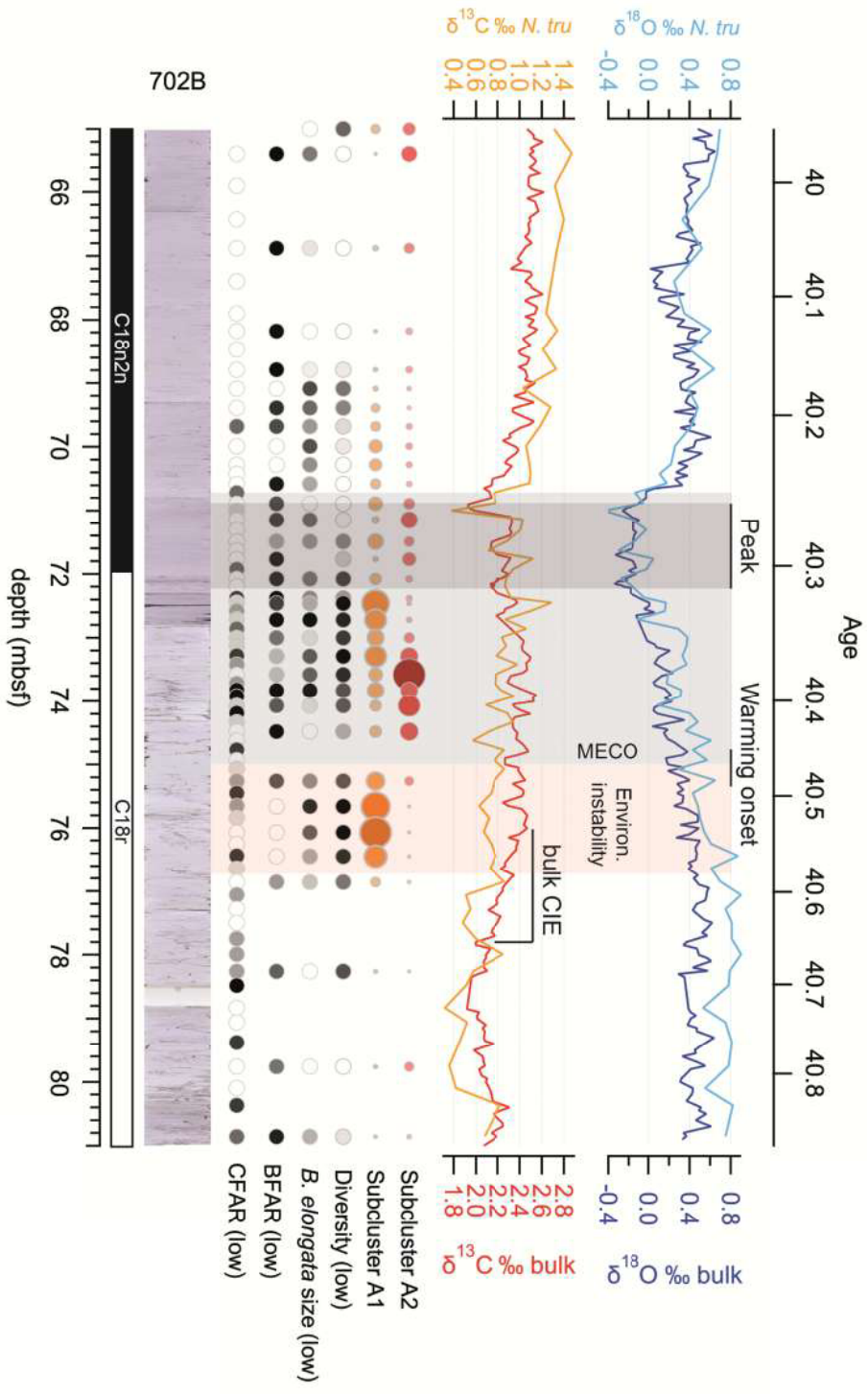

Figure 5. Summary figure from Rivero-Cuesta et al. (2019) illustrating **t**he main results of benthic foraminifera analysis across the MECO at ODP Site 702.

The benthic foraminiferal turnover, as reflected in changes in relative abundance of species but no extinctions, points to environmental changes across the MECO as well as before the start of the event. A classical hierarchical cluster of

species shows two main clusters (A and B) and four subclusters (A1, A2, B1 and B2). Subcluster A1 shows the largest changes in relative abundance, yielding significant paleoecological information. This subcluster is composed by the species *Alabamina weddellensis, Caucasina* sp. and *Epistominella exigua*, which are largely known as "phytodetritus exploiting taxa" (PET) (Boscolo-Galazzo et al., 2015 and references therein). These species have a small size and an opportunistic mode of life, profiting from seasonal blooms of phytodetritus. The relative abundance of subcluster A1 significantly increased between 76.9 and 72.1 mbsf (Fig. 5), which is described as an interval of environmental instability.

The species *Bulimina* cf. *huneri* and *Fursenkoina* sp. 2 (subcluster A2), which have been associated with strong seasonality (D'haenens et al., 2012), also increased noticeably in abundance within this environmental instability interval. Interestingly, this interval coincides with increased positive carbon isotopic values (Fig. 5), pointing to a correlation with a carbon component. This interval and the associated environmental changes described above started 150 kyr before the onset of the oxygen negative excursion that marks the beginning of the MECO warming (, i.e., the bulk CIE is recorded before "warming onset", Fig. 5). Since no significant changes in oxygenation nor in export productivity have been inferred across the study interval (e.g., steady infaunal/epifaunal ratio), the assemblage turnover is interpreted as result of changes in the type (rather than in the amount) of organic matter reaching the seafloor. The isotopic data suggest that this paleoecological disturbance in the deep sea predates MECO OIE, hence the benthic turnover is apparently unrelated to the warming associated with this event.

Coincident with the start of the environmental instability interval, the absolute abundance of *B. elongata*, the main component of subcluster B2, decreased. This species is a major component of the assemblages, and it shows lower abundance and accumulation rates from the middle to the upper part of the study interval. The different response of subcluster B2 to the changing environmental conditions is also suggested by a decrease in maximum test size of this species in the middle part of the study interval. This is further supported by DCA analysis, which differentiates between subclusters A1 - A2 (to the right of axis

1) and subcluster B2 (to the left of axis A2). The response of *B. elongata* is further discussed in section 5.1.3.

The paleoceanographic proxies BFAR and CFAR provide further information at Site 702. Lower BFAR and CFAR values are recorded coinciding with the warming interval of the MECO (Fig. 5), suggesting a relation between temperature and accumulation rates. This has been also inferred from the benthic foraminiferal turnover at other localities across the MECO (e.g. Boscolo-Galazzo et al., 2015) and other Eocene hyperthermal events (e.g. Arreguín-Rodríguez et al., 2016). The metabolic hypothesis, as explained in the previous section, might have increased respiration rates throughout the water column in both planktic (CFAR) and benthic (BFAR) foraminifera, decreasing nutrient availability and eventually reproduction rates. This suggests that, despite that fact that MECO warming did not strongly affect benthic assemblages, it did have an impact on benthic (and planktic) foraminifera abundance and accumulation rates.

The benthic assemblages studied across the MECO at other locations (Fig. 6) yield different paleoecological interpretations, suggesting that the faunal response was strongly site-related. A summary of the main results is shown in Table 2.

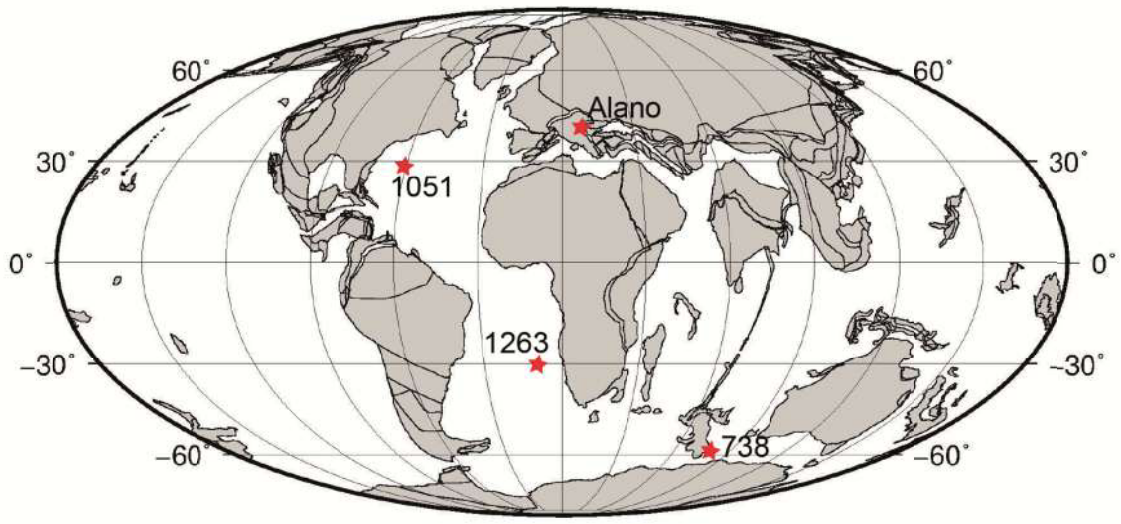

Figure 6. Location of drilling sites and sections where benthic foraminifera have been analysed across the MECO. Plate Tectonic Reconstruction map (40 Ma) from ODSN.

	ODP Site 1263 (*Boscolo-Galazzo et al., 2015*)	**Alano section** (*Boscolo-Galazzo et al., 2013*)	**ODP Site 1051** (*Moebius et al., 2015*)	**ODP Site 738** (*Moebius et al., 2014*)
Basin	SE Atlantic	Central-W Tethys	NW Atlantic	Southern Ocean (Indian sector)
Paleodepth	2000 m	600 – 1000 m	1000 – 2000 m	1700 m
Setting	Open ocean (pelagic)	Hemipelagic, marginal marine	Open ocean (pelagic)	Open ocean (pelagic)
Benthic assemblages	Restructured but no extinctions	Restructured but no extinctions	Unchanged composition	Restructured but no extinctions
Fraction studied	63 μm	63 μm	125 μm	125 μm
MECO warming	PET taxa increase (seasonal/pulsed flux of organic matter)	Refractory organic matter (*B. crenulata* increase)	No notable changes recorded	Change from epifaunal to infaunal-dominated assemblages
MECO peak conditions	Increase in infaunal taxa Lowest BFAR and CFAR Decline in organic matter flux	Decrease in infaunal taxa Increase in agglutinated taxa Minimum foraminiferal N/g	BFAR and PFAR increase by an order of magnitude	Brief drop infaunal taxa
Post-MECO	Rebound of PET Recovery of BFAR and CFAR to pre-MECO levels	Opportunistic bi-triserial taxa Decrease in diversity Organic-rich layers ORG1 and ORG2	High productivity intervals HPI 1 and HPI 2	Return to epifaunal-dominated assemblage
Oxygen	No signs of oxygen deficiency	Depletion during ORG1 and 2 Geochemical proxies (Mn/Al)	No signs of oxygen deficiency	Brief depletion during peak conditions (Ce/Ce fish teeth)
Productivity	Oligotrophic conditions, no evidence of changes in surface primary productivity (FFAR)	Eutrophic conditions Increased during ORG 1 and 2	Eutrophic conditions Increased during HPI 1 and 2	Eutrophic conditions Increased during warming
Dissolution (CCD)	No signs of dissolution	Local CCD shallowing during MECO peak and ORG2	No signs of dissolution	No signs of dissolution

Table 2. Summary of benthic foraminifera studies across the MECO.

ODP Site 1263 (Boscolo Galazzo et al., 2015) is located in the SE Atlantic (Walvis Ridge) (Fig. 6) and deposition took place in an open ocean setting at 2000 m paleodepth during the middle Eocene. Benthic foraminiferal assemblages do not show major faunal changes during and after the MECO, and they are mainly dominated by phytodetritus-exploiting taxa, indicative of a seasonal or pulsed flux of organic matter. However, the MECO peak is coeval with a marked decline in BFARs and CFARs. This has been related to a decrease in the transfer of organic matter to the seafloor, likely as an effect of warming which affected pelagic food webs. It has been suggested that higher temperatures increased heterotrophs metabolic rates, which would have led to a decrease in numbers of both planktic and benthic foraminifera in food-limiting (oligotrophic) settings such as at Site 1263.

Alano section (Boscolo Galazzo et al., 2013) was deposited in a marginal-marine basin of central western Tethys (Fig. 6) at 600-1000 m paleodepth. During the gradual warming of the MECO, marine export productivity increased, causing a transient restructuring of benthic fauna. The aftermath of the MECO shows even higher export productivity, which led to bottom-water oxygen depletion. Opportunistic stress-tolerant taxa (buliminids, bolivinids and uvigerinids) dominate in coincidence with the deposition of organic-rich sediments during a 0.5 Ma period of environmental instability after MECO peak conditions. However, there were no permanent changes (extinctions) in the structure and composition of the benthic foraminiferal assemblages, which recovered to pre-MECO conditions after the post-MECO instability period. Signs of dissolution (increased percentage of agglutinated taxa and minimum numbers of benthic foraminifera per gram) are registered especially during peak-MECO conditions. The inferred higher productivity has been attributed to an increased influx of nutrient-bearing fresh water into the basin, caused by a strengthened hydrological cycle during MECO warming. This mechanism continued after peak conditions, leading to the deposition of organic rich layers and eventually hypoxic conditions.

ODP Site 1051 (Moebius et al., 2015) is located in the Northwest Atlantic (Blake Nose) (Fig. 6) , and its estimated depositional setting lies between 1000 to 2000 m paleodepth. Similar to Site 1263, it corresponds to an open ocean (pelagic)

environment and its benthic foraminiferal response to the MECO event is also similar to that at Site 1263: largely unchanged faunal composition. However, BFAR and PFAR (planktic foraminiferal accumulation rates) values increase during peak MECO conditions, and two high productivity intervals have been recorded (one at peak MECO and the second one 300 kyr later). An increase in biological productivity has been interpreted during and after the MECO peak, which led to eutrophic conditions and suggests correlation with the two organic intervals at the Alano section (Boscolo Galazzo et al., 2013).

ODP Site 738 (Moebius et al., 2014) is located in the Indian sector of the Southern Ocean (Kerguelen Plateau) (Fig. 6) and was deposited at 1700 m paleodepth during the middle Eocene. A change in benthic foraminiferal dominance, from epifaunal to infaunal morphotypes, is recorded during warming and peak MECO conditions. Cerium content of fish teeth suggests lower oxygen levels during peak conditions. Changes in benthic assemblages and oxygen depletion have been related to an increase in export productivity, associated with warming and possibly increased continental runoff and arrival of additional nutrients to surface waters. This conclusion matches the interpretations from the Alano section and Site 1051.

Benthic foraminifera analyses at ODP Site 702 (Rivero-Cuesta et al., 2019) show a benthic faunal turnover but no extinctions across the MECO. This has been also reported at the studied sites described above except for ODP Site 1051, the only site from the North Atlantic region. This could suggest that the North Atlantic region was less affected by the effects of the MECO, however more records are needed to support this hypothesis. Other common characteristics of the sites analysed are the lack of dissolution and largely unchanged oxygen levels except for the Alano section (Table 2). Its marginal marine setting in a restricted basin may account for the differences recorded.

Changes recorded across SE Atlantic Site 1263 are the most similar to those at Site 702. Site 1263 records an increase in PET taxa during MECO warming, pointing to higher seasonality; and a decrease in BFAR and CFAR values during peak MECO, suggesting lower flux of organic matter due to warming (metabolic hypothesis) (Boscolo-Galazzo et al., 2015). Nannofossil analyses report warm-

water taxa extending at high latitudes at Site 702, suggesting a strong ecological connection between Site 702 and other South Atlantic sites such as Site 1263 (see section 5.3 of Rivero-Cuesta et al., 2019) rather than other sites at a similar latitudes such as Site 738 in the Indian sector of the Southern Ocean. It is noticeable that the environmental effects of the MECO are variable not only in space (different settings and basins), but also in time, with environmental instability extending long before (e.g. Site 702) or after (e.g. Alano and Site 1051) the isotopic excursion. This enhances the importance and interest of paleoenvironmental data in order to understand complex climatic events such as the MECO.

5.1.3 Comparison of climatic events

The analysis of benthic foraminifera assemblages across the LLTM and MECO events at the same location (ODP Site 702) provides a unique opportunity to compare and discuss differences and similarities between these two climatic events for the first time. Despite certain differences between these events, such as duration (30 kry of the LLTM vs. 300 kyr of the MECO) and other characteristics shown in Table 3, there are remarkable similarities in the benthic response at Site 702. Both events are recorded during the gradual cooling trend of the middle-late Eocene, in contrast to the early Eocene hyperthermals, which are recorded during a gradual warming trend superimposed on the general warm climate background of the early Eocene.

ODP Site 702	LLTM (41.52 Ma)	MECO (40.51 Ma)
OIE magnitude	0.23‰ bulk / 0.48‰ benthic	0.65‰ bulk / 1.35‰ benthic
OIE onset to peak (bulk)	7 kyr	150 kyr
Deep-sea warming	2ºC	4º - 6ºC
CIE magnitude	0.55‰ bulk / 0.77‰ benthic	0.69‰ bulk / 1.14‰ benthic
CIE duration (bulk)	30 kyr	150 kyr (not coeval with OIE)
$CaCO_3$ content decrease	15 kyr	none

Table 3. Main characteristics of the LLTM and MECO warming events at Site 702. Data from Westerhold et al. (2018) and Rivero-Cuesta et al. (2019).

The lack of extinctions across both LLTM and MECO events suggests that their duration and rate of environmental changes were within the tolerance limits of the benthic species analysed. Neither the fast warming of the LLTM (2ºC in 7 kyr; Westerhold et al., 2018) nor the long duration of the MECO (ca. 300 kyr; Rivero-Cuesta et al., 2019) passed any critical thresholds to trigger extinctions among benthic foraminifera at Southern high latitudes such as Site 702. The lack of extinctions across the MECO has been previously reported from other Atlantic and Pacific sites (Boscolo Galazzo et al., 2013, 2015; Moebius et al., 2014, 2015), similar to other late Paleocene and early Eocene hyperthermals (e.g., Alegret et al., 2016; Arreguín-Rodríguez et al., 2016; Arreguín-Rodríguez and Alegret, 2016; Deprez et al., 2017), excluding the PETM (e.g. Thomas, 1998, 2003, 2007; Alegret et al., 2009a, b, 2018; Arreguín-Rodríguez et al., 2018).

Detailed analysis of the benthic foraminiferal turnover provides new insights into these events. Benthic foraminiferal assemblages reported across the LLTM (Rivero-Cuesta et al., 2020) are very similar to those described across the MECO at Site 702 (Rivero-Cuesta et al., 2019), except for a few species that are present (*Hanzawaia ammophila, Cibicidoides dohmi* and *Fursenkoina* sp. 2) to common (*Bolivina cf. huneri*) across the MECO which have not been reported across the LLTM. *Caucasina* sp., which is included in the phytodetritus exploiting taxa (PET) cluster across the MECO (Rivero-Cuesta et al., 2019), is very scarce across the LLTM. The general characteristics of the assemblages reported at Site 702 across the LLTM and MECO events are very similar, both largely dominated by calcareous taxa (agglutinated species > 4%). This suggests that the CCD was well below the seafloor (1000-2000 m paleodepth) and no significant dissolution took place during the middle Eocene, as also observed in the analysis of calcareous nannofossil assemblages at this site across the MECO (Pea, 2011). The infaunal/epifaunal morphogroup ratio is also very similar, ca. 50%, and it points to oligo-mesotrophic conditions at the seafloor. The infaunal/epifaunal ratio did not vary noticeably across the study events, ruling out large changes in bottom water oxygenation or organic matter flux. Additionally, no evidence for low oxygenation at the seafloor (e.g. species tolerant to low-oxygen conditions or dark organic rich sediments) has been found across the LLTM or the MECO at Site 702.

The number of species is slightly lower across the LLTM (n=62) than across the MECO (n=73), but diversity (Fisher-α index) of the benthic assemblages is very similar, varying between ~10 and ~18 across both events. The alikeness of the assemblages (same species in similar relative abundance), the same size fraction analysed (63 μm) and the similar sampling resolution (slightly higher across the LLTM due to its shorter duration) allows a detailed comparison of the benthic foraminifera response to these two climatic events. Site 702 had very similar accumulation rates across the LLTM (1.340 cm/kyr) and the MECO (1.224 cm/kyr), and no significant core breaks or hiatuses are recorded across these events.

Hierarchical cluster analysis of benthic foraminifera assemblages generated 3 clusters across the LLTM and 4 subclusters across the MECO study intervals. Despite the aforementioned minor differences in species composition of the assemblages, their main components and characteristics are similar: subcluster A1 from the MECO cluster analysis is comparable to cluster 3 from the LLTM analysis, with PET taxa (especially *A. weddellensis*) dominating both clusters. To facilitate comparison, these two clusters have been represented in the same color (orange) in their respective figures in Rivero-Cuesta et al. (2019, 2020). Subcluster B1 (MECO) is analogous to cluster 2 (LLTM), where *N. truempyi*, *O. umbonatus* and other cosmopolitan species are common. These clusters are represented in blue. Finally, subcluster B2 (MECO) is equivalent to cluster 1 (LLTM), being *B. elongata* the most common species (represented in green).

The *N. truempyi* - *O. umbonatus* clusters (subcluster B1 of MECO and cluster 2 of LLTM; blue plots) show a very similar response, increasing in relative abundance across both events. Nevertheless, the accumulation rates of the most common species (*N. truempyi* and *O. umbonatus*) do not vary significantly, suggesting that their absolute abundance (and likely the rest of the species constituting these clusters) was largely unaffected by the environmental changes related to these climatic events.

The *B. elongata* clusters (subcluster B2 of MECO and cluster 1 of LLTM; green plots) show a decrease in both relative and absolute abundance across the

MECO and LLTM. These changes are coeval with higher carbon isotopic values across the MECO, and lower values across the LLTM. One might speculate that changes in the type of organic matter arriving to the seafloor during the MECO and LLTM (discussed previously in sections 5.1.1 and 5.1.2) may have led to differences in the carbon isotopic signal and to the ecological response of *B. elongata*, but further analyses are needed to link the isotopic signal and differences in the type of organic matter. Interestingly, *B. elongata* was reported to become extinct during the late Eocene (Thomas, 1989; 1990), and it did not recover to pre-event abundances after the MECO (River-Cuesta et al., 2019). This suggests that the profound climatic changes of the middle-late Eocene passed the threshold limit of this species.

The cluster with the most different behaviour across both events is the *A. weddellensis* – *E. exigua* cluster (subcluster A1 of MECO and cluster 3 of LLTM; orange plots). The relative and absolute abundance of this cluster strongly fluctuates across the LLTM studied interval, with no clear trends across the event. This has been interpreted as a changing but overall intense seasonality, and is supported by the high abundance of PET species. On the other hand, this cluster has a distinct pattern across the MECO, showing a large increase in abundance before the onset of the event, coinciding with a positive CIE. The MECO A2 subcluster (which has no analog clusters in the LLTM) shows a similar behaviour, and it is also related to enhanced seasonality (see section 5.1.2). These results point to paleoenvironmental changes predating the onset of the MECO, mostly a large increase in seasonality (phytodetritus) and associated changes in the type of organic matter arriving to the seafloor, which triggered a benthic foraminiferal turnover. The inferred changes in organic matter type across the LLTM, however, seem to be of a different nature and may not be related to seasonality. Due to the small test size of the PET, some paleoenvironmental studies have traditionally overlooked their presence, but more data regarding these taxa is needed to shed light on seasonality changes across Eocene hyperthermal events.

A decrease in surface and export productivity, as inferred from decreased CFAR and BFAR values, is recorded across both the MECO and the LLTM, coeval with negative oxygen isotopic values, especially across the LLTM where data

shows a positive correlation between CFAR and bulk oxygen isotopic values (see supplementary figure 2 in Rivero-Cuesta et al., 2020). These results point to a significant relation between temperature and accumulation rates. Interestingly, the magnitude of the CFAR and BFAR decrease is very similar across both events, despite the different magnitude of the oxygen isotopic excursion (Table 3). This suggests that accumulation rates decreased at the same rate during these warming events in spite of their different magnitude and duration. This might be related to a specific warming threshold which, once overpassed, the metabolic feedback starts to operate. However, more BFAR data is needed to test this hypothesis.

The metabolic hypothesis has been previously invoked to account for low accumulation rates across Eocene hyperthermal events (e.g. Olivarez Lyle and Lyle, 2006; O'Connor et al., 2009; Boscolo-Galazzo et al., 2014; Arreguín-Rodríguez et al., 2016). Low BFAR values have also been recorded during MECO peak conditions at Site 1263 (Boscolo Galazzo et al., 2015), suggesting less organic matter arriving to the seafloor in this oligo-mesotrophic setting. Higher temperatures increase the metabolic rates of heterotroph organisms such as planktic and benthic foraminifera, which then require a higher nutrient intake (e.g., John et al., 2013; Laws et al., 2000). If the food demand increase is not compensated (e.g., by an increase in primary productivity), it results in an overall decrease in heterotroph productivity (Boscolo-Galazzo et al., 2014). Oligotrophic settings are more likely to display this mechanism and register lower benthic and planktic foraminifera ARs across a warming period, as nutrient availability is already low and primary productivity is not able to cope with the increasing demand.

This mechanism could have played a significant role as a positive feedback in the ocean carbon budget in the short term. If export productivity decreased during MECO warming (as reported by low CFARs) and less organic matter arrived at the seafloor (as inferred from low BFARs), the organic carbon pump was likely less efficient during this warming period. As a consequence, less organic carbon was being buried at the seafloor (Diester-Haass and Faul, 2019), and this oceanic region would have been less efficient or slower taking up carbon from the atmosphere and favoring CO_2 accumulation in the ocean during the warming phases. Although this mechanism accounts for the observed faunal changes at Sites

702 and 1263 and for the decreased export productivity registered at Equatorial Atlantic ODP Site 959 (Cramwinckel et al., 2019), it does not apply to eutrophic settings (e.g., Site 1051, North Atlantic Ocean) where BFARs and CFARs have been reported to increase during MECO peak conditions (Moebius et al., 2015). Further AR estimates, accompanied by revised sedimentation rates (calculated with robust age models), are needed to accurately assess foraminiferal ARs and their role in the ocean organic carbon budget during MECO warming and other Eocene hyperthermal events.

5.2 Stratigraphic boundaries

5.2.1 Benthic turnover across the Eocene Oligocene transition

Benthic foraminifera analysis at the Menzel bou Zelfa and Jhaff composite section reflects paleoecological changes across the upper Eocene and lower Oligocene (section 4.1.3). The quantitative benthic and planktic foraminiferal data contributed to the paleoenvironmental reconstruction on this area for the first time.

Benthic foraminifera assemblages show a dominance of calcareous over agglutinated taxa, pointing to deposition well above the CCD. The relatively diverse assemblages (30 – 50 species per sample) and the abundance of bathyal taxa indicate an upper to middle bathyal paleodepth, which seems to decrease towards the upper part of the study interval. The dominance of infaunal morphogroups (around 80%) and a particularly high abundance of bolivinids, buliminids and triserial taxa points to eutrophic conditions (Gooday, 2003; Alegret et al., 2008; Fenero et al., 2012). At the Eocene/Oligocene boundary (EOB) there is an increase in the bi- and triserial taxa coupled with a decrease in diversity, suggesting a further increase in the food supply. Trophic changes across the EOB have also been recorded in the South Atlantic (Bordiga et al., 2015), where species indicative of seasonal delivery of food to the seafloor (e.g. *Epistominella* spp.) and buliminid taxa peaked at the EOB. Increased productivity across the EOB has been reported even at high latitudes (Antarctic Ocean ODP Site 689, Diester-Haass, 1995), and attributed to a stronger ocean mixing due to polar-equator temperature gradient increase. Certainly, there are records of export nutrient-rich waters at the EOB which could be related to the onset of the North Atlantic Deep Water Formation (e.g. Coxall et al., 2018), suggesting the changes in global oceanic circulation might have played a key role across the EOT.

Benthic foraminifera analysis in the western Tethys (Fuente Caldera section, Spain) has some similarities with the results at the MBZ section, such as the dominance of bolivinids in the lower Rupelian, which points to a sudden increase in the nutrient flux to the seafloor (Alegret et al., 2008). These authors identified three major biotic and paleoenvironmental events across the EOT at

Fuente Caldera, including a dramatic sea-level fall after the Oi1 that may have been tectonically controlled. Shallow-water taxa were commonly found across this section, as well as other epiphytic taxa which may have been transported by turbidites, suggesting a strong locally tectonic control. This hinders direct comparison with the record at MNZ section and emphasizes that regional features, especially in the Tethys area, need to be addressed. Indeed, regional factors seem to have influenced the carbon isotopic signal in the Neo-Tethys area (Cornacchia et al., 2018), which has been interpreted as short periods of higher productivity linked to enhanced nutrient availability.

The abundance of infaunal morphotypes, especially elongate uniseral taxa, increases after the EOB at the MBZ section. Benthic foraminifera across the EOT in the North Atlantic do not show significant taxonomic turnover of the Elongate Group (benthic foraminifera with elongate cylindrical morphologies) (Ortiz and Kaminski, 2012), hence this increase in elongate taxa could be a regional feature of the MBZ section area.

The disappearance of two species (*N. truempyi* and *Angulogerina muralis*) across the EOT at MBZ section indicates that the paleoecological changes might not have been beneficial for all benthic species, especially for oligotrophic taxa such as *N. truempyi*. Early studies across the EOT already reported the extinction of *N. truempyi, Clinapertina* spp. and *Abyssamina* spp. in the Bay of Biscay, and the proliferation of *Nuttallides umbonifera*, a species that is positively correlated with increased corrosiveness of bottom waters (Miller, 1983).

It has been suggested that the transition from the Eocene greenhouse to the Oligocene and its changes in temperature, ice-volume and sea-level were stepwise according to oxygen isotopes and Mg/Ca ratio of benthic foraminifera (Katz et al., 2008). This might account for the pattern of local disappearances of benthic foraminifera across the early Oligocene at the MBZ section. Certainly, lower bathyal benthic foraminifera faunas from Weddell Sea (Thomas, 1992) show gradual, stepped faunal changes between 34 and 31.5 Ma, with decreased diversity and increased relative abundance of epifaunal species in combination with high dominance of *Nuttallides umbonifera*. The gradual nature of the faunal changes in lower bathyal benthic foraminiferal assemblages and the absence of catastrophic

extinctions may reflect the reaction of the fauna to the E/O gradual cooling and an increase in corrosiveness of deep waters.

5.2.2 The Bartonian GSSP

The analysis of benthic foraminifera assemblages at the Alum Bay section (parastratotype of the Bartonian GSSP) has contributed to the paleoecological interpretation of this section. Early studies by Murray and Wright (1974) inferred a near shore shelf depositional setting at Alum Bay, with fine substrate and turbid water for this part of the sequence. Our new data (section 4.2.1) corroborates this interpretation and identifies different intervals of paleoenvironmental change along the study section. The small benthic foraminifera genera identified at Alum Bay (*Bolivina, Brizalina, Buccella, Buliminella, Cibicides*, *Discorbis, Nonion, Quinqueloculina* and *Rosalina*) are common in inner shelf environments (0-100 m; Murray, 2006). Dominance of calcareous and epifaunal taxa, low diversity (Fisher-α = 2.8 – 6.2), high dominance and low P/B ratio also point to a shallow setting close to the coastline. This environmental interpretation is further supported by the analysis of the larger benthic foraminifera assemblages in Cotton et al. (2020).

The dominance of a single genus (*Cibicides*), commonly associated with cold waters (Murray 2006), is the most remarkable feature of the small benthic foraminifera assemblages at Alum Bay (Fig. 7). The upper half of the studied section is not only dominated by this one genus, but it also has a strong dominance of one species (>50% of *C. pygmeus* in interval B, and *C. ungerianus* in interval C), which accounts for the low diversity and high dominance of the assemblages reported.

Interval A (14 – 20.5 m) represents a near shore, shallow and stable shelf setting. The low diversity values recorded and the occurrence of *Protelphidium* sp. suggest a partially restricted and/or slightly hyposaline setting, as this genus is associated with low salinity environments (Murray and Wright, 1974; Murray, 2006). Dinoflagellate assemblages also point towards a restricted, inner neritic environment (see details in section 4.2.1). The maximum values of diversity, P/B ratio and foraminifera per gram in sample AB16 (19.5 m) may reflect a condensed

horizon, possibly caused by reduced sedimentation rates and/or changes in sea level.

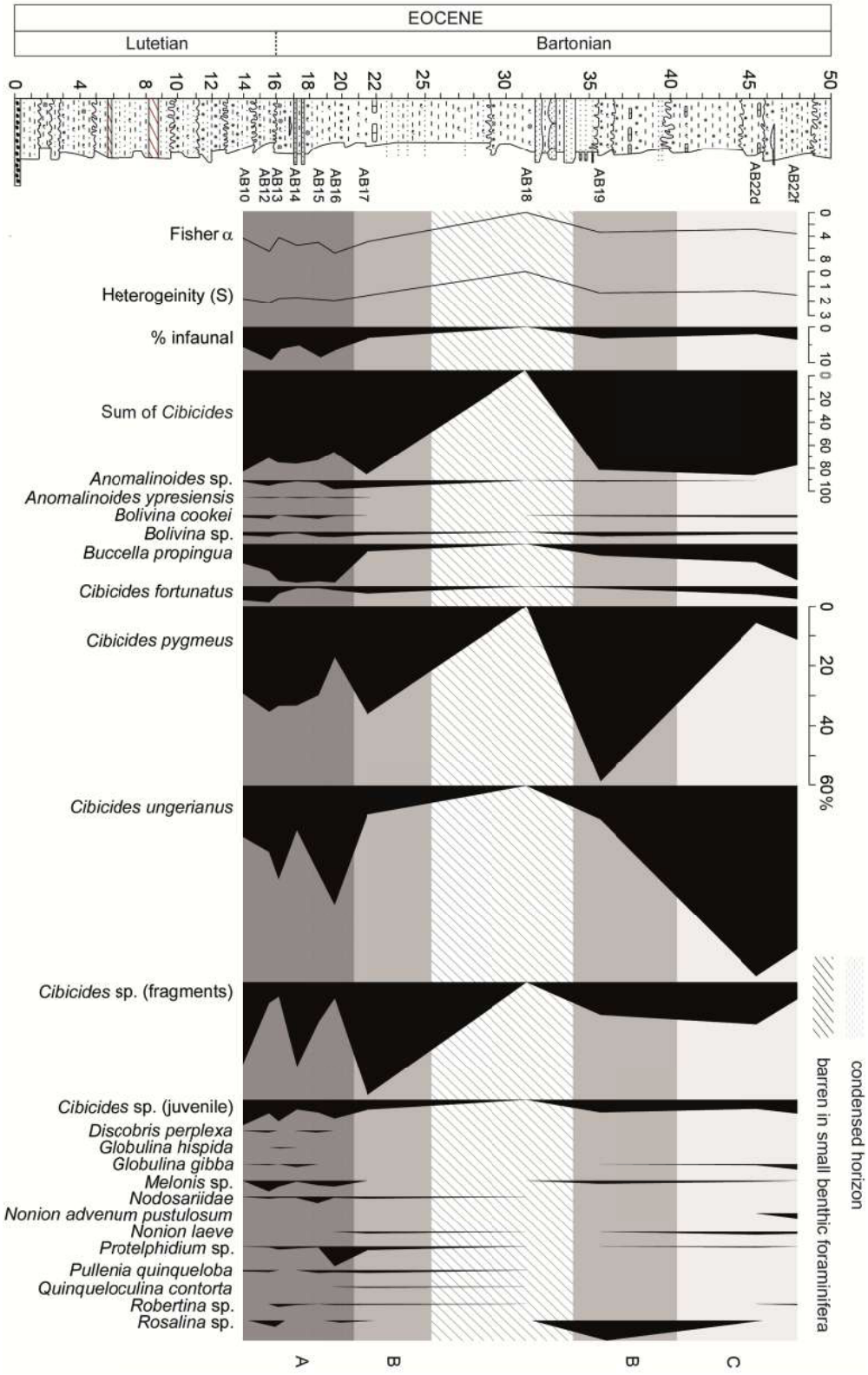

Figure 7. Summary figure from Cotton et al. (2020) showing the main results of smaller benthic foraminifera analysis across the base of the Bartonian at Alum Bay.

Interval B (20.5 – 40.5 m) is dominated by the species *C. pygmeus*, and it contains one sample barren of foraminifera. Murray and Wright (1974) interpreted barren samples from this part of the log as reflecting intertidal conditions, which might point to variations in sea level and unstable conditions. We argue that *C. pygmeus* may have adapted to environmental instability related to rapidly changing sea level, becoming more abundant in this interval. *Rosalina* spp. has been argued to have a clinging mode of life (attached with organic 'glue' to the seaweeds or hard substrates), indicative of a high-energy environment (Kitazato, 1988), pointing to an energetic, near-shore setting with episodes of intertidal settings.

Interval C (40.5 – 48 m) is characterized by a strong dominance of *C. ungerianus*, and by a small increase in percentage of species present in interval A such as *Buccella propingua, Cibicides fortunatus* and *Globulina gibba*. These results point to a return to conditions similar to those inferred from the lower part (interval A) of the section. However, diversity and the percentage of infaunal morphogroups are lower, possibly due to the proliferation of opportunistic species (C*. ungerianus* and *Buccella propingua*). After the instability recorded in interval B, the assemblages seem to recover and reflect environmental conditions similar to those from interval A.

Our results agree with the interpretation and intervals defined by Murray and Wright (1974) for this part of the section, corresponding to the "Upper Bracklesham Beds" and "Lower Barton Beds". However, the interpretation given by Dawber et al. (2011) for the same section slightly differs from our results. They infer a shallowing-upward trend from the lower part of the section (70-120 m paleodepth, equivalent to our interval A) to 30-70 m palaeodepth towards our interval B, and 0-30 m towards our interval C . Diversity values are also slightly lower, with Fisher-α values ranging from 0 to 5 and H (S) values from 0 to 1.5. The trends described by Dawber et al. (2011) do not fit our observations. We do not know the source of these discrepancies, and we cannot evaluate the results in that publication as it does not provide information regarding the methodology followed in the study of benthic foraminifera (e.g., number of specimens counted per sample, permanent record of the picked specimens, taxonomic criteria used in the

identification of taxa, etc.), and a table with the benthic foraminiferal counts is missing.

The integrated analysis of further sections across the Bartonian base within the Hampshire basin will shed more light on the paleoecological reconstruction in this area, however reliable correlation between sections is necessary in order to have a clear picture of the evolution of the basin across the middle Eocene and to clearly define the Bartonian base in this area.

Early studies on calcareous nannofossils at Alum Bay showed relatively impoverished assemblages with NP zone, being largely recognized by secondary markers. The occurrence of *Reticulofenestra umbilicus*, primary marker of CP14a within the CP zonation (Okada and Bukry, 1980), was recognized by Aubry (1983, 1986) suggesting further correlation potential for calcareous nannoplankton in the section. Our study places the Alum Bay section within nannoplankton Zones CNE14 and CNE15 and middle upper part of NP16, but also using secondary markers. Only a single long-ranged planktic foraminifera species (*Dipsidripella danvillensis*) has been found at Alum Bay, hence planktic foraminifera biozones cannot be identified.

Dinoflagellate cyst studies have reported a taxonomic turnover close to the base Bartonian stratotype (Bujak et al., 1980) with the species *Rhombodinium draco* occurring a few centimetres above the level of the *N. prestwichianus* bed at Alum Bay and other several localities in the Hampshire basin; however this is not consistent outside this region. Our study, performed at higher resolution, reports the base of *R. draco* coinciding with the acme of *N. prestwichianus*. Other biostratigraphic markers such as the renowned *N. prestwichianus* bed do not allow long-distance correlation, hence they are not useful outside the Hampshire basin.

Our multidisciplinary study (Cotton et al., 2020) concludes that the parastratotype Alum Bay section is not viable as the Bartonian GSSP. The C19n/C18r magnetochron boundary, the most reliable geological marker of the base of the Bartonian (Gradstein et al., 2012), has not been clearly identified at Alum Bay (Dawber et al., 2011; Cotton et al., 2020) and there are scarce primary biostratigraphic markers which can be correlated worldwide.

CONCLUSIONS

Benthic foraminiferal assemblages were analysed across two middle to late Eocene climatic events (LLTM and MECO) and two stratigraphic boundaries (Lutetian/Bartonian and Eocene/Oligocene) at three land sections from the Tethys and NE Atlantic Ocean (Torre Cardela section in Spain, Alum Bay in England and Menzel Bou Zelfa in Tunisia) and an ocean drilling site (ODP Site 702, South Atlantic Ocean). The data has been analysed and interpreted as the ecological response of the benthic fauna to these events in a variety of settings.

The climatic and stratigraphic events analysed did not cause large extinctions among benthic foraminifera. Instead, transient changes in benthic assemblages point to temporary shifts in the environmental conditions. The common driver of these faunal turnovers in our study cases seems to be closely related to changes in the flux of organic matter to the seafloor, especially in the deeper settings. Salinity, current activity and eustatic changes also influenced benthic foraminifera distribution across the Lutetian/Bartonian boundary at Alum Bay and the Eocene/Oligocene transition at Menzel Bou Zelfa.

Benthic foraminifera reflect paleoenvironmental instability across the LLTM and MECO global warming events that lasted longer than the isotopic excursion that defines both events. These paleoenvironmental perturbations are likely related to changes in the type of organic matter arriving to the seafloor, which affected abundance and distribution of the benthic foraminiferal species. The dominance of calcareous taxa and the balanced infaunal/epifaunal ratio across both events rules out major changes in the trophic conditions and in the $CaCO_3$ saturation of bottom waters at ODP Site 702, suggesting that no significant dissolution took place across these events at this site.

The decrease in abundance of *Bulimina elongata* across both the LLTM and MECO events at ODP Site 702 points to a higher sensitivity of this species to the middle and late Eocene climatic changes, but the correlation between its abundance and the carbon isotope record is not clear, and further analyses are needed to understand its paleoecology in detail.

Phytodetritus exploiting taxa (PET) reveal as a key group with paleoenvironmental significance across the MECO at ODP Site 702. Their abundance increased coupled with a positive carbon isotope excursion that predates the onset of the MECO by 150 kyr. This correlation suggests that the carbon flux –rather than temperature- played a key role in the distribution and abundance of benthic foraminifera at Site 702 across this event.

The amount and type of food reaching the seafloor, possibly influenced by current activity, are here suggested as the main factor controlling benthic assemblages at the Torre Cardela section, which comprises the base of the Bartonian stage and the MECO. The increase in abundance of the species *Bolivinoides crenulata* points to a higher input of low-quality, refractory organic matter that is correlated with an increase in allochthonous taxa.

At ODP Site 702, benthic foraminifera and coarse fraction accumulation rates (BFARs and CFARs) decreased during the warming events studied, showing a positive correlation with the oxygen isotopic records. Increased metabolic rates of heterotroph organisms may account for the decreased CFAR and BFAR values across two warming events of different magnitude and duration, the LLTM (OIE ~ 0.5 ‰) and the MECO (OIE ~ 1 ‰). Interestingly, the decrease rate in CFARs and BFARs is very similar across both events despite the different characteristics of their OIEs. This suggests that metabolic rates accelerated during warm events in spite of their different magnitude and duration.

Regarding the stratigraphic boundaries, analysis of benthic foraminifera across the Eocene-Oligocene transition at Menzel Bou Zelfa section has been performed for the first time, allowing the paleoenvironmental reconstruction of this area and contributing with new foraminiferal data across this boundary. The benthic assemblages studied are characteristic of a relatively warm climate during the middle to late Eocene, whereas eustatic changes and cooling have been inferred at the base of the Oligocene. These interpretations are in line with the global framework of the Eocene-Oligocene transition. The gradual pattern of disappearances of benthic foraminifera in the basal Oligocene is coeval with the decrease in temperature and sea level fall related to the Oi1 glaciation.

The reassessment of the Lutetian/Bartonian boundary in the classic Alum Bay section has been carried out through a multidisciplinary analysis that combines nannofossil, smaller and larger benthic foraminifera, planktic foraminifera, dinoflagellates and paleomagnetic data. This thesis has contributed with the analysis of smaller benthic foraminifera and its paleoecological interpretations, which has been integrated with paleoecological data from larger benthic foraminifera and dinoflagellates. This work has contributed to the analysis of the base of the Bartonian at the parastratotype section, providing further information for correlation within the Hampshire basin, and contributing to the search of a potential GSSP for the base of the Bartonian.

CONCLUSIONES

Se han analizado las asociaciones de foraminíferos bentónicos a través de dos eventos climáticos del Eoceno medio y superior (el LLTM y el MECO) y dos límites estratigráficos (Luteciense/Bartoniense y Eoceno/Oligoceno) que se localizan en tres secciones del Océano Tetis y Atlántico NE (afloramiento de Torre Cardela en España, Alum Bay en Inglaterra y Menzel Bou Zelfa en Túnez) y un sondeo oceánico (ODP 702, Atlántico Sur). Estos datos han sido analizados e interpretados como la respuesta ecológica de la fauna bentónica a estos eventos en diferentes ambientes.

Los eventos climáticos y estratigráficos analizados no causaron extinciones significativas entre en los foraminíferos bentónicos. Sin embargo, se observan cambios transitorios en las asociaciones que indican variaciones temporales de las condiciones ambientales. La causa de estos cambios faunísticos parece estar estrechamente relacionada con cambios en el flujo de materia orgánica hacia los fondos oceánicos, especialmente en los ambientes más profundos. Cambios en la salinidad, en la actividad de las corrientes y en el nivel del mar también influyeron en la distribución de los foraminíferos bentónicos a través del límite Luteciense/Bartoniense en el afloramiento de Alum Bay y del límite Eoceno/Oligoceno en Menzel Bou Zelfa.

Los foraminíferos bentónicos revelan que la inestabilidad paleoambiental durante los eventos globales del LLTM y el MECO duró más que la excusión isotópica que define ambos eventos. Las perturbaciones paleoambientales están probablemente relacionadas con cambios en el tipo de materia orgánica que llegaba a los fondos oceánicos, lo cual afectó a la abundancia y distribución de las especies de foraminíferos bentónicos. La dominancia de taxones calcáreos y la equilibrada proporción de formas infaunales y epifaunales a través de ambos eventos descarta grandes cambios en las condiciones tróficas así como en la saturación de $CaCO_3$ en las aguas de fondo del sondeo ODP 702, sugiriendo que no hubo disolución importante durante estos eventos.

La disminución en la abundancia de *Bulimina elongata* durante el LLTM y el MECO en el sondeo ODP 702 indica una mayor susceptibilidad de esta especie a los cambios climáticos del Eoceno medio y superior, aunque no se ha encontrado una correlación directa con los valores isotópicos del carbono. Se precisan análisis adicionales para ahondar en el conocimiento de su paleoecología.

Los taxones con preferencia por el fitodetritus (PET por sus siglas en inglés) son un grupo relevante por su significado paleoambiental durante el MECO en el sondeo ODP 702. Esto taxones aumentaron en coincidencia con la excursión positiva de los isótopos del carbono unos 150 kyr antes del inicio del MECO. Esta correlación sugiere que el flujo de carbono –en vez de la temperatura- jugó un papel clave en la distribución y abundancia de los foraminíferos bentónicos durante este evento.

La cantidad y el tipo de alimento que llegaba a los fondos oceánicos, posiblemente influenciados por la actividad de corrientes, se sugieren como el factor principal que controló las asociaciones bentónicas en la sección de Torre Cardela, que abarca la base del Bartoniense y el MECO. El aumento en abundancia de la especie *Bolivinoides crenulata* indica un mayor aporte de materia orgánica refractaria, de baja calidad, que se correlaciona además con un incremento en taxones alóctonos.

En el sondeo ODP 702, las tasas de acumulación de los foraminíferos bentónicos y de la fracción gruesa (BFARs y CFARs, por sus siglas en inglés) disminuyeron durante los eventos de calentamiento, mostrando una correlación positiva con los isótopos de oxígeno. El incremento en las tasas metabólicas de organismos heterótrofos puede explicar el descenso de las tasas de acumulación durante dos eventos de calentamiento de diferente magnitud y duración, el LLTM (OIE ~ 0.5 ‰) y el MECO (OIE ~ 1 ‰).

Respecto a los límites estratigráficos, los foraminíferos bentónicos del tránsito Eoceno-Oligoceno se han estudiado por primera vez en la sección de Menzel Bou Zelfa, dando lugar a la reconstrucción paleoambiental de esta zona y contribuyendo con nuevos datos al estudio de este interesante límite estratigráfico. Las asociaciones de foraminíferos bentónicos estudiadas son características de un

clima relativamente cálido durante el Eoceno medio y superior, mientras que se han detectado cambios eustáticos y enfriamiento en la base del Oligoceno. Estas interpretaciones concuerdan con el marco global del tránsito Eoceno-Oligoceno. El patrón gradual de desapariciones de foraminíferos bentónicos en el Oligoceno basal es sincrónico con la disminución de temperatura y el descenso del nivel del mar relacionados con la glaciación Oi1.

La reevaluación del límite Luteciense/Bartoniense en el afloramiento clásico de Alum Bay se ha llevado a cabo mediante un análisis multidisciplinario que combina nanofósiles, macro- y microforaminíferos bentónicos, foraminíferos planctónicos, dinoflagelados y datos de paleomagnetismo. Esta tesis ha contribuido con el análisis de los microforaminíferos bentónicos, y con interpretaciones paleoecológicas en las que encajan los datos paleoecológicos de macroforaminíferos y dinoflagelados. Este trabajo ha contribuido al análisis de la base del Bartoniense en la sección paraestratotípica, proporcionando información adicional para su correlación en la cuenca de Hampshire y en la búsqueda de un potencial GSSP para la base del Bartoniense.

References

Adl, S.M., Simpson, A.G.B., Farmer, M.A., Andersen, R.A., Anderson, O.R., Barta, J.R., Bowser, S.S., Brugerolle, G., Fensome, R.A., Fredericq, S., James, T.Y., Karpov, S., Kugrens, P., Krug, J., Lane, C.E., Lewis, L.A., Lodge, J., Lynn, D.H., Mann, D.G., Mccourt, R.M., Mendoza, L., Moestrup, O., Mozley-Standridge, S.E., Nerad, T.A., Shearer, C.A., Smirnov, A.V., Spiegel, F.W., and Taylor, M.F.J.R., 2005. The new higher cevel classification of Eukaryotes with emphasis on the taxonomy of Protists. Journal of Eukaryotic Microbiology 52, 399–451.

Agnini, C., Macrì, P., Backman, J., Brinkhuis, H., Fornaciari, E., Giusberti, L., Luciani, V., Rio, D., Sluijs, A., and Speranza, F., 2009. An early Eocene carbon cycle perturbation at ~52.5 Ma in the Southern Alps: chronology and biotic response. Paleoceanography 24, PA2209.

Alegret, L., and Thomas, E., 2001. Upper Cretaceous and lower Paleogene benthic foraminifera from northeastern Mexico. Micropaleontology 47, 269–316.

Alegret, L., and Thomas, E., 2005. Cretaceous/Paleogene boundary bathyal paleo-environments in the central North Pacific (DSDP Site 465), the Northwestern Atlantic (ODP Site 1049), the Gulf of Mexico and the Tethys: The benthic foraminiferal record. Palaeogeography, Palaeoclimatology, Palaeoecology 224, 53–82.

Alegret, L., and Thomas, E., 2009. Food supply to the seafloor in the Pacific Ocean after the Cretaceous/Paleogene boundary event. Marine Micropaleontology 73, 105–116.

Alegret, L., Cruz, L.E., Fenero, R., Molina, E., Ortiz, S., and Thomas, E., 2008. Effects of the Oligocene climatic events on the foraminiferal record from Fuente Caldera section (Spain, western Tethys). Palaeogeography, Palaeoclimatology, Palaeoecology 269, 94–102.

Alegret, L., Ortiz, S., and Molina, E., 2009a. Extinction and recovery of benthic foraminifera across the Paleocene–Eocene Thermal Maximum at the Alamedilla section (Southern Spain). Palaeogeography, Palaeoclimatology, Palaeoecology 279, 186–200.

Alegret, L., Ortiz, S., Orue-Etxebarria, X., Bernaola, G., Baceta, J.I., Monechi, S., Apellaniz, E., and Pujalte, V., 2009b. The Paleocene-Eocene Thermal Maximum: new data on microfossil turnover at the Zumaia Section, Spain. PALAIOS 24, 318–328.

Alegret, L., Ortiz, S., Arreguín-Rodríguez, G.J., Monechi, S., Millán, I., and Molina, E., 2016. Microfossil turnover across the uppermost Danian at Caravaca, Spain: Paleoenvironmental inferences and identification of the latest Danian event. Palaeogeography, Palaeoclimatology, Palaeoecology 463, 45–59.

Alegret, L., Reolid, M., and Vega Pérez, M., 2018. Environmental instability during the latest Paleocene at Zumaia (Basque-Cantabric Basin): The bellwether of the Paleocene-Eocene Thermal Maximum. Palaeogeography, Palaeoclimatology, Palaeoecology 497, 186–200.

Alegret, L., Arreguín-Rodríguez, G.J., Trasviña-Moreno, C.A., and Thomas, E. (2020). Turnover and stability in the deep sea: Benthic foraminifera as tracers of Paleogene global change. Global and Planetary Change 196, 103372.

Altenbach, A.V., 1992. Short term processes and patterns in the foraminiferal response to organic flux rates. Marine Micropaleontology 19, 119–29.

Altenbach, A.V., and Struck, U., 2001. On the coherence of organic carbon flux and benthic foraminiferal biomass. Journal of Foraminiferal Research 31, 79–85.

Alve, E., 1995. Benthic foraminiferal responses to estuarine pollution; a review. The Journal of Foraminiferal Research 25, 190–203.

Alve, E., 2003. A common opportunistic foraminiferal species as an indicator of rapidly changing conditions in a range of environments. Estuarine, Coastal and Shelf Science 57, 501–514.

Alve, E., and Murray, J.W., 1994. Ecology and taphonomy of benthic foraminifera in a temperate mesotidal inlet. The Journal of Foraminiferal Research 24, 18–27.

Alve, E. and Murray, J.W., 1997. High benthic fertility and taphonomy of foraminifera: a case study of the Skagerrak, North Sea. Marine Micropaleontology 31, 157–75.

Anderson, L.D., and Delaney, M.L., 2005. Middle Eocene to early Oligocene paleoceanography from Agulhas Ridge, Southern Ocean (Ocean Drilling Program Leg 177, Site 1090). Paleoceanography 20, PA1013.

Arreguín-Rodríguez, G.J., and Alegret, L., 2016. Deep-sea benthic foraminiferal turnover across early Eocene hyperthermal events at Northeast Atlantic DSDP Site 550. Palaeogeography, Palaeoclimatology, Palaeoecology 451, 62–72.

Arreguín-Rodríguez, G. J., Alegret, L., Sepúlveda, J., Newman, S., and Summons, R. E. 2014. Enhanced terrestrial input supporting the *Glomospira* acme across the Paleocene-Eocene boundary in Southern Spain. Micropaleontology 60(1), 43-51.

Arreguín-Rodríguez, G.J., Alegret, L., and Thomas, E., 2016. Late Paleocene-middle Eocene benthic foraminifera on a Pacific seamount (Allison Guyot, ODP Site 865): Greenhouse climate and superimposed hyperthermal events: Benthic Foraminifera on Pacific Seamount. Paleoceanography 31, 346–364.

Arreguín-Rodríguez, G.J., Thomas, E., D'haenens, S., Speijer, R.P., and Alegret, L., 2018. Early Eocene deep-sea benthic foraminiferal faunas: Recovery from the Paleocene Eocene Thermal Maximum extinction in a greenhouse world. PLOS ONE 13, e0193167.

Aubry, M-P., 1983. Biostratigraphie du Paléogène épicontinental de l'Europe du nord-ouest. Étude fondée sur les nannofossiles calcaries. Documents del Laboratories de Géologie de la Faculté des Sciences de Lyon 89, 317 pp.

Aubry, M-P., 1986. Paleogene calcareous nannoplankton biostratigraphy of northwestern Europe. Palaeogeography, Palaeoclimatology, Palaeoecology 55, 267-334.

Aubry, M.-P., 1992. Late Paleogene calcareous nannoplankton evolution: a tale of climatic deterioration. In: Prothero, D.R., and Berggren, W.A. (Eds.), Eocene-Oligocene Climatic and Biotic Evolution. Princeton Legacy Library, 272–309.

Aubry, M.-P., Berggren, W., Van Couvering, J.A., Ali, J., Brinkhuis, H., Cramer, B., Kent, D.V., Swicher, C.C., Dupuis, C., Gingerich, P.D., Heilmann-Clausen, C., King, C., Ward, D.J., Knox, R.W.O., Ouda, K., Stott, L.D., and Thiry, M., 2003. Chronostratigraphic terminology at the Paleocene/Eocene boundary. In: Wing, S.L., et al. (Eds), Causes and Consequences of Globally Warm Climates in the Early Paleogene. Geological Society of America, Special Paper 369, 551-566.

Barnet, J.S.K., Littler, K., Westerhold, T., Kroon, D., Leng, M.J., Bailey, I., Röhl, U., and Zachos, J.C., 2019. A High-Fidelity Benthic Stable Isotope Record of Late Cretaceous–Early Eocene Climate Change and Carbon-Cycling. Paleoceanography and Paleoclimatology 34, 672-691.

Bemis, B.E., Spero, H., Bijma, J. and Lea, D.W., 1988. Reevaluation of the oxygen isotopic composition of planktonic foraminifera: experimental results and revised paleotemperature equations. Paleoceanography 13, 150–60.

Berggren, W.A., and Pearson, P.N., 2005. A revised tropical to subtropical Paleogene planktonic foraminiferal zonation. The Journal of Foraminiferal Research 35, 279–298.

Bernaola, G., Baceta, J.I., Orue-Etxebarria, X., Alegret, L., Martin-Rubio, M., Arostegui, J., and Dinares-Turell, J., 2007. Evidence of an abrupt environmental disruption during the mid-Paleocene biotic event (Zumaia section, western Pyrenees). Geological Society of America Bulletin 119, 785–795.

Bignot, G., 1998. Middle Eocene benthic foraminifers from holes 960A and 960C, central Atlantic Ocean. In: Mascle, J., Lohmann, G.P., Moullade, M. (Eds.), Proceedings of the Ocean Drilling Program, Scientific Results. Texas A&M University, 433–444.

Bijl, P.K., Houben, A.J.P., Schouten, S., Bohaty, S.M., Sluijs, A., Reichart, G.-J., Damsté, J.S.S., and Brinkhuis, H., 2010. Transient Middle Eocene Atmospheric CO_2 and Temperature Variations. Science 330, 819–821.

Bock, W.D., and Moore, D.R., 1968. A commensal relationship between a foraminifer and a bivalve mollusk. Gulf Research Reports 2 (3), 273-279.

Boersma, A., 1998. Foraminifera. In: Haq, B.O., and Boersma, A. (Eds.), Introduction to marine micropaleontology. Elsevier, 19-77.

Bohaty, S.M., and Zachos, J.C., 2003. Significant Southern Ocean warming event in the late middle Eocene. Geology 31, 1017–1020.

Bohaty, S.M., Zachos, J.C., Florindo, F., and Delaney, M.L., 2009. Coupled greenhouse warming and deep-sea acidification in the middle Eocene. Paleoceanography 24, PA2207.

Bolli, H.M., Beckmann, J.-P., and Saunders, J.B., 1994. Benthic foraminiferal biostratigraphy of the south Caribbean region. Cambridge University Press, 804 pp.

Boltovskoy, E., 1991. On the destruction of foraminiferal tests (laboratory experiments). Revue de micropaleontologie, 34, 19–25.

Boltovskoy, E. and Lena, H., 1969. Los epibiontes de 'Macrocystis' flotante como indicadores hidrológicos. Neotropicana, 15, 135–137.

Boltovskoy, E. and Wright, R., 1976. Recent foraminifera. Springer Netherlands, 515 pp.

Bordiga, M., Henderiks, J., Tori, F., Monechi, S., Fenero, R., Legarda-Lisarri, A., and Thomas, E., 2015. Microfossil evidence for trophic changes during the Eocene–Oligocene transition in the South Atlantic (ODP Site 1263, Walvis Ridge). Climate of the Past 11, 1249–1270.

Boscolo-Galazzo, F., Giusberti, L., Luciani, V., and Thomas, E., 2013. Paleoenvironmental changes during the Middle Eocene Climatic Optimum (MECO) and its aftermath: The benthic foraminiferal record from the Alano section (NE Italy). Palaeogeography, Palaeoclimatology, Palaeoecology 378, 22–35.

Boscolo-Galazzo, F., Thomas, E., Pagani, M., Warren, C., Luciani, V., and Giusberti, L., 2014. The middle Eocene climatic optimum (MECO): A multiproxy record of paleoceanographic changes in the southeast Atlantic (ODP Site 1263, Walvis Ridge): MECO repercussions in the SE Atlantic. Paleoceanography 29, 1143–1161.

Boscolo-Galazzo, F., Thomas, E., and Giusberti, L., 2015. Benthic foraminiferal response to the Middle Eocene Climatic Optimum (MECO) in the South-Eastern Atlantic (ODP Site 1263). Palaeogeography, Palaeoclimatology, Palaeoecology 417, 432–444.

Boscolo-Galazzo, F., Crichton, K.A., Barker, S., and Pearson, P.N., 2018. Temperature dependency of metabolic rates in the upper ocean: A positive feedback to global climate change? Global and Planetary Change 170, 201–212.

Bowen, G.J., Bralower, T.J., Delaney, M.L., Dickens, G.R., Kelly, D.C., Koch, P.L., Kump, L.R., Meng, J., Sloan, L.C., Thomas, E., Wing, S.L., and Zachos, J.C., 2006. Eocene hyperthermal event offers insight into greenhouse warming. Eos, Transactions American Geophysical Union 87, 165-169.

Bujak, J. P., Downie, C., Eaton, G. L., and Williams, G. L., 1980. Dinoflagellate cysts and acritarchs from the Eocene of southern England. Special Papers in Palaeontology 24, 1-100.

Burgess, C.E., Pearson, P.N., Lear, C.H., Morgans, H.E.G., Handley, L., Pancost, R.D., and Schouten, S., 2008. Middle Eocene climate cyclicity in the southern Pacific: Implications for global ice volume. Geology 36, 651-654.

Buzas, M.A., Culver, S.J., and Jorissen, F.J., 1993. A statistical evaluation of the microhabitats of living (stained) infaunal benthic foraminifera. Marine Micropaleontology 20, 311–320.

Ciesielski, P.F., and Kristoffersen, Y., 1991. Proceedings of the Ocean Drilling Program, Initial Reports, vol. 114. Texas A&M University, 797 pp.

Ciesielski, P.F., and Kristoffersen, Y., 1988. Proceedings of the Ocean Drilling Program, Scientific Results, vol. 114. Texas A&M University, 813 pp.

Coccioni, R., Frontalini, F., Bancalà, G., Fornaciari, E., Jovane, L., and Sprovieri, M., 2010. The Dan-C2 hyperthermal event at Gubbio (Italy): Global implications, environmental effects, and cause(s). Earth and Planetary Science Letters 297, 298–305.

Corliss, B.H., 1985. Microhabitats of benthic foraminifera within deep-sea sediments. Nature 314, 435–438.

Corliss, B.H., 1991. Morphology and microhabitat preferences of benthic foraminifera from the northwest Atlantic Ocean. Marine micropaleontology 17, 195–236.

Corliss, B.H., and Chen, C., 1988. Morphotype patterns of Norwegian Sea deep-sea benthic foraminifera and ecological implications. Geology 16, 716–719.

Corliss, B.H. and Emerson, S. 1990. Distribution of rose Bengal stained deep-sea benthic foraminifera from the Nova Scotian continental margin and Gulf of Maine. Deep-Sea Research, 37, 381–400.

Corliss, B.H., and Honjo, S., 1981. Dissolution of Deep-Sea Benthonic Foraminifera. Micropaleontology 27(4), 356-378.

Cornacchia, I., Brandano, M., Raffi, I., Tomassetti, L., and Flores, I., 2018. The Eocene–Oligocene transition in the C-isotope record of the carbonate successions in the Central Mediterranean. Global and Planetary Change 167, 110–122.

Cotton, L., Rivero-Cuesta, L., Franceschetti, G., Iakovleva, A., Alegret, L., Dinarès-Turell, J., Hooker, J., King, C., Fluegeman, R., Yager, S., Monechi, S., 2020. Reassessing the Bartonian unit stratotype at Alum Bay (Isle of Wight, UK): an integrated approach. Newsletters on Stratigraphy 54(1), 17-42.

Coxall, H.K., and Pearson, P.N., 2007. The Eocene – Oligocene Transition, in: Williams, M., Haywood, A.M., Gregory, F.J., Schmidt, D.N. (Eds.), Deep-Time Perspectives on Climate Change: Marrying the Signal from Computer Models and Biological Proxies, Special Publications. The Geological Society, London, pp. 351–387.

Coxall, H.K., Wilson, P.A., Pälike, H., Lear, C.H., and Backman, J., 2005. Rapid stepwise onset of Antarctic glaciation and deeper calcite compensation in the Pacific Ocean. Nature 433, 53–57.

Coxall, H.K., Huck, C.E., Huber, M., Lear, C.H., Legarda-Lisarri, A., O'Regan, M., Sliwinska, K.K., van de Flierdt, T., de Boer, A.M., Zachos, J.C., and Backman, J., 2018. Export of nutrient rich Northern Component Water preceded early Oligocene Antarctic glaciation. Nature Geoscience 11, 190–196.

Cramer, B.S., Wright, J.D., Kent, D.V., and Aubry, M.-P., 2003. Orbital climate forcing of δ13C excursions in the late Paleocene-early Eocene (chrons C24n-C25n). Paleoceanography 18, 1097.

Cramer, B.S., Toggweiler, J.R., Wright, J.D., Katz, M.E., and Miller, K.G., 2009. Ocean overturning since the Late Cretaceous: Inferences from a new benthic foraminiferal isotope compilation. Paleoceanography 24, PA4216.

Cramwinckel, M.J., van der Ploeg, R., Bijl, P.K., Peterse, F., Bohaty, S.M., Röhl, U., Schouten, S., Middelburg, J.J., and Sluijs, A., 2019. Harmful algae and export production collapse in the equatorial Atlantic during the zenith of Middle Eocene Climatic Optimum warmth. Geology 47, 247–250.

Culver, S. J. and Buzas, M. A., 2000. Global latitudinal species diversity gradient in deep-sea benthic foraminifera. Deep-Sea Research I 47, 259–275.

Curry, D., 1981. Bartonian. In: Pomerom, C. (Ed.), Stratotypes of Paleogene stages. Bulletin d'Information des Géologues du Bassin de Paris. Mémorie hors série 2, 23-36.

Cushman, J.A., 1948. Foraminifera. Their Classification and Economic Use. Harvard University Press, 605 pp.

Dawber, C.F., Tripati, A.K., Gale, A.S., MacNiocaill, C., and Hesselbo, S.P., 2011. Glacioeustasy during the middle Eocene? Insights from the stratigraphy of the Hampshire Basin, UK. Palaeogeography, Palaeoclimatology, Palaeoecology 300, 84–100.

DeConto, R.M., Pollard, D., 2003. Rapid Cenozoic glaciation of Antarctica induced by declining atmospheric CO_2. Nature 421, 245–249.

Den Dulk, M., Reichart, G.-J., Van Heyst, S., Zachariasse, W.J., and Van der Zwaan, G.J., 2000. Benthic foraminifera as proxies of organic matter flux and bottom water oxygenation? A case history from the northern Arabian Sea. Palaeogeography, Palaeoclimatology, Palaeoecology 161, 337–359.

Denne, R.A., and Gupta, B.K.S., 1989. Effects of Taphonomy and Habitat on the Record of Benthic Foraminifera in Modern Sediments. PALAIOS 4, 414-423.

Deprez, A., Jehle, S., Bornemann, A., and Speijer, R.P., 2017. Differential response at the seafloor during Palaeocene and Eocene ocean warming events at Walvis Ridge, Atlantic Ocean (ODP Site 1262). Terra Nova 29, 71–76.

D'haenens, S., Bornemann, A., Stassen, P., and Speijer, R.P., 2012. Multiple early Eocene benthic foraminiferal assemblage and δ13C fluctuations at DSDP Site 401 (Bay of Biscay — NE Atlantic). Marine Micropaleontology 88–89, 15–35.

D'haenens, S., Bornemann, A., Claeys, P., Röhl, U., Steurbaut, E., and Speijer, R.P., 2014. A transient deep-sea circulation switch during Eocene Thermal Maximum 2. Paleoceanography 29, 370–388.

Diester-Haass, L., 1995. Middle Eocene to early Oligocene paleoceanography of the Antarctic Ocean (Maud Rise, ODP Leg 113, Site 689): change from a low to a high productivity ocean. Palaeogeography, Palaeoclimatology, Palaeoecology 113, 311–334.

Diester-Haass, L., and Faul, K., 2019. Paleoproductivity reconstructions for the Paleogene Southern Ocean: a direct comparison of geochemical and micropaleontological proxies. Paleoceanography and Paleoclimatology 34, 79–97.

Diester-Haass, L. and Zachos, J., 2003. The Eocene-Oligocene transition in the Equatorial Atlantic (ODP Site 925); paleoproductivity increase and positive d13C excursion. In: D.R. Prothero, L.C. Ivany and E.A. Nesbitt (Eds). Columbia University Press.

Diester-Haass, L., and Zahn, R., 1996. Eocene-Oligocene transition in the Southern Ocean: History of water mass circulation and biological productivity. Geology 24 (2), 163-166.

Douglas, R.G., Liestman, J., Walch, C., Blake, G. and Cotton, M.L. 1980. The transition from live to sediment assemblages in benthic foraminifera from the southern California borderland. Quaternary depositional environments of the Pacific. Society of Economic Paleontologists and Mineralogists, Pacific Section Symposium, 4, 257–280.

Dunkley Jones, T., Bown, P.R., Pearson, P.N., Wade, B.S., Coxall, H.K., and Lear, C.H., 2008. Major shifts in calcareous phytoplankton assemblages through the Eocene-Oligocene transition of Tanzania and their implications for low-latitude primary production. Paleoceanography 23, PA4204.

Dupuis, C., Aubry, M.P., Steurbaut, E., Berggren, W.A., Cramer, B.S., Kent, D.V., Speijer, R.P., and Heilmann-Clausen, C., 2003. The Dababiya Quarry Section: Lithostratigraphy, clay mineralogy, geochemistry and paleontology. Micropaleontology 49, 41–59.

Edelman-Furstenberg, Y., 2001. Deep-sea benthic foraminifera from the central Red Sea. The Journal of Foraminiferal Research 31, 48–59.

Edgar, K.M., Wilson, P.A., Sexton, P.F., and Suganuma, Y., 2007. No extreme bipolar glaciation during the main Eocene calcite compensation shift. Nature 448, 908–911.

Edgar, K.M., Wilson, P.A., Sexton, P.F., Gibbs, S.J., Roberts, A.P., and Norris, R.D., 2010. New biostratigraphic, magnetostratigraphic and isotopic insights into the Middle Eocene Climatic Optimum in low latitudes. Palaeogeography, Palaeoclimatology, Palaeoecology 297, 670–682.

Fenero, R., Thomas, E., Alegret, L., and Molina, E., 2012. Oligocene benthic foraminifera from the Fuente Caldera section (Spain, western Tethys): taxonomy and paleoenvironmental inferences. The Journal of Foraminiferal Research 42, 286–304.

Finger, K. L. and Lipps, J. H., 1981. Foraminiferal decimation and repopulation in an active volcanic caldera, Deception Island, Antarctica. Micropaleontology, 27, 111–39.

Fisher, R.A., Corbet, A.S., and Williams, C.B., 1943. The relation between the number of species and the number of individuals in a random sample of an animal population. The Journal of Animal Ecology 12, 42.

Flach, E.C., 2003. Factors controlling soft bottom macrofauna along and across European continental margins. In: Wefer, G., Billett, D., Hebbeln, D. et al., (Eds), Ocean Margin Systems. Springer-Verlag, 351–363.

Fontanier, C., Jorissen, F.J., Chaillou, G., Anschutz, P., Grémare, A., and Griveaud, C., 2005. Live foraminiferal faunas from a 2800m deep lower canyon station from the Bay of Biscay: Faunal response to focusing of refractory organic matter. Deep Sea Research Part I: Oceanographic Research Papers 52, 1189–1227.

Foster, L.C., Schmidt, D.N., Thomas, E., Arndt, S., and Ridgwell, A., 2013. Surviving rapid climate change in the deep sea during the Paleogene hyperthermals. Proceedings of the National Academy of Sciences 110, 9273–9276.

Francis, J.E., 1999. Evidence from fossil plants for Antarctica paleoclimates over the past 100 million years. Terra Antartica 3, 43-52.

Friedrich, O., 2010. Benthic foraminifera and their role to decipher paleoenvironment during mid-Cretaceous Oceanic Anoxic Events – the "anoxic benthic foraminifera" paradox. Revue de Micropaléontologie 53, 175–192.

Frontalini, F., Coccioni, R., Catanzariti, R., Jovane, L., Savian, J.F., and Sprovieri, M., 2016. The Eocene Thermal Maximum 3: Reading the environmental perturbations at Gubbio (Italy). In: Geological Society of America Special Papers. Geological Society of America, 161–175.

Funakawa, S., and Nishi, H., 2008. Radiolarian Faunal Changes during the Eocene-Oligocene Transition in the Southern Ocean (Maud Rise, ODP Leg 113, Site 689) and its Significance in Paleoceanographic Change. Micropaleontology 54, 15–26.

Funakawa, S., Nishi, H., Moore, T.C., and Nigrini, C.A., 2006. Radiolarian faunal turnover and paleoceanographic change around Eocene/Oligocene boundary in the central equatorial Pacific, ODP Leg 199, Holes 1218A, 1219A, and 1220A. Palaeogeography, Palaeoclimatology, Palaeoecology 230, 183–203.

Gage, J. D. and Tyler, P. A., 1991. Deep-Sea Biology: a natural history of organisms at the deep-sea floor. Cambridge University Press, 504 pp.

Galeotti, S., Krishnan, S., Pagani, M., Lanci, L., Gaudio, A., Zachos, J.C., Monechi, S., Morelli, G., and Lourens, L., 2010. Orbital chronology of Early Eocene hyperthermals from the Contessa Road section, central Italy. Earth and Planetary Science Letters 290, 192–200.

García-Gallardo, Á., Grunert, P., Voelker, A.H.L., Mendes, I., and Piller, W.E., 2017. Re-evaluation of the "elevated epifauna" as indicator of Mediterranean Outflow Water in the Gulf of Cadiz using stable isotopes ($\delta^{13}C$, $\delta^{18}O$). Global and Planetary Change 155, 78–97.

Gaucher, C., and Sprechmann, P., 1999. Upper Vendian skeletal faunas of the Arroyo del Soldado Group, Uruguay. Berinegria 23, 55-921.

George, M. and Murray, J. W., 1977. Glauconite in Celtic Sea sediments. Proceedings of the Ussher Society 4, 94–101.

Giorgioni, M., Jovane, L., Rego, E.S., Rodelli, D., Frontalini, F., Coccioni, R., Catanzariti, R., and Özcan, E., 2019. Carbon cycle instability and orbital forcing during the Middle Eocene Climatic Optimum. Scientific Reports 9, 9357.

Giraldo-Gómez, V.M., Mutterlose, J., Podlaha, O.G., Speijer, R.P., and Stassen, P., 2018. Benthic Foraminifera and Geochemistry Across the Paleocene–eocene Thermal Maximum Interval in Jordan. Journal of Foraminiferal Research 48, 100–120.

Giusberti, L., Coccioni, R., Sprovieri, M., and Tateo, F., 2009. Perturbation at the sea floor during the Paleocene–Eocene Thermal Maximum: Evidence from benthic foraminifera at Contessa Road, Italy. Marine Micropaleontology 70, 102–119.

Giusberti, L., Boscolo Galazzo, F., and Thomas, E., 2016. Variability in climate and productivity during the Paleocene–Eocene Thermal Maximum in the western Tethys (Forada section). Climate of the Past 12, 213–240.

Gonzalvo, C., and Molina, E., 1996. Bioestratigrafía y cronoestratigrafía del tránsito Eoceno Medio-Eoceno Superior en la Cordillera Bética. Revista Española de Micropaleontología XXVIII, 25–44.

Gooday, A.J., 1986. Soft-shelled foraminifera in meiofaunal samples from the bathyal northeast Atlantic. Sarsia 71, 275–287.

Gooday, A.J., 1988. A response of benthic Foraminifera to deposition of phytodetritus in the deep sea. Nature 332, 70–73.

Gooday, A.J., 1993. Deep-sea benthic foraminiferal species which exploit phytodetritus: Characteristic features and controls on distribution. Marine Micropaleontology 22, 187–205.

Gooday, A. J. 1999. Biovidersity of foraminifera and other protists in the deep sea: scales and patterns. Belgian Journal of Zoology 129, 61–80.

Gooday, A.J., 2002. Biological Responses to Seasonally Varying Fluxes of organic matter to the ocean floor: a review. Journal of Oceanography 58, 302–332.

Gooday, A.J., 2003. Benthic foraminifera (protista) as tools in deep-water Palaeoceanography: environmental infuences on faunal characteristics. Advances in Marine Biology 46, 1–90.

Gooday, A.J., and Hughes, J.A., 2002. Foraminifera associated with phytodetritus deposits at a bathyal site in the northern Rockall Trough (NE Atlantic): seasonal contrasts and a comparison of stained and dead assemblages. Marine Micropaleontology 46, 83–110.

Gooday, A.J., and Rathburn, A.E., 1999. Temporal variability in living deep-sea benthic foraminifera: a review. Earth-Science Reviews 46, 187–212.

Gooday, A.J., and Turley, C.M., 1990. Responses by benthic organisms to inputs of organic material to the ocean floor: a review. Philosophical Transactions of the Royal Society A 331, 119–138.

Gooday, A.J., Levin, L.A., Linke, P., and Heeger, T., 1992. The role of benthic foraminifera in deep-sea food webs and carbon cycling. In: Rowe, G.T., Pariente, V. (Eds.), Deep-sea food chains and the global carbon cycle. Springer Netherlands, 63–91.

Gooday, A.J., Nomaki, H., and Kitazato, H., 2008. Modern deep-sea benthic foraminifera: a brief review of their morphology-based biodiversity and

trophic diversity. Geological Society, London, Special Publications 303, 97–119.

Gradstein, F.M., Ogg, J.G., Schmitz, M., and Ogg, G., 2012. The Geologic Time Scale 2012. Elsevier Science, 1176 pp.

Grira, C., Karoui-Yaakoub, N., Negra, M.H., Rivero-Cuesta, L., and Molina, E., 2018. Paleoenvironmental and ecological changes during the Eocene-Oligocene transition based on foraminifera from the Cap Bon Peninsula in North East Tunisia. Journal of African Earth Sciences 143, 145–161.

Gross, O., 2000. Influence of temperature, oxygen and food availability on the migrational activity of bathyal benthic foraminifera: evidence by microcosm experiments., In: Liebezeit, G., Dittmann, S., and Kröncke, I. (Eds.), Life at interfaces and under extreme conditions. Springer Netherlands, 123–137.

Grünig, A., 1985. Systematical description of Eocene Benthic Foraminifera of Possagno (northern Italy), Sansoain (northern Spain) and Biarritz (Aquitaine, France). In: Memorie Degli Instituti Di Geologia e Mineralogia Dell'Università Di Padova, 251–302.

Grünig, A., and Herb, R., 1980. Paleoecology of Late Eocene benthonic Foraminifera from Possagno (Treviso-Northern Italy). Cushman Foundation, Special Publication 19, 68–85.

Hallock, P., 1985. Why are larger foraminifera large? Paleobiology 11, 195–208.

Hammer, Ø., and Harper, D.A.T., Ryan, P.D., 2001. PAST: Paleontological statistics software package for education and data analysis. Paleontologia Electronica 4(1), 9.

Hammer, Ø., and Harper, D., 2005. Paleontological Data Analysis. Blackwell Publishing, 351 pp.

Haslett. S.K., 2002. Quaternary Environmental Micropalaeontology. Routledge, 288 pp.

Hayek, L.A.C., and Buzas, M.A., 1997. Surveying natural populations. Columbia University Press, 563 pp.

Hayward, B.W., Johnson, K., Sabaa, A.T., Kawagata, S., and Thomas, E., 2010. Cenozoic record of elongate, cylindrical, deep-sea benthic foraminifera in the North Atlantic and equatorial Pacific Oceans. Marine Micropaleontology 74, 75–95.

Hayward, B.W., Kawagata, S., Sabaa, A., Grenfell, H., Van Kerckhoven, L., Johnson, K., and Thomas, E., 2012. The last global extinction (Mid-Pleistocene) of deep-sea benthic foraminifera (Chrysalogoniidae, Ellipsoidinidae, Glandulonodosariidae, Plectofrondicularиidae, Pleurostomellidae, Stilostomellidae), their Late Cretaceous-Cenozoic history and taxonomy, Cushman Foundation for Foraminiferal Research Special Publications 43, 408 pp.

Herguera, J.C., 2000. Last glacial paleoproductivity patterns in the eastern equatorial Pacific: benthic foraminifera records. Marine Micropaleontology 40, 259–275.

Herguera, J.C., and Berger, W.H., 1991. Paleoproductivity from benthic foraminifera abundance: Glacial to postglacial change in the west-equatorial Pacific. Geology 19, 1173–1176.

Hohenegger, J., Pillar, W. and Baal, C., 1993. Horizontal and vertical spatial distribution of foraminifers in the shallow subtidal Gulf of Trieste, northern Adriatic Sea. Journal of Foraminiferal Research 23, 79–101.

Holbourn, A., Henderson, A.S., and MacLeod, N., 2013. Atlas of Benthic Foraminifera. Wiley-Blackwell Publishing, 642 pp.

Hooker, J.J., 1986. Mammals from the Bartonian (middle/late Eocene) of the Hampshire Basin, southern England. Bulletin of the British Museum of Natural History (Geology) 39, 191-478.

Hooker, J.J., and King, C., 2019. The Bartonian unit stratotype (S. England): Assessment of its correlation problems and potential. Proceedings of the Geologists' Association 130, 157–169.

Hooker, J.J., Collinson, M.E., and Sille, N.P., 2004. Eocene–Oligocene mammalian faunal turnover in the Hampshire Basin, UK: calibration to the global time scale and the major cooling event. Journal of the Geological Society 161, 161–172.

Ingle, J.C. Jr., 1980. Cenozoic paleobathymetry and depositional history of selected sequences within the southern California Continental Borderland. Cushman Foundation, Special Publication 19, 163–195.

Intxauspe-Zubiaurre, B., Martínez-Braceras, N., Payros, A., Ortiz, S., Dinarès-Turell, J., and Flores, J.-A., 2018. The last Eocene hyperthermal (Chron C19r event, ~41.5 Ma): Chronological and paleoenvironmental insights from a continental margin (Cape Oyambre, N Spain). Palaeogeography, Palaeoclimatology, Palaeoecology 505, 198–216.

Ivany, L.C., Lohmann, K.C., Hasiuk, F., Blake, D.B., Glass, A., Aronson, R.B., and Moody, R.M., 2008. Eocene climate record of a high southern latitude continental shelf: Seymour Island, Antarctica. Geological Society of America Bulletin 120, 659–678.

Jaramillo, C., Rueda, M., J., and Mora, G., 2006. Cenozoic plant diversity in the neotropics. Science 311, 1893–1896.

Jennions, S.M., Thomas, E., Schmidt, D.N., Lunt, D., and Ridgwell, A., 2015. Changes in benthic ecosystems and ocean circulation in the Southeast Atlantic across Eocene Thermal Maximum 2. Paleoceanography 30, 1059–1077.

John, E.H., Pearson, P.N., Coxall, H.K., Birch, H., Wade, B.S., and Foster, G.L., 2013. Warm ocean processes and carbon cycling in the Eocene. Philosophical Transactions of the Royal Society A: Mathematical, Physical and Engineering Sciences 371, 20130099–20130099.

Jones, R.W., and Charnock, M.A., 1985. "Morphogroups" of agglutinated foraminifera. Their life positions and feeding habits and potential applicability in (paleo)ecological studies. Revue de Palèobiologie 4(2), 311–320.

Jorissen, F.J., 1999. Benthic foraminiferal microhabitats below the sediment-water interface. In: Modern Foraminifera. Springer Netherlands, 161–179.

Jorissen, F.J., Barmawidjaja, D.M., Puskaric, S. and van der Zwaan, G.J., 1992. Vertical distribution of benthic foraminifera in the northern Adriatic Sea: the relation with organic flux. Marine Micropaleontology 19, 131–46.

Jorissen, F.J., Buzas, M.A., Culver, S.J. and Kuehl, S.A., 1994. Vertical distribution of living benthic foraminifera in submarine canyons off New Jersey. Journal of Foraminiferal Research 24, 28–36.

Jorissen, F.J., de Stigter, H.C., and Widmark, J.G., 1995. A conceptual model explaining benthic foraminiferal microhabitats. Marine micropaleontology 26, 3–15.

Jorissen, F.J., Wittling, I., Peypouquet, J.P., Rabouille, C., and Relexans, J.C., 1998. Live benthic foraminiferal faunas off Cape Blanc, NW-Africa: Community structure and microhabitats. Deep Sea Research Part I: Oceanographic Research Papers 45, 2157–2188.

Jorissen, F.J., Fontanier, C., and Thomas, E., 2007. Chapter seven: paleoceanographical proxies based on deep-sea benthic foraminiferal assemblage characteristics. In: Developments in Marine Geology. Elsevier, 263–325.

Jovane, L., Florindo, F., Coccioni, R., Dinares-Turell, J., Marsili, A., Monechi, S., Roberts, A.P., and Sprovieri, M., 2007. The middle Eocene climatic optimum event in the Contessa Highway section, Umbrian Apennines, Italy. Geological Society of America Bulletin 119, 413–427.

Jovane, L., Sprovieri, M., Coccioni, R., Florindo, F., Marsili, A., and Laskar, J., 2010. Astronomical calibration of the middle Eocene Contessa Highway section (Gubbio, Italy). Earth and Planetary Science Letters 298, 77–88.

Kamikuri, S., and Wade, B.S., 2012. Radiolarian magnetobiochronology and faunal turnover across the middle/late Eocene boundary at Ocean Drilling Program Site 1052 in the western North Atlantic Ocean. Marine Micropaleontology 88, 41–53.

Katz, M.E., 1999. The source and fate of massive carbon input during the Latest Paleocene Thermal Maximum. Science 286, 1531–1533.

Katz, M.E., and Miller, K.G., 1991. Early Paleogene benthic foraminiferal assemblages and stable isotopes in the Southern Ocean. In: Ciesielski, P.F., and Kristoffersen, Y. (Eds.), Proceedings of the Ocean Drilling Program, Scientific Results vol. 114, 481–512.

Katz, M.E., Miller, K.G., Wright, J.D., Wade, B.S., Browning, J.V., Cramer, B.S., and Rosenthal, Y., 2008. Stepwise transition from the Eocene greenhouse to the Oligocene icehouse. Nature Geoscience 1(5), 329–334.

Katz, M.E., Tjalsma, R.C., and Miller, K.G., 2003. Oligocene bathyal to abyssal benthic foraminifera of the Atlantic Ocean. Micropaleontology 49, 1–45.

Katz, M.E., Cramer, B.S., Franzese, A., Honisch, B., Miller, K.G., Rosenthal, Y., and Wright, J.D., 2010. Traditional and emerging geochemical proxies in Foraminifera. The Journal of Foraminiferal Research 40, 165–192.

Kennett, J.P., and Stott, L.D., 1991. Abrupt deep-sea warming, palaeoceanographic changes and benthic extinctions at the end of the Paleocene. Nature 353, 225–229.

Kennett, J.P., Houtz, R.E., Andrews, P.B., Edwards, A.R., Gostin, V.A., Hajós, M., Hampton, M., Jenkins, D.G., Margolis, S.V., Ovenshine, A.T. and Perch-Nielsen, K., 1975. Cenozoic Paleoceanography in the southwest Pacific Ocean, Antarctic glaciation, and the current development of the circum-Antarctic current. In: Initial Reports of the Deep Sea Drilling Project 29, Initial Reports, 1155-1169.

Kirtland Turner, S., and Ridgwell, A., 2013. Recovering the true size of an Eocene hyperthermal from the marine sedimentary record. Paleoceanography 28, 700–712.

Kirtland Turner, S., Sexton, P.F., Charles, C.D., and Norris, R.D., 2014. Persistence of carbon release events through the peak of early Eocene global warmth. Nature Geoscience 7, 748–751.

Kitazato, H., 1988. Ecology of benthic foraminifera in the tidal zone of a rocky shore. Revue de Paléobiologie 2, 815-825.

Koeberl, C., and Montanari, A., 2009. The late Eocene Earth: hothouse, icehouse, and impacts. The Geological Society of America Special Paper 452, 322 pp.

Kurbjeweit, F., Schmiedl, G., Schiebel, R., Hemleben, C., Pfannkuche, O., Wallmann, K., and Schäfer, P., 2000. Distribution, biomass and diversity of benthic foraminifera in relation to sediment geochemistry in the Arabian Sea. Deep Sea Research Part II: Topical Studies in Oceanography 47, 2913–2955.

Lambshead, P.J.D., and Gooday, A.J., 1990. The impact of seasonally deposited phytodetritus on epifaunal and shallow infaunal benthic foraminiferal populations in the bathyai northeast Atlantic: the assemblage response. Deep-Sea Research 37, 1263–1283.

Lauretano, V., Littler, K., Polling, M., Zachos, J.C., and Lourens, L.J., 2015. Frequency, magnitude and character of hyperthermal events at the onset of the Early Eocene Climatic Optimum. Climate of the Past 11, 1313–1324.

Lauretano, V., Hilgen, F.J., Zachos, J.C., and Lourens, L.J., 2016. Astronomically tuned age model for the early Eocene carbon isotope events: A new high-resolution δ13 Cbenthic record of ODP Site 1263 between ~ 49 and ~ 54 Ma. Newsletters on Stratigraphy 49, 383–400.

Laws, E.A., Falkowski, P.G., Smith, W.O., Ducklow, H., and McCarthy, J.J., 2000. Temperature effects on export production in the open ocean. Global Biogeochemical Cycles 14, 1231–1246.

Lawver, L.A., and Gahagan, L.M., 2003. Evolution of Cenozoic seaways in the circum-Antarctic region. Palaeogeography, Palaeoclimatology, Palaeoecology 198, 11–37.

Lear, C.H., 2000. Cenozoic deep-sea temperatures and global ice volumes from Mg/Ca in benthic foraminiferal calcite. Science 287, 269–272.

Lear, C.H., Bailey, T.R., Pearson, P.N., Coxall, H.K., and Rosenthal, Y., 2008. Cooling and ice growth across the Eocene-Oligocene transition. Geology 36, 251.

Lee, J.J. and Anderson, O. R., 1991. Symbiosis in Foraminifera. In: Lee, J.J. and Anderson, O.R. (Eds.), Biology of Foraminifera. Academic Press Inc, 157–220.

Lee, J.J. and Hallock, P., 2000. Advances in the biology of foraminifera. Micropaleontology, 46 (Supplement 1), 1–198.

Lee, J.J., Tietjen, J. H., Mastropaolo, C. and Rubin, H., 1977. Food quality and the heterogeneous spatial distribution of meiofauna. Helgoländer wissenschalftliche Meeresuntersuchungen, 30, 272–82.

Leon-Rodriguez, L., and Dickens, G.R., 2010. Constraints on ocean acidification associated with rapid and massive carbon injections: The early Paleogene record at ocean drilling program site 1215, equatorial Pacific Ocean. Palaeogeography, Palaeoclimatology, Palaeoecology 298, 409–420.

Li, Q., Davies, P. J., McGowran, B. and Linden, T. van der, 2003. Foraminiferal ecostratigraphy of late Oligocene sequences, southeastern Australia: patterns and inferred sea levels at third-order and Milankovitch cycles. Society of Economic Paleontologists and Mineralogists Special Publication 75, 147–71.

Linke, P. and Lutze, G. F., 1993. Microhabitat preferences of benthic foraminifera: a static concept or a dynamic adaptation to optimise food acquisition? Marine Micropaleontology 20, 215–34.

Littler, K., Röhl, U., Westerhold, T., and Zachos, J.C., 2014. A high-resolution benthic stable-isotope record for the South Atlantic: Implications for orbital-scale changes in Late Paleocene–Early Eocene climate and carbon cycling. Earth and Planetary Science Letters 401, 18–30.

Liu, Z., Zhao, Q., Cheng, X., and Huang, W., 2004. Deep-water Earliest Oligocene Glacial Maximum (EOGM) in South Atlantic. Chinese Science Bulletin 49, 2190.

Liu, Z., Pagani, M., Zinniker, D., DeConto, R.M., Huber, M., Brinkhuis, H., Shah, S.R., Leckie, R.M., and Pearson, A., 2009. Global cooling during the Eocene-Oligocene climate transition. Science 323, 1187–1190.

Loeblich, A.R., Jr., and Tappan, H., 1987. Foraminiferal genera and their classification. Van Nostrand Reinhold Company Inc, 970 pp.

Loubere, P., 1998. The impact of seasonality on the benthos as reflected in the assemblages of deep-sea foraminifera. Deep Sea Research Part I: Oceanographic Research Papers 45, 409–432.

Loubere, P., and Fariduddin, M., 1999. Benthic foraminifera and the flux of organic carbon to the seabed. In: Modern Foraminifera. Springer Netherlands, 181–199.

Lourens, L.J., Sluijs, A., Kroon, D., Zachos, J.C., Thomas, E., Röhl, U., Bowles, J., and Raffi, I., 2005. Astronomical pacing of late Palaeocene to early Eocene global warming events. Nature 435, 1083–1087.

Luciani, V., Dickens, G.R., Backman, J., Fornaciari, E., Giusberti, L., Agnini, C., and D'Onofrio, R., 2016. Major perturbations in the global carbon cycle and photosymbiont-bearing planktic foraminifera during the early Eocene. Climate of the Past 12, 981–1007.

Lunt, D.J., Ridgwell, A., Sluijs, A., Zachos, J.C., Hunter, S., and Haywood, A., 2011. A model for orbital pacing of methane hydrate destabilization during the Palaeogene. Nature Geoscience 4, 775–778.

Lyle, M., Lyle, A.O., Backman, J., and Tripati, A.K., 2005. Biogenic Sedimentation in the Eocene Equatorial Pacific - The Stuttering Greenhouse and Eocene Carbonate Compensation Depth. Proceedings of the Ocean Drilling Program, Scientific Results 199, 1–35.

Mackensen, A., and Licari, L., 2004. Carbon isotopes of live benthic foraminifera from the South Atlantic: sensitivity to bottom water carbonate saturation state and organic matter rain rates. In: Wefer, G., Mulitza, S., and Ratmeyer, V. (Eds.), The South Atlantic in the Late Quaternary: Reconstruction of Material Budgets and Current Systems. Springer Berlin Heidelberg,. 623–644.

Martin, R.E., 2000. Environmental Micropaleontology. The Application of Microfossils to Environmental Geology. Springer US, 481 pp.

Mayer-Eymar, K., 1858. Versuch einer neuen Klassifikation der Tertiär-Gebilde Europa's. Verhandlungen der SchweizerNaturforschendenGesellschaft fur die Gesammten Naturwissenschaften Trogen 42, 165-199.

McInerney, F.A., and Wing, S.L., 2011. The Paleocene-Eocene Thermal Maximum: a perturbation of carbon cycle, climate, and biosphere with implications for the future. Annual Review of Earth and Planetary Sciences 39, 489–516.

Merico, A., Tyrrell, T., and Wilson, P.A., 2008. Eocene/Oligocene ocean de-acidification linked to Antarctic glaciation by sea-level fall. Nature 452, 979–982.

Meyer-Reil, L.A. and Köster, M., 1991. Fine-scale distribution of hydrolytic activity associated with foraminiferans and bacteria in deep-sea sediments in the Norwegian–Greenland Sea. Kieler Meereforschungen 8, 121–6.

Mikhalevich, V.I., 2004. The general aspects of the distribution of Antarctic foraminifera. Micropaleontology 50, 179–194.

Miller, K.G., 1983. Eocene-Oligocene paleoceanography of the deep Bay of Biscay: benthic foraminiferal evidence. Marine Micropaleontology 7, 403–440.

Miller, K.G., Fairbanks, R.G., and Mountain, G.S., 1987a. Tertiary oxygen isotope synthesis, sea level history, and continental margin erosion. Paleoceanography 2, 1–19.

Miller, K.G., Janecek, T.R., Katz, M.E., and Keil, D.J., 1987b. Abyssal circulation and benthic foraminiferal changes near the Paleocene/Eocene boundary. Paleoceanography 2, 741–761.

Miller, K.G., Wright, J.D., and Fairbanks, R.G., 1991. Unlocking the Ice House: Oligocene-Miocene oxygen isotopes, eustasy, and margin erosion. Journal of Geophysical Research: Solid Earth 96, 6829–6848.

Miller, K.G., Wright, J.D., Katz, M.E., Wade, B.S., Browning, J.V., Cramer, B.S., and Rosenthal, Y., 2009. Climate threshold at the Eocene-Oligocene transition: Antarctic ice sheet influence on ocean circulation. In: Koeberl, C. and Montanari, A. (Eds.), The Late Eocene Earth—Hothouse, Icehouse, and Impacts. Geological Society of America Special Papers 452, 169-178.

Moebius, I., Friedrich, O., and Scher, H.D., 2014. Changes in Southern Ocean bottom water environments associated with the Middle Eocene Climatic Optimum (MECO). Palaeogeography, Palaeoclimatology, Palaeoecology 405, 16–27.

Moebius, I., Friedrich, O., Edgar, K.M., and Sexton, P.F., 2015. Episodes of intensified biological productivity in the subtropical Atlantic Ocean during the termination of the Middle Eocene Climatic Optimum (MECO): Intensified Productivity During the MECO. Paleoceanography 30, 1041–1058.

Molina, E., 2015. Evidence and causes of the main extinction events in the Paleogene based on extinction and survival patterns of foraminifera. Earth-Science Reviews 140, 166–181.

Molina, E., Gonzalvo, C., Ortiz, S., and Cruz, L.E., 2006. Foraminiferal turnover across the Eocene–Oligocene transition at Fuente Caldera, southern Spain: No cause–effect relationship between meteorite impacts and extinctions. Marine Micropaleontology 58, 270–286.

Molina, E., Alegret, L., Apellaniz, E., Bernaola, G., Caballero, F., Dinares-Turell, J., Hardenbol, J., Heilmann-Clausen, C., Larrasoaña, J.C., Luterbacher, H.P., Monechi, S., Ortiz, S., Orue-Etxebarria, X., Payros, A., Pujalte, V., Rodríguez-Tovar, F.J., Tori, F., Tosquella, J., and Uchman, A., 2011. The Global Stratotype Section and Point (GSSP) for the base of the Lutetian Stage at the Gorrondatxe section, Spain. Episodes 34, 86–108.

Molina, E., Torres-Silva, A.I., Ćorić, S., and Briguglio, A., 2016. Integrated biostratigraphy across the Eocene/Oligocene boundary at Noroña, Cuba, and the question of the extinction of orthophragminids. Newsletters on Stratigraphy 49, 85412.

Morse, J.W., and Arvidson, R.S., 2002. The dissolution kinetics of major sedimentary carbonate minerals. Earth-Science Reviews 58, 51–84.

Müller-Merz, E., and Oberhänsli, H., 1991. Eocene bathyal and abyssal benthic foraminifera from a South Atlantic transect at 20–30 S. Palaeogeography, Palaeoclimatology, Palaeoecology 83, 117–171.

Murray, J.W., 1991. Ecology and Paleoecology of Benthic Foraminifera. Longman, 397 pp.

Murray, J.W., 2000. When Does Environmental Variability Become Environmental Change? In: Martin, R.E. (Ed.), Environmental Micropaleontology, Topics in Geobiology. Springer US, 7–37.

Murray, J.W., 2001. The niche of benthic foraminifera, critical thresholds and proxies. Marine Micropaleontology 41, 1–7.

Murray, J.W., 2006. Ecology and Applications of Benthic Foraminifera. Cambridge University Press, 426 pp.

Murray, J.W., 2007. Biodiversity of living benthic foraminifera: How many species are there? Marine Micropaleontology 64, 163–176.

Murray, J.W., and Pudsey, C.J., 2004. Living (stained) and dead foraminifera from the newly ice-free Larsen Ice Shelf, Weddell Sea, Antarctica: ecology and taphonomy. Marine Micropaleontology 53, 67–81.

Murray, J.W., and Wright, C.A., 1974. Paleogene Foraminiferida and Palaeoecology, Hampshire and Paris basins and the English Channel. The Palaeontological Association, Special papers in Palaeontology 14, 171 pp.

Newsam, C., Bown, P.R., Wade, B.S., and Jones, H.L., 2017. Muted calcareous nannoplankton response at the Middle/Late Eocene Turnover event in the western North Atlantic Ocean. Newsletters on Stratigraphy 50, 297–309.

Nicolo, M.J., Dickens, G.R., Hollis, C.J., and Zachos, J.C., 2007. Multiple early Eocene hyperthermals: Their sedimentary expression on the New Zealand continental margin and in the deep sea. Geology 35, 699-702.

O'Connor, M.I., Piehler, M.F., Leech, D.M., Anton, A., and Bruno, J.F., 2009. Warming and resource availability shift food web structure and metabolism. PLoS Biology 7, e1000178.

Ogg, J.G., Ogg, G., and Gradstein, F.M., 2008. The Concise Geologic Time Scale. Cambridge University Press, 177 pp.

Ohkushi, K., Thomas, E., and Kawahata, H., 2000. Abyssal benthic foraminifera from the northwestern Pacific (Shatsky Rise) during the last 298 kyr. Marine Micropaleontology 38, 119-147.

Okada, H., and Bukry, D., 1980. Supplementary modification and introduction of code numbers to the low-latitude coccolith biostratigraphic zonation (Bukry, 1973; 1975). Marine Micropaleontology 5, 321–325.

Olivarez Lyle, A., and Lyle, M.W., 2006. Missing organic carbon in Eocene marine sediments: Is metabolism the biological feedback that maintains end-member climates? Paleoceanography 21, PA2007.

Ortiz, S., and Kaminski, M.A., 2012. Record of deep-sea, benthic elongate-cylindrical foraminifera across the Eocene-Oligocene Transition in the North Atlantic Ocean (ODP Hole 647A). The Journal of Foraminiferal Research 42, 345–368.

Ortiz, S., and Thomas, E., 2006. Lower-middle Eocene benthic foraminifera from the Fortuna section (Betic Cordillera, southeastern Spain). Micropaleontology 52, 97–150.

Ortiz, S., and Thomas, E., 2015. Deep-sea benthic foraminiferal turnover during the early–middle Eocene transition at Walvis Ridge (SE Atlantic). Palaeogeography, Palaeoclimatology, Palaeoecology 417, 126–136.

Pagani, M., Zachos, J.C., Freeman, K.H., Tipple, B., and Bohaty, S., 2005. Marked decline in atmospheric carbon dioxide concentrations during the Paleogene. Science 309, 600–603.

Pälike, H., Lyle, M.W., Nishi, H., Raffi, I., Ridgwell, A., Gamage, K., Klaus, A., Acton, G., Anderson, L., Backman, J., Baldauf, J., Beltran, C., Bohaty, S.M., Bown, P., Busch, W., Channell, J.E.T., Chun, C.O.J., Delaney, M., Dewangan, P., Dunkley Jones, T., Edgar, K.M., Evans, H., Fitch, P., Foster, G.L., Gussone, N., Hasegawa, H., Hathorne, E.C., Hayashi, H., Herrle, J.O., Holbourn, A., Hovan, S., Hyeong, K., Iijima, K., Ito, T., Kamikuri, S., Kimoto, K., Kuroda, J., Leon-Rodriguez, L., Malinverno, A., Moore Jr, T.C., Murphy, B.H., Murphy, D.P., Nakamura, H., Ogane, K., Ohneiser, C., Richter, C., Robinson, R., Rohling, E.J., Romero, O., Sawada, K., Scher, H., Schneider, L., Sluijs, A., Takata, H., Tian, J., Tsujimoto, A., Wade, B.S., Westerhold, T., Wilkens, R., Williams, T., Wilson, P.A., Yamamoto, Y., Yamamoto, S., Yamazaki, T., and Zeebe, R.E., 2012. A Cenozoic record of the equatorial Pacific carbonate compensation depth. Nature 488, 609–614.

Pälike, H., Norris, R.D., Herrle, J.O., Wilson, P.A., Coxall, H.K., Lear, C.H., Shackleton, N.J., Tripati, A.K., and Wade, B.S., 2006. The Heartbeat of the Oligocene Climate System. Science 314, 1894–1898.

Pawlowski, J., 2000. Introduction to the Molecular Systematics of Foraminifera. Micropaleontology 46, 1–12.

Pawlowski, J., and Holzmann, M., 2008. Diversity and geographic distribution of benthic foraminifera: a molecular perspective. Biodiversity and Conservation 17, 317–328.

Pawlowski, J., Vargas, C. de, Fahrni, J. and Bowser, S., 1998. Reticulomyxa filoda – an 'athalamiid' freshwater foraminifer. Forams '98, International Symposium on Foraminifera, Sociedad Mexicana de Paleontología Special Publication, 78–79.

Pawlowski, J., Holzmann, M., and Tyszka, J., 2013. New supraordinal classification of Foraminifera: Molecules meet morphology. Marine Micropaleontology 100, 1–10.

Payros, A., Ortiz, S., Alegret, L., Orue-Etxebarria, X., Apellaniz, E., and Molina, E., 2012. An early Lutetian carbon-cycle perturbation: Insights from the Gorrondatxe section (western Pyrenees, Bay of Biscay). Paleoceanography 27, PA2213.

Payros, A., Dinarès-Turell, J., Monechi, S., Orue-Etxebarria, X., Ortiz, S., Apellaniz, E., and Martínez-Braceras, N., 2015. The Lutetian/Bartonian transition (middle Eocene) at the Oyambre section (northern Spain): Implications for standard chronostratigraphy. Palaeogeography, Palaeoclimatology, Palaeoecology 440, 234–248.

Pea, L., 2011. Eocene-Oligocene paleoceanography of the subantarctic South Atlantic: Calcareous Nannofossil reconstructions of temperature, nutrient, and dissolution history (Doctoral thesis, University of Parma, Italy).

Pearson, P.N., 2010. Increased Atmospheric CO_2 during the Middle Eocene. Science 330, 763–764.

Pearson, P.N., and Palmer, M.R., 2000. Atmospheric carbon dioxide concentrations over the past 60 million years. Nature 406, 695–699.

Pearson, P.N., McMillan, I.K., Wade, B.S., Jones, T.D., Coxall, H.K., Bown, P.R., and Lear, C.H., 2008. Extinction and environmental change across the Eocene-Oligocene boundary in Tanzania. Geology 36, 179-182.

Peebles, M.W., and Lewis, R.D., 1991. Surface textures of benthic foraminifera from San Salvador, Bahamas. The Journal of Foraminiferal Research 21, 285–292.

Pekar, S.F., Christie-Blick, N., Kominz, M.A., and Miller, K.G., 2002. Calibration between eustatic estimates from backstripping and oxygen isotopic records for the Oligocene. Geology 30, 903-906.

Phleger, F.B., 1960. Ecology and distribution of recent foraminifera. John Hopkins Press, 297 pp.

Premoli Silva, I., and Jenkins, D.G., 1993. Decision on the Eocene-Oligocene boundary stratotype. Episodes 16, 379–381.

Prentice, M.L., and Matthews, R.K., 1988. Cenozoic ice-volume history: Development of a composite oxygen isotope record. Geology 16, 963–966.

Rathburn, A.E., and Corliss, B.H., 1994. The ecology of living (stained) deep-sea benthic foraminifera from the Sulu Sea. Paleoceanography 9, 87–150.

Rathburn, A.E., Pérez, M.E., and Martin, J.B., 2003. Relationships between the distribution and stable isotopic composition of living benthic foraminifera and cold methane seep biogeochemistry in Monterey Bay, California. Geochemistry, Geophysics and Geosystems 4, 1106.

Rea, D.K., and Lyle, M.W., 2005. Paleogene calcite compensation depth in the eastern subtropical Pacific: Answers and questions. Paleoceanography 20, PA1012.

Reizopoulou, S., and Nicolaidou, A., 2004. Benthic diversity of coastal brackish-water lagoons in western Greece. Aquatic Conservation: Marine and Freshwater Ecosystems 14, 93–102.

Rivero-Cuesta, L., Molina, E., and Alegret, L., 2018. Eocene (Bartonian) benthic foraminifera and paleoenvironmental changes in the Western Tethys. Palaeogeography, Palaeoclimatology, Palaeoecology 503, 102–111.

Rivero-Cuesta, L., Westerhold, T., Agnini, C., Dallanave, E., Wilkens, R.H., and Alegret, L., 2019. Paleoenvironmental changes at ODP Site 702 (South Atlantic): anatomy of the Middle Eocene Climatic Optimum. Paleoceanography and Paleoclimatology 34, 2019PA003806.

Rivero-Cuesta, L., Westerhold, T., and Alegret, L., 2020. The Late Lutetian Thermal Maximum (middle Eocene): first record of deep-sea benthic foraminiferal response. Palaeogeography, Palaeoclimatology, Palaeoecology 545, 109637.

Rohling, E.J. and Cooke, S., 1999. Stable oxygen and carbon isotopes in foraminiferal carbonate shells. In: Sen Gupta, B.K., (Ed.), Modern Foraminifera. Springer Netherlands, 239–258.

Salamy, K.A., and Zachos, J.C., 1999. Latest Eocene–Early Oligocene climate change and Southern Ocean fertility: inferences from sediment accumulation and stable isotope data. Palaeogeography, Palaeoclimatology, Palaeoecology 145, 61–77.

Schmiedl, G., Mackensen, A., and Müller, P.J., 1997. Recent benthic foraminifera from the eastern South Atlantic Ocean: Dependence on food supply and water masses. Marine Micropaleontology 32, 249–287.

Schmitz, B., Alegret, L., Apellaniz, E., Arenillas, I., Aubry, M.-P., Baceta, J.-U., Berggren, W.A., Bernaola, G., Caballero, F., Clemmensen, A., Dinarés-Turell, J., Dupuis, C., Heilmann-Clausen, C., Knox, R., Martín-Rubio, M., Molina, E., Monechi, S., Ortiz, S., Orue-Etxebarria, X., Payros, A., Petrizzo, M.R., Pujalte, V., Speijer, R., Sprong, J., Steurbaut, E., and Thomsen, E., 2008. Proposed Global Stratotype Sections and Points for the bases of the Selandian and Thanetian stages (Paleocene Series). Report of the International Subcommission on Paleogene Stratigraphy, 52.

Schmitz, B., Pujalte, V., Molina, E., Monechi, S., Orue-Etxebarria, X., Speijer, R.P., Alegret, L., Apellaniz, E., Arenillas, I., Aubry, M.-P., Baceta, J.I., Berggren, W.A., Bernaola, G., Caballero, F., Clemmensen, A., Dinarés-Turell, J., Dupuis, C., Heilmann-Clausen, C., Hilario Orús, A., Knox, R., Martín-Rubio, M., Ortiz, S., Payros, A., Petrizzo, M.R., von Salis, K., Sprong, J., Steurbaut, E., and Thomsen, E., 2011. The Global Stratotype Sections and Points for the bases of the Selandian (Middle Paleocene) and Thanetian (Upper Paleocene) stages at Zumaia Spain. Episodes 34, 220e243.

Schönfeld, J., 1997. The impact of the Mediterranean Outflow Water (MOW) on benthic foraminiferal assemblages and surface sediments at the southern Portuguese continental margin. Marine Micropaleontology 29, 211–236.

Schönfeld, J., 2002. A new benthic foraminiferal proxy for near-bottom current velocities in the Gulf of Cadiz, northeastern Atlantic Ocean. Deep Sea Research Part I: Oceanographic Research Papers 49, 1853–1875.

Scott, D.B., Medioli, F. S. and Schafer, C.T., 2001. Monitoring in coastal environments using foraminifera and thecamoebian indicators. Cambridge University Press, 177 pp.

Scott, G.A., Scourse, J.D. and Austin, W.E.N., 2003. The distribution of benthic foraminifera in the Celtic Sea: the significance of seasonal stratification. The Journal of Foraminiferal Research 33, 32–61.

Sen Gupta, B.K., 1999. Modern Foraminifera. Springer Netherlands, 371 pp.

Sexton, P.F., Wilson, P.A., and Norris, R.D., 2006. Testing the Cenozoic multisite composite δ18O and δ13C curves: New monospecific Eocene records from a single locality, Demerara Rise (Ocean Drilling Program Leg 207). Paleoceanography 21, PA2019.

Sexton, P.F., Norris, R.D., Wilson, P.A., Pälike, H., Westerhold, T., Röhl, U., Bolton, C.T., and Gibbs, S., 2011. Eocene global warming events driven by ventilation of oceanic dissolved organic carbon. Nature 471, 349–352.

Shackleton, N.J., and Kennett, J.P., 1975. Paleotemperature history of the Cenozoic and the initiation of Antarctic glaciation: Oxygen and carbon isotope analyses in DSDP sites 277, 279, and 281. In: Kennett, J.P., Houtz, R.E., et al. (Eds.), Initial Reports of the Deep Sea Drilling Project, 29.

Shannon, C.E., 1948. A Mathematical Theory of Communication. The Bell System Technical Journal 27, 379–423.

Sluijs, A., Bowen, G.J., Brinkhuis, H., Lourens, L.J., and Thomas, E., 2007. The Palaeocene–Eocene Thermal Maximum super greenhouse: biotic and geochemical signatures, age models and mechanisms of global change. In: Williams, M., Haywood, A.M., Gregory, F.J., and Schmidt, D.N. (Eds.), Deep-time perspectives on climate change: Marrying the signal from computer models and biological proxies. The Geological Society of London on behalf of The Micropalaeontological Society, 323–349.

Sluijs, A., Schouten, S., Donders, T.H., Schoon, P.L., Röhl, U., Reichart, G.-J., Sangiorgi, F., Kim, J.-H., Sinninghe Damsté, J.S., and Brinkhuis, H., 2009. Warm and wet conditions in the Arctic region during Eocene Thermal Maximum 2. Nature Geoscience 2, 777–780.

Sluijs, A., Zachos, J.C., and Zeebe, R.E., 2012. Constraints on hyperthermals. Nature Geoscience 5, 231.

Sluijs, A., Zeebe, R.E., Bijl, P.K., and Bohaty, S.M., 2013. A middle Eocene carbon cycle conundrum. Nature Geoscience 6, 429–434.

Smart, C.W., King, S.C., Gooday, A.J., Murray, J.W., and Thomas, E., 1994. A benthic foraminiferal proxy of pulsed organic matter paleofluxes. Marine Micropaleontology 23, 89–99.

Smart, C.W., Thomas, E., and Ramsay, A.T.S., 2007. Middle–late Miocene benthic foraminifera in a western equatorial Indian Ocean depth transect: Paleoceanographic implications. Palaeogeography, Palaeoclimatology, Palaeoecology 247, 402–420.

Snider, L.J., Burnet, B.R., and Hessler, R.R., 1984. The composition and distribution of meiofauna and nanobiota in a central North Pacific deep-sea area. Deep-Sea Research I 31, 1225-1249.

Speijer, R.P., 1994. Extinction and recovery patterns in benthic foraminiferal paleocommunities across the Cretaceous/Paleogene and Paleocene/Eocene boundaries, (Doctoral thesis, Universiteit Utrecht, Utrecht).

Spindler, M., 1980. The pelagic gulfweed *Sargassum natans* as a habitat for the benthic foraminifera *Planorbulina acervalis* and *Rosalina globularis*. Neues Jahrbuch für Geologie und Paläntologie Monatheft 9, 569–80.

Spofforth, D.J.A., Agnini, C., Pälike, H., Rio, D., Fornaciari, E., Giusberti, L., Luciani, V., Lanci, L., and Muttoni, G., 2010. Organic carbon burial following the middle Eocene climatic optimum in the central western Tethys. Paleoceanography 25, PA3210.

Sprong, J., Kouwenhoven, T.J., Bornemann, A., Schulte, P., Stassen, P., Steurbaut, E., Youssef, M., and Speijer, R.P., 2012. Characterization of the Latest Danian Event by means of benthic foraminiferal assemblages along a depth transect at the southern Tethyan margin (Nile Basin, Egypt). Marine Micropaleontology 86–87, 15–31.

Sprong, J., Kouwenhoven, T.J., Bornemann, A., Dupuis, C., Speijer, R.P., Stassen, P., and Steurbaut, E., 2013. In search of the Latest Danian Event in a paleobathymetric transect off Kasserine Island, north-central Tunisia. Palaeogeography, Palaeoclimatology, Palaeoecology 379–380, 1–16.

Stap, L., Lourens, L., van Dijk, A., Schouten, S., and Thomas, E., 2010a. Coherent pattern and timing of the carbon isotope excursion and warming during Eocene Thermal Maximum 2 as recorded in planktic and benthic foraminifera. Geochemistry, Geophysics, Geosystems 11, Q11011.

Stap, L., Lourens, L.J., Thomas, E., Sluijs, A., Bohaty, S., and Zachos, J.C., 2010b. High-resolution deep-sea carbon and oxygen isotope records of Eocene Thermal Maximum 2 and H2. Geology 38, 607–610.

Suto, I., 2006. The explosive diversification of the diatom genus Chaetoceros across the Eocene/Oligocene and Oligocene/Miocene boundaries in the Norwegian Sea. Marine Micropaleontology 58, 259–269.

Thiel, H., Schriever, G., Lochte, K., Gooday, A.J., Hemleben, C., Manidura, R.F.G., and Turley, C.M., 1988. Phytodetritus on the Deep-Sea Floor in a Central Oceanic Region of the Northeast Atlantic. Biological Oceanography 6, 203–239.

Thomas, E., 1985. Late Eocene to recent deep-sea benthic foraminifers from the Central Equatorial Pacific Ocean. In: Mayer, L., and Theyer, F., et al. (Eds.), Initial Reports of the Deep Sea Drilling Project 85. U.S. Government Printing Office, 655-694.

Thomas, E., 1989. Development of Cenozoic deep-sea benthic foraminiferal faunas in Antarctic waters. Geological Society Special Publications 47, 283–296.

Thomas, E., 1990. Late Cretaceous through Neogene Deep-sea benthic foraminifers (Maud Rise, Weddell Sea, Antarctica). In: Barker, P.E., and Kennett, J.P. (Eds.), Proceedings of the Ocean Drilling Program, Scientific Results. Texas A&M University, 571–594.

Thomas, E., 1992. Middle Eocene-Late Oligocene Bathyal Benthic Foraminifera (Weddell Sea): Faunal Changes and Implications for Ocean Circulation. In: Prothero, D.R., and Berggren, W.A. (Eds.), Eocene-Oligocene Climatic and Biotic Evolution. Princeton University Press, 245-271.

Thomas, E., 1998. The biogeography of the Late Paleocene benthic foraminiferal extinction. In: Aubry, M.P., Lucas, S., and Berggren, W.A. (Eds.), Late Paleocene-Early Eocene Biotic and Climatic Events in the Marine and Terrestial Records. Columbia University Press, 214–243.

Thomas, E., 2003. Extinction and food at the seafloor: A high-resolution benthic foraminiferal record across the initial Eocene thermal maximum, Southern Ocean site 690. In: Scott, L.W., Gingerich, P.D.., Schmitz, B., and Thomas, E. (Eds.), Causes and Consequences of Globally Warm Climates in the Early Paleogene. Geological Society of America Special Paper 369, 319–332.

Thomas, E., 2007. Cenozoic mass extinctions in the deep sea: What perturbs the largest habitat on Earth? In: Monechi, S., Coccioni, R., and Rampino, M. (Eds.), Large Ecosystem Perturbations: Causes and Consequences. Geological Society of America Special Paper 424, 1–23.

Thomas, E., and Gooday, A.J., 1996. Cenozoic deep-sea benthic foraminifers: Tracers for changes in oceanic productivity? Geology 24, 355.

Thomas, E., and Shackleton, N.J., 1996. The Paleocene-Eocene benthic foraminiferal extinction and stable isotope anomalies. Geological Society London Special Publications 101, 401–441.

Thomas, E., Zachos, J.C., and Bralower, T.J., 2000. Deep-sea environments on a warm earth: latest Paleocene-early Eocene. In: Huber, B.T., Macleod, K.G., and Wing, S.L. (Eds.), Warm Climates in Earth History. Cambridge University Press, 132–160.

Thomas, E., Boscolo-Galazzo, F., Balestra, B., Monechi, S., Donner, B., and Röhl, U., 2018. Early Eocene Thermal Maximum 3: biotic response at Walvis Ridge (SE Atlantic Ocean). Paleoceanography and Paleoclimatology 33, 862–883.

Tipple, B.J., Pagani, M., Krishnan, S., Dirghangi, S.S., Galeotti, S., Agnini, C., Giusberti, L., and Rio, D., 2011. Coupled high-resolution marine and terrestrial records of carbon and hydrologic cycles variations during the Paleocene–Eocene Thermal Maximum (PETM). Earth and Planetary Science Letters 311, 82–92.

Titelboim, D., Almogi-Labin, A., Herut, B., Kucera, M., Schmidt, C., Hyams-Kaphzan, O., Ovadia, O., and Abramovich, S., 2016. Selective responses of benthic foraminifera to thermal pollution. Marine Pollution Bulletin 105, 324–336.

Tjalsma, R.C., and Lohmann, G.P., 1983. Paleocene - Eocene Bathyal and Abyssal Benthic Foraminifera from the Atlantic Ocean. Micropaleontology Special Edition, 89 pp.

Tripati, A., Backman, J., Elderfield, H., and Ferretti, P., 2005. Eocene bipolar glaciation associated with global carbon cycle changes. Nature 436, 341–346.

Tsuchiya, M., Kitazato, H. and Pawlowski, J., 2000. Phylogenetic relationships among species of Glabratellidae (Foraminifera) inferred from ribosomal DNA sequences: comparison with morphological and reproductive data. Micropaleontology 46 (Supplement 1), 13–20.

Uthicke, S., Momigliano, P., and Fabricius, K.E., 2013. High risk of extinction of benthic foraminifera in this century due to ocean acidification. Scientific Reports 3, 1769.

Van Andel, T.H., 1975. Mesozoic/cenozoic calcite compensation depth and the global distribution of calcareous sediments. Earth and Planetary Science Letters 26, 187–194.

Van der Zwaan, G.J., Duijnstee, I.A.P., Den Dulk, M., Ernst, S.R., Jannink, N.T., and Kouwenhoven, T.J., 1999. Benthic foraminifers: proxies or problems?: a review of paleocological concepts. Earth-Science Reviews 46, 213–236.

Van Morkhoven, F.P.C.M., Berggren, W.A., and Edwards, A.S., 1986. Cenozoic cosmopolitan deep-water benthic foraminifera. Elf-Aquitaine, 421 pp.

Vandenberghe, N., Hilgen, F.J., and Speijer, R.P., 2012. The Paleogene Period. In: Gradstein, F.M., Ogg, J.G., Schmitz, M., and Ogg, G. (Eds), The Geologic Time Scale. Elsevier, 855–921.

Vénec-Peyré, M.T. and Le Calvez, Y. 1986. Foraminifères benthiques et phénomenès de transfert; importance des études comparatives de la biocénose et de la thanatocénose. Annales de l'Institut Océanographique 57, 79–110.

Verity, P.G., Smetacek, V., and Smayda, T., 2002. Status, trends and the future of the marine pelagic ecosystem. Environmental conservation 29, 207–237.

Villa, G., Fioroni, C., Pea, L., Bohaty, S., and Persico, D., 2008. Middle Eocene–late Oligocene climate variability: Calcareous nannofossil response at Kerguelen Plateau, Site 748. Marine Micropaleontology 69, 173–192.

Wade, B.S., and Kroon, D., 2002. Middle Eocene regional climate instability: Evidence from the western North Atlantic. Geology 30, 1011–1014.

Wade, B.S., and Pälike, H., 2004. Oligocene climate dynamics. Paleoceanography 19, PA4019.

Wade, B.S., and Pearson, P.N., 2008. Planktonic foraminiferal turnover, diversity fluctuations and geochemical signals across the Eocene/Oligocene boundary in Tanzania. Marine Micropaleontology 68, 244-255.

Wade, B.S., Pearson, P.N., Berggren, W.A., and Pälike, H., 2011. Review and revision of Cenozoic tropical planktonic foraminiferal biostratigraphy and calibration to the geomagnetic polarity and astronomical time scale. Earth-Science Reviews 104, 111–142.

Weinmann, A.E., and Langer, M.R., 2017. Diverse thermotolerant assemblages of benthic foraminiferal biotas from tropical tide and rock pools of eastern Africa. Revue de Micropaléontologie 60, 511–523.

Westerhold, T., and Röhl, U., 2013. Orbital pacing of Eocene climate during the Middle Eocene Climate Optimum and the chron C19r event: Missing link found in the tropical western Atlantic: Orbital Pacing of Eocene Climate. Geochemistry, Geophysics, Geosystems 14, 4811–4825.

Westerhold, T., Röhl, U., Laskar, J., Raffi, I., Bowles, J., Lourens, L.J., and Zachos, J.C., 2007. On the duration of magnetochrons C24r and C25n and the timing of early Eocene global warming events: Implications from the Ocean Drilling Program Leg 208 Walvis Ridge depth transect. Paleoceanography 22, PA2201.

Westerhold, T., Röhl, U., Pälike, H., Wilkens, R., Wilson, P.A., and Acton, G., 2014. Orbitally tuned timescale and astronomical forcing in the middle Eocene to early Oligocene. Climate of the Past 10, 955–973.

Westerhold, T., Röhl, U., Frederichs, T., Bohaty, S.M., and Zachos, J.C., 2015. Astronomical calibration of the geological timescale: closing the middle Eocene gap. Climate of the Past 11, 1181–1195.

Westerhold, T., Röhl, U., Donner, B., Frederichs, T., Kordesch, W.E.C., Bohaty, S.M., Hodell, D.A., Laskar, J., and Zeebe, R.E., 2018. Late Lutetian Thermal Maximum-Crossing a Thermal Threshold in Earth's Climate System? Geochemistry, Geophysics, Geosystems 19, 73–82.

Westerhold, T., Marwan, N., Drury, A.J., Liebrand, D., Agnini, C., Anagnostou, E., Barnet, J.S.K., Bohaty, S.M., De Vleeschouwer, D., Florindo, F., Frederichs, T., Hodell, D.A., Holbourn, A.E., Kroon, D., Lauretano, V., Littler, K., Lourens, L.J., Lyle, M., Pälike, H., Röhl, U., Tian, J., Wilkens, R.H., Wilson, P.A., and Zachos, J.C., 2020. An astronomically dated record of Earth's climate and its predictability over the last 66 million years. Science 369, 1383–1387.

Wing, S.L., 2005. Transient floral change and rapid global warming at the Paleocene-Eocene boundary. Science 310, 993–996.

Wollenburg, J.E. and Mackensen, A. 1998. On the vertical distribution of the living (rose Bengal stained) benthic foraminifers in the Arctic Ocean. Journal of Foraminiferal Research 28, 268–85.

Wynn, R.B., Weaver, P.P.E., Masson, D.G., and Stow, D.A.V., 2002. Turbidite depositional architecture across three interconnected deep-water basins on the north-west African margin. Sedimentology 49, 669–695.

Zachos, J.C., 2001. Trends, rhythms, and aberrations in global climate 65 Ma to present. Science 292, 686–693.

Zachos, J.C., 2005. Rapid acidification of the ocean during the Paleocene-Eocene Thermal Maximum. Science 308, 1611–1615.

Zachos, J.C., Stott, L.D., and Lohmann, K.C., 1994. Evolution of Early Cenozoic marine temperatures. Paleoceanography 9, 353–387.

Zachos, J.C., Quinn, T.M., and Salamy, K.A., 1996. High-resolution (10^4 years) deep-sea foraminiferal stable isotope records of the Eocene-Oligocene climate transition. Paleoceanography 11, 251–266.

Zachos, J.C., Schouten, S., Bohaty, S., Quattlebaum, T., Sluijs, A., Brinkhuis, H., Gibbs, S.J., and Bralower, T.J., 2006. Extreme warming of mid-latitude coastal ocean during the Paleocene-Eocene Thermal Maximum: Inferences from TEX86 and isotope data. Geology 34, 737.

Zachos, J.C., Dickens, G.R., and Zeebe, R.E., 2008. An early Cenozoic perspective on greenhouse warming and carbon-cycle dynamics. Nature 451, 279–283.

Zachos, J.C., McCarren, H., Murphy, B., Röhl, U., and Westerhold, T., 2010. Tempo and scale of late Paleocene and early Eocene carbon isotope cycles: Implications for the origin of hyperthermals. Earth and Planetary Science Letters 299, 242–249.

Zeebe, R.E., Westerhold, T., Littler, K., and Zachos, J.C., 2017. Orbital forcing of the Paleocene and Eocene carbon cycle. Paleoceanography 32, 440–465.

Appendices

Appendix I: Information about the published articles

Grira, C., Karoui-Yaakoub, N., Hédi Negra, M., Rivero-Cuesta, L., and Molina, E., 2018. Paleoenvironmental and ecological changes during the Eocene-Oligocene transition based on foraminifera from the Cap Bon Peninsula in North East Tunisia. *Journal of African Earth Sciences*, 143, 145-161.

Journal Impact Factor (Journal Citations Reports): 0.889 in Geosciences multidisciplinary.
The doctoral candidate contributed to the classification of benthic foraminifera and the interpretation and discussion of results.

Rivero-Cuesta, L., Molina, E., and Alegret, L., 2018. Eocene (Bartonian) benthic foraminifera and paleoenvironmental changes in the Western Tethys. *Palaeogeography, Palaeoclimatology, Palaeoecology*, 503, 102-111.

Journal Impact Factor (Journal Citations Reports): 2.833 in Paleontology. The doctoral candidate picked and classified the benthic foraminiferal specimens, picked and prepared the isotope samples, carried out the statistical analyses, created the figures, took SEM images and wrote the paper.

Rivero-Cuesta, L., Westerhold, T., Agnini, C., Dallanave, E., Wilkens, R., and Alegret, L., 2019. Paleoenvironmental changes at ODP Site 702 (South Atlantic): anatomy of the Middle Eocene Climatic Optimum. *Paleoceanography and Paleoclimatology*, 34, PA003806.

Journal Impact Factor (Journal Citations Reports): 2.888/Paleontology. The doctoral candidate picked, classified and measured the benthic foraminiferal specimens, picked and prepared the isotope and carbonate samples, carried out statistical analyses, created figures (except magnetostratigraphy, age model and nannofossil data) and wrote the paper (except coauthor's results and materials and methods used by them).

Rivero-Cuesta, T. Westerhold, L., and Alegret, L., 2020. The Late Lutetian Thermal Maximum (middle Eocene): first record of deep-sea benthic foraminifera response. Palaeogeography, Palaeoclimatology, Palaeoecology, 545, 109637.

Journal Impact Factor (Journal Citations Reports): 2.833 in Paleontology. The doctoral candidate picked and classified the benthic foraminiferal specimens, carried out the statistical analyses, created the figures, took SEM images and wrote the paper.

Cotton, L., Rivero-Cuesta, L., Franceschetti, G., Iakovleva, A., Alegret, L., Dinarès-Turell, J., Hooker, L., King, C., Fluegeman, R., Yager, S., and Monechi, S., 2020. Reassessing the Bartonian unit stratotype at Alum Bay (Isle of Wight, UK): an integrated approach. Newsletters on Stratigraphy, 54(1), 17-42.

Journal Impact Factor (Journal Citations Reports): 3.025 in Geology. The doctoral candidate picked and classified the small benthic foraminiferal specimens, prepared the dinoflagellates and large benthic foraminifera samples, carried out statistical analyses, interpretation and discussion from the small benthic foraminifera data, created figures (stratigraphic column and small benthic data), took SEM images and wrote the parts of the paper related to the small benthic foraminifera.

Appendix II: Supplementary material (Rivero-Cuesta et al., 2020)

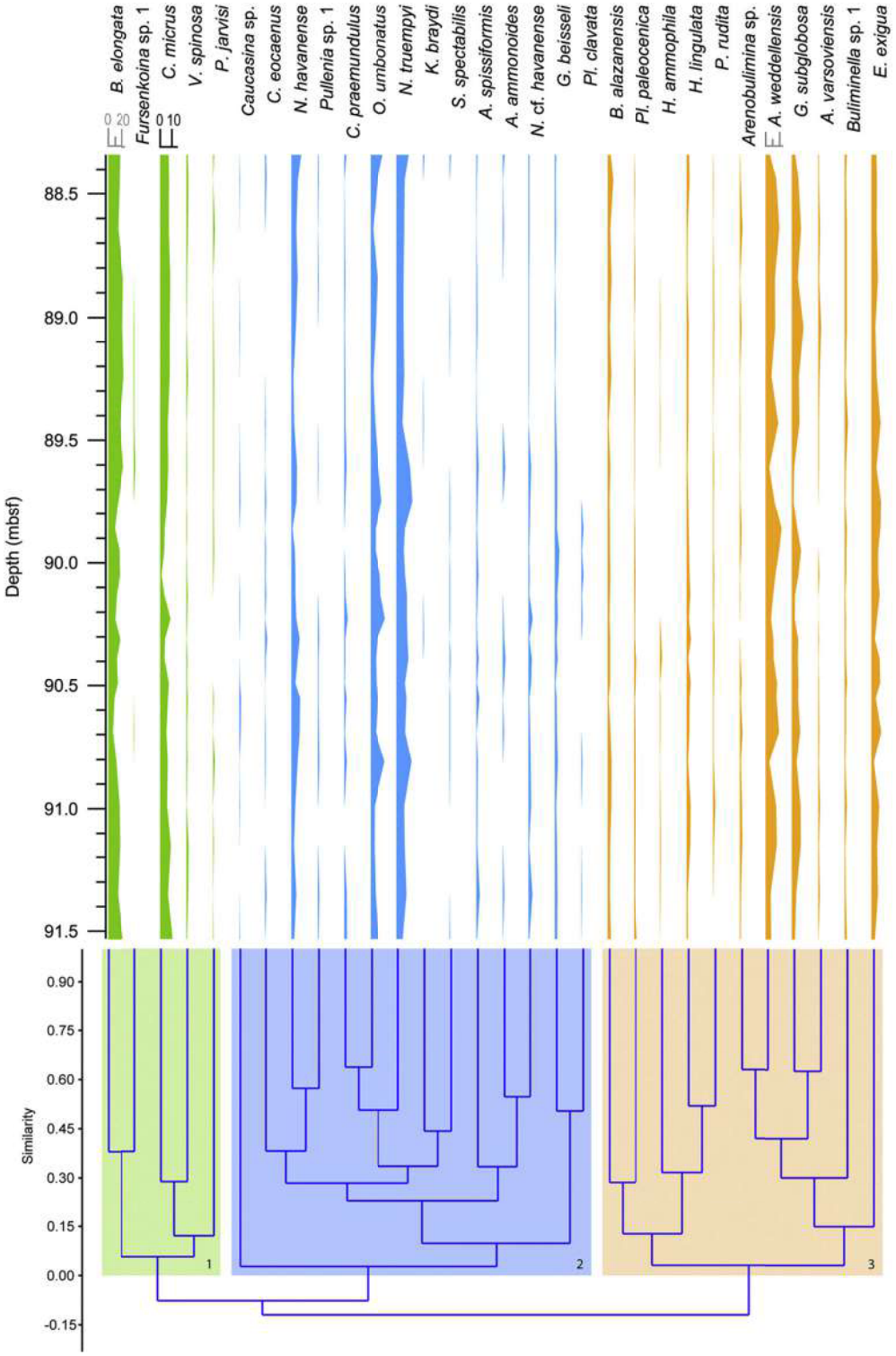

Supplementary Figure 1. Hierarchical cluster analysis of the benthic foraminiferal assemblages at Site 702 across the LLTM event. Three clusters (1, 2, and 3) have been differentiated according to similarity >0. Plots show the relative abundance of each of the 30 species included in the cluster analysis.

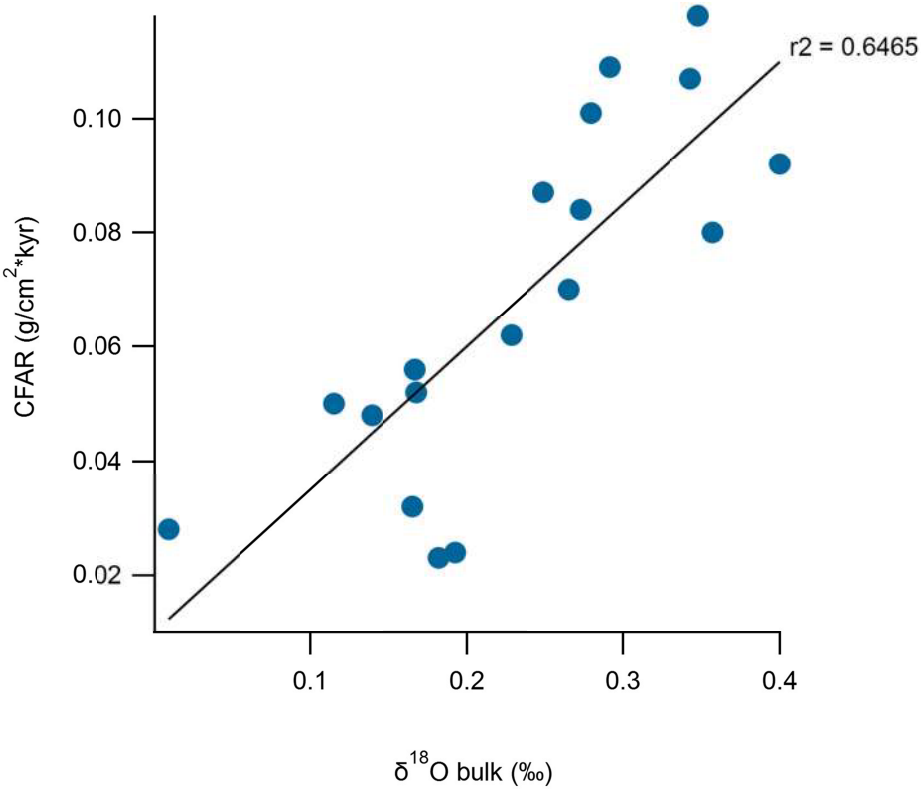

Supplementary Figure 2. Cross-plot of $\delta^{18}O$ values in bulk sediment (in ‰, data from Westerhold et al., 2018) against the coarse fraction accumulation rate (CFAR in $g/cm^2 * kyr$, this study). The regression line is shown ($r^2 = 0.6465$).

Supplementary Table 2 containing benthic foraminiferal data from Site 702 across the LLTM (relative abundances of all the species identified and the environmental indices calculated) can be found in a separate Excel file (Appendices folder).

Appendix III: Supplementary material (Rivero-Cuesta et al., 2019)

Supporting information Tables S1, S2 and S3 can be found in a separate Excel file (Appendices folder).

Paleoceanography and Paleoclimatology

Supporting Information for

Paleoenvironmental changes at ODP Site 702 (South Atlantic): anatomy of the Middle Eocene Climatic Optimum

L. Rivero-Cuesta[1], T. Westerhold[2], C. Agnini[3], E. Dallanave[4], R. H. Wilkens[5] and L. Alegret[1]

[1]Departamento de Ciencias de la Tierra & Instituto Universitario de Ciencias Ambientales, Universidad de Zaragoza, Zaragoza, Spain, [2]MARUM – Center for Marine Environmental Sciences, University of Bremen, Bremen, Germany, [3]Dipartamento di Geoscienze, Università di Padova, Padua, Italy, 4Faculty of Geosciences of Bremen, Bremen, Germany, [5]Hawaii Institute of Geophysics & Planetology, University of Hawaii, Honolulu, HI, USA.

Contents of this file

Figures S1 to S8 with captions
Tables S3 and S4 with captions

Additional Supporting Information (Files uploaded separately)

Captions for Tables S1, S2 and S5 (larger than 1 page, upload as separate files)

Introduction

This supporting information file contains graphic visualization of data generated during this study that are named and/or used in the material and methods, results and/or discussion sections in a derived or secondary way and hence not included in the main article. Small tables have also been included in this file, however large datasets can be found as separate .xlsx files (captions in this document). Scanning Electron Microscope (SEM) images of the most relevant benthic foraminiferal species cited in the main text are shown here too.

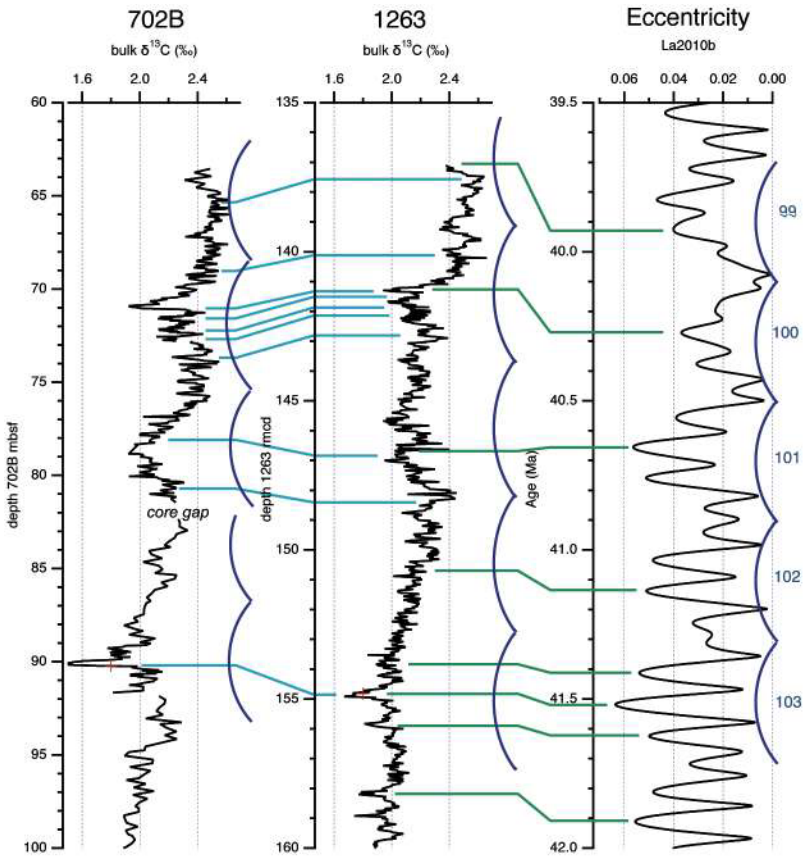

Figure S1. Hole 702B age model derived from calibrated age model of Site 1263. Tie points between both sites (blue lines) and cyclicity tuning points (green lines) ages are shown.

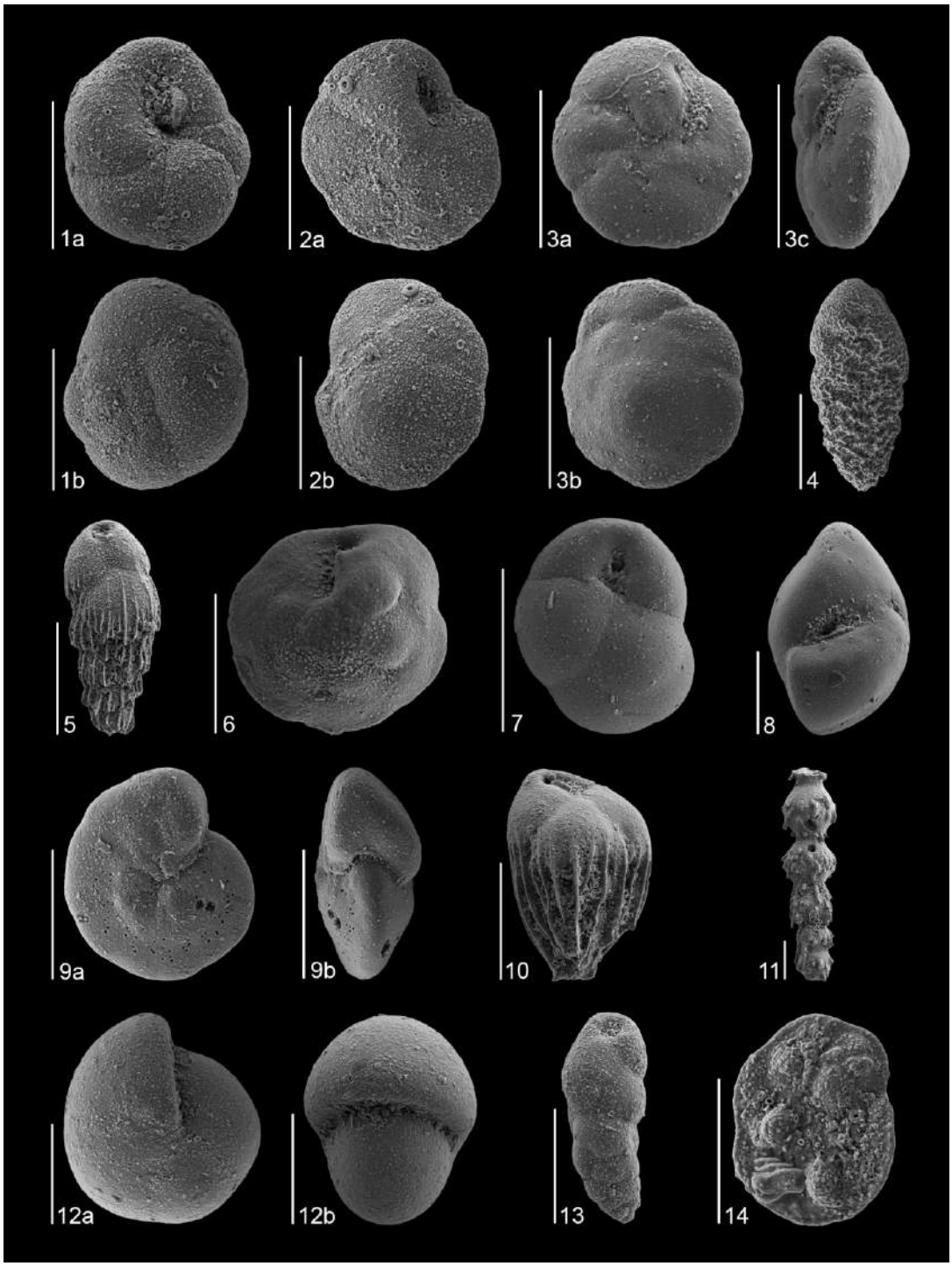

Figure S2. SEM images of most abundant (> 3%) benthic foraminiferal species at Site 702. 1, *Caucasina* sp.: a) ventral, b) dorsal; 2, *Epistominella exigua*: a) ventral, b) dorsal; 3, *Alabaminella weddellensis*: a) ventral, b) dorsal, c) apertural; 4, *Bulimina* cf. *huneri*; 5, *Fursenkoina* sp. 2; 6, *Nuttallides truempyi*: ventral; 7, *Globocassidulina subglobosa*; 8, *Oridorsalis umbonatus*: apertural; 9, Cibicidoides micrus: a) dorsal, b) apertural; 10, *Bulimina alazanensis*; 11, *Stilostomella subspinosa*; 12, *Pullenia* sp. 1: a) lateral, b) apertural; 13. *Bulimina elongata*; 14, *Heronallenia lingulata*. All scale bars = 100 μm.

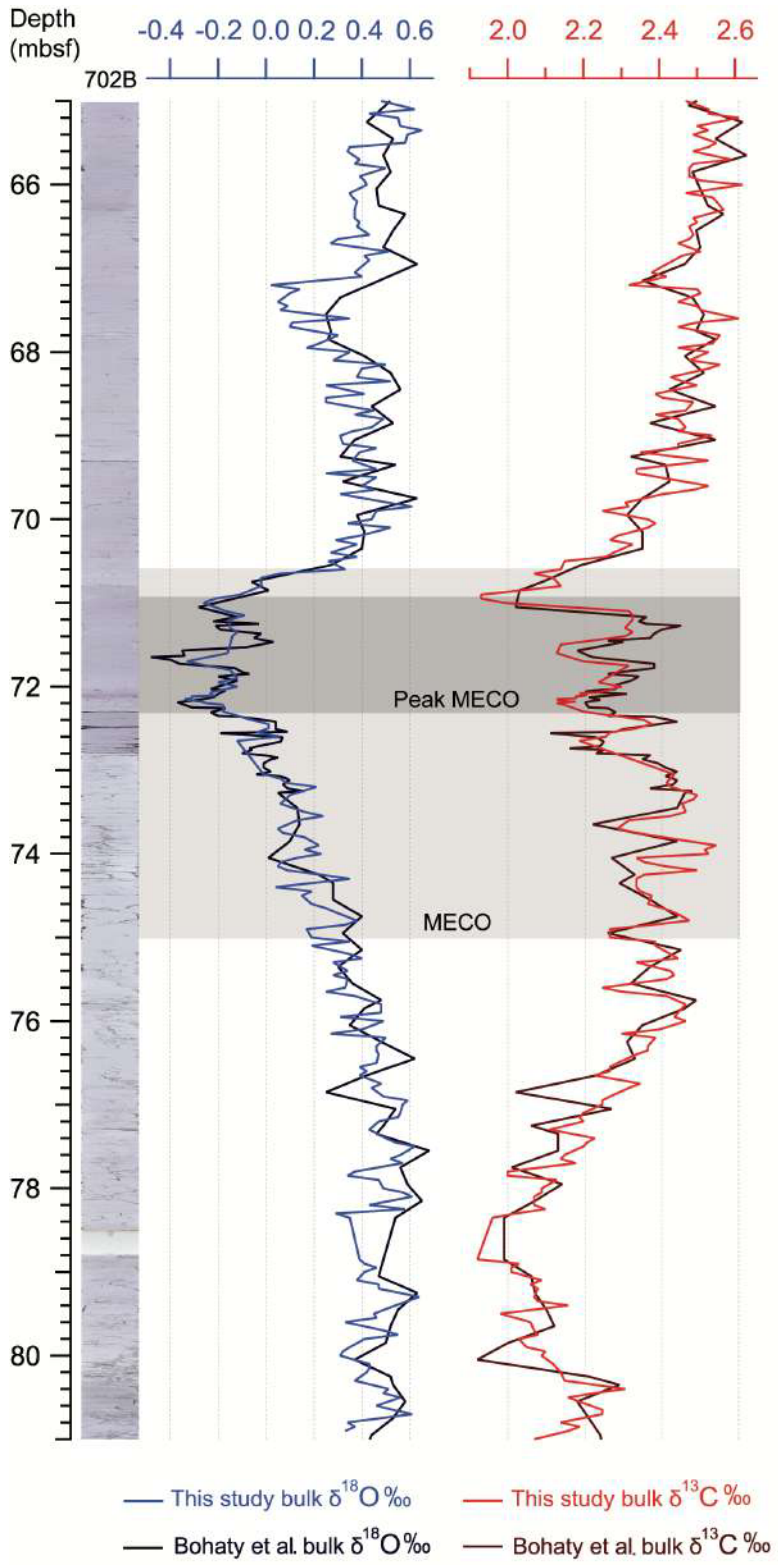

Figure S3. ODP Site 702 isotopic records (bulk) plotted against depth (mbsf) across the MECO. Darker lines correspond to data from Bohaty et al. 2009. Brighter lines correspond to bulk isotopic data generated in this study.

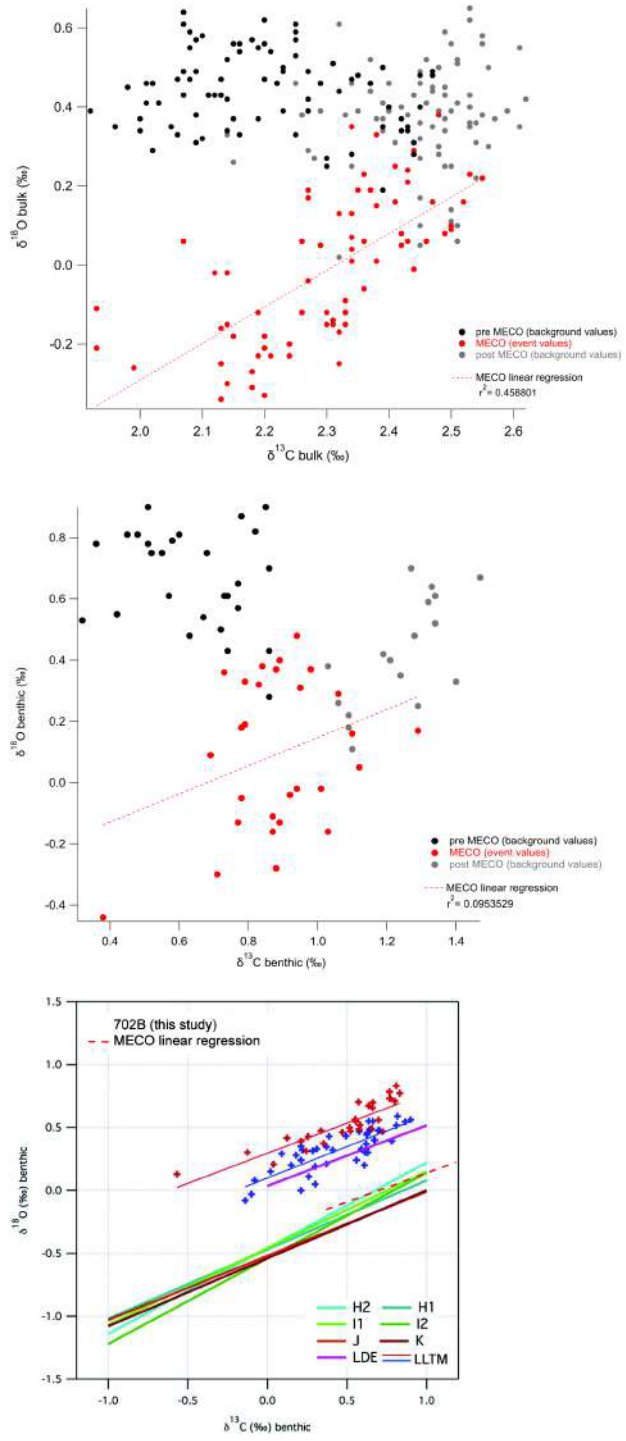

Figure S4. Oxygen *vs.* carbon cross-plots of bulk (a) and benthic (b) isotope analysis. Samples are color-coded in background and event values (see legend). MECO linear regressions (red dashed lines) and r^2 correlation values are shown; c) comparison of our benthic isotopic data and the resulting MECO linear regression (red dashed line) with several early and middle Eocene hyperthermal events from Westerhold et al. 2018 (see figure caption and references therein for details).

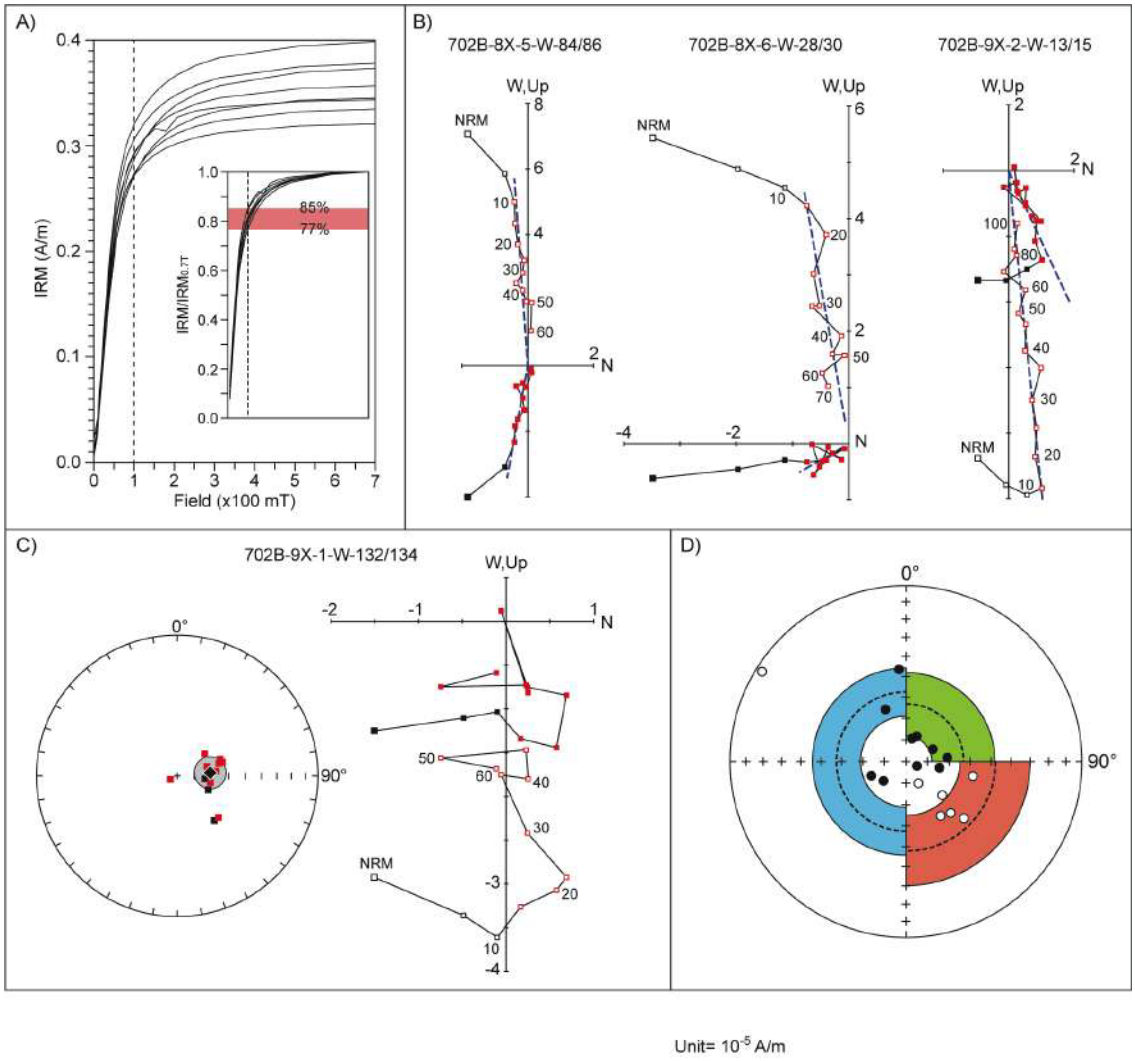

Figure S5. Rock- and paleomagnetism results. A) Isothermal remanent acquisition (IRM) of 8 representative samples up to 0.7 T; the inset shows the same data normalized by the maximum IRM (IRM0.7T); all samples reach between 77% and 85% of the IRM0.7T within 100 mT of inducing field. B, C) Representative vector end-point demagnetization diagrams with characteristic remanent directions isolated by (B) linear interpolation (Kirschvink, 1980) or (C) Fisher (1953) mean; the diagram of panel C is shown together with the equal-area projection, where the diamond represent the average direction with associated 95% confidence circle; in all diagrams, open and filled symbols are the projection onto the vertical and the horizontal plane, respectively; demagnetization steps unit is in mT, while the axes unit is 10-5 A/m; N= north; W, Up= west and up. D) Stereographic projection of the characteristic remanent magnetization (ChRM) directions; open and filled circles are negative (up-pointing) and positive (down-pointing) directions, respectively; average inclinations with associated 95% confidence boundaries (McFadden and Reid, 1982) are represented by the red (negative directions), green (positive directions) and blue (all directions plotted on a common polarity) hemicycles.

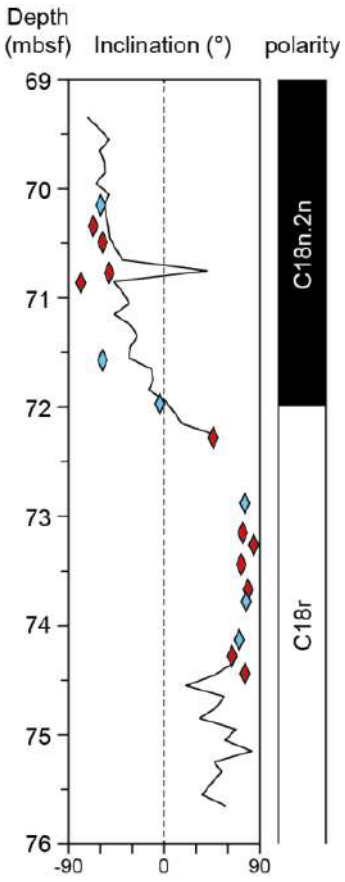

Figure S6. Inclination of the paleomagnetic vectors plotted versus depth (mbsf); red diamonds are inclination derived by linear interpolation of vector end-points (Kirschvink, 1980), while blue diamonds are inclination derived by calculating spherical mean (Fisher, 1953) of vector end-points failing to trend linearly to the origin of the demagnetization axes. Data are shown together with archive-halves measurement (Clement and Hailwood, 1991). Magnetostratigraphic interpretation is shown on the right-hand panel.

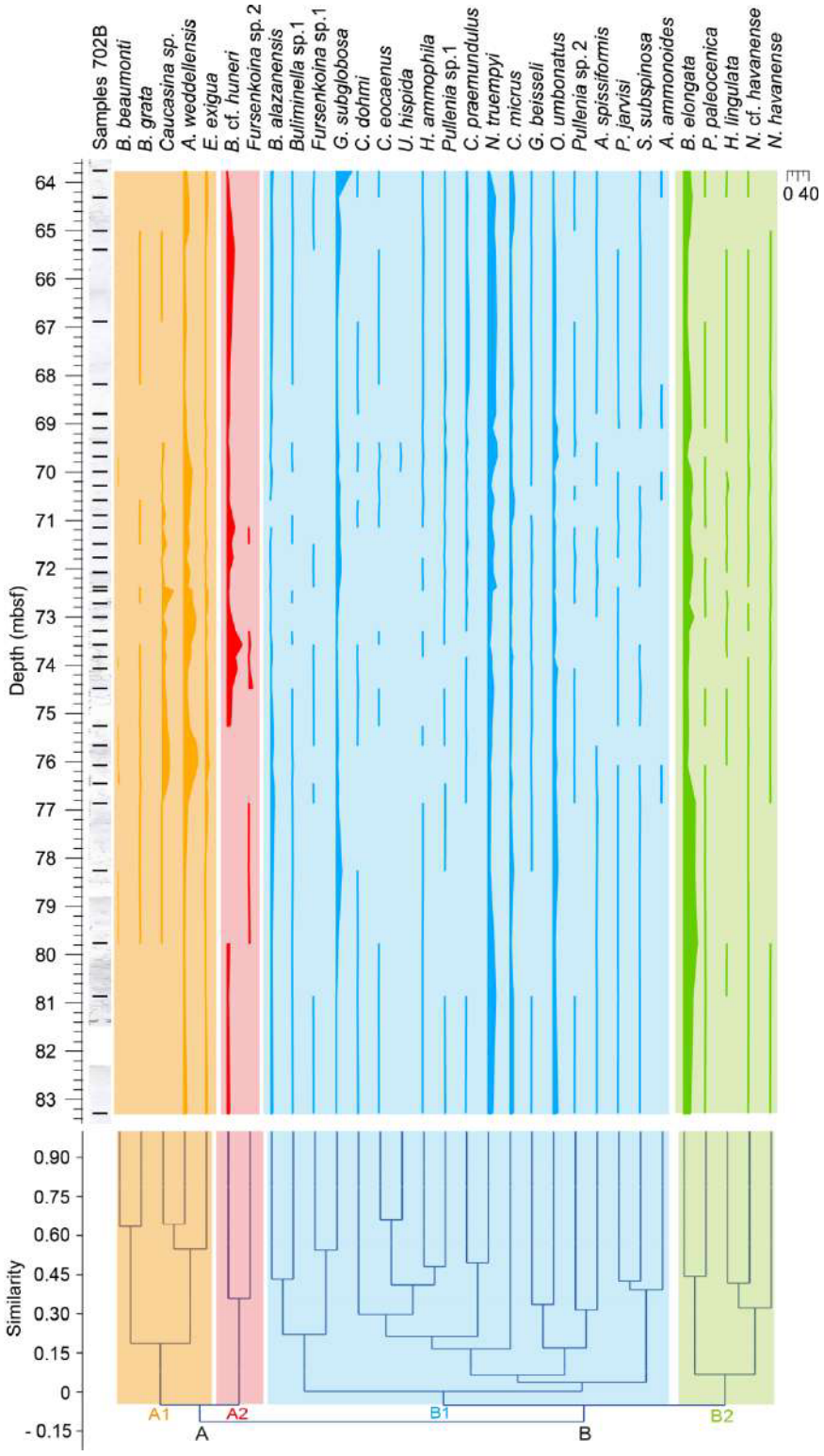

Figure S7. Relative abundances of most representative (>1.5 %) benthic foraminiferal species against depth (mbsf) at ODP Site 702. At the bottom of the figure are shown the species grouped into 4 subclusters (A1, A2, B1 and B2) according to cluster analysis (Pearson similarity index and unweighted pair group method with arithmetic mean, PAST Software).

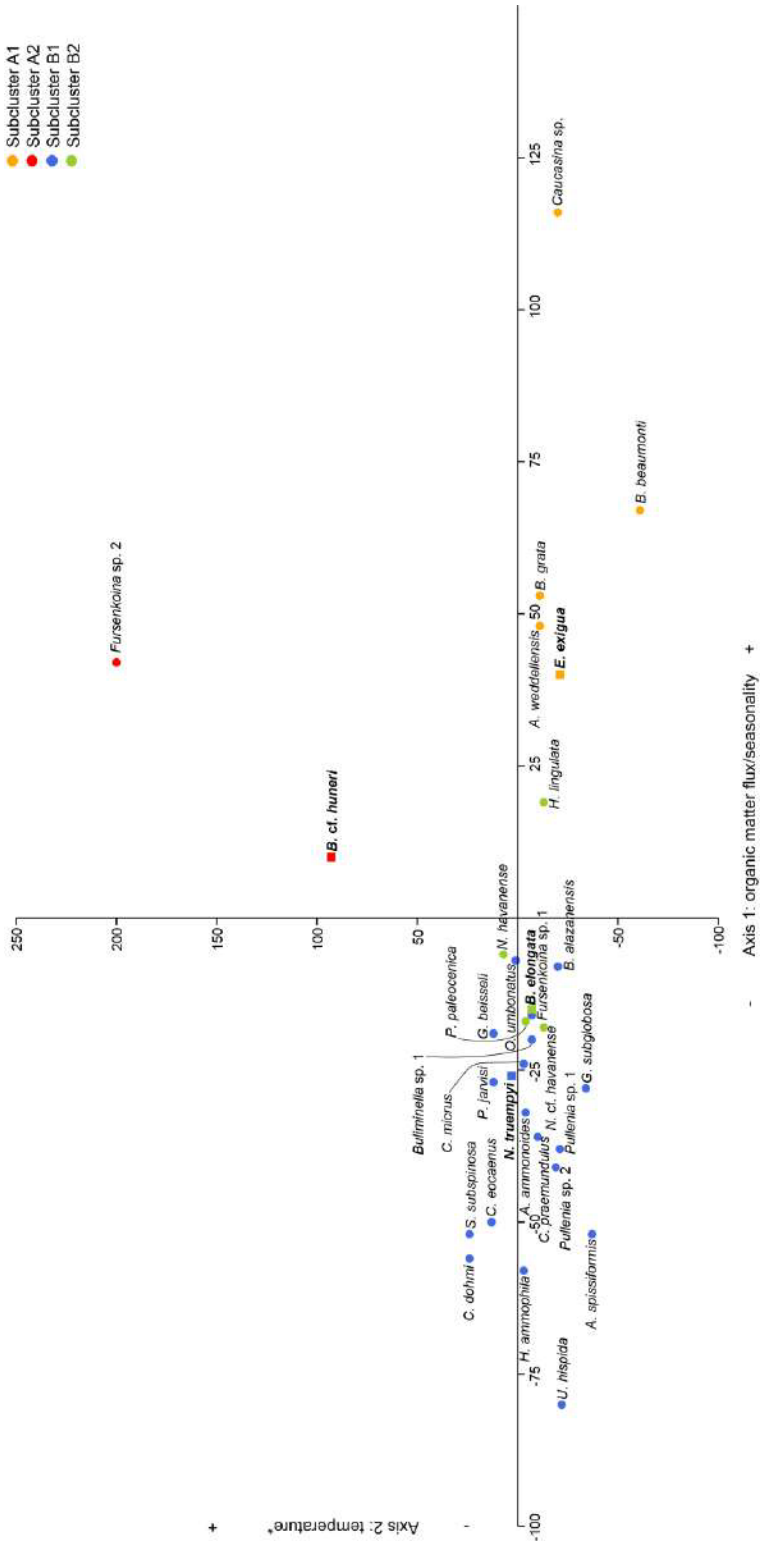

Figure S8. DCA analysis (Q-mode) of benthic foraminiferal species (n =31). Species are color-coded according to the subclusters from the hierarchical cluster analysis (see legend). Squares highlights the dominant species of each subcluster, circles are used for the rest of the species.

Table S1. Stable isotope analysis from Site 702, bulk (sheet 1) and benthic (sheet 2). Includes errors and corrections of the measurements.

Table S2. Benthic foraminiferal data from Site 702 across the MECO. Sheet 1: relative abundances of all the species identified and environmental indices calculated. Sheet 2: measurements of *B. elongata*. Sheet 3: benthic foraminiferal accumulation rates. Sheet 4: coarse fraction accumulation rates.

Site	Hole	Core	Section	Top-Depth	Bottom-Depth	MBSF_Top	NRM intensity	N	Dec	Inc	MAD	Anchored	k	R	a95
702	B	8	5	84	86	70.14	4.096E-05	8	147.45	-59.94			31.21	7.78	10.07
702	B	8	5	103	105	70.33	7.231E-05	9	132.91	-67.05	5.81	yes			
702	B	8	5	118	120	70.48	8.330E-05	10	102.26	-58.03	6.76	no			
702	B	8	5	146	148	70.76	4.380E-05	9	134.50	-51.96	13.82	no			
702	B	8	6	5	7	70.85	6.493E-05	10	150.31	-78.47	4.97	yes			
702	B	8	6	76	78	71.56	2.375E-05	9	139.07	-58.16			12.29	8.35	15.29
702	B	8	6	116	118	71.96	2.580E-05	8	302.00	-3.98			31.89	7.78	9.96
702	B	8	6	147	149	72.27	1.590E-04	8	355.66	46.37	8.88	no			
702	B	9	1	7	9	72.87	3.894E-05	7	229.34	76.27			26.48	6.77	11.95
702	B	9	1	34	36	73.14	5.405E-05	9	100.38	74.24	6.98	yes			
702	B	9	1	45	47	73.25	3.936E-05	9	111.76	84.55	10.74	no			
702	B	9	1	63	65	73.43	3.221E-05	9	247.85	72.72	10.01	yes			
702	B	9	1	86	88	73.66	5.499E-05	10	14.29	79.09	3.68	yes			
702	B	9	1	97	99	73.77	6.451E-05	9	22.97	77.36			37.28	8.79	8.54
702	B	9	1	132	134	74.12	3.519E-05	9	84.48	70.80			32.21	8.75	9.21
702	B	9	1	147	149	74.27	4.853E-05	10	338.39	63.99	4.70	yes			
702	B	9	2	13	15	74.43	9.408E-05	13	65.20	76.35	3.69	yes			

Table S3. List of paleomagnetic directions and associated confidence boundaries; MBSF= meter below seafloor; NRM= intensity of the natural remanent magnetization in A/m; N= number of vector end-points; Dec, Inc= declination and inclination of the paleomagnetic vector; MAD= maximum angular deviation of Kirschvink (1980), calculated for paleomagnetic vector either anchored or not anchored (anchored yes/no) to the origin of the demagnetization axes; k, R, a95 = statistical precision parameters of Fisher (1953).

Event	Species	Base Zone*	Sample Base ID	Sample Top ID	Depth Base (mbsf)	Depth Top (mbsf)	Mid point (mbsf)	Chron position to the top	Age (Ma) GST 2012	Reference
T	*C. solitus*	NP17-CP14b	-	-	-	-	-	C18n.2n 0.21-C18n.1n 0.24	39.8 - 38.8	Agnini et al. 2014
Tc	*S. spiniger*	MNP17A	702B-8x-6w, 10	702B-8x-5w, 140	70.90	70.70	70.80	C18n.1n 0.94	40.10	Fornaciari et al. 2010
Bc	*D. bisectus*	CNE15	702B-9x-1w, 50	702B-9x-1w, 30	73.30	73.10	73.20	C18r 0.20	40.36	Agnini et al. 2014
Bc	*D. hesslandii*		702B-9x-2w, 20	702B-9x-1w, 140	74.50	74.20	74.35	C18r 0.22	40.37	Agnini et al. 2014
T	*S. furcatolithoides*	MNP16B	-	-	-	-	-	C18r 0.33	40.48	Agnini et al. 2014
Bc	*C. reticulatum*	CNE14	-	-	-	-	-	C19r 0.84	42.16	Agnini et al. 2014
Bc	*R. umbilicus*	NP16-CP14a-CNE13	-	-	-	-	-	C20n 0.42	42.77	Agnini et al. 2014

*CN zones: NP(Martini, 1971); CP(Okada & Bukry, 1980); CNE (Agnini et al., 2014); MNP (Fornaciari et al., 2010)

Table S4. Calcareous nannofossil biostratigraphic data from Site 702. The position of biohorizons (i.e., Top ID sample, Base ID samples and depth in mbsf) are provided. Biochronology adopted (Top chron position Time Scale reference, calibration reference) is also reported.

Table S5. XRF analysis from Site 702 (sheet 1), isotopic data from Site 702 (sheet 2) and Site 1263 (sheet 3) used for the age model, correlation tie points and cyclostratigraphic ages (sheet 4).

Appendix IV: Supplementary material (Rivero-Cuesta et al., 2018)

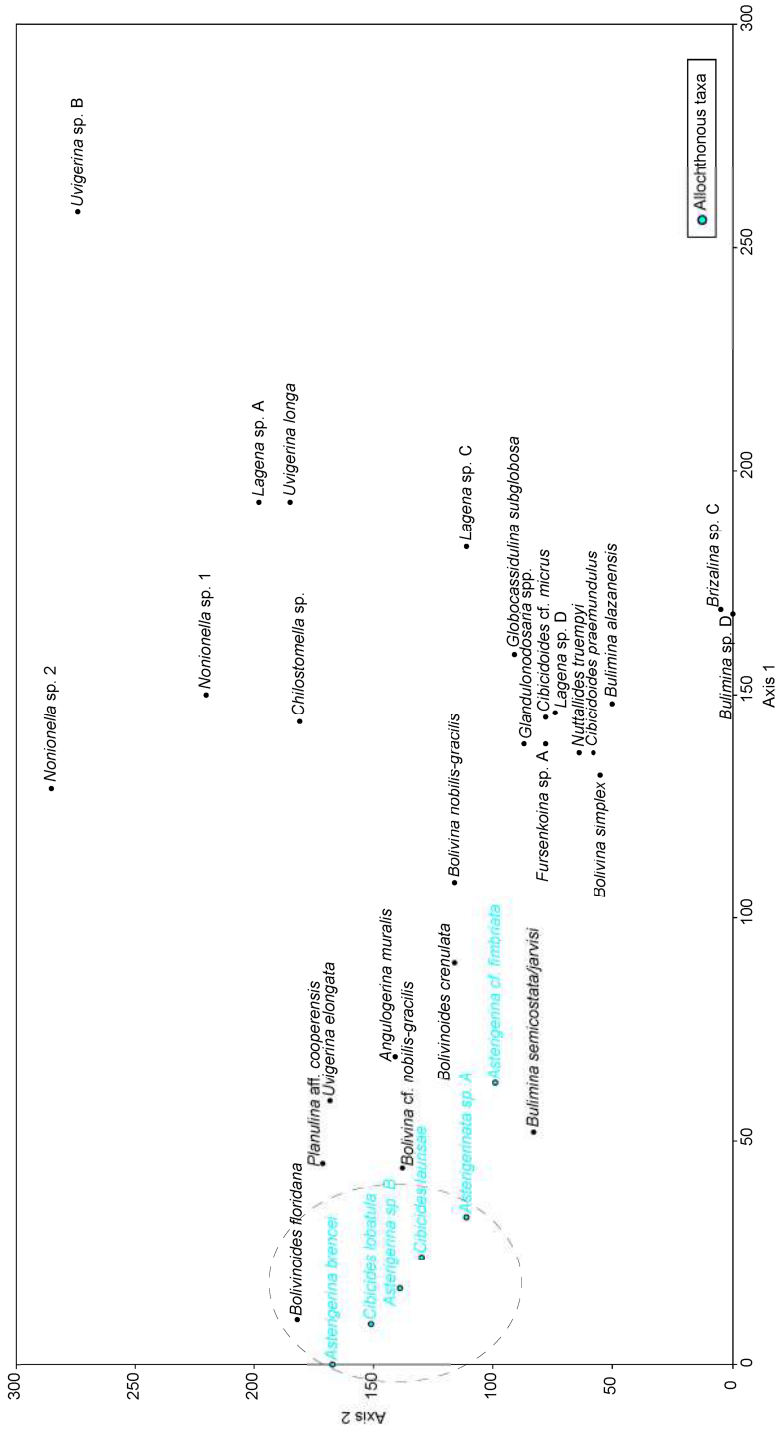

Supplementary Figure 1. R-mode DCA analysis performed on total assemblages of benthic foraminifera. The dashed ellipse includes species with the lowest values along Axis 1, which are considered as allochthonous. Two outliers where identified: *Bolivinoides floridan*a (autochthonous species inside the ellipse) and *Asterigerina* cf. *fimbriata* (outside the ellipse, but marked in blue as it is interpreted as an allochthonous taxon).

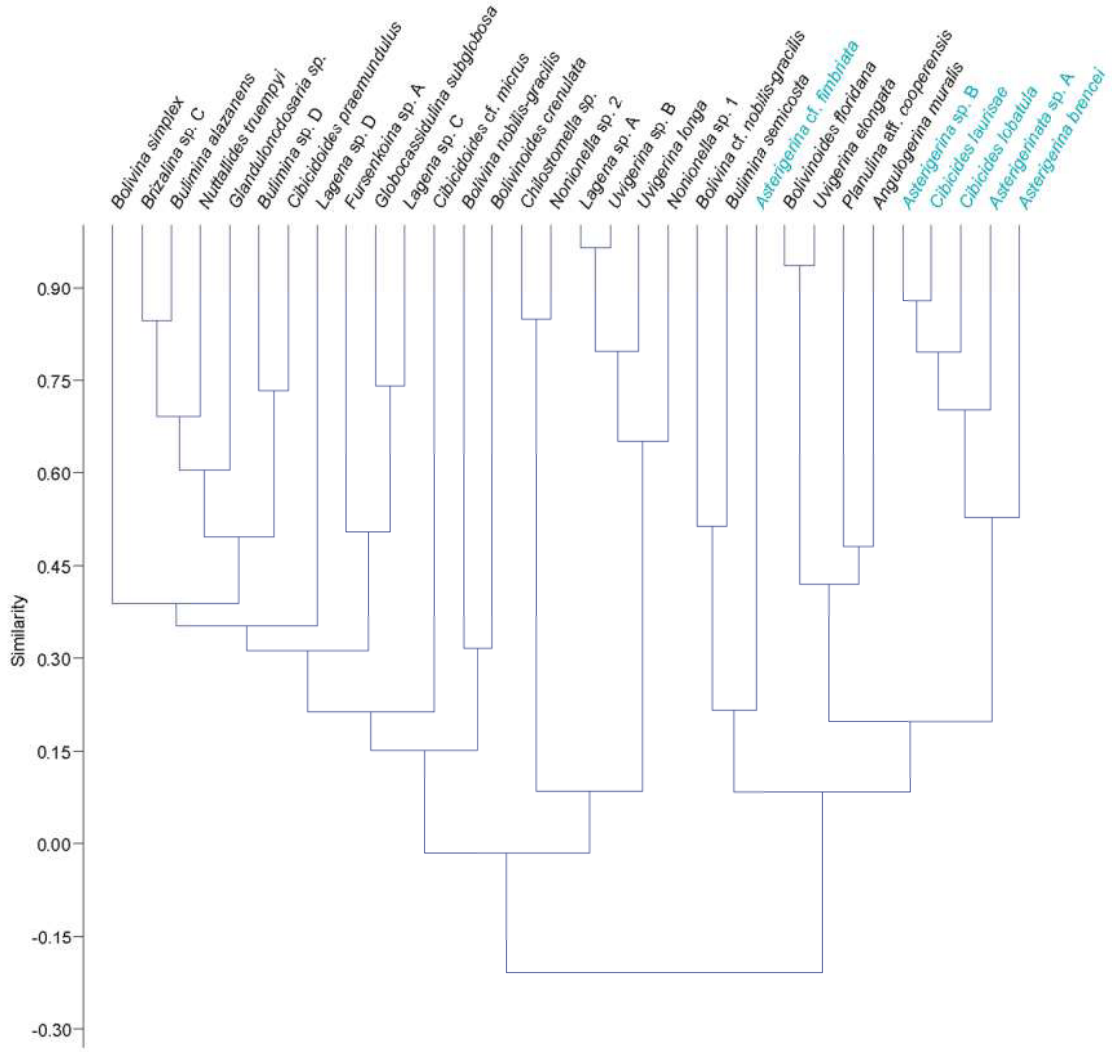

Supplementary Figure 2. Cluster analysis performed on total assemblages of benthic foraminifera. Species in blue are interpreted as allochthonous.

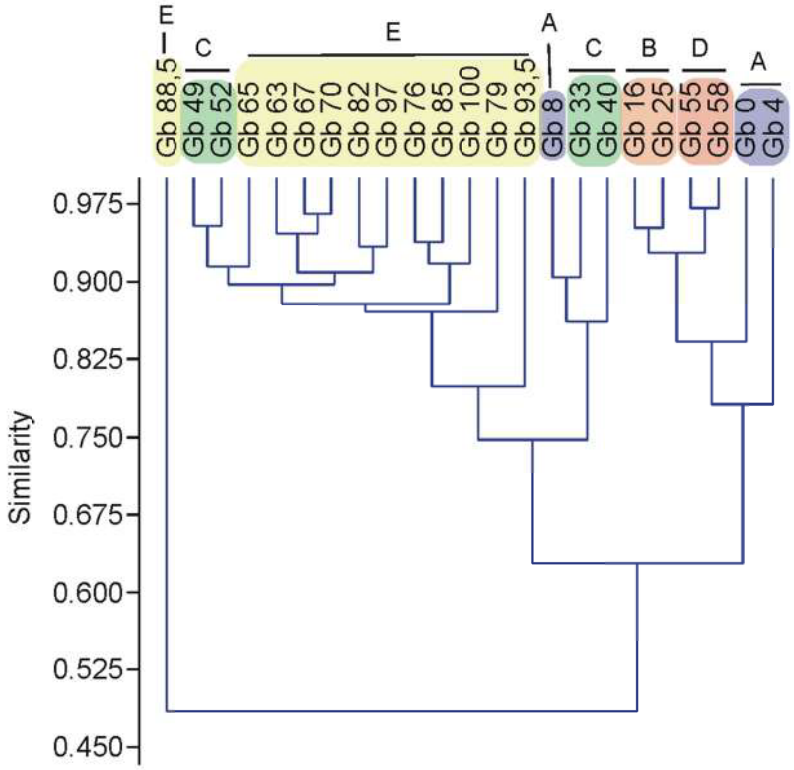

Supplementary Figure 3. Cluster analysis performed on samples from Torre Cardela.

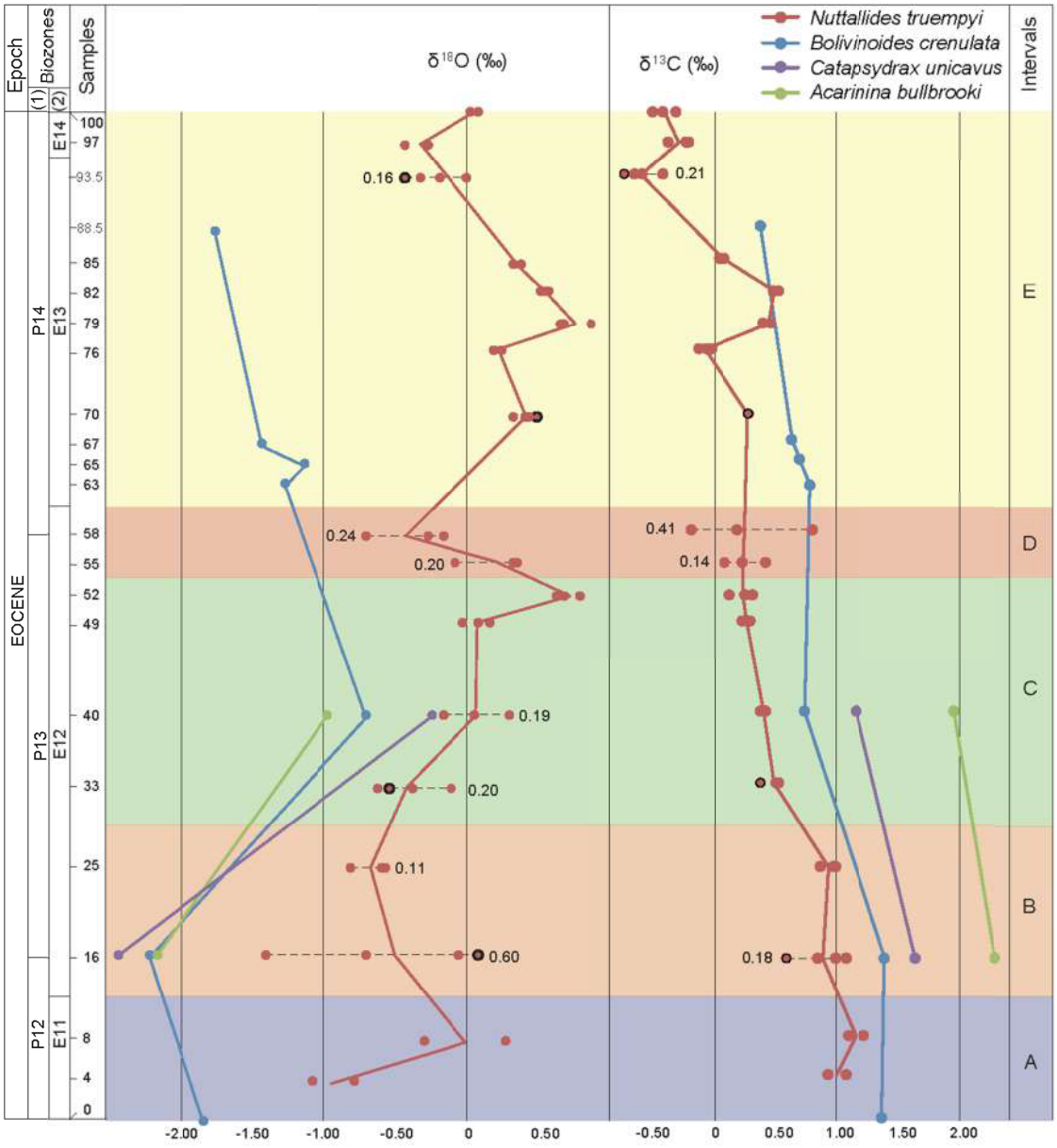

Supplementary Figure 4. Species-specific oxygen and carbon stable isotope data from Torre Cardela section. Dashed lines represent standard deviation; red circles with a black ring represent "rusty" specimens. Planktonic foraminiferal biozones (1) Gonzalvo and Molina (1996) and (2) this work.

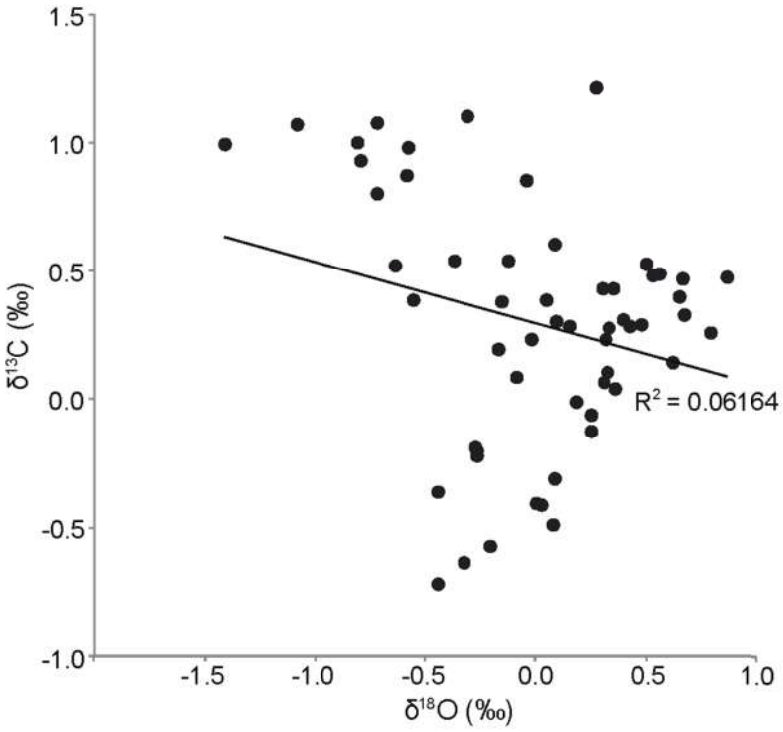

Supplementary Figure 5. Plot of carbon versus oxygen stable isotope values of Nuttallides truempyi from the Torre Cardela section. Correlation values are low: r = -0.25 and p = 0.064.

Supplementary Data 1 contains benthic foraminiferal data from the Torre Cardela section across the base of the Bartonian (total count and relative abundances of all the species identified and the environmental indices calculated).

Supplementary Data 2 contains the isotopic data analyzed in this paper.

Supplementary data can be found in a separate Excel file (Appendices folder).